



# Deciphering Deafness in Down Syndrome: Finding the Otitis Media Gene

---

A thesis presented for the degree of Doctor of Philosophy (DPhil)

Trinity Term, 2022

**Amy Southern**

Mammalian Genetics Unit, MRC Harwell Institute

Linacre College, University of Oxford

Department of Biochemistry

**Supervisors:**

Dr Hilda Tateossian (MRC Harwell Institute)

Professor Steve Brown (MRC Harwell Institute)

Associate Professor Duncan Sparrow (DPAG, Oxford)

Professor Matthew Whitby (Biochemistry, Oxford)

**Word count:** 39,535

DEPARTMENT OF BIOCHEMISTRY  
UNIVERSITY OF OXFORD



Mary Lyon  
Centre at  
MRC Harwell



Linacre College  
University of Oxford

## Abstract

---

### **Deciphering Deafness in Down syndrome: Finding the Otitis Media Gene**

Hearing impairment, particularly in children with Down syndrome (DS), can lead to isolation and developmental issues. The most common cause of hearing loss in children with DS is otitis media with effusion (OME). OME is defined as inflammation of the middle ear epithelial lining and the accumulation of fluid in the middle ear cavity, without the presence of a pathogen. The middle ear fluid impedes the passage of sound waves to the inner ear. OME is known to have a strong genetic component, and children with DS are particularly susceptible.

With the aid of a mapping panel of partial trisomy mouse models, it was found that mice carrying a duplication of the genes in the Dp5Tyb region demonstrate highly penetrant OME affecting one or both ears. The Dp5Tyb region only contains 12 protein coding genes, all of which have human chromosome 21 orthologues. The DS and deafness phenotypes of Dp5Tyb mice were investigated, and also the expression of the 12 genes in the middle ear environment. Single gene knockout mice for Dp5Tyb genes were crossed to Dp5Tyb or Dp3Tyb mice, thus restoring disomy of one gene in double mutant offspring. Analysis of these double mutants identified *Dyrk1a* as a key gene of interest. When *Dyrk1a* dosage was restored to two copies in a DS mouse the OME phenotype was rescued to wildtype levels. Investigations into how increased *Dyrk1a* dosage contributes to OME pathogenesis provided evidence that it impacts on a number of processes, including promoting TGF- $\beta$  signalling and driving the differentiation of naïve CD4<sup>+</sup> T cells into pro-inflammatory Th17 cells.

These studies suggest that the administration of DYRK1A inhibitors to Dp5Tyb mice could ameliorate the OME phenotype. The application of this to young children with DS could make a big difference to their speech and language development.

## Acknowledgements

---

Firstly, I would like to thank my supervisors, Hilda Tateossian and Steve Brown, for their guidance and support throughout my project. I am also incredibly grateful to Duncan Sparrow for stepping in during my final year to offer additional supervision due to the closure of the Mammalian Genetics Unit at Harwell. Thank you also to Matthew Whitby, for helping with departmental and university related matters.

I am so pleased that I had the opportunity to work at MRC Harwell, surrounded by a community of experts in their respective fields, who are always willing to help others. In particular I'd like to thank the Histology team – Maz Yon, Adele Austin and Caroline Barker – not only for the huge amount of work they've done to support my project, but also for their friendship over the past four years. I am very grateful to Simon Gillard and the Ward 6 team in the Mary Lyon Centre for managing the mouse colonies. Thanks also goes to Lee Moir for helping with any MSD assay-related queries. Our resident PCR expert Debbie Williams has been wonderful, thank you for all your help. I would also like to extend my gratitude to Victor Tybulewicz (Francis Crick Institute) and Lizzie Fisher (University College London) for providing the DpTyb mouse lines.

I have made friends for life at Harwell, with our relationships made even stronger due to the shared hardship of COVID-19, MGU closure, and general PhD life. Thank you to all the students, past and present, for your friendship throughout this emotional rollercoaster, in particular my girls since day one – Louisa Zolkiewski and Gurpreet Bharj.

Thank you to my Mum, Dad and sister (Pauline, Nick and Katie Southern) for your unwavering support and understanding. To my Grandad, Derek Southern – thank you for inspiring me to follow in your footsteps and become a scientist at Harwell. I really appreciate you encouraging me to reach my full potential - I never imagined that would mean doing a PhD at Oxford University!

And finally, thank you to my partner, Ben Dolby. You've been by my side for my entire further education journey, and I couldn't have done it without your unconditional love and motivational pep talks. You're the best life partner I could wish for, and I'm grateful for you every day.

## Statement of Contributions

---

This thesis contains original, unpublished work undertaken primarily by me, Amy Southern. However, components of this project were recently added to a manuscript for publication, on which myself and Hilda Tateossian are co-first authors.

The core facilities at MRC Harwell have been incredibly useful. The Necropsy team helped collect lungs from Dp5Tyb mice and heads from the mouse crosses in the Mary Lyon Centre (MLC). The Histology department embedded and sectioned the lungs and heads, and also performed haematoxylin and eosin (H&E) and Alcian blue periodic acid Schiff (AB-PAS) staining when required. Ward 6 in the MLC took care of the animal husbandry, set up matings, and took ear biopsies for genotyping. The Genotyping team then performed all genotyping.

Others have also contributed to this work, and I am very grateful for their time.

Andrew Parker and Lucy Dunbar assisted with scanning electron microscopy (SEM) sample processing and taught me how to do the imaging. Zsombor Szoke-Kovacs performed the micro-computed tomography (microCT) imaging. Debbie Williams helped with real time quantitative PCR (RT-qPCR) experimental design, provided protocols and helped with the initial analysis of results. Assistance with RT-qPCR statistical analysis and data visualisation was sought from Heena Lad and George Nicholson. George also helped with analysis of the Meso Scale Discovery (MSD) assay data. Regie Santos-Cortez performed RT-qPCR on human saliva samples with my primers and shared her findings.

## Publications Arising from DPhil

---

Shortlisted for Max Perutz Science Writing Award 2019. Story published online.

<https://www.ukri.org/publications/max-perutz-science-writing-award-2019-winning-and-shortlisted-essays/>

Hilda Tateossian\*, **Amy Southern**\*, Pratik Vikhe, Eva Lana-Elola, Sheona Watson-Scales, Dorota Gibbins, Debbie Williams, Thomas Purnell, Philomena Mburu, Andrew Parker, Dominic P Norris, Regie Lyn P Santos-Cortez, Brian W Herrmann, Sara Wells, Heena V Lad, Elizabeth MC Fisher, Victor LJ Tybulewicz and Steve DM Brown. **DYRK1A kinase trisomy is the major cause of Otitis Media in Down Syndrome** (2022). *Manuscript in preparation, draft included in the Appendix.*

\*co-first authors

## Conference presentations

---

June 2019 – International Society for Otitis Media (ISOM). Los Angeles, CA, USA. Presented a lightning talk and a poster, awarded 1<sup>st</sup> prize.

July 2019 – Oxford Medical Sciences Division DPhil day. Poster presentation, awarded the runner-up prize.

October 2020 – MRC Harwell student symposium, presented a short talk.

July 2021 – MRC Harwell student symposium, presented a short talk.

June 2022 – Trisomy 21 Research Society (T21RS) conference. Long Beach, CA, USA. Poster presentation.

## List of Figures

Figure 1.1. Anatomy of the human ear .....	2
Figure 1.2. Inflammation in the middle ear due to otitis media with effusion (OME).....	6
Figure 1.3. Schematic of the duplicated chromosomal regions in DS mouse models and the OME incidence in each mouse line.....	20
Figure 2.1. Setup of electrodes for measuring auditory-evoked brainstem response (ABR) .....	29
Figure 2.2. Diagram showing the anatomical plane of the histological sections.....	32
Figure 2.3. Measuring middle ear epithelial lining thickness.....	33
Figure 2.4. Mean linear intercept calculation.....	35
Figure 2.5. Craniofacial measurements.....	38
Figure 2.6. Meso Scale Discovery (MSD) assay .....	41
Figure 3.1. Mapping panel of the duplicated regions of DpTyb and DpYey mice.....	48
Figure 3.2. Weights of Dp5Tyb mice and their WT littermates.....	51
Figure 3.3. Thickness of middle ear epithelial lining in WT and Dp5Tyb mice from three weeks to one year of age.....	53
Figure 3.4. Auditory-evoked brainstem response thresholds for WT and Dp5Tyb mice from four weeks to six months of age.....	55
Figure 3.5. Scanning electron microscopy and H&E staining of cochlear hair cells....	56
Figure 3.6. Micro-computed tomography (microCT) images of the middle ear ossicles.....	58
Figure 3.7. Photographs of tympanic membranes.....	59
Figure 3.8. Mean linear intercept (Lm) graph and images of the lungs.....	61
Figure 3.9. Craniofacial measurements carried out on WT and Dp5Tyb skulls following bone preparation.....	62
Figure 4.1. Incidence of OME in Dp1Tyb, Dp3Tyb and Dp5Tyb compared to their respective WT littermates .....	72
Figure 4.2. Alcian Blue Periodic Acid Schiff (AB-PAS) staining of the middle ear epithelial lining near the Eustachian tube entrance.....	74
Figure 4.3. Dp5Tyb middle ear cilia from the dorsal and ventral regions.....	76
Figure 4.4. Dp3Tyb middle ear cilia from the dorsal and ventral regions.....	77
Figure 4.5. RT-qPCR data from Dp5Tyb blood and middle ear fluid using primers for Hif1a and downstream genes.....	80
Figure 4.6. Meso Scale Discovery (MSD) assay on WT and Dp5Tyb blood serum, and Dp5Tyb middle ear fluid.....	81
Figure 4.7. Immunohistochemistry of proteins present in Dp5Tyb middle ear fluid....	83
Figure 5.1. RT-qPCR data showing expression of the 12 Dp5Tyb genes in Dp5Tyb and WT white blood cells and middle ear epithelium, and Dp5Tyb middle ear fluid.....	97
Figure 5.2. Exploration of RT-qPCR data.....	100
Figure 5.3. Gene expression in the saliva of children with DS, relative to the saliva of their non-DS mothers.....	101
Figure 5.4. Immunohistochemistry with antibody against DYRK1A.....	104
Figure 5.5. Immunohistochemistry with antibody against GIRK2 (KCNJ6).....	105

Figure 5.6. Immunohistochemistry with antibody against KCNJ15.....	106
Figure 5.7. Immunohistochemistry with antibody against ERG.....	107
Figure 5.8. Immunohistochemistry with antibody against phosphorylated ETS2.....	108
Figure 5.9. Immunohistochemistry with antibody against PSMG1.....	109
Figure 5.10. Immunohistochemistry with antibody against BRWD1.....	110
Figure 5.11. Immunohistochemistry with antibody against HMGN1.....	111
Figure 5.12. Immunohistochemistry with antibody against GET1 (WRB).....	112
Figure 5.13. Immunohistochemistry with antibody against LCA5L.....	113
Figure 5.14. Immunohistochemistry with antibody against SH3BGR.....	114
Figure 5.15. Immunohistochemistry with antibody against B3GALT5.....	115
Figure 5.16. Percentage of mice with OME when knockouts of single genes in the Dp5Tyb region were crossed to Dp3Tyb or Dp5Tyb mice to create double mutants.....	118
Figure 6.1. Immunohistochemistry showing expression of DYRK1A and associated proteins.....	133
Figure 6.2. Meso Scale Discovery (MSD) assay to quantify protein levels in WT and Dp5Tyb blood serum, and Dp5Tyb middle ear fluid.....	135
Figure 8.1. Lower magnification images for cilia SEM.....	II
Figure 8.2. Primers for all 12 genes in the Dp5Tyb region.....	II
Figure 8.3. Negative controls for immunohistochemistry.....	III
Figure 8.4. Examples of western blots with antibodies against the 12 Dp5Tyb proteins.....	IV
Figure 8.5. Genotyping using quantitative PCR (qPCR).....	VI
Figure 8.6. Duplicated regions present in the DpTyb mouse lines.....	VII
Figure 8.7. Primers and probe sequences for the VIC-labelled internal control, Dot1l.....	VII
Figure 8.8. Primer sequences and FAM-labelled probes for the Dp5Tyb, Dp1Tyb and Dp3Tyb assays, respectively.....	VIII
Figure 8.9. Master mix for each qPCR.....	IX
Figure 8.10. Example of 5b18 and 3c09 assay copy calling.....	X
Figure 8.11. The Qiagen QIAxcel machine used to run the PCR, alongside an example readout showing WT and mutant bands.....	XI
Figure 8.12. The PCR protocol, and gel based primers and PCR master mixes for all seven mouse lines using the gel based genotyping method.....	XIII
Figure 8.13. Example of a Dyrk1a gel based assay.....	XIV
Figure 8.14. Schematics showing CRISPR/Cas9 technology removing an exon.....	XV
Figure 8.15. FAM-labelled primers and probes used in the genotyping of Kcnj6 <sup>+/-</sup> mice.....	XVI
Figure 8.16. Master mix used for Kcnj6 <sup>+/-</sup> genotyping.....	XVI
Figure 8.17. Example result from qPCR copy calling for Kcnj6 <sup>+/-</sup> .....	XVII
Figure 8.18. Sequences of the primers and probes used for ETS2-B6JNM genotyping.....	XVIII
Figure 8.19. The master mix and PCR protocol for Ets2 <sup>+/-</sup> genotyping.....	XIX
Figure 8.20. An example of Ets2 <sup>+/-</sup> allelic discrimination assay results.....	XX
Figure 8.21. Schematic of Psmg1 genotyping technique.....	XXI
Figure 8.22. Schematic of the full Knockout-First mutant allele (Tm1a).....	XXII

## List of Tables

---

Table 1.1. Genes associated with OME in humans.....	8
Table 2.1. Details of the knockout mouse lines used for this project.....	27
Table 8.1. Primary antibodies used for immunohistochemistry (IHC).....	I
Table 8.2. Secondary antibodies used for immunohistochemistry (IHC).....	I

## Abbreviations

---

<b>ABR</b>	Auditory-evoked brainstem response
<b>AOM</b>	Acute otitis media
<b>AR</b>	Antigen retrieval
<b>B3GALT5</b>	Beta-1,3-galactosyltransferase 5
<b>BRWD1</b>	Bromodomain and WD repeat-containing protein 1
<b>BSA</b>	Bovine serum albumin
<b>CC-3</b>	Cleaved caspase 3
<b>cDNA</b>	Complimentary/copy DNA
<b>COME</b>	Chronic otitis media with effusion
<b>CPD</b>	Critical point drying
<b>CSOM</b>	Chronic suppurative otitis media
<b>DAB</b>	3,3'-Diaminobenzidine
<b>dB SPL</b>	Decibel sound pressure level
<b>DC</b>	Detergent compatible
<b>df</b>	Degrees of freedom
<b>DNA</b>	Deoxyribonucleic acid
<b>Dp3Tyb</b>	Down syndrome phenotype 3 mouse line by Victor Tybulewicz
<b>Dp5Tyb</b>	Down syndrome phenotype 5 mouse line by Victor Tybulewicz
<b>DPOAE</b>	Distortion product otoacoustic emissions
<b>DS</b>	Down syndrome
<b>DYRK1A</b>	Dual specificity tyrosine-phosphorylation-regulated kinase 1A
<b>EDTA</b>	Ethylenediaminetetraacetic acid
<b>EL</b>	Epithelial lining of the middle ear cavity
<b>EMMA</b>	European mouse mutant archive
<b>ENU</b>	N-ethyl-N-nitrosourea
<b>ERG</b>	Erythroblast transformation-specific (ETS)-related gene
<b>ET</b>	Eustachian tube
<b>ETS2</b>	Erythroblast transformation-specific (ETS) proto-oncogene 2
<b>FDR</b>	False discovery rate
<b>GET1</b>	Guided entry of tail-anchored proteins factor 1 (a.k.a. WRB)
<b>GWAS</b>	Genome-wide association study

<b>H&amp;E</b>	Hematoxylin and eosin
<b>HC</b>	Hair cell
<b>HIF(-1<math>\alpha</math>)</b>	Hypoxia inducible factor (-1 $\alpha$ )
<b>HMGN1</b>	High Mobility Group Nucleosome Binding Domain 1
<b>hr</b>	Hour
<b>ICS</b>	Institut Clinique de la Souris
<b>IDA</b>	Industrial denatured alcohol
<b>IFN</b>	Interferon
<b>Ig</b>	Immunoglobulin
<b>IHC</b>	Immunohistochemistry
<b>IL</b>	Interleukin
<b>IMPC</b>	International Mouse Phenotyping Consortium
<b>IP</b>	Intraperitoneal
<b>ISOM</b>	International Society for Otitis Media
<b>KCNJ6</b>	Potassium Inwardly Rectifying Channel Subfamily J Member 6
<b>KCNJ15</b>	Potassium Inwardly Rectifying Channel Subfamily J Member 15
<b>KO</b>	Knockout
<b>LCA5L</b>	Leber Congenital Amaurosis 5-Like
<b>MEC</b>	Middle ear cavity
<b>MGU</b>	Mammalian Genetics Unit at MRC Harwell
<b>MICER</b>	Mutagenic Insertion and Chromosome Engineering Resource
<b>MicroCT</b>	Micro-computed tomography
<b>mins</b>	Minutes
<b>MLC</b>	Mary Lyon Centre at MRC Harwell
<b>MMRRC</b>	Mutant Mouse Resource and Research Center
<b>MRC</b>	Medical Research Council
<b>NDP</b>	NanoZoomer Digital Pathology
<b>NF<math>\kappa</math>B</b>	Nuclear factor kappa-light-chain-enhancer of activated B cells
<b>OM</b>	Otitis media
<b>OME</b>	Otitis media with effusion
<b>o/n</b>	Overnight
<b>PBS</b>	Phosphate buffered saline
<b>PBST</b>	Phosphate buffered saline with 0.05% tween

<b>PFA</b>	Paraformaldehyde
<b>PSMG1</b>	Proteasome Assembly Chaperone 1
<b>rcf</b>	Relative centrifugal force
<b>RNA</b>	Ribonucleic acid
<b>RT</b>	Room temperature
<b>RT-qPCR</b>	Real time quantitative PCR
<b>SEM</b>	Scanning electron microscopy
<b>SEM (statistics)</b>	Standard error of mean
<b>SH3BGR</b>	SH3 Domain Binding Glutamate-Rich Protein
<b>SMAD</b>	Contraction of: <i>C. elegans</i> SMA (small worm phenotype) and <i>Drosophila</i> MAD (Mothers Against Decapentaplegic)
<b>T21RS</b>	Trisomy 21 Research Society
<b>TBST</b>	Tris buffered saline with tween
<b>TCP</b>	The Centre for Phenogenomics
<b>TGF-<math>\beta</math></b>	Transforming growth factor $\beta$
<b>TNF-<math>\alpha</math></b>	Tumour necrosis factor $\alpha$
<b>VEGF-A</b>	Vascular endothelial growth factor A
<b>WBC</b>	White blood cell
<b>WRB</b>	Tryptophan Rich Basic Protein (also known as GET1)
<b>WT</b>	Wildtype

# Table of Contents

---

Abstract.....	i
Acknowledgements .....	ii
Statement of Contributions.....	iii
Publications Arising from DPhil .....	iv
Conference presentations .....	iv
List of Figures.....	v
List of Tables.....	vii
Abbreviations.....	viii
Table of Contents .....	xi
CHAPTER 1: Introduction.....	1
1.1. Anatomy of the mammalian ear .....	1
1.2. Hearing loss.....	3
1.2.1. Sensorineural hearing loss.....	3
1.2.2. Conductive hearing loss .....	4
1.3. Human genetic studies into the causes of OM.....	6
1.4. Mouse models of OM.....	11
1.4.1. <i>Jeff</i> .....	11
1.4.2. <i>Junbo</i> .....	12
1.4.3. <i>Tgif1</i> .....	14
1.4.4. <i>edison</i> .....	15
1.5. Down syndrome .....	16
1.6. Otitis media in Down syndrome .....	17
1.7. Mouse models of DS.....	19
1.7.1. Ts65Dn.....	20
1.7.2. Ts1Rhr .....	21
1.7.3. Tc1 .....	21

1.7.4. DpTyb.....	22
1.8. The Dp5Tyb genes .....	24
1.9. Thesis aims.....	25
CHAPTER 2: Materials and Methods .....	26
2.1. Mouse lines.....	26
2.1.1. Animal husbandry.....	26
2.1.2. Dp5Tyb and Dp3Tyb mice.....	26
2.1.3. Knock-out and point-mutation mouse lines .....	27
2.1.4. Generation of double mutants .....	27
2.1.5. Dp12Tyb, Dp1Tyb <i>Dyrk1a</i> <sup>+/-</sup> , Dp5Tyb <i>Hmgn1</i> <sup>+/-</sup> , and Dp3Tyb <i>Dyrk1a</i> <sup>+/-</sup> mice.....	28
2.2. Genotyping .....	28
2.3. Auditory-evoked Brainstem Response (ABR) .....	28
2.4. Schedule 1 cull of mice .....	30
2.5. Tympanic membrane observations .....	30
2.6. Histology .....	30
2.6.1. Sample collection and fixation.....	30
2.6.2. Decalcification .....	31
2.6.3. Dehydration, clearance and paraffin impregnation processing.....	31
2.6.4. Embedding and sectioning.....	31
2.6.5. Haematoxylin and Eosin (H&E) staining.....	33
2.6.6. Imaging .....	33
2.7. Measuring the middle ear epithelial lining.....	33
2.8. Lung phenotype .....	34
2.8.1. Mean linear intercept (Lm) calculation.....	34
2.9. Immunohistochemistry (IHC) .....	35
2.9.1. De-waxing .....	36
2.9.2. Blocking.....	36

2.9.3. Antigen retrieval (AR) .....	36
2.9.4. Antibody incubation .....	36
2.9.5. Visualisation and counterstaining .....	37
2.9.6. Quantification of staining .....	37
2.9.7. Special stains .....	37
2.10. Bone preparation .....	37
2.10.1. Craniofacial measurements.....	38
2.11. Real Time Quantitative Polymerase Chain Reaction (RT-qPCR) .....	38
2.11.1. Sample collection .....	38
2.11.2. RNA extraction and cDNA synthesis .....	39
2.11.3. PCR amplification.....	39
2.11.4. Analysis.....	40
2.12. Meso Scale Discovery (MSD) assay.....	40
2.12.1. Sample collection .....	40
2.12.2. Plate coating .....	41
2.12.3. Assay protocol.....	42
2.12.4. MSD data analysis .....	42
2.13. Micro-Computed Tomography (microCT) .....	43
2.13.1. Sample collection .....	43
2.13.2. Imaging .....	43
2.13.3. Segmentation .....	44
2.14. Scanning Electron Microscopy (SEM).....	44
2.14.1. Sample collection .....	44
2.14.2. Decalcification and fine dissection (inner ears only).....	44
2.14.3. Processing .....	45
2.14.4. Critical point drying, mounting and sputter coating.....	45
2.14.5. Imaging .....	45
2.15. Statistical analysis.....	45

CHAPTER 3: Phenotypic characterisation of Dp5Tyb mice .....	47
3.1. Introduction .....	47
3.2. Results.....	50
3.2.1. Trisomy of the Dp5Tyb region has no effect on survival.....	50
3.2.2. Dp5Tyb mice do not weigh significantly less than their WT littermates at two-months-old.....	51
3.2.3. Dp5Tyb mice have inflamed middle ears from three weeks of age .....	52
3.2.4. Dp5Tyb mice have a small increase in ABR thresholds, which is indicative of conductive hearing loss.....	54
3.2.5. No sensorineural hearing loss was found in Dp5Tyb mice.....	56
3.2.6. Investigation of additional conductive elements to the hearing loss .....	57
3.2.7. Dp5Tyb mice have a mild lung phenotype .....	60
3.2.8. Mild craniofacial defect in Dp5Tyb mice .....	62
3.3. Discussion .....	64
CHAPTER 4: Further exploration of the Dp5Tyb otitis media phenotype .....	70
4.1. Introduction .....	70
4.2. Results.....	72
4.2.1. Incidence of OME in DS mouse lines relative to WT littermates .....	72
4.2.2. Dp5Tyb mice do not appear to have more goblet cells than WT littermates at two-months-old.....	73
4.2.3. Dp5Tyb and Dp3Tyb mice have impaired middle ear cilia maintenance at two months of age.....	75
4.2.4. Hypoxia and inflammation markers are upregulated in the middle ear of Dp5Tyb mice .....	78
4.2.5. Macrophages and neutrophils are present in the inflamed Dp5Tyb middle ear, and there is widespread proliferation and cell death .....	82
4.3. Discussion .....	84
CHAPTER 5: Middle ear expression of the 12 genes in the Dp5Tyb region, and analysis of double mutants.....	90

5.1. Introduction .....	90
5.1.1. <i>Dual-specificity tyrosine-regulated kinase 1A (Dyrk1a)</i> .....	90
5.1.2. <i>Potassium Inwardly Rectifying Channel Subfamily J Member 6 (Kcnj6)</i> ..	91
5.1.3. <i>Potassium Inwardly Rectifying Channel Subfamily J Member 15 (Kcnj15)</i> .....	92
5.1.4. <i>Erythroblast transformation-specific (ETS)-related gene (Erg)</i> .....	92
5.1.5. <i>Erythroblast transformation-specific (ETS) Proto-Oncogene 2 (Ets2)</i> .....	92
5.1.6. <i>Proteasome Assembly Chaperone 1 (Psmg1)</i> .....	93
5.1.7. <i>Bromodomain and WD Repeat Domain Containing 1 (Brwd1)</i> .....	93
5.1.8. <i>High Mobility Group Nucleosome Binding Domain 1 (Hmgn1)</i> .....	93
5.1.9. <i>Guided Entry of Tail-Anchored Proteins Factor 1 (Get1)</i> .....	94
5.1.10. <i>Leber Congenital Amaurosis 5-Like (Lca5l)</i> .....	94
5.1.11. <i>SH3 Domain Binding Glutamate Rich Protein (Sh3bgr)</i> .....	94
5.1.12. <i>Beta-1,3-Galactosyltransferase 5 (B3galt5)</i> .....	95
5.2. Results.....	96
5.2.1. Expression of the 12 Dp5Tyb genes at the RNA level.....	96
5.2.2. Human saliva qPCR data found differential expression of <i>DYRK1A</i> and <i>KCNJ6</i> in children with DS compared to their non-DS mothers .....	101
5.2.3. Expression of the 12 Dp5Tyb genes at the protein level .....	103
5.2.4. Generation and phenotypic analysis of double mutants .....	116
5.3. Discussion .....	122
5.3.1. Expression of the Dp5Tyb genes at the transcript level .....	122
5.3.2. Expression of the Dp5Tyb genes at protein level .....	123
5.3.3. Restoring disomy of each Dp5Tyb gene to find the dosage-sensitive gene(s) causing OME.....	125
CHAPTER 6: Investigating the role of <i>DYRK1A</i> in otitis media .....	128
6.1. Introduction .....	128
6.2. Results.....	131

6.2.1. DYRK1A, SMAD proteins, VEGF-A and IL-6 were restored to WT levels when <i>Dyrk1a</i> copy number was normalised.....	131
6.2.2. The pro-inflammatory Th17 lineage is activated in Dp5Tyb mice, and hypoxia-related proteins are upregulated in Dp5Tyb middle ear fluid .....	134
6.3. Discussion .....	136
CHAPTER 7: Discussion .....	141
7.1. Project overview .....	141
7.2. Summary of results .....	142
7.2.1. Dp5Tyb as a mouse model of DS.....	142
7.2.2. Dp5Tyb as a mouse model of OME in DS.....	142
7.2.3. Expression of the 12 genes in the Dp5Tyb region.....	144
7.2.4. Crossing single gene knockouts to Dp5Tyb or Dp3Tyb mice .....	145
7.2.5. Hypoxia signalling in the Dp5Tyb middle ear .....	146
7.2.6. Mechanisms for <i>Dyrk1a</i> involvement in OME pathogenesis .....	147
7.3. Wider impact and contribution to the field.....	148
7.4. Future directions .....	149
7.4.1. Hearing loss .....	149
7.4.2. Craniofacial defects.....	150
7.4.3. Cilia morphology.....	150
7.4.4. Hypoxia .....	151
7.4.5. DYRK1A inhibitors.....	151
7.4.6. Additional genetic loci involved in OME.....	151
7.5. Conclusion .....	152
References .....	153
Appendix .....	I
8.1. Primary antibodies .....	I
8.2. Secondary antibodies .....	I
8.3. Lower magnification images for cilia SEM .....	II

8.4. RT-qPCR primers for Dp5Tyb genes .....	II
8.5. Negative controls for immunohistochemistry .....	III
8.6. Examples of western blots for the 12 Dp5Tyb proteins.....	IV
8.7. Genotyping .....	V
8.7.1. Genotyping of Dp lines .....	V
8.7.2. Genotyping of knockout and point mutation lines .....	XI
8.7.3. Genotyping of double mutants .....	XXII
8.8. Tateossian <i>et al.</i> 2022 – unpublished draft .....	XXIII

# CHAPTER 1: Introduction

---

Hearing impairment in childhood can lead to isolation and developmental issues (Rosenfeld et al., 2016). For children with Down syndrome (DS) these issues are further compounded by their learning difficulties (Nightengale et al., 2017). The most common cause of hearing loss in children with DS is otitis media with effusion (OME) (Park et al., 2012), which occurs without the presence of a pathogen (Fortnum et al., 2014) and is known to have a significant genetic component (Bhutta et al., 2013, Tateossian et al., 2022). OME affects up to 93% of one-year-olds with DS (Barr et al., 2011). I will use mouse models to investigate the cause of OME in DS. Identifying the dosage-sensitive gene(s) responsible could support the development of therapies, with the aim of enabling these children to develop their speech and language skills, and ultimately improve their quality of life.

## 1.1. Anatomy of the mammalian ear

The ear is the sensory organ responsible for hearing. It is comprised of the outer, middle and inner ear. All components must develop and function properly in order for hearing to take place at its full capacity (Anthwal and Thompson, 2016). The outer ear is what can be seen externally. It includes the auricle and the external auditory canal, finishing at the eardrum (tympanic membrane) (*Figure 1.1*) (Fuchs and Tucker, 2015). Behind the tympanic membrane is the middle ear, an air-filled cavity lined with ciliated epithelium which is continuous with the Eustachian tube and nasopharynx (Anthwal and Thompson, 2016). The middle ear epithelium derives from two distinct developmental origins (Thompson and Tucker, 2013), with the neural crest-derived dorsal region lightly littered with bundles of motile cilia, and the endoderm-derived ventral region (around the Eustachian tube entrance) heavily covered with a lawn of motile cilia (Luo et al., 2017, Tateossian et al., 2022).

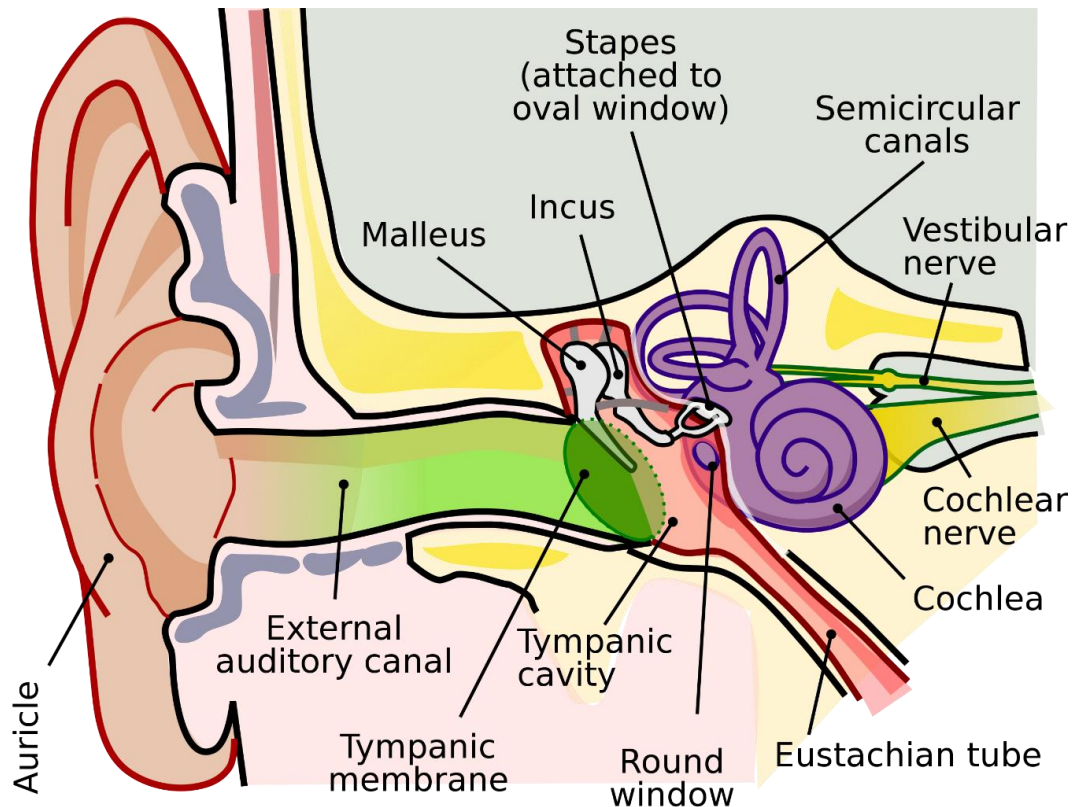


**Figure 1.1. Anatomy of the human ear.** The outer ear encompasses the parts of the ear that can be viewed from the outside, such as the auricle and the external auditory canal, and also the eardrum (tympanic membrane). Behind the tympanic membrane is the middle ear - an air-filled cavity that houses the ossicles (malleus, incus, and stapes). The middle ear is connected to the nasopharynx via the Eustachian tube. Behind the oval window is the inner ear, which includes the cochlea and auditory nerves. The cochlea contains hair cells, which transduce sound waves into electrochemical signals for the brain. Source: (Chittka and Brockmann, 2005), reproduced under Creative Commons License 2.5.

Goblet cells are also present in the ventral epithelium, and secrete mucins (the main component of mucus) to trap dust and airborne particles (Lim et al., 1973). As with airway mucociliary clearance, the middle ear cilia waft the mucus and cellular excretions down the Eustachian tube to be swallowed or expelled from the body (Bustamante-Marin and Ostrowski, 2017). The middle ear also contains the three ossicle bones - malleus, incus and stapes (*Figure 1.1*), suspended between the tympanic membrane and the oval window - a membrane separating the middle and inner ear (Anthwal and Thompson, 2016). The inner ear mainly comprises of the

cochlea, which is a fluid-filled spiral containing mechanosensory hair cells (Fuchs and Tucker, 2015).

In order for hearing to take place, the auricle and ear canal focus sound waves towards the tympanic membrane (Fuchs and Tucker, 2015). The membrane vibrates, and passes the vibrations onto the malleus, incus and stapes which amplify the sound waves (Fuchs and Tucker, 2015). The stapes then connects to the oval window, which further amplifies the sound and vibrates the fluid within the cochlea (Fuchs and Tucker, 2015). Hair cells are organised along the basilar membrane of the cochlea according to the sound frequencies they can detect (Mann et al., 2014), with high frequency sounds detected nearer the basal region and low frequency sounds detected near the apex of the cochlea (Li et al., 2021). The hair cells transduce the sound waves into electrical energy, which travels along the cochlear nerve to the brain (Fuchs and Tucker, 2015).

### 1.2. Hearing loss

According to the Royal National Institute for Deaf People (RNID), 12 million people in the UK currently suffer from hearing loss, which can be caused by a number of factors, including ageing, noise exposure, injury, genetics and disease. Some hearing loss is degenerate, whereas some is short term and will improve. Hearing loss can broadly be categorised into sensorineural, conductive, or a mixture of both.

#### 1.2.1. Sensorineural hearing loss

Sensorineural hearing loss is caused by inner ear problems, and is usually degenerative so will worsen over time if not managed (Kreicher et al., 2018). Age-related hearing loss (presbycusis) is sensorineural, and affects social interaction and quality of life (Michels et al., 2019, Bowl and Dawson, 2019). People with

sensorineural hearing loss tend to use hearing aids, although these can come with discomfort and social stigma (Lin et al., 2022).

### 1.2.2. Conductive hearing loss

Conductive hearing loss is due to pathology within the middle ear which causes the sound waves to have difficulty reaching the inner ear (Anthwal and Thompson, 2016). In humans it is diagnosed using pure-tone audiometry, or simple tuning fork methods such as Weber and Rinne tests (Abdullah et al., 2022). For pure-tone audiometry, the difference between the thresholds recorded by air conduction and bone conduction audiometry (known as the air-bone conduction gap) is used to differentiate between conductive, sensorineural and mixed hearing loss (Margolis et al., 2016). In mice, elevated DPOAE thresholds combined with reduced DPOAE amplitudes and mildly elevated ABR thresholds across all frequencies is indicative of conductive hearing loss (Chen et al., 2022). Causes of conductive hearing loss include a perforated eardrum (tympanic membrane), abnormal growth of the middle ear bones (ossicles), or a blockage of the middle ear cavity with fluid and white blood cells (otitis media) (De Schrijver et al., 2019).

#### 1.2.2.1. Tympanic membrane perforations

The tympanic membrane is a thin layer of tissue which separates the external ear canal from the middle ear (*Figure 1.1*). When sound waves reach the tympanic membrane it vibrates, and transfers these vibrations to the ossicles (Anthwal and Thompson, 2016). A perforation of the tympanic membrane reduces its ability to vibrate efficiently, leading to conductive hearing loss (Manickam et al., 2016).

#### 1.2.2.2. Ossicle overgrowth/malformation

The ossicles are the malleus, incus and stapes bones (*Figure 1.1*). They carry vibrations from the tympanic membrane to the oval window (Anthwal and Thompson,

2016). Their morphology is important to ensure effective transfer of the vibrations. If the bones form incorrectly they may not connect properly to each other or to the membranes either side (Anthwal and Thompson, 2016).

### 1.2.2.3. Inflammation of the middle ear cavity (otitis media)

Otitis media (OM) is a term used to describe inflammation of the middle ear, and consists of thickening of the epithelial lining (mucoperiosteum) and the accumulation of fluid (effusion) in the middle ear cavity, usually containing white blood cells (Bhutta et al., 2019). OM is considered a spectrum of disease, including acute OM (AOM) and OM with effusion (OME) (Schilder et al., 2016). AOM is inflammation of the middle ear due to a bacterial or viral infection, and is usually associated with pain and fever (Schilder et al., 2016). Frequent reinfections (three or more AOM episodes in six months) lead to a diagnosis of recurrent AOM (Schilder et al., 2016). A complication of AOM is chronic suppurative otitis media (CSOM), where the bulging eardrum ruptures and infected fluid leaks out into the auditory canal (Schilder et al., 2016). Conversely, OME is the inflammation of the middle ear mucosa and occurrence of fluid behind the tympanic membrane with no sign of an infectious agent (Fortnum et al., 2014) (*Figure 1.2*). AOM usually resolves within two months, but OME can last longer, and is diagnosed as chronic OME (COME) when it persists for over three months (Blanc et al., 2018). OM is considered a spectrum as after an episode of AOM, once the pathogen has been neutralised, the inflammation and effusion often persists and becomes OME (Schilder et al., 2016). OM leads to conductive hearing loss as the presence of fluid in the middle ear cavity restricts the vibration of the eardrum and ossicles.

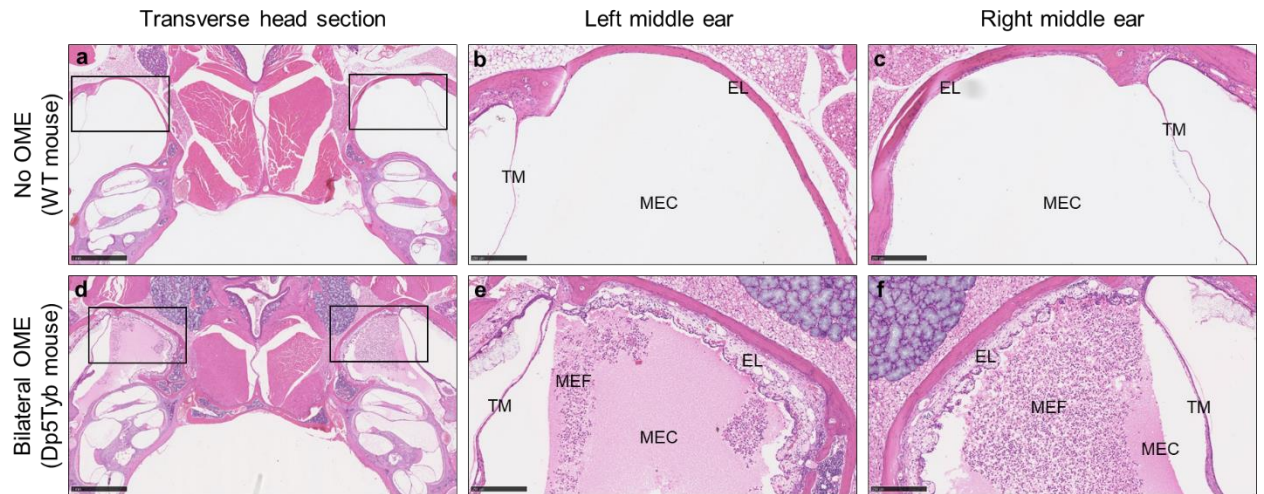


**Figure 1.2. Inflammation in the middle ear due to otitis media with effusion (OME).** Head sections from mice, cut in the transverse plane and stained with H&E (haematoxylin and eosin). (a) Section from a WT mouse with no OME, followed by magnified images of the left (b) and right (c) middle ear cavities. The epithelial lining is very thin, and the middle ear cavity is an air-filled space. (d) Section from a Dp5Tyb mouse with bilateral OME, followed by magnified images of the left (e) and right (f) middle ear cavities. The epithelial lining is much thicker, and cellular fluid has accumulated in the middle ear cavity. TM = tympanic membrane; EL = epithelial lining; MEC = middle ear cavity; MEF = middle ear fluid. Scale bar for transverse head sections (a, d): 1 mm; scale bar for individual ears (b, c, e, f): 250  $\mu$ m.

### 1.3. Human genetic studies into the causes of OM

In humans, it is known that susceptibility to infections has a strong genetic component, but only 4% of genome-wide association studies (GWAS) have been carried out to identify causative genes for infectious diseases (Mozzi et al., 2018).

Before 2012, the main method used to identify genes which confer susceptibility to OM was association analysis of candidate genes, chosen for their known roles in inflammation, or due to findings from animal models of OM (Rye et al., 2012). For one study, patients treated with tympanostomy tubes for COME and their relatives underwent ear examination and hearing tests, and completed a form detailing any OM-related history (Sale et al., 2011). Blood samples were taken, and the isolated DNA was genotyped to identify single nucleotide polymorphisms (SNPs) with minor allele frequency  $\geq 0.05$  in 15 candidate genes. Of the 99 SNPs successfully genotyped, only a handful of variants (found in genes *MUC2*, *MUC5B*, *MUC5AC*,

*SCN1B*, *SFTPD* and *TLR4*) showed a positive association with COME when analysed using the Generalised Disequilibrium test (GDT). Confidence in these results is elevated due to samples being taken from closely related individuals, however the authors conclude that it is unlikely that these SNPs in the chosen candidate genes are making a major contribution to COME susceptibility as the associations were not replicated in an independent cohort of families (Sale et al., 2011).

Another study (Rye et al., 2011b) looked at SNPs involved in TGF- $\beta$  signalling, due to the mouse models *Jeff* and *Junbo* which develop severe OM due to mutations in the TGF- $\beta$  signalling pathway members *Fbxo11* and *Evi1*, respectively (Tateossian et al., 2009, Parkinson et al., 2006). They collected DNA samples (from saliva or blood) from children with a history of tympanostomy tubes along with their parents and any siblings also affected by COME (Rye et al., 2011b). Haplotype tagging SNPs with minor allele frequency  $\geq 0.2$  were chosen from an online database (International HapMap Project) for a total of 19 TGF- $\beta$ -related genes. SNPs in *SMAD2*, *SMAD4* and *FBXO11* were found to be positively associated with OM in western Australian families, however, the only gene to maintain this association amongst an independent cohort of families was *FBXO11* (Rye et al., 2011b).

In summary, these studies identified several candidate genes as having a positive association with OME: *FBXO11*, *MUC2*, *MUC5AC*, *MUC5B*, *SCN1B*, *SMAD2*, *SMAD4*, *SFTPD*, and *TLR4* (Table 1.1).

## CHAPTER 1: Introduction

**Table 1.1. Genes associated with OME in humans.** The table lists the human chromosome where each gene can be found, and the known functions of that gene. Any mouse studies related to the gene are also included. The table focuses on genes related to OME, rather than AOM, when the studies have discriminated between these conditions. Information on gene loci and protein functions was sourced from the referenced papers, or from GeneCards and NCBI.

Gene	Chr.	Function	OME-related mouse studies	References
<i>FBXO11</i>	2	Subunit of a ubiquitin protein ligase complex, which functions in phosphorylation-dependent ubiquitination	Mice carrying Jeff and Mutt alleles had craniofacial abnormalities, hearing loss and OM. Jeff mice also have defects in middle ear bulla development.	(Segade et al., 2006; Rye et al., 2011b) (Hardisty-Hughes et al., 2006; Del-Pozo et al., 2019)
<i>MUC2</i>	11	This mucin is secreted as part of the mucus barrier which protects the gut lumen	Mucins expressed in human middle ear epithelium are also expressed in mouse middle ear epithelium	(Sale et al., 2011) (Kerschner et al., 2010)
<i>MUC5AC/MUC5B</i>	11	Gel-forming glycoproteins (mucins) which form mucus to protect the respiratory tract from pathogens	Mucins expressed in human middle ear epithelium are also expressed in mouse middle ear epithelium	(Sale et al., 2011; Ubell et al., 2010; MacArthur et al., 2014) (Kerschner et al., 2010)
<i>SCN1B</i>	19	Forms the smaller subunits of voltage-gated sodium channels	None	(Sale et al., 2011)
<i>SMAD2</i>	18	Transcription factor that mediates TGF- $\beta$ signalling	None	(Rye et al., 2011b)
<i>SMAD4</i>	18	Transcription factor that mediates TGF- $\beta$ signalling	None	(Rye et al., 2011b)
<i>SFTPD</i>	10	Lung surfactant protein which protects the lungs from inhaled pathogens as part of the innate immune system	None	(Sale et al., 2011)
<i>TLR4</i>	9	Activation of this transmembrane protein leads to NF- $\kappa$ B signalling and inflammatory cytokine production	C3H/HeJ mice have an increased incidence and duration of OM due to a mutation in TLR4. TLR4 <sup>-/-</sup> mice have more persistent inflammation than WT mice	(Emonts et al., 2007; Sale et al., 2011; Alpay et al., 2010; MacArthur et al., 2014; Hafrén et al., 2015) (MacArthur et al., 2006)
<i>FUT2</i>	19	Enzyme involved in the protein glycosylation pathway, and the formation of blood group antigens	<i>Fut2</i> expression in the murine middle ear increases until 1 day after infection, then drops again. <i>FUT2</i> variants are thought to alter the middle ear microbiome by regulating A antigen levels, therefore increasing OM susceptibility	(Pickrell et al., 2016; Tian et al., 2017; Santos-Cortez et al., 2018)
<i>TBX1</i>	22	Transcription factor involved in organ formation during embryonic development	<i>Tbx1</i> heterozygous knockout mice had a 30 dB elevated ABR threshold compared to WT mice, and were found to have OM. <i>Tbx1</i> <sup>+/-</sup> mice with unilateral OME have smaller muscles surrounding the Eustachian tube on that side, leading to reduced clearing ability	(Pickrell et al., 2016; Tian et al., 2017) (Chen et al., 2016; Fuchs et al., 2015)
<i>ABO</i>	9	Enzyme which determines blood group by modifying oligosaccharides on cell surface glycoproteins	None	(Pickrell et al., 2016; Tian et al., 2017; Wiesen et al., 2019)
<i>CDCA7-[]- SP3</i>	2	The genes bordering this SNP encode nuclear proteins with transcription factor activities	None	(Allen et al., 2013)
<i>FNDC1</i>	6	Potential activator of G-protein signalling	Expressed in murine middle ear epithelium, and may modulate inflammatory responses	(van Ingen et al., 2016)
<i>NUBPL</i>	14	Nucleotide binding protein	None	(Jiang et al., 2022)
<i>CDHR3</i>	7	Expressed highly in ciliated respiratory epithelium, and is involved in cell adhesion and cell signalling	<i>Cdhr3</i> expression is restricted to ciliated epithelial cells in the murine middle ear	(Tian et al., 2017; Jiang et al., 2022) (Hirsch et al., 2021)

However, these candidate gene-based studies were conducted on relatively small sample sizes (studies varied from 20 to 441 cases). As OM is a complex disease, incorporating both environmental and genetic risk factors, studies must be sufficiently powered to identify small genetic effect sizes, and the findings must be replicable in other independent cohorts (Rye et al., 2012). It has been suggested that even large sample sizes (1500 cases and matched controls) may not detect the rare genetic variants associated with OM, despite being sufficiently powered (>90%) to identify small genetic effect sizes (odds ratio  $\leq 1.5$ ) (Rye et al., 2012). When this review was published only very limited GWAS datasets were available for OM, however, the authors concluded that GWAS combined with Next Generation Sequencing (NGS) should be able to detect rare variants that the candidate gene approach was unable to identify (Rye et al., 2012).

Over the past decade, several studies have used GWAS to look for OM-associated genes in humans (Allen et al., 2013, Einarisdottir et al., 2016, van Ingen et al., 2016, Pickrell et al., 2016, Tian et al., 2017). In total, these five studies highlighted 21 significant loci, however, only five of these loci were still significant when investigated in an independent human cohort (Santos-Cortez et al., 2020). These loci were *FUT2*, *TBX1* variant rs1978060, *ABO*, intergenic variant rs10497394 between *CDCA7* and *SP3*, and *FNDC1* (Table 1.1). All of these loci were found to be expressed in mucosal and epithelial tissue (according to the Genotype-Tissue Expression (GTEx) database), however, expression data for specifically the middle ear epithelial lining was unavailable (Santos-Cortez et al., 2020). The reproducibility of these findings in an independent cohort increases confidence in their causal link to OM, as does their localisation to tissues with similar properties to the middle ear.

Recently, GWAS was used again to identify several new loci significantly associated with increased risk of OM (Jiang et al., 2022), and also supported some of the findings from a previous study by 23andMe (Tian et al., 2017). The two new OM-related loci were both variants of the *nucleotide binding protein like (NUBPL)* gene, and the only gene with replicable significance from the 23andMe study was *cadherin related family member 3 (CDHR3)* (Table 1.1) (Jiang et al., 2022). The Jiang study was carried out using medically diagnosed infections, and was sufficiently powered to draw conclusions about which genes are likely playing a role in OM pathogenesis (Jiang et al., 2022). However, the 23andMe study (Tian et al., 2017) was performed on self-reported infections. Tian's research was not repeated in a cohort of medically diagnosed patients until 2022, when a post-analysis power calculation indicated that the majority of Tian's OM-related findings were underpowered (Jiang et al., 2022). It has been found that most genetic-association studies in humans remain underpowered, and it has therefore been suggested that these studies are unable to identify loci that pose a lower disease risk (Bhutta et al., 2017b).

## 1.4. Mouse models of OM

Human twin studies have shown that a person's genetics can determine whether they are predisposed to chronic or recurring episodes of OM, however the genes that confer susceptibility are still unknown (Casselbrant et al., 2004). Mice have similar middle ear anatomy and function to humans, making them a good model organism for OM (Brown et al., 2008).

Mouse models of OM have been reviewed extensively by others (Rye et al., 2011a, Tyrer et al., 2013, Bhutta, 2012). Here I will focus on the OM mouse models discovered and studied by previous members of the Deafness lab at MRC Harwell, as their findings helped shape this DPhil project. The majority of these models were identified from the phenotype-driven mouse ENU (N-ethyl-N-nitrosourea) mutagenesis screen performed at MRC Harwell (Nolan et al., 2000). ENU mutagenesis creates point mutations, then animals are screened based on phenotypes observed rather than genotype and subsequently the underlying mutation is mapped and identified by sequencing (Brown, 2021). Mutant mice were tested for deafness using a 90 dB click box to elicit a startle response (known as Preyer's reflex) in mice with normal hearing (Nolan et al., 2000). The deaf mutants identified from the initial screening include *Jeff* (Hardisty et al., 2003) and *Junbo* (Parkinson et al., 2006), and later the *edison* mutant was identified (Crompton et al., 2017).

### 1.4.1. *Jeff*

The *Jeff* mouse (Hardisty et al., 2003) has a point mutation in an F-box gene, *Fbxo11*, on mouse chromosome 17 (Mmu17) which leads to chronic OME in heterozygotes (Hardisty-Hughes et al., 2006, Hardisty et al., 2003). Specifically, the point mutation was chemically induced, and involved an A to T transversion at base

1472, leading to a Q491L substitution in exon 13 (The National Mouse Archive). *Jeff* heterozygotes have no abnormalities regarding their tympanic membranes, ossicles or cochlea hair cells, so these mice were used to study the genetic cause of OME (Hardisty et al., 2003). Human studies have highlighted an association between mutations in *FBXO11* and chronic OME (Bhutta et al., 2017a).

TGF- $\beta$  signalling plays a role in inflammation and immunity. The *FBXO11* protein is a transcription factor involved in this signalling pathway as it regulates levels of phosphorylated SMAD2 (pSMAD2) in epithelial cells (Hardisty-Hughes et al., 2006, Tateossian et al., 2009). A genetic interaction between *Fbxo11* and *Smad2* was also identified (Tateossian et al., 2009). *Jeff* mutants have decreased p53 and increased pSMAD2, which directly regulates the TGF- $\beta$  pathway (Tateossian et al., 2009, Tateossian et al., 2015). The mutation is thought to be gain of function and also leads to changes in the immune response to inflammation (Kubinyecz et al., 2020, Vikhe et al., 2020). The cellular content of *Fbxo11<sup>Jf/+</sup>* blood and middle ear fluid was studied using flow cytometry, and it was found that the mutation causes disruption to immune cell balance (Vikhe et al., 2020). *Fbxo11<sup>Jf/+</sup>* mice had elevated neutrophils, dendritic cells and natural killer T cells, and decreased levels of B cells and T helper cells in their blood and middle ear fluid compared to WT littermates. Children with OME also had raised levels of natural killer T cells, suggesting that *Jeff* is a good model of human OME (Vikhe et al., 2020).

### 1.4.2. *Junbo*

*Junbo* mice have a dominant mutation in the gene *Evi1* on mouse chromosome 3 (Parkinson et al., 2006). The mutation is a chemically-induced A2288T transversion causing an Asn763Ile change in the second zinc-finger domain of the EVI1 protein

(The National Mouse Archive). *EVI1* is a transcription factor which can suppress TGF- $\beta$  signalling by binding to SMAD3 (Kurokawa et al., 1998).

*Jbo/+* mice have hearing loss which is likely caused by OME as they have no morphological defects in the middle or inner ear. The age of OME onset, incidence amongst WT littermates and severity of phenotype varied according to the sterility of the housing conditions (Parkinson et al., 2006).

When housed in standard low microbe conditions all *Jbo/+* mice and one-third of WT littermates had OME by two weeks of age (Parkinson et al., 2006). Any WT OME resolved by weaning age, but 94% of *Jbo/+* mice still had middle ear fluid, inflammation of the epithelial lining and polyps at six months old (Parkinson et al., 2006). In the 6% of *Jbo/+* mice without OME at six months tympanic membrane perforations were present, which may have helped the OME to resolve (Parkinson et al., 2006).

When housed in the pathogen-free MLC (Mary Lyon Centre, MRC Harwell) facility, it took longer for the whole colony to develop OME. In low pathogen conditions all *Jbo/+* mice had OME by two weeks old, but in the MLC it took two months before all of them had OME in at least one ear (90% bilateral, 10% unilateral). No OME was found in WT mice before weaning age, and one adult WT mouse had OME (Parkinson et al., 2006).

Despite the differences between facilities, these findings suggest that the *Evi1* mutation predisposes *Jbo/+* mice to OME, which later develops into chronic OME (Parkinson et al., 2006). Since this study, *EVI1* has been found to inhibit inflammation by downregulating NF- $\kappa$ B. The mutation in *Evi1* in *Junbo* mice is therefore thought to enhance inflammation through NF- $\kappa$ B activation (Xu et al., 2012).

Both *Jeff* and *Junbo* implicate TGF- $\beta$  signalling in susceptibility to OME (Hardisty-Hughes et al., 2006, Parkinson et al., 2006, Tateossian et al., 2009). Identification of the *Jeff* and *Junbo* mutants and their impact on TGF- $\beta$  signalling has led to further research into the role of TGF- $\beta$  in the inflamed middle ear environment associated with OME (Cheeseman et al., 2011). However, to date, human studies have not found a link between mutations at the EVI1 locus and chronic OME (Bhutta et al., 2017a).

### 1.4.3. *Tgif1*

*Transforming growth interacting factor 1 (Tgif1)* is a mouse model of chronic OME (Tateossian et al., 2013). *Tgif1* mice have a conditional knockout allele for the *Tgif* gene, created by Cre excision of a floxed segment encompassing exon 2 and exon 3 (The Jackson Laboratory). TGIF is a negative regulator of TGF- $\beta$  signalling and a SMAD2-binding protein. TGIF prevents phosphorylation of SMAD2 (Tateossian et al., 2013).

As TGIF regulates TGF- $\beta$  signalling, and *Jeff* and *Junbo* mice indicate that TGF- $\beta$  signalling is involved in OME, it was investigated whether *Tgif1* mice have a similar OME phenotype to the other OME mouse models (Tateossian et al., 2013). *Tgif1* heterozygous knockout mice do exhibit the key signs of OME, such as conductive hearing loss, increased goblet cells, and middle ear fluid containing raised levels of VEGF, TNF- $\alpha$  and IL1- $\beta$  (Tateossian et al., 2013). These findings support the theory that TGF- $\beta$  is involved in chronic OME (Tateossian et al., 2013). In addition, a positive association between TGIF1 mutations and chronic OME has been identified in humans (Bhutta et al., 2017a).

#### 1.4.4. *edison*

The *edison* mouse has a missense mutation in the *Nisch* gene (Crompton et al., 2017). The mutation is a Leu972Pro substitution resulting from a T3079C base change (Crompton et al., 2017). NISCH interacts with another protein, Integrin  $\alpha 5$  (ITGA5), which regulates vascular endothelial growth factor (VEGF)-dependent angiogenesis. Mice homozygous for the *edison* mutation have chronic OME, with hearing loss and inflamed middle ear epithelial lining. The severity of the OME is enhanced when an additional *Itga5*-null heterozygous mutation is present (Crompton et al., 2017). Only the double mutants (*Itga5*<sup>tm1Hyn/+</sup> *Nisch*<sup>edsn/edsn</sup>) had upregulated pSMAD2, implicating elevated TGF- $\beta$  signalling as the result of severe middle ear inflammation rather than the cause (Crompton et al., 2017). PAK1, RAC1, LIMK1 and NF- $\kappa$ B were proposed to be involved in OME pathogenesis. RAC1 signalling mediates cellular functions through effector proteins such as PAK1, and NISCH binds to PAK1 (an association which is enhanced by ITGA5) but can also bind directly to RAC1. LIMK1 is downstream of PAK1 and enhances vascular permeability, and is also a target for inhibition by NISCH. Another role of RAC1 is the upregulation of NF- $\kappa$ B, which enhances the inflammatory response (Crompton et al., 2017). In WT mice NISCH inhibits LIMK1, PAK1, RAC1 and ITGA5. In *edison* mutants (*Itga5*<sup>+/+</sup> *Nisch*<sup>edsn/edsn</sup>) this inhibition is reduced, leading to increased expression of LIMK1, PAK1, NF- $\kappa$ B and also FAK, which indirectly activates VEGF. In double mutants (*Itga5*<sup>tm1Hyn/+</sup> *Nisch*<sup>edsn/edsn</sup>) the inhibitory power of NISCH is reduced to an even greater extent, causing elevated expression of LIMK1, NF- $\kappa$ B and RAC1, leading to increased inflammation in the middle ear (Crompton et al., 2017). This study has provided *Nisch* as a new candidate gene for increased susceptibility to chronic OME, and offers possible mechanisms for its involvement in OME pathogenesis. However,

no association between chronic OME and the NISCH locus has been identified in humans (Bhutta et al., 2017a).

These studies of OME mouse models have identified protein mutations and signalling pathways that are likely contributing to OME pathogenesis. It is noteworthy that all of these OME models ultimately involve TGF- $\beta$  signalling, which is known to cross talk with VEGF signalling and the hypoxia response (Crompton et al., 2017). Upregulation of VEGF increases angiogenesis and vascular leakage; a key contributor to the accumulation of middle ear fluid in OME. In addition to this, the hypoxia response was found to be involved in the development of OME in *Jeff* and *Junbo* mice (Cheeseman et al., 2011).

### 1.5. Down syndrome

Down syndrome (DS) is a common chromosomal abnormality involving full or partial trisomy of human chromosome 21 (Hsa21). In the UK, around two babies every day are born with DS (Down's Syndrome Association, 2021). The third copy of Hsa21 causes gene dosage problems, leading to many different phenotypes including congenital heart defects, developmental delays, early onset Alzheimer's disease (Antonarakis et al., 2020), increased incidence of leukaemia (Mowery et al., 2018), gastrointestinal issues (Ravel et al., 2020) and a high incidence of recurrent infections (Mitwalli et al., 2018). Children with DS also have learning difficulties, which are compounded by the fact they often also have hearing loss (Nightengale et al., 2017).

Up to 78% of children with DS have some form of hearing loss (Nightengale et al., 2017), which can be sensorineural, conductive or a mixture of both. One study showed that of the DS children with reduced hearing, 88.2% had conductive hearing loss (Park et al., 2012). It has been suggested that craniofacial differences may

predispose these children to conductive hearing loss, as they often have narrow ear canals, hypotonia of the muscle surrounding the Eustachian tube and malformation of the joints between the ossicles (Fausch and Roosli, 2015). However, notably, children with DS commonly suffer from conductive hearing loss due to OME (Barr et al., 2011).

### 1.6. Otitis media in Down syndrome

OME persists for much longer in children with DS (Fortnum et al., 2014). The length of an episode of OME varies amongst individuals, but one study found that 83% of children with DS require tympanostomy tubes (grommets) due to chronic OME (Shott et al., 2001). Each set of grommets typically lasts 6-12 months, and over half of the children with DS returned for repeated surgery to insert at least one more set of grommets (Shott et al., 2001). In comparison, OME in children without DS usually resolves within three months without any need for treatment (Schilder et al., 2016). The persistence in children with DS is an issue particularly as OME develops at the age they are learning language and communication skills (Fortnum et al., 2014). Studies have shown that children with conductive hearing loss due to recurrent OM have significantly lower IQ scores than their peers with normal hearing (Balkany et al., 1979). For children with DS the hearing loss will have an even more severe impact due to their existing learning difficulties (Balkany et al., 1979).

Studies vary on the incidence of OME in DS, ranging from 55-93% of children (Selikowitz, 1992, Schwartz and Schwartz, 1978, Barr et al., 2011). It has also been found that OME affects younger DS children the most, with 93% of one-year-olds affected, decreasing to 68% by the age of five (Barr et al., 2011). In children without DS OME affects 50% of one-year-olds and 15-40% of children under five (Simon et al., 2018).

The Eustachian tube connects the middle ear and nasopharynx (*Figure 1.1*). Children in general have short, narrow and more horizontal Eustachian tubes, which leads to increased OM incidence (Anthwal and Thompson, 2016). In children with DS the angle and position of the Eustachian tubes develop incorrectly due to their craniofacial defects (Mazzoni et al., 1994). They also have hypotonia of muscles surrounding the Eustachian tubes, which likely exacerbates the accumulation of middle ear fluid associated with OM (Kreicher et al., 2018). DS causes immune system dysfunction which increases susceptibility to infections (Ugazio et al., 1990), meaning they could develop AOM which then persists as OME.

Tympanostomy tubes (grommets) are the most common treatment for OME (Maris et al., 2014). Some clinicians recommend surgical intervention (grommet insertion) when the OME has persisted for two to three months, or the child had suffered from OME over three times in one year (Shott et al., 2001). However the grommets are usually extruded from the eardrum in three to twelve months (Sacks and Wood, 2003) so repeated surgeries are required if the OME is persistent or recurrent, thereby increasing the risk of infection and potentially leading to long term complications (Paulson et al., 2014).

Children with DS also have narrow ear canals, which makes accessing the tympanic membrane difficult (Kreicher et al., 2018). Therefore, it would be hugely beneficial to uncover the genetic cause of OME in DS so that non-surgical treatments could be explored.

## 1.7. Mouse models of DS

DS in humans is caused by full or partial trisomy of Hsa21. The mouse orthologues to these genes are found mostly on mouse chromosome 16 (Mmu16), with some genes on Mmu17 and Mmu10 (*Figure 1.3*). The order of Hsa21 orthologues on Mmu16 is highly conserved, with only one insertion (*Itgb2l*) and one inversion of two adjacent genes (*Mx1* and *D16Jhu19e*) (Pletcher et al., 2001).

As genetic engineering technology has improved so have the techniques with which it's possible to create mouse models of DS. Each model has a different approach, with some having duplications of mouse chromosomes containing Hsa21 orthologues (Yu et al., 2010), and others carrying a copy of the human chromosome itself (O'Doherty et al., 2005). Some models have full duplications, whereas others have partial duplications which allow mapping of the dosage-sensitive genes responsible for specific DS phenotypes (Davisson et al., 1990, Olson et al., 2004, Lana-Elola et al., 2016).

## CHAPTER 1: Introduction

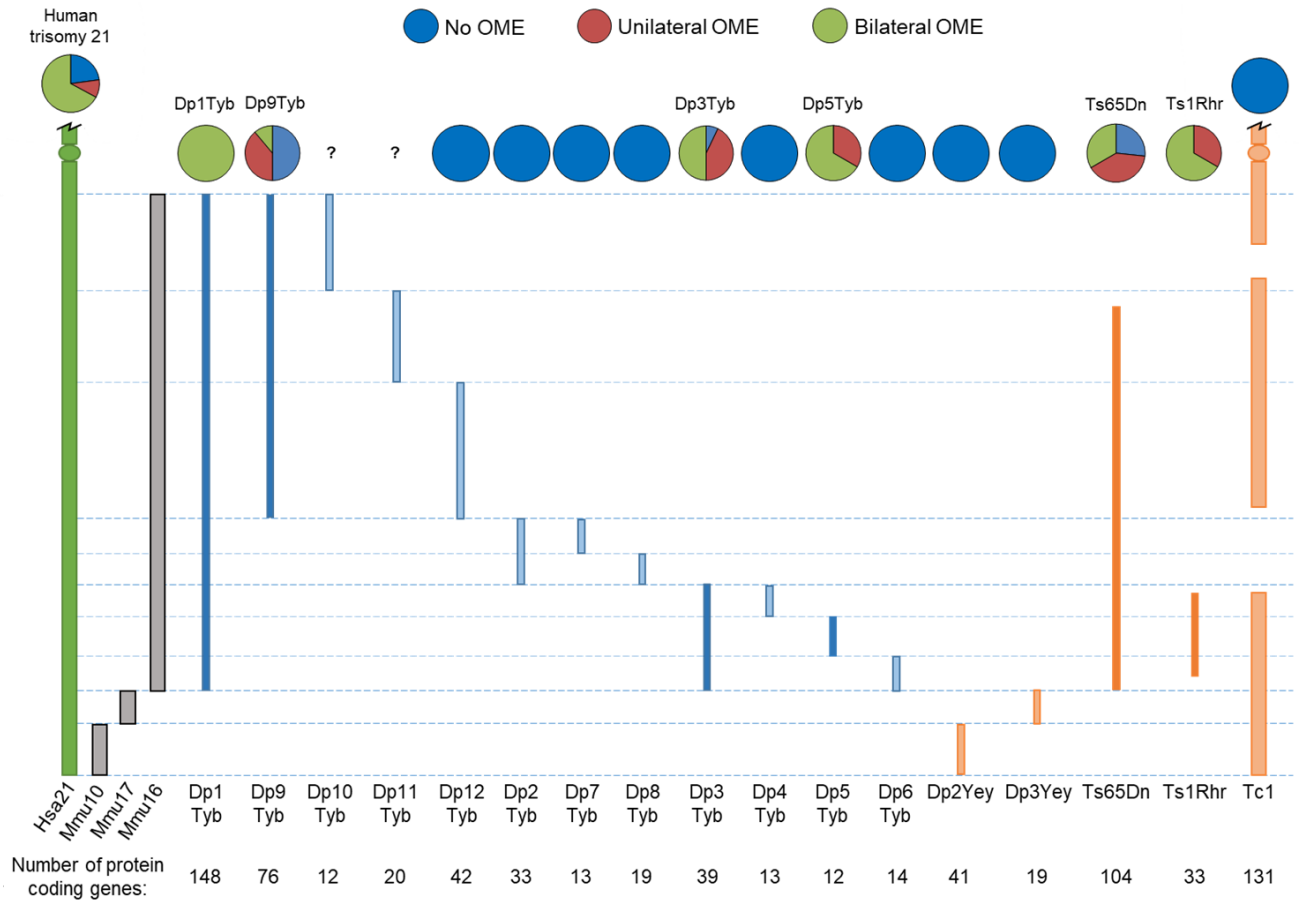


**Figure 1.3. Schematic of the duplicated chromosomal regions in DS mouse models and the OME incidence in each mouse line.** This research was carried out by the Deafness lab at MRC Harwell. On the left is the human chromosome, Hsa21, alongside the mouse chromosomes which contain Hsa21 orthologues. Blue lines indicate the duplicated regions in DpTyb mouse models, with those with OME coloured dark blue. The duplicated regions in other DS mouse models are shown with orange bars, with darker orange highlighting the mice with OME. The duplicated region in Ts1Rhr mice is called the Down syndrome critical region (DSCR). The pie charts indicate the number of mice with no OME (blue), unilateral OME (red) or bilateral OME (green). Dp10Tyb and Dp11Tyb mice are not available yet so their OME incidence is unknown. Image modified from figures by (Lana-Elola et al., 2016) and (Tateossian et al., 2022), plus additional information on Ts65Dn (Han et al., 2009) and Tc1 mice (Bhutta et al., 2013). The number of protein coding genes was sourced from (Lana-Elola et al., 2016, Yu et al., 2010, Olson et al., 2004, O'Doherty et al., 2005) and unpublished data provided by Lana-Elola. Limited data are available on the proportion of unilateral and bilateral OME in humans with DS, but findings vary depending on the age and heritage of the child. The pie chart shown above Hsa21 represents the incidence amongst 70 British children with DS, aged 18-24 months, as reported by the National Institute for Health and Clinical Excellence (NICE, 2008).

### 1.7.1. Ts65Dn

Ts65Dn mice were created over 30 years ago (Davisson et al., 1990) and have since been used to study several DS phenotypes, including OME (Han et al., 2009).

Ts65Dn mice were found to have hearing loss, and histological analysis of the middle

ears confirmed that this was likely due to OME (Han et al., 2009) (*Figure 1.3*). Ts65Dn mice have trisomy of 90 protein coding genes from Mmu16 plus a small section of Mmu17. In total they have a duplication of around two-thirds of the genes orthologous to those on Hsa21. Unfortunately, some of the duplicated Mmu17 genes are not orthologous to any on Hsa21, so the duplication of these genes may be interfering with results from phenotyping experiments (Duchon et al., 2011, Reinholdt et al., 2011).

### 1.7.2. Ts1Rhr

Until 2004 it was widely believed that trisomy of a “Down syndrome critical region” (DSCR) was responsible for many of the common DS phenotypes, such as craniofacial defects. Olson and colleagues then genetically engineered the Ts1Rhr mouse (which has a duplication of the 33 Hsa21 orthologues in the DSCR) plus the Ms1Rhr/Ts65Dn mouse (which has a duplication of the Ts65Dn region but not the DSCR) (Olson et al., 2004). They concluded that the DSCR was not required for the craniofacial phenotype seen in Ts65Dn mice, and therefore the DSCR cannot be said to be responsible for all key DS phenotypes.

However, when studied by members of the Deafness lab (MRC Harwell), the DSCR was shown to be involved in the OME phenotype. Ts1Rhr mice had reduced hearing, indicated by increased click-evoked auditory brainstem response (ABR) thresholds. Histological analysis of the middle ear also showed that all Ts1Rhr mice had OME; one-third had unilateral and the rest bilateral OME (Tateossian et al., 2022) (*Figure 1.3*).

### 1.7.3. Tc1

O'Doherty and colleagues were the first to introduce a copy of Hsa21 into the mouse genome (O'Doherty et al., 2005). The aim was to create a mouse that was trisomic

only for the genes on Hsa21 as this would be a better model of human trisomy 21. They named this transchromosomal mouse Tc1, and it successfully expressed the human mRNA transcripts and proteins. Unfortunately, the mice were mosaic as the extra copy of Hsa21 was often lost from cells during mitosis. A more recent study also found that Hsa21 had been unintentionally rearranged during the introduction of the chromosome into mouse embryonic stem cells using gamma radiation (Gribble et al., 2013). Nevertheless, the Tc1 mouse has been used to study many DS phenotypes, including heart defects (Dunlevy et al., 2010), learning and memory deficits (Morice et al., 2008, Galante et al., 2009), and differences in tumour angiogenesis (Reynolds et al., 2010). Unfortunately Tc1 mice don't appear to be a good model for studying OME, as they don't have hearing loss (Kuhn et al., 2012) or middle ear inflammation (Bhutta et al., 2013) (*Figure 1.3*). An explanation could be that Tc1 mice don't have a duplication of all Hsa21 genes, for example they only have two copies of some genes which are present in three copies in Ts65Dn mice. As Ts65Dn mice have OME, it is likely one of these genes that is dosage sensitive and causes OME when three copies are present (Kuhn et al., 2012). The absence of OME phenotype could also be explained by the different regulatory elements that are present in humans and mice, or genetic mosaicism in Tc1 mice (Patterson, 2009).

### 1.7.4. DpTyb

The phenotypes seen in DS are likely caused by increased dosage of one or multiple genes, which then has a knock-on effect on downstream signalling pathways. By using mice with partial duplications of Hsa21 orthologous regions we can observe which duplications create mice exhibiting the phenotype of interest and thereby map the causative genes.

A comprehensive series of mouse strains carrying partial duplications of Mmu16 has been engineered (Lana-Elola et al., 2016). The duplicated chromosomal regions are shown on the mapping panel illustrated in *Figure 1.3*. This panel has previously been used to map causative genes for the heart and locomotor phenotypes seen in DS (Lana-Elola et al., 2016, Watson-Scales et al., 2018).

The Deafness lab (MRC Harwell) checked the OME phenotypes of all available DpTyb mice (Tateossian et al., 2022). Sections of the middle ears were analysed for thickening of the middle ear epithelial lining and presence of cellular middle ear fluid, and the occurrence of this in one, both, or neither ears was recorded (represented as pie charts in *Figure 1.3*).

The mouse genes orthologous to those on Hsa21 are spread across Mmu16, 17 and 10, but the DpTyb mice only cover those on Mmu16. However, Dp2Yey (Dp(10Prmt2-Pdxk)2Yey) and Dp3Yey (Dp(17Abcg1-Rrp1b)3Yey) mice have duplications of the Mmu10 and Mmu17 regions respectively (Yu et al., 2010). In addition to checking the OME phenotypes of the DpTyb lines, the Deafness lab (MRC Harwell) also checked the OME phenotype of Dp2Yey and Dp3Yey mice, and no OME was found in either mouse line (*Figure 1.3*) (Tateossian et al., 2022).

By checking the OME phenotype of mice with duplications of Hsa21 orthologues, the mapping panel (*Figure 1.3*) can be used to attempt to identify the causative genes for OME. The fully penetrant bilateral OME seen in Dp1Tyb mice must be contributed to by genes in the Dp9Tyb and Dp5Tyb region. Highly penetrant OME is observed in both Dp5Tyb and Dp3Tyb mice (which includes the entire Dp5Tyb region), while only moderately penetrant OME is observed in Dp9Tyb. These results indicate that a major locus for OME lies within the Dp5Tyb region, and a minor locus within the Dp9Tyb region. In the future it would be interesting to investigate the OME

phenotypes of Dp10Tyb and Dp11Tyb mice to further refine the position of the minor locus within Dp9Tyb. For my DPhil project I will focus on identifying the causative genes within the Dp5Tyb region.

## 1.8. The Dp5Tyb genes

Dp5Tyb is a 1.8Mb region containing only 12 protein coding genes, all of which are orthologous to Hsa21 genes (Lana-Elola et al., 2016). When mice have three copies of this region they all have OME in one or both ears (*Figure 1.3*). This was the starting point for my DPhil project. My project will explore the expression of these 12 genes in the middle ear environment at transcript and protein level. I will also explore how restoring disomy of one Dp5Tyb gene at a time affects the Dp5Tyb OME phenotype.

The 12 Dp5Tyb genes are: *Dyrk1a*, *Kcnj6*, *Kcnj15*, *Erg*, *Ets2*, *Psmg1*, *Brwd1*, *Hmgn1*, *Wrb*, *Lca5l*, *Sh3bgr* and *B3galt5*. They encode a range of proteins, including transcription factors, channel proteins, and membrane glycoproteins. Others play roles in chromatin remodelling, protein complex assembly, cell proliferation, apoptosis and inflammation.

Of these genes, overexpression of *Dyrk1a* in particular is thought to play a role in many different DS phenotypes, including early onset Alzheimer's disease (García-Cerro et al., 2014), craniofacial defects (McElyea et al., 2016) and motor dysfunction (Watson-Scales et al., 2018). If *Dyrk1a* is identified as a dosage-sensitive gene responsible for causing OME, the underlying mechanism will be explored.

## 1.9. Thesis aims

I hypothesise that there is a major locus in the Dp5Tyb region that, when present in three copies, leads to OME. To investigate this, I have established the following research aims:

- 1) Phenotypically characterise Dp5Tyb mice
- 2) Study expression of the 12 Dp5Tyb genes at the transcript and protein level in the middle ear
- 3) Generate and phenotypically analyse double mutants
- 4) Investigate the mechanism of DYRK1A involvement in OME pathogenesis

These aims will allow me to observe how well Dp5Tyb mice recapitulate some of the DS phenotypes seen in humans and other mouse models of DS, including OME. I will also compare the OME phenotype seen in Dp5Tyb mice to other mouse models of OME without DS. By crossing single gene knockouts to mice with DS, double mutants will be generated with disomy of one of the Dp5Tyb genes. Using these mice I will be able to identify which genes, when present in three copies, are involved in the development of OME. Once these gene(s) are identified I will perform further experiments to uncover how overexpression of these gene(s) is playing a role in OME pathogenesis. Understanding the underlying mechanism could offer insight into possible future treatment options for OME in children with DS.

## CHAPTER 2: Materials and Methods

---

### 2.1. Mouse lines

#### 2.1.1. Animal husbandry

Most of the mice were housed in the Mary Lyon Centre (MLC) at MRC Harwell, which is a pathogen-free facility. They were kept in individually ventilated cages (Techniplast UK Ltd) with a 12 hour light/dark cycle and were fed and watered ad-libitum. Dp12Tyb mice and some of the double mutants (Dp1Tyb *Dyrk1a*<sup>+/-</sup>, Dp3Tyb *Dyrk1a*<sup>+/-</sup> and Dp5Tyb *Hmgn1*<sup>+/-</sup>) were bred and maintained at the Francis Crick Institute. All procedures complied with the Animals (Scientific Procedures) Act 1986 and were covered by my personal licence (I2A0B45CD), the OM project licence (20/0004) and the establishment licence (X9BFFDAE2), all awarded by the UK Home Office. Mice were euthanized using Home Office Schedule 1 methods (section 2.4).

#### 2.1.2. Dp5Tyb and Dp3Tyb mice

The full names of these mouse lines are C57BL/6J.129P2-Dp(16Dyrk1a-B3galt5)5TybEmcf/Nimr (Dp5Tyb) and C57BL/6J.129P2-Dp(16Mir802-Zbtb21)3TybEmcf/Nimr (Dp3Tyb), respectively. The mouse lines were created by the Tybulewicz lab at the Francis Crick Institute (Lana-Elola et al., 2016). Briefly, *in vivo* Cre-mediated recombination was used to duplicate the specific 12-gene region (Dp5Tyb), or 39-gene region (Dp3Tyb), on mouse chromosome 16 (Mmu16). For Dp5Tyb, loxP sites were inserted in the trans configuration proximal to *Dyrk1a* and distal to *B3galt5* in female mice containing the *Hprt*<sup>tm1(cre)Mnn</sup> allele (Tang et al., 2002). For Dp3Tyb, the loxP sites were inserted proximal to *Mir802* and distal to *Zbtb21* in females containing the same allele. Both sets of females were then bred to C57BL/6JNimr males, and the Cre activity led to duplication between the loxP sites in

## CHAPTER 2: Materials and Methods

0.7-6% of pups (Lana-Elola et al., 2016). To maintain these lines in the MLC, Dp5Tyb and Dp3Tyb males were backcrossed to B6JNM (WT) females.

### 2.1.3. Knock-out and point-mutation mouse lines

Mouse lines were sourced using the IMPC website are detailed in *Table 2.1* below.

**Table 2.1. Details of the knockout mouse lines used for this project.** The *Hmgn1* heterozygous knockout was crossed to Dp5Tyb, and the *Dyrk1a* knockout was crossed to Dp3Tyb at the Francis Crick Institute and we received the heads for analysis. A *Kcnj15* knockout mouse was unavailable. MLC = Mary Lyon Centre; MMRRC = Mutant Mouse Resource and Research Center; EMMA = European Mouse Mutant Archive; TCP = The Centre for Phenogenomics; ICS = Institut Clinique de la Souris.

Gene	Full name	Knockout line	Source	Website	Details
<i>Dyrk1a</i>	Dual-specificity tyrosine-(Y)-phosphorylation regulated kinase 1a	C57BL/6J.129P2-Dyrk1a <sup>tm1Mia</sup>	Francis Crick Institute	<a href="http://www.informatics.jax.org/allele/MGI:2386937">http://www.informatics.jax.org/allele/MGI:2386937</a>	Created on 129P2/OlaHsd ES cells in the Arbonés lab, then backcrossed to C57BL/6J. Imported from the Tybulewicz lab at the Francis Crick institute
<i>Kcnj6</i>	Potassium inwardly-rectifying channel, subfamily J, member 6	<i>Kcnj6</i> <sup>em1(IMPC)H</sup>	MLC	<a href="https://www.mousephenotype.org/data/genes/MGI:104781#order">https://www.mousephenotype.org/data/genes/MGI:104781#order</a>	Produced on C57BL/6N through CRISPR technology at Harwell as part of IMPC project
<i>Erg</i>	ETS transcription factor	C57BL/6N-Erg <sup>em1(IMPC)Bay/Mmucd</sup>	MMRRC (047583-UCD)	<a href="https://www.mmrc.org/catalog/sds.php?mmrc_id=47583">https://www.mmrc.org/catalog/sds.php?mmrc_id=47583</a>	Live mice imported on a C57BL/6N background, rederived on C57BL/6N Tac
<i>Ets2</i>	E26 avian leukemia oncogene 2, 3' domain	C3HeB/FeJ-Ets2 <sup>tm1Mhda/leg</sup>	EMMA (EM:07468)	<a href="https://www.infrafrontier.eu/search?keyword=07468">https://www.infrafrontier.eu/search?keyword=07468</a>	Frozen sperm imported on C3HeB/FeJ background, rederived onto C57BL/6JNimr
<i>Psmg1</i>	proteasome (prosome, macropain) assembly chaperone 1	C57BL/6N-Psmg1 <sup>tm1a(KOMP)Wsj/BayMmucd</sup>	MMRRC (049256-UCD)	<a href="https://www.mmrc.org/catalog/sds.php?mmrc_id=49256">https://www.mmrc.org/catalog/sds.php?mmrc_id=49256</a>	Live mice imported on C57BL/6N background, rederived on C57BL/6JNimr with cre-deletion at the same time to produce the tm1b allele
<i>Brwd1</i>	bromodomain and WD repeat domain containing 1	C57BL/6N-Crl-Brwd1 <sup>em1(IMPC)Tcp</sup>	TCP (MGI:6156470)	<a href="http://www.cmmr.ca/gene-detail.php?gene=MGI:1890651">http://www.cmmr.ca/gene-detail.php?gene=MGI:1890651</a>	Frozen sperm imported on C57BL/6N-Crl background, rederived onto C57BL/6JNimr
<i>Hmgn1</i>	high mobility group nucleosomal binding domain 1	<i>Hmgn1</i> <sup>em1Tyb</sup>	Francis Crick Institute	Unpublished	<i>Hmgn1</i> <sup>em1Tyb</sup> allele has a 360 bp CRISPR/Cas9-generated deletion which removes all of exon 1, intron 1 and part of exon 2. Maintained on C57BL/6JNimr
<i>Wrb (Get1)</i>	guided entry of tail-anchored proteins factor 1	C57BL/6N-Wrb <sup>tm1.1(KOMP)Vlcs/MbpMmucd</sup>	MMRRC (050392-UCD)	<a href="https://www.mmrc.org/catalog/sds.php?mmrc_id=50392">https://www.mmrc.org/catalog/sds.php?mmrc_id=50392</a>	Frozen sperm imported on C57BL/6N background, rederived on C57BL/6JNimr
<i>Lca5l</i>	Leber congenital amaurosis 5-like	<i>Lca5l</i> <sup>em1(IMPC)ics</sup>	ICS	N/A	Frozen sperm imported on C57BL/6N background, rederived on C57BL/6N Tac
<i>Sh3bgr</i>	SH3-binding domain glutamic acid-rich protein	<i>Sh3bgr</i> <sup>em1(IMPC)ics</sup>	ICS	N/A	Frozen sperm imported on C57BL/6N background, rederived on C57BL/6N Tac
<i>B3galt5</i>	UDP-Gal:betaGlcNAc beta 1,3-galactosyltransferase, polypeptide 5	<i>B3galt5</i> <sup>em1(IMPC)ics</sup>	ICS	N/A	Frozen sperm imported on C57BL/6N background, rederived on C57BL/6N Tac

### 2.1.4. Generation of double mutants

DpTyb males were mated with females that were heterozygous for the gene of interest (due to knockout or point mutation). Some of the offspring were double mutant, meaning they have two copies of the gene of interest, and three copies of the other Dp1Tyb/Dp3Tyb/Dp5Tyb genes.

### 2.1.5. Dp12Tyb, Dp1Tyb *Dyrk1a*<sup>+/-</sup>, Dp5Tyb *Hmgn1*<sup>+/-</sup>, and Dp3Tyb

#### *Dyrk1a*<sup>+/-</sup> mice

These lines were created and genotyped at the Francis Crick Institute. The heads were put in formalin and shipped to MRC Harwell. The Histology team sectioned and H&E stained them. The sections were then imaged using the NanoZoomer RS digital pathology slide scanner (Hamamatsu) and viewed using NDP.view2 software. They were scored 0, 1 or 2 regarding the number of ears with OME present.

## 2.2. Genotyping

All genotyping was performed by the Genotyping team at MRC Harwell. Detailed genotyping methods can be found in the Appendix. Briefly, pinna biopsies were taken from mice at three weeks of age. Genotyping for Dp1Tyb, Dp3Tyb and Dp5Tyb was performed by searching for the mutant break point sequences at the ends of the inserted region using quantitative polymerase chain reaction (qPCR). Other lines were genotyped using qPCR with primers either side of the deleted/mutated region, gel-based assays, allelic discrimination assays or knockout first genotyping.

## 2.3. Auditory-evoked Brainstem Response (ABR)

Mice were anaesthetized using a mixture of ketamine hydrochloride (100 mg/kg) and xylazine (10 mg/kg), administered by intraperitoneal (IP) injection, and placed in a heat box (Datesand Ltd.) until immobilized. Mice were then placed on a heated mat to maintain body temperature at 37°C, inside a sound attenuating chamber (ETS-Lindgren SD enclosure). Recording electrodes (Grass Telefactor F-E2-12) were placed sub-dermally over the vertex (active), right mastoid (reference), and left flank (ground) (*Figure 2.1*). 'Artificial tears' (Viscotears®, Novartis) were administered to the eyes of the mouse to prevent the eyes becoming dry whilst sedated.

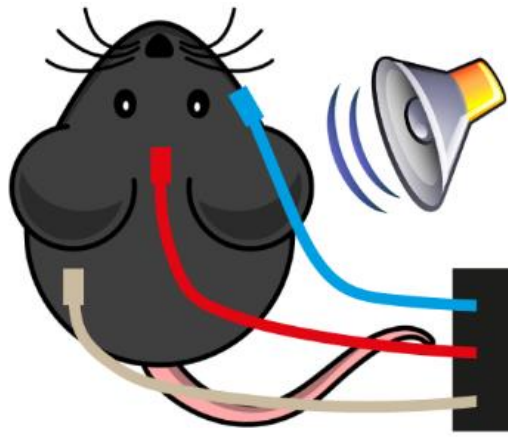


*Figure 2.1. Setup of electrodes for measuring auditory-evoked brainstem response (ABR).* Once the mouse was anaesthetised, recording electrodes were placed sub-dermally in the following positions: active electrode over the vertex (red), reference electrode in the right mastoid (blue) and ground electrode in the left flank (grey). A speaker played the acoustic stimuli 1.5 cm away from the right ear, starting at 90 dB and decreasing in increments of 5 dB. The reference electrode (blue) was then moved to the left mastoid, the speaker to the left ear, and the ground electrode (grey) to the right flank. The pattern of acoustic stimuli was then repeated. Image modified under Creative Commons License 2.5.

Acoustic stimuli were delivered monaurally to the right ear at a distance of 1.5 cm via a free field transducer (ES1 Tucker Davis Technology (TDT), Alachua, FL), controlled by TDT SigGen/BioSig software, using TDT RZ6 hardware. The transducer output was calibrated using a ¼" measuring microphone (7016 ACO-Pacific, Belmont, CA) and SigCal software (TDT) and calibrated levels checked using a Brüel and Kjær PULSE system with a type 4939 ¼" microphone and a high frequency 3110 processing module. The speaker and electrode positions were then moved to deliver the stimuli to the left ear and record the response. ABR responses were collected, amplified and averaged using TDT RZ6 hardware and BioSig software (Tucker Davis Technology (TDT), Alachua, FL). Stimuli consisted of 0.1 ms broadband clicks of alternating polarity presented at a rate of 21/sec for a total of 300 averages. Stimuli were presented at 90 dB SPL followed by decreasing steps of 5 dB SPL until a threshold was determined visually by the absence of replicable response peaks.

Recovery of mice was accelerated by administration of atipamezole (Antisedan™, 5 mg/ml) at the rate of 1 mg/kg of body weight.

#### 2.4. Schedule 1 cull of mice

Mice were given an IP injection of Euthatal (sodium pentobarbital) (0.2 ml/20g body weight). However when collecting samples for scanning electron microscopy the mice were culled by cervical dislocation instead as the cochleae must be fixed quickly to preserve hair cell and cilia morphology. Once death was confirmed, the required samples were collected. All mice were two-months-old at time of death unless otherwise stated.

#### 2.5. Tympanic membrane observations

Following a Schedule 1 cull, the head was removed and skinned. The skull was placed under a light microscope and a visual inspection was carried out to look for perforations of the tympanic membranes.

#### 2.6. Histology

Once fixed, all stages of processing, sectioning and H&E staining were performed by the Histology department at MRC Harwell. The Necropsy team collected the lungs.

##### 2.6.1. Sample collection and fixation

Following a Schedule 1 cull, the heads were removed and skinned, and submerged in 10% neutral buffered formalin (NBF) (Leica) for at least 48 hours.

To collect the lungs, the thorax was cut open and the lungs were inflated with 10% NBF via an injection into the bronchus. The lungs were then removed from the mouse and submerged in 10% NBF for one week.

### 2.6.2. Decalcification

The fixed heads were then washed in phosphate buffered saline (PBS) (three x 15 mins) before decalcification (with either 18% D.F.B. decalcifying agent (Kristensen; Pioneer Research Chemicals) for three days, or 4.3% EDTA in PBS for three weeks). EDTA was used if the sections were for immunohistochemistry requiring antigen retrieval.

### 2.6.3. Dehydration, clearance and paraffin impregnation processing

Decalcified heads were placed into an Excelsior™ AS processor (Thermo Scientific™) which is pre-programmed to perform the dehydration, clearance and paraffin wax impregnation required to prepare the samples for microtome sectioning. The samples were dehydrated in increasing concentrations of industrial denatured alcohol (IDA) (70, 90 and 100%), cleared using 100% xylene to removed lipids and residual alcohol, and impregnated with molten paraffin wax under vacuum.

Lungs were also put through the Excelsior™ AS processor (Thermo Scientific™).

### 2.6.4. Embedding and sectioning

Heads were then embedded in paraffin wax following routine procedures. Sections were cut using a Finesse™ ME+ microtome (ThermoFisher). The sections were guided into a 45°C water bath, charged slides were placed underneath and lifted out of the water with the section.

For IHC and most H&E, 5 µm transverse sections were cut (*Figure 2.2a*). Sagittal 5 µm sections (at the mid-modiolar level) were cut from other skulls and H&E stained to see the hair cells in the cochlea (*Figure 2.2b*).

## CHAPTER 2: Materials and Methods

Lungs were embedded in paraffin following routine procedures, then the left lobe was cut in the transverse plane (*Figure 2.2c*). Three step sections were cut, with three 5  $\mu\text{m}$  sections cut at each depth. All were H&E stained. Some lung sections were left unstained as an epithelial tissue on which to test the IHC antibodies.

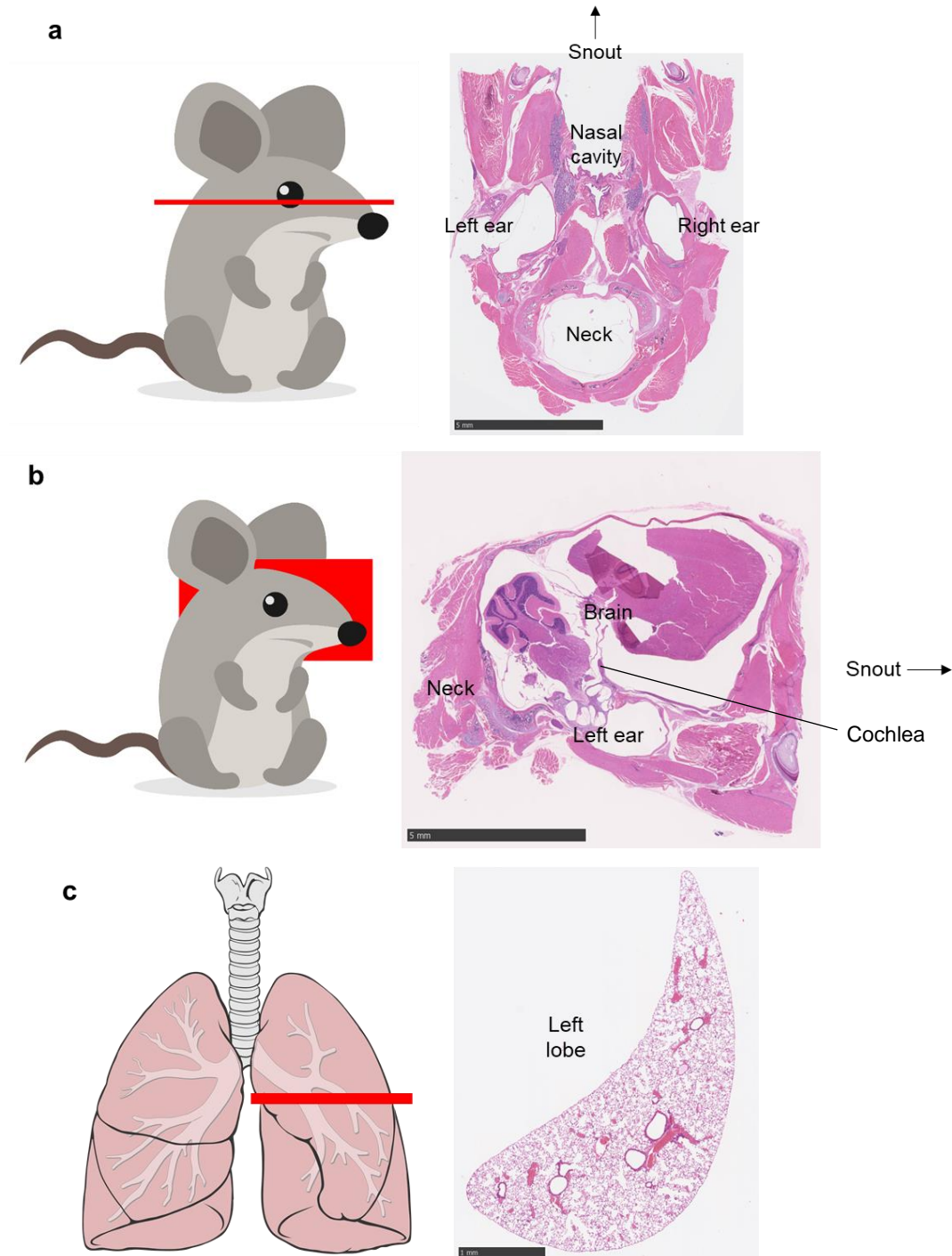


**Figure 2.2. Diagram showing the anatomical plane of the histological sections.** (a) Mouse head cut in the transverse plane. Scale bar = 5 mm. (b) Mouse head cut in the sagittal plane. Scale bar = 5 mm. (c) Left lobe of mouse lung cut in the transverse plane. Scale bar = 1 mm. Mouse and lung images modified under creative commons license 2.5.

### 2.6.5. Haematoxylin and Eosin (H&E) staining

Paraffin sections from heads and lungs were H&E stained using an Automatic Stainer, which first dewaxed the sections using 100% xylene and rehydrated using 100% and 70% IDA before applying the haematoxylin and eosin stains.

Sections were then mounted in Clearium solution (Leica) and glass coverslips were applied.

### 2.6.6. Imaging

Images were taken using NDPscan software on a NanoZoomer Digital Pathology scanner (Hamamatsu).

### 2.7. Measuring the middle ear epithelial lining

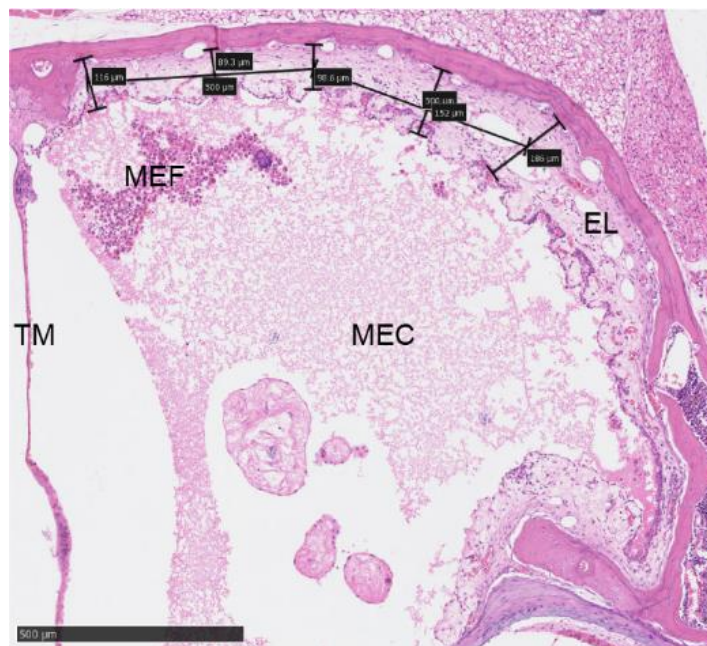


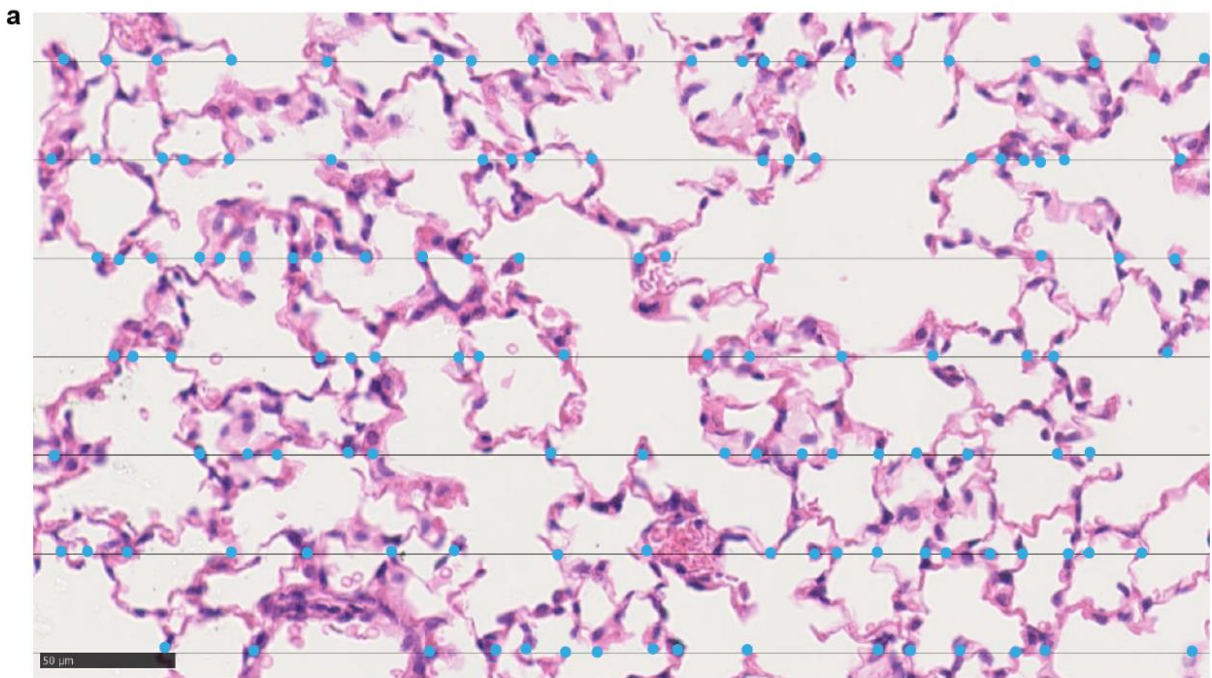
**Figure 2.3. Measuring middle ear epithelial lining thickness.** Example shown is the left ear of a two-month-old Dp5Tyb mouse. Images were opened in NDP.view2 software and annotated using the ruler tool. A 500 µm line was drawn from the start of the epithelial lining (area furthest from the cochlea, next to where TM joins), followed by another 500 µm line. Measurements were then taken from the ends and midpoints of these lines (five measurements in total per ear). TM = tympanic membrane; MEF = middle ear fluid; MEC = middle ear cavity; EL = epithelial lining. Scale bar = 500 µm.

The middle ear epithelial lining was measured on images taken of H&E stained 5  $\mu\text{m}$  transverse sections. Using NDP.view2 software, two 500  $\mu\text{m}$  lines were drawn starting from the area of middle ear furthest from the cochlear/inner ear region. Measurements were then taken from the ends and midpoints of these lines, totalling five measurements (*Figure 2.3*). An average (mean) thickness was calculated for each mouse, then WT mice were compared to Dp5Tyb at each time-point (three-weeks, four-weeks, two-months, four-months, six-months and one-year-old).

## 2.8. Lung phenotype

### 2.8.1. Mean linear intercept (Lm) calculation

The lung sections used were H&E stained 5  $\mu\text{m}$  transverse sections from two-month-old mice. Images were taken from three areas at three different depths (step sections) on NDP viewer at x40 magnification (nine images per mouse). Using ImageJ, seven grid lines were superimposed onto each image and the number of times the alveoli crossed the lines was counted using a cell counter on ImageJ. The mean linear intercept was then calculated using the equations shown in *Figure 2.4*.



**b** True length of line =  $\frac{\text{Scale bar} \times \text{Length of line}}{\text{Length of scale bar}}$

$$\text{Mean linear intercept (Lm)} = \frac{\text{Number of lines counted} \times \text{True length of line}}{\text{Total number of intersects}}$$

**Figure 2.4. Mean linear intercept calculation.** (a) Images of WT and Dp5Tyb H&E stained lung sections were opened in ImageJ software. A grid was superimposed, consisting of seven horizontal lines. The cell counter was used to mark each time an alveolar wall crossed a grid line (blue dot). Scale bar = 50 $\mu$ m. (b) The equations used to calculate the mean linear intercept. A total of nine images were analysed for each mouse (three images from three longitudinal step sections through the lung), and then an average (mean) was taken.

## 2.9. Immunohistochemistry (IHC)

The IHC protocol was optimised extensively regarding: the method of skull decalcification, the coating on the microscopy slides, the use of heat-mediated antigen retrieval and the concentration of primary antibody. The antibodies were also tested on lung tissue first to preserve precious middle ear sections. EDTA was used to decalcify skulls as it was found that this caused the thin WT middle ear epithelial lining to adhere better to the slide, particularly when combined with Series 2 Adhesive microscope slides (TRAJAN, 472042491).

### 2.9.1. De-waxing

Sections were de-waxed in xylene and rehydrated in graded ethanol using the Tissue-Tek® DRS™ automated processor (Sakura).

### 2.9.2. Blocking

For IHC, endogenous peroxidase was blocked by submerging the slides in 3% hydrogen peroxide in propan-2-ol for 20 mins then washed in PBS.

### 2.9.3. Antigen retrieval (AR)

Heat mediated AR was performed if required (see Appendix) using a microwave. Slides were loaded into the container and either citrate buffer or water was added to cover the slides. Citrate buffer (pH 6) was used for AR of lung sections, ddH<sub>2</sub>O for head sections. The microwave was set to 50% power, run for 7 mins, topped up with water and run again for 7 mins. The whole container was left to cool for at least 30 mins before proceeding.

### 2.9.4. Antibody incubation

The VECTASTAIN® Elite® ABC HRP Kit (Peroxidase, Rabbit IgG) kit (Cat. No: PK-6101) was used following the manufacturer's instructions. Nearly all of the primary antibodies were raised in rabbit (see appendix for exceptions). An ImmEdge pen was used to outline the sections with a waterproof barrier. Goat serum from the kit was diluted in PBS and added to the sections for 20 mins. Sections were then incubated with primary antibodies overnight at 4°C (see Appendix for concentrations).

Secondary and tertiary antibodies from the kit were used for antibodies raised in rabbit. For antibodies raised in other species, HRP-linked secondary antibodies were used (see Appendix) and no tertiary was required.

### 2.9.5. Visualisation and counterstaining

3, 3'-Diaminobenzidine (DAB)+ substrate chromogen system (Dako) was used for development of the signal. DAB was added to the sections for 1-5 mins. The slides were then washed in PBS and taken to the Histology department for counterstaining with Haematoxylin and sealing with Clearium solution and coverslips. Once dry, images were taken using the NanoZoomer scanner and NDP.view2 software.

### 2.9.6. Quantification of staining

The scans were opened in NDP.view2 software, and an image at 40x magnification was taken of each epithelial lining. I took the images from the same area of each ear. I opened the magnified images in ImageJ software, and using the cell counter tool I manually counted 200 cells (any colour). Of these cells, I then counted how many were brown (expressing the protein of interest) and represented it as a percentage.

### 2.9.7. Special stains

Haematoxylin and eosin (H&E), and Alcian blue and Periodic acid-Schiff (AB-PAS) staining were carried out using standard methods by the Histology team.

### 2.10. Bone preparation

Skulls were stored in 95% ethanol before undergoing bone preparation by the Histology team. Bone preparation briefly involved maceration in 1% potassium hydroxide and staining with Alcian blue for cartilage and alizarin red for bone. The skulls were stored in glycerol until measurements were taken.

### 2.10.1. Craniofacial measurements

The skulls were imaged with a Zen microscope and measured using ImageJ software. The frontal bone length and width, nasal bone length and skull length were measured (*Figure 2.5*), and allometric ratios were calculated against skull length for each mouse.

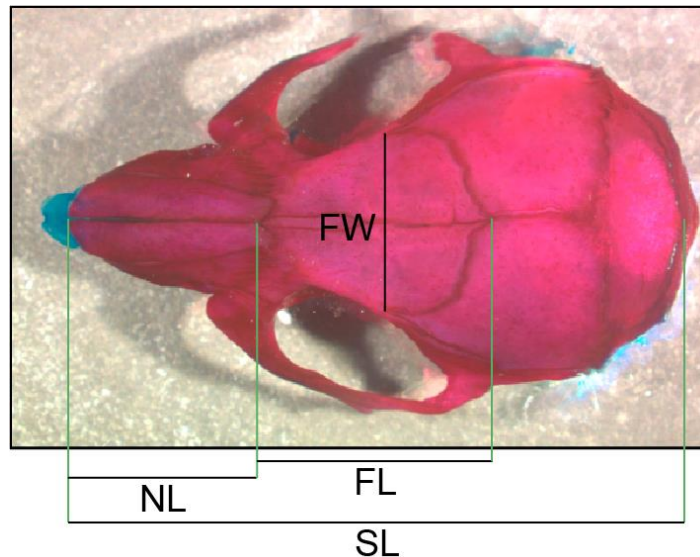


*Figure 2.5. Craniofacial measurements.* WT and Dp5Tyb skulls underwent bone preparation, which highlighted cartilage in light blue and bone in pink. Photographs were taken on a Zen microscope camera, and measured using ImageJ software. FW = frontal bone width; NL = nasal bone length; FL = frontal bone length; SL = skull length.

## 2.11. Real Time Quantitative Polymerase Chain Reaction (RT-qPCR)

### 2.11.1. Sample collection

For qPCRs, after the IP injection, blood was taken by retro-orbital bleed using capillary microvettes, and middle ear exudates were collected with a P2 pipette after removing the tympanic membrane with forceps. In Dp5Tyb mice, the total exudate ranged from 0-3  $\mu$ l per ear. The middle ear epithelial lining was collected using a microcuvette. To allow RNA isolation for qPCR, blood was collected into EDTA tubes (stored in the fridge for up to one week) and the middle ear epithelial cells and exudate were added to 20  $\mu$ l aliquots of RNase-free water (stored in -80 freezer).

### 2.11.2. RNA extraction and cDNA synthesis

RNA from larger tissues, such as lung, was extracted using Precellyus bead tubes with lysis buffer (shaken on precellyus24 at 4500 rpm for 20 secs) followed by the Qiagen RNeasy Plus Mini Kit (cat no. 74134). For blood samples, the Maxwell® RSC simplyRNA blood kit (Promega, AS1380) was used, and for middle ear epithelial cells and ear exudate the Maxwell® RSC simply RNA cells kit (Promega, AS1390) was used. Both kits were used following the manufacturer's instructions.

A NanoDrop ND8000 (Labtech) and 2100 Bioanalyzer (Agilent) were used to test the quantity and quality of RNA respectively, before cDNA was synthesised using a High-Capacity cDNA Reverse Transcription Kit (ThermoFisher, 4368813).

### 2.11.3. PCR amplification

#### 2.11.3.1. Taqman assays

Probes for *Hif1α*, *Tnfa*, *Ii1β* and *Vegfa* had already been designed and used for other mouse models by the Deafness lab. RT-qPCR was performed using TaqMan gene expression assays, Fast Universal PCR Master Mix and a 7500 Fast RealTime PCR System (Applied Biosystems). Reactions were performed in triplicate.

#### 2.11.3.2. SYBR® Green assays

Primers for genes in the Dp5Tyb region were designed on PrimerExpress3 (see Appendix) then tested on cDNA from WT control tissue (e.g. lung). The control tissue for each gene was chosen using expression data on the GTEx portal. RNA extraction was performed as described earlier, following Qiagen's instructions.

The qPCR plates were run with SYBR® Green Master Mix on an ABI 7500 Fast machine on the following setting: one cycle at 95°C for 20 secs; 40 cycles at 95°C for 3 secs; then 60°C for 30 secs. Reactions were performed in triplicate.

#### 2.11.4. Analysis

Data were normalized using *Ppia* as the endogenous control and fold changes of expression were calculated using Applied Biosystems 7500 software v2.3. Gene expression across multiple plates was normalized to the reference sample (usually a WT F blood), then to the endogenous control gene, *Ppia*. Thresholds were manually adjusted to sit at the exponential phase (centre of the straight line). Clear outliers were manually removed.

#### 2.12. Meso Scale Discovery (MSD) assay

MSD assays use electrochemiluminescent labels (SULFO-TAG™), which generate light when stimulated by electricity in the correct chemical environment. The MSD instrument applies electricity to the plate electrodes, causing the labels to emit light. This light intensity corresponds to the quantity of analyte present. A plate was designed to contain analytes of interest from the U-PLEX Biomarker Group 1 mouse assays (catalogue number K15069L-1). U-PLEX Mouse: IL-1 $\beta$ , IL-6, IL-10, IL-17A, IL-21, TNF- $\alpha$ , and VEGF-A.

##### 2.12.1. Sample collection

After the IP injection with terminal anaesthetic, blood was collected into brown z-gel tubes (no anticoagulant) via retro-orbital bleed using glass capillary microvettes.

Serum was isolated by allowing the blood to clot at room temperature for one hour before centrifuging (16000 x g, 5 mins, 4°C). Supernatant (serum) was removed into a clean Eppendorf on dry ice, and was later loaded neat into the plate (25  $\mu$ l/well).

Middle ear exudate was collected using forceps to remove the tympanic membrane and a pipette to collect the fluid. The fluid from both ears (1-3.5  $\mu$ l) was combined into

50  $\mu$ l ice cold PBS, vortexed for 30 secs and centrifuged (500 x g, 10 mins, 4°C) to pellet the cells and debris. The supernatant was later added to the plate neat (25  $\mu$ l/well).

### 2.12.2. Plate coating

Each well of the 96-well plate contained 10 miniature wells for the different linkers to attach (*Figure 2.6b*). The plate was coated following the manufacturer's instructions. To summarise, 200  $\mu$ l of each antibody was coupled to 300  $\mu$ l of a unique linker (numbered 1-10), vortexed and incubated (RT, 30 mins). Then 200  $\mu$ l of stop solution was added to each tube, vortexed and incubated (RT, 30 mins). A 600  $\mu$ l aliquot of each linker-coupled antibody was combined into one tube, vortexed, then 50  $\mu$ l was added to each well to coat the plate. After incubating (RT, one hour shaking) the plate was washed three times (150  $\mu$ l/well PBS-T) and was ready for use.

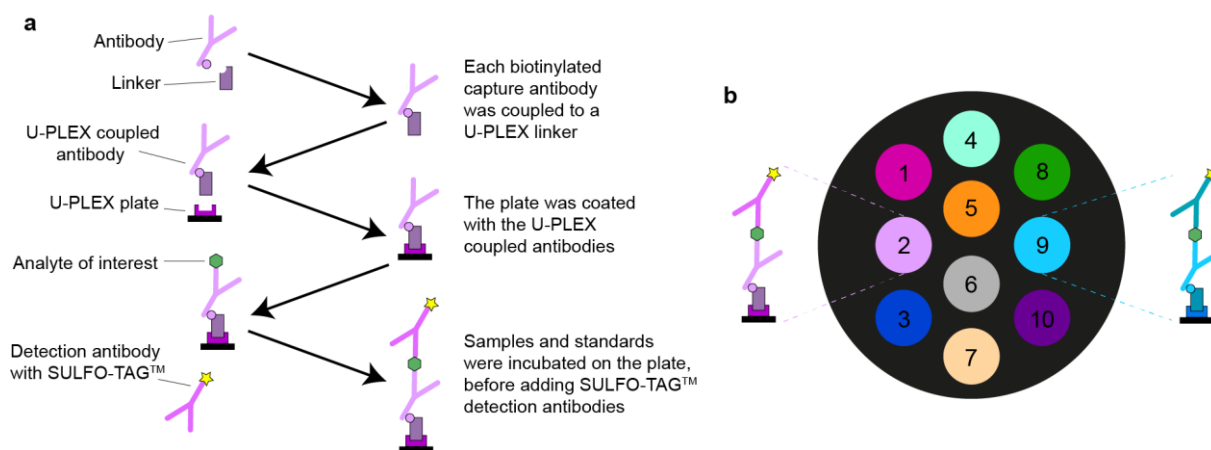


**Figure 2.6. Meso Scale Discovery (MSD) assay.** (a) Schematic diagram of the main steps in the MSD protocol. (b) A magnified image representing the bottom of a well in the 96-well MSD plate. Each well contains 10 miniature wells where the 10 antibodies and linkers can bind (shown as different coloured spots). The images either side show the contents of each miniature well after the protocol has been followed. One sample is added to the whole well, and as each miniature well is binding to a different analyte of interest, 10 results are given per well. Image modified from MSD booklet provided with the kit.

### 2.12.3. Assay protocol

Lyophilized standards were reconstituted with 250  $\mu$ l Diluent 41. Multiple calibrators were combined (50  $\mu$ l of each) into a final volume of 250  $\mu$ l Diluent 41. The subsequent six dilutions for the standard curve were prepared by 4-fold serial dilutions in Diluent 41. Diluent 41 alone was used for the 8<sup>th</sup> standard. Diluent 41 was added (25  $\mu$ l/well), followed by 25  $\mu$ l standard or sample. The plate was covered and incubated (RT, 1 hour shaking). Detection antibodies are pre-coupled to electrochemiluminescent tags (SULFO-TAG™). A 60  $\mu$ l aliquot of each detection antibody was combined and brought to a final volume of 6 ml using Diluent 45. After washing three times (150  $\mu$ l/well PBS-T), 50 $\mu$ l of the detection antibody solution was added per well, sealed and incubated (RT, one hour, shaking). After a final three washes (150  $\mu$ l/well PBS-T), read buffer was added 150  $\mu$ l/well and the plate was read on an MSD Sector Imager 2400. The assay protocol is summarised in *Figure 2.6a*.

### 2.12.4. MSD data analysis

#### 2.12.4.1. Data pre-processing

- 1) Replaced missing values with limit of detection (LOD / 2 for the specific assay (Lower LODs in pg/ml are IL-17A = 0.3, IL-21 = 6.5, IL-22 = 1.2, IL-6 = 4.8, IL-10 = 3.8, IL-1 $\beta$  = 3.1, TNF- $\alpha$  = 1.3, VEGF-A = 0.77)).
- 2) Applied logarithmic (base 2) transformation.
- 3) Regressed out plate effects (subtract plate means and add global mean).
- 4) Calculated the mean of data for each sample (12 samples have four technical replicates averaged from across two plates, and 24 samples have two technical replicates averaged from a single plate).

#### 2.12.4.2. Statistical analysis

For each pairwise comparison in a panel a two-sided Mann–Whitney–Wilcoxon (MWW) test was performed and raw p-values were denoted according to (\*\*\*\*<0.0001, \*\*\* < 0.001, \*\* < 0.01, \* < 0.05). In order to control for multiple testing, we applied the Benjamin-Hochberg procedure to the complete set of 24 p-values arising from all the MWW tests across all assays and pairs of groups. Rejecting the null in all starred cases (\*, \*\*, \*\*\* and \*\*\*\*) controlled the false discovery rate (FDR) below 5%.

### 2.13. Micro-Computed Tomography (microCT)

#### 2.13.1. Sample collection

The skull was bisected and the middle and inner ear were isolated from the skull together and fixed in 4% PFA. After six hours on the Belly Dancer Orbital platform shaker (Stovall) the PFA was replaced with fresh 4% PFA and left overnight. After three washes with PBS the samples were left in PBS in the fridge ready for microCT.

MicroCT was performed with the assistance of Zsombor Szoke-Kovacs, and his methods are as follows.

#### 2.13.2. Imaging

Skyscan 1172 Micro-Computed Tomography (microCT), by Bruker, was used for the scanning of samples. Mouse auditory bullae were glued using dental cement to a Skyscan 1172 sample holding metal rod, and were scanned at a standard set of parameters specifically developed for ear scanning (X-ray power 80-85 kV, Al 0.5 mm filter, small camera pixel, image pixel size 2.5  $\mu\text{m}$ , rotation step 0.250, frame averaging 2, random movement 10). The collected x-ray images were reconstructed

in NRecon (Bruker), followed by a standardization/scaling process (downsized by 2 and rescaled by 14  $\mu\text{m}$ ) using the Harwell Automated Reconstruction Processor (HARP), developed at MRC Harwell.

### 2.13.3. Segmentation

Manual segmentation of the ossicles using the 'Thresholding' option was done in ITKSnap, then surface mesh models were viewed and exported in 3DSlicer.

## 2.14. Scanning Electron Microscopy (SEM)

SEM was performed with the assistance of Andrew Parker and his methods are as follows.

### 2.14.1. Sample collection

For cochlear and middle ear SEM, mice were culled by cervical dislocation, then the head was removed, bisected and the bullae were separated from the skull.

For cochlear SEM, the middle ear was discarded and forceps were used to pierce the oval window and scratch a small hole in the apex of the cochlea. Glutaraldehyde (2.5% in 0.1M phosphate buffer) was injected through the oval window to fix the cochlea before submerging in the same glutaraldehyde.

For middle ear SEM, the inner ear was discarded and the middle ear was fixed in glutaraldehyde. Both sets of samples were submerged overnight at 4°C on a rocking platform.

### 2.14.2. Decalcification and fine dissection (inner ears only)

The samples were rinsed in 0.1M phosphate buffer three times for 15 mins, before submersion in EDTA (4.3% in 0.1M phosphate buffer) to decalcify for 24-48 hours at

room temperature. Fine dissection was performed to remove the decalcified shell and reveal the cochlear organ of Corti.

### 2.14.3. Processing

Osmium tetroxide thiocarbohydrazide (OTO) processing was done using a Leica EM-TP (Leica Microsystems). Briefly, the samples were immersed in 1% v/v osmium tetroxide ( $\text{OsO}_4$ ) (Electron Microscopy Supplies) in 0.1M sodium cacodylate buffer (Sigma Aldrich) for one hour, washed six times for 5 mins in ddH<sub>2</sub>O, immersed in 1% v/v thiocarbohydrazide (TCH) (Fluka) in ddH<sub>2</sub>O for 30 mins, washed times for 5 mins in ddH<sub>2</sub>O, immersed in  $\text{OsO}_4$  again for one hour and washed six times for 5 mins in ddH<sub>2</sub>O.

### 2.14.4. Critical point drying, mounting and sputter coating

The samples were then dehydrated through six increasing concentrations of ethanol (25-100%) (Fisher Scientific) for 45 mins each before being transferred to 100% acetone (Fisher Scientific) and critical point dried using a Leica EM CPD300 (Leica Microsystems). Samples were then mounted on stubs using silver paint (Agar Scientific) and sputter coated with platinum in an argon atmosphere using a Quorum Q150T sputter coater (Quorum Technologies).

### 2.14.5. Imaging

The cochleae and middle ears were then visualised with a JEOL LSM-6010 (Jeol Ltd.) scanning electron microscope.

## 2.15. Statistical analysis

Data were tested for normality using a D'Agostino and Pearson test. If normally distributed, an unpaired student's t-test was performed to compare two datasets of  $n \geq 3$ . For datasets with unequal standard deviations Welch's correction was used. If

## CHAPTER 2: Materials and Methods

not normal, a non-parametric test (Mann-Whitney Test) was performed instead. Error bars on graphs show mean  $\pm$  standard deviation (SD).

Statistical analysis was performed using GraphPad Prism 9 software. The significance threshold was set at  $p < 0.05$ . On graphs, significance levels are represented by: ns =  $p > 0.05$  (not significant), \* =  $p \leq 0.05$ , \*\* =  $p \leq 0.01$ , \*\*\* =  $p \leq 0.001$ , \*\*\*\* =  $p \leq 0.0001$ .

## CHAPTER 3: Phenotypic characterisation of Dp5Tyb mice

---

### 3.1. Introduction

Humans with Down syndrome (DS) have trisomy of human chromosome 21 (Hsa21), which leads to a broad range of characteristic phenotypes (Antonarakis, 2017).

Understanding the genetic cause of these phenotypes could allow therapies to be developed to improve quality of life for people with DS. In order to do this, mouse models of DS have been created. The mouse orthologues to genes on Hsa21 are found mostly on mouse chromosome 16 (Mmu16), with some also on Mmu10 and Mmu17. In 2016 the Tybulewicz lab published their segmental trisomy models of Mmu16, which were used to investigate congenital heart defects (Lana-Elola et al., 2016). These models were shared with MRC Harwell so that other DS phenotypes could be investigated, such as otitis media with effusion (OME).

These mice, known as DpTyb, have two full copies of Mmu16, plus an additional duplication of a specific region of Mmu16, ranging from 12 to 148 genes (all Hsa21 orthologues on Mmu16) (Lana-Elola et al., 2016). The duplicated regions have discrete end points so there are no overlaps. This allows a mapping panel to be created (*Figure 3.1*), and the causative genes for a DS phenotype can be tracked by analysing mice with smaller and smaller duplicated regions.

The Hsa21 orthologues on Mmu10 and Mmu17 are duplicated in the mouse models Dp(10Prmt2-Pdxk)2Yey (Dp2Yey) and Dp(17Abcg1-Rrp1b)3Yey (Dp3Yey), respectively (Yu et al., 2010). The Deafness lab (Harwell) found no OME in these mice (*Figure 3.1*) (Tateossian et al., 2022).

### CHAPTER 3: Phenotypic characterisation of Dp5Tyb mice

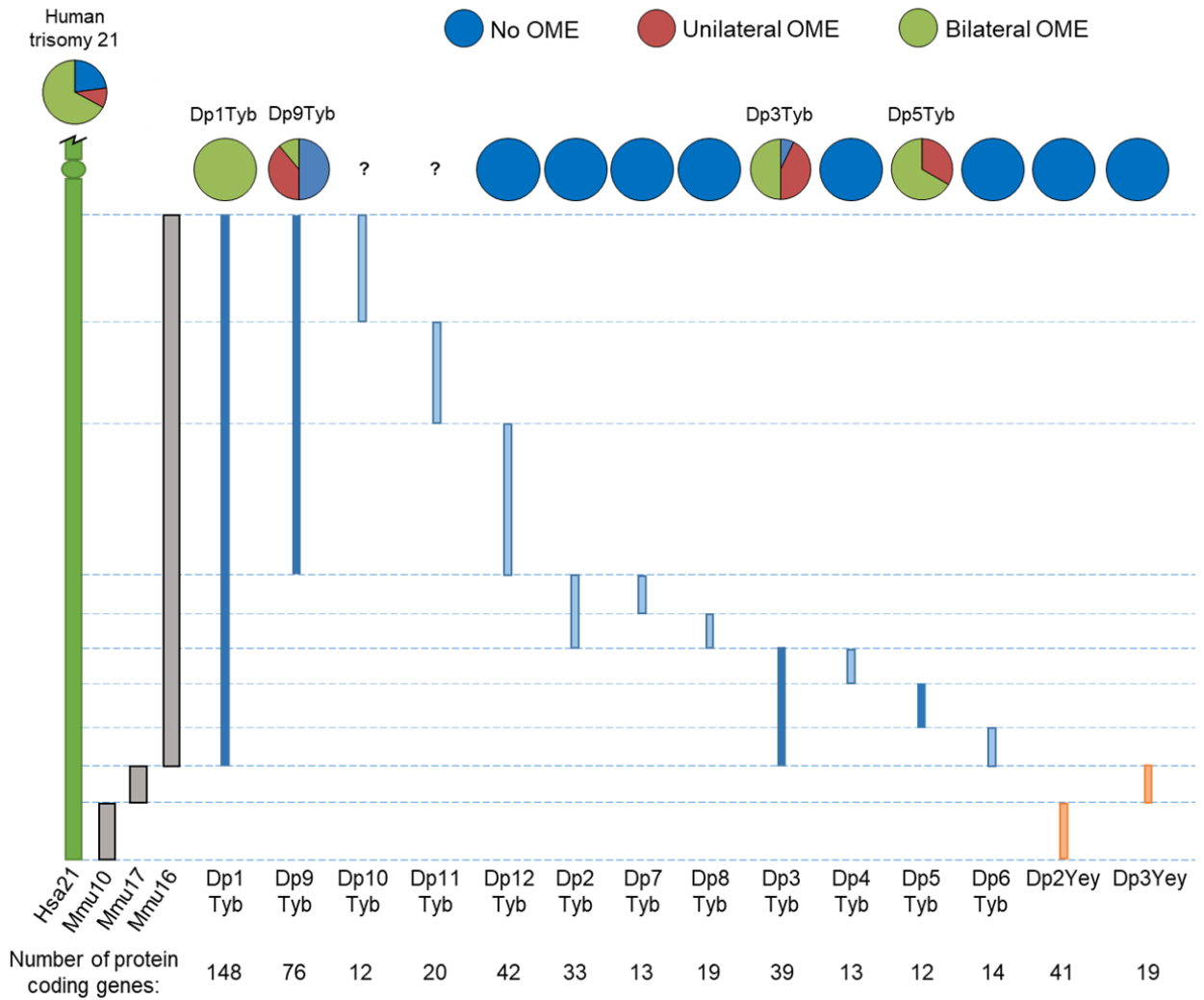


**Figure 3.1. Mapping panel of the duplicated regions of DpTyb and DpYey mice, and the OME incidence in each mouse line.** Mmu10, 16 and 17 are orthologous to Hsa21. Most of the DpTyb mice have trisomy of a section of Mmu16, apart from Dp1Tyb mice, which have a duplication of all Hsa21 orthologues on the chromosome. Dp2Yey and Dp3Yey have three copies of the Hsa21 orthologues on Mmu10 and Mmu17 respectively. Blue lines represent the duplicated region in DpTyb lines, with those with otitis media with effusion (OME) coloured dark blue. The orange lines represent the duplications in DpYey mice. The pie charts show the incidence of OME in each mouse line, with segments representing those which don't have OME, and those with OME in one or both ears (termed unilateral and bilateral, respectively). Image modified from figures by (Lana-Elola et al., 2016, Tateossian et al., 2022). Human data sourced from a report by the National Institute for Health and Clinical Excellence (NICE, 2008), which details the OME incidence in 70 British children with DS, aged 18-24 months.

Dp1Tyb mice have a duplication of the majority of Mmu16 (148 protein coding genes, 114 of which are orthologous to those on Hsa21). Along with other DS phenotypes, the Deafness lab (MRC Harwell) found fully penetrant OME in Dp1Tyb mice (Tateossian et al., 2022). The mapping panel was then used to investigate the Dp2Tyb, Dp3Tyb and Dp9Tyb segmental duplications, covering the region duplicated

### CHAPTER 3: Phenotypic characterisation of Dp5Tyb mice

in Dp1Tyb, to ascertain which region contained the causative gene(s). Only half of Dp9Tyb mice had OME, nearly all Dp3Tyb mice were affected and none of the Dp2Tyb mice had OME. Mice with duplication of shorter sections of the Dp3Tyb region – Dp4Tyb, Dp5Tyb and Dp6Tyb – were analysed next. Dp4Tyb and Dp6Tyb mice had no OME, but all Dp5Tyb mice had OME in one or both ears. In summary, the data indicates that a major locus predisposing to OME lies within the Dp5Tyb segment. In addition, a minor locus contributing to OME is present within Dp9Tyb. This was the starting point for my DPhil project.

Dp1Tyb mice display a wide range of DS phenotypes, including modified craniofacial morphology and reduced hearing (Lana-Elola et al., 2021). The Deafness lab also studied the hearing loss and associated OME phenotypes of the Dp1Tyb mice, and these phenotypes will be discussed further in relation to those seen in Dp5Tyb mice.

The Dp5Tyb region contains 12 genes, all of which are orthologous to genes found on Hsa21. After establishing that all Dp5Tyb mice have OME, which is a main contributor to conductive hearing loss, I further explored the deafness phenotype.

Other possible causes of reduced hearing were investigated, such as issues with the inner ear (sensorineural hearing loss) or other reasons for conductive hearing loss, such as malformation of the ossicles (middle ear bones) or a perforated eardrum.

The age of OME onset, and the extent to which the hearing loss and inflammation persisted as the mice aged were also explored. When studying Dp1Tyb mice we found that they had abnormalities regarding the size of alveoli in their lungs and the shape of their skulls, so these phenotypes were also investigated in Dp5Tyb mice for comparison.

This chapter discusses the deafness and DS phenotypes seen in Dp5Tyb mice compared to their wildtype (WT) littermates, and also compared to Dp1Tyb where data are available from others (Tateossian et al., 2022, Lana-Elola et al., 2021).

## 3.2. Results

### 3.2.1. Trisomy of the Dp5Tyb region has no effect on survival

Dp1Tyb and Dp3Tyb mice have a reduced survival rate, with 50% less Dp1Tyb and 25% less Dp3Tyb mice surviving to weaning age compared to WT littermates (Lana-Elola et al., 2016). Carriers of the duplicated region should comprise 50% of the population if the genotype has no negative effects on survival. I therefore investigated the survival rate of Dp5Tyb mice. From a sample of 10 litters, 56 mice survived past weaning stage. When genotyped, 24 were WT and 32 were Dp5Tyb mice. These values do not differ significantly from the expected value of 28 ( $p = 0.5700$ , two-tailed Fisher's exact test). Therefore, duplication of the Dp5Tyb region has no effect on the survival of these mice relative to their WT littermates.

## 3.2.2. Dp5Tyb mice do not weigh significantly less than their WT

## littermates at two-months-old

Upon first examination, Dp5Tyb mice appear smaller than their WT littermates.

However, when averaged over several cages, there's no significant difference in weight at two-months-old between the genotypes in either sex (*Figure 3.2*). The males follow a trend of lower weight in Dp5Tyb mice than WT littermates (mean WT: 26.16 g; mean Dp5Tyb: 25.35 g;  $p = 0.0571$ ), but the mean weight of Dp5Tyb females was slightly higher than their WT littermates (mean WT: 20.24 g; mean Dp5Tyb: 20.59 g;  $p = 0.4285$ ).

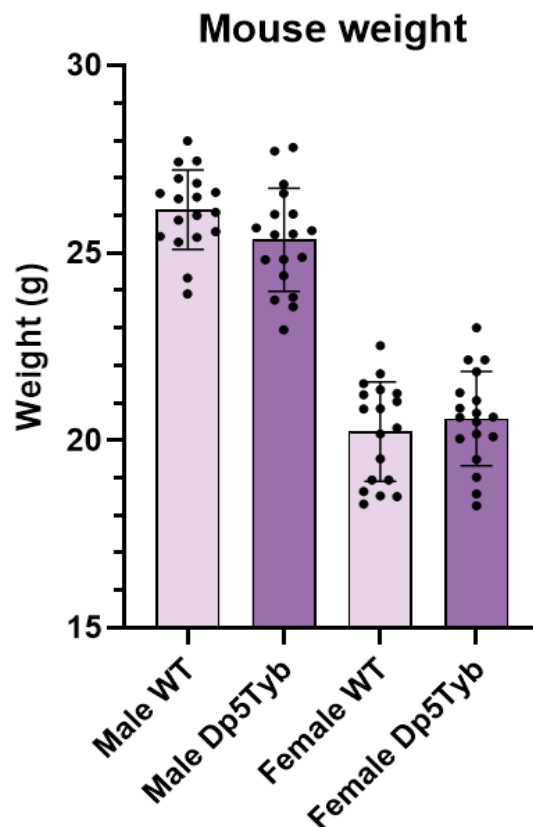


**Figure 3.2. Weights of Dp5Tyb mice and their WT littermates.** Mice were two-months-old. All cohorts  $n = 18$ . Male  $p = 0.0571$ ; female  $p = 0.4285$ . Both calculated using two-tailed unpaired t tests. Error bars show mean  $\pm$  standard deviation.

### 3.2.3. Dp5Tyb mice have inflamed middle ears from three weeks of age

The OME phenotype of the Dp5Tyb mice was analysed histologically at different time points, from 3-52 weeks of age. For this study the mice were culled, and their heads were fixed in formalin, sliced into transverse sections and haematoxylin and eosin (H&E) stained.

OME typically presents as thickening of the middle ear epithelial lining (mucoperiosteum) and an accumulation of fluid and white blood cells in the middle ear cavity. To analyse the OME phenotype of Dp5Tyb mice I examined the H&E sections and measured the ear with the thickest mucoperiosteum per mouse, always starting from the top of the middle ear and taking five measurements (see methods). Mucoperiosteal thickening was observed in Dp5Tyb mice from the first time point of three weeks, all the way through to the last time point of one-year-old. Measurements of the mucoperiosteal thickness revealed that the most significant difference between WT and Dp5Tyb epithelial thickness was at two months of age ( $p = 0.0002$ ) (*Figure 3.3*). It was therefore decided that two-months-old would be the standard age of mice used for all future experiments, unless multiple time points were needed. At two-months-old, mice are still classed as juvenile (Jackson et al., 2017), which is relevant to the human disease being modelled as humans with DS are most affected by OME during childhood. Using this time point also allows comparison with Dp1Tyb research done by others in the Deafness lab (Tateossian et al., 2022).

The thickness of WT mucoperiosteum remained constant through all time points. A Kruskal-Wallis test (non-parametric one-way ANOVA) showed there was no significant difference overall between the groups ( $p = 0.0636$ ). Dunn's multiple comparisons test showed no significant differences between the WT mice of any two time points, with all  $p$ -values  $> 0.0745$ .

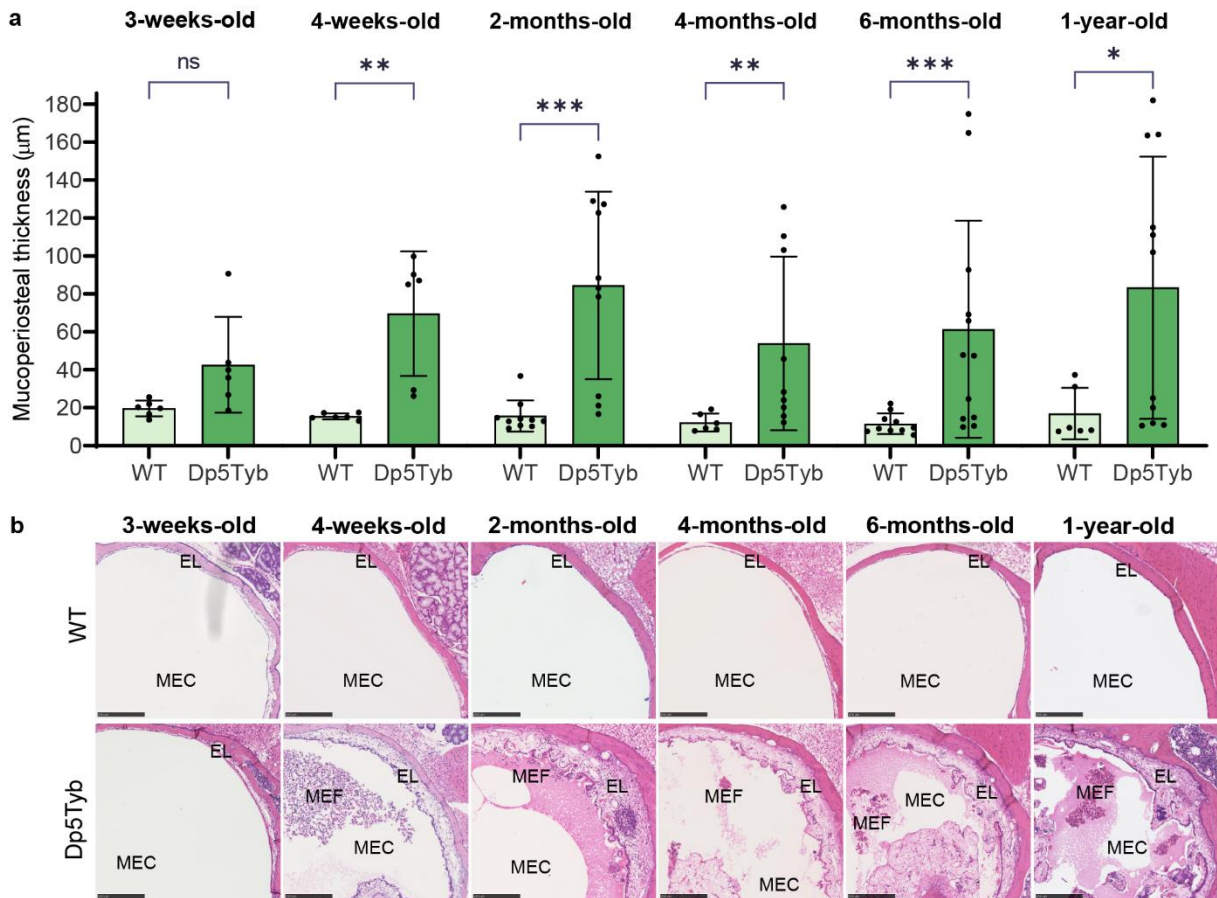


**Figure 3.3. Thickness of middle ear epithelial lining in WT and Dp5Tyb mice from three weeks to one year of age.** (a) Error bars show mean  $\pm$  standard deviation. Unpaired two-tailed t-test with Welch's correction. Three-weeks-old: WT  $n = 6$ , Dp5Tyb  $n = 6$ ,  $p = 0.0764$  (unpaired t test with Welch's correction); Four-weeks-old: WT  $n = 6$ , Dp5Tyb  $n = 6$ ,  $p = 0.0022$  (Mann Whitney test); Two-months-old: WT  $n = 10$ , Dp5Tyb  $n = 10$ ,  $p = 0.0002$  (Mann Whitney test); Four-months-old: WT  $n = 6$ , Dp5Tyb  $n = 9$ ,  $p = 0.0048$  (Mann Whitney test); Six-months-old: WT  $n = 10$ , Dp5Tyb  $n = 12$ ,  $p = 0.0008$  (Mann Whitney test); One-year-old: WT  $n = 6$ , Dp5Tyb  $n = 11$ ,  $p = 0.0202$  (Mann Whitney test). Each point on the graph represents the middle ear with the thickest mucoperiosteum per mouse. (b) Images of WT and Dp5Tyb middle ears, taken from H&E stained transverse paraffin-embedded sections. EL = epithelial lining; MEC = middle ear cavity; MEF = middle ear fluid. Scale bar = 250  $\mu\text{m}$ .

### 3.2.4. Dp5Tyb mice have a small increase in ABR thresholds, which is indicative of conductive hearing loss

All Dp5Tyb mice have at least one ear affected by OME, which is a common cause of conductive hearing loss in children, particularly those with DS (Fortnum et al., 2014, Park et al., 2012). Children with DS sometimes have mixed hearing loss, which is caused by a combination of conductive (middle ear) and sensorineural (inner ear) elements (Kreicher et al., 2018). To better understand the deafness phenotype of Dp5Tyb mice I measured their auditory-evoked brainstem response (ABR) to broadband click stimuli. Dp5Tyb mice and WT littermates were anaesthetised and three sub-dermal electrodes were inserted – one below the ear being tested, one along the midline of the head, and one in the flank. A tone was then played near the mouse's ear, gradually decreasing in intensity from 90 dB to 5 dB. The brainstem response was shown in waves on the screen. Once the limit of the mouse's hearing was reached the waves became disordered and the threshold was noted. A mild hearing impairment (a small increase in ABR threshold compared to WT littermates) is categorised as conductive, whereas more severe hearing loss is indicative of sensorineural hearing loss. The exact thresholds vary, but one study performed click-evoked ABRs at 30 dB and 65 dB. Children who couldn't hear the 65 dB stimulus were diagnosed with sensorineural hearing loss, those that could hear at 65 dB but not 30 dB had conductive hearing loss, and those that could hear the 30 dB stimulus had normal hearing (Watson et al., 1996).

Click-evoked ABRs were carried out from four weeks to six months of age. A small but statistically significant increase in threshold was seen in Dp5Tyb mice compared to WT littermates at every time point (Figure 3.4). At two months, Dp5Tyb mice had a mean threshold 21.87 dB above their WT littermates ( $p = 0.0366$ ). For comparison, at

two-months-old Dp1Tyb mice had a mean ABR threshold 27.5 dB above WT littermates ( $p < 0.0001$ ) (Tateossian et al., 2022). The small threshold increase of 20-30 dB is indicative of conductive hearing loss, rather than sensorineural. However, it is important to note that mild sensorineural hearing loss is a possibility (Zaitoun et al., 2021). Another study performed click-evoked ABRs on Dp1Tyb mice at 14 weeks of age, and found the mean threshold was around 25 dB higher than that of WT littermates (Lana-Elola et al., 2021).

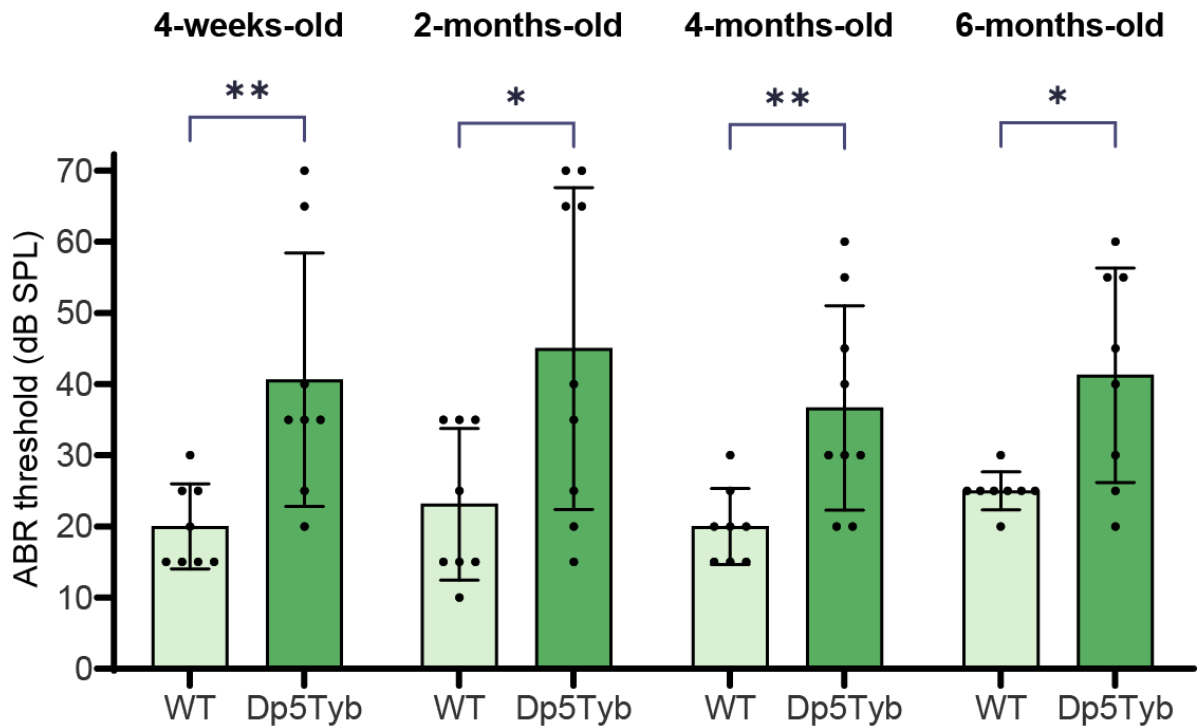


**Figure 3.4. Auditory-evoked brainstem response thresholds for WT and Dp5Tyb mice from four weeks to six months of age.** Each data point represents one ear, both ears of each mouse were tested, apart from a two-month-old and four-month-old Dp5Tyb for which only one ear was tested. Error bars show mean  $\pm$  standard deviation. Four-weeks-old: WT  $n = 8$ , Dp5Tyb  $n = 8$ ,  $p = 0.0036$  (Mann Whitney test); Two-months-old: WT  $n = 8$ , Dp5Tyb  $n = 9$ ,  $p = 0.0366$  (Mann Whitney test); Four-months-old: WT  $n = 8$ , Dp5Tyb  $n = 9$ ,  $p = 0.0085$  (unpaired t test with Welch's correction); Six-months-old: WT  $n = 8$ , Dp5Tyb  $n = 8$ ,  $p = 0.0308$  (Mann Whitney test). db SPL = decibels sound pressure level.

## 3.2.5. No sensorineural hearing loss was found in Dp5Tyb mice

To ascertain whether the reduced hearing detected in Dp5Tyb mice was due to conductive hearing loss only or sensorineural hearing loss as well, the organ of Corti in the inner ear was examined at two-months-old. Hair cells are part of the organ of Corti, they convert sound waves into electrochemical energy, stimulating the auditory nerve to pass the information to the brain. Organ of Corti and hair cell morphology were observed using scanning electron microscopy (SEM) and H&E stained sections (*Figure 3.5*). Images were taken at the top (apical), middle (mid) and bottom (basal) turns of the cochlea.

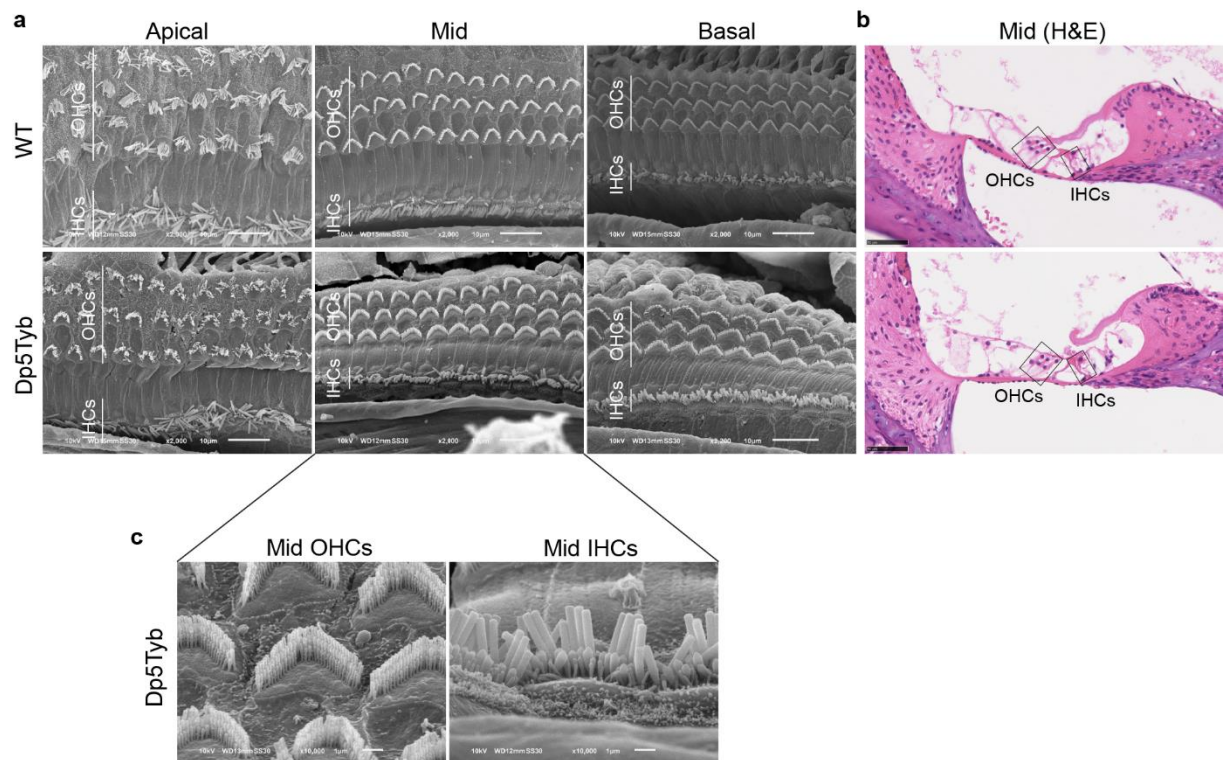


**Figure 3.5. Scanning electron microscopy and H&E staining of cochlear hair cells.** (a) Scanning electron microscopy images of a WT and Dp5Tyb organ of Corti. Images are of hair cells at the apical, mid and basal turns of the cochlea. IHCs = inner hair cells; OHCs = outer hair cells. WT n = 2; Dp5Tyb n = 2. Images taken at x2000 magnification. Scale bar = 10  $\mu$ m. (b) Histological images of WT and Dp5Tyb cochlear hair cells from the mid turn of the cochlea. Sagittal head sections were haematoxylin and eosin (H&E) stained, imaged and the mid turn was identified. WT n = 2, Dp5Tyb n = 2. Scale bar = 50  $\mu$ m. (c) Higher magnification images of Dp5Tyb hair cells from the mid turn of the cochlea. Images taken at x10000 magnification. Scale bar = 1  $\mu$ m. SEM images were taken by Andrew Parker.

On the SEM images, healthy hair cells present as three rows of outer hair cells (OHCs) with one row of inner hair cells (IHCs) below (*Figure 3.5a*). On the H&E sections, the cochlea has been bisected in the sagittal plane, so healthy hair cells would now appear as three OHCs converging with one IHC at each turn of the cochlea (*Figure 3.5b*).

At two-months-old, Dp5Tyb hair cells are indistinguishable from WT hair cells when observed through histological examination and SEM imaging. The hair cell bundles have normal morphology at all turns of the cochlea. *Figure 3.5a* shows example SEM images of a WT and Dp5Tyb organ of Corti, above a higher magnification image of the mid cochlear turn (*Figure 3.5c*) to allow the hair cell bundles to be viewed more easily. H&E images of the mid turn are shown alongside (*Figure 3.5b*).

These findings suggest that it is unlikely that Dp5Tyb mice have a sensorineural element to their hearing loss. However, in-depth analysis was not performed, such as verifying the health of the supporting cells, for example.

### 3.2.6. Investigation of additional conductive elements to the hearing loss

After confirming that the hearing loss is due to middle ear dysfunction, other potential causes of this conductive hearing loss were investigated - malformation of the middle ear ossicles, and perforation of the tympanic membranes.

### 3.2.6.1. Micro-computed tomography shows no malformation of ossicles

To study the morphology of the middle ear ossicles, micro-computed tomography (microCT) imaging was used to acquire 3D x-ray images of eight WT and eight Dp5Tyb bullae, which were then reconstructed, scaled and the ossicles segmented. Example images of WT and Dp5Tyb bullae of two-month-old mice in 2D are shown in *Figure 3.6*, with the bones shown in different colours for clarity. Visual inspections were carried out, and no difference in ossicle shape or size, or distance between ossicles was observed between WT and Dp5Tyb bullae.

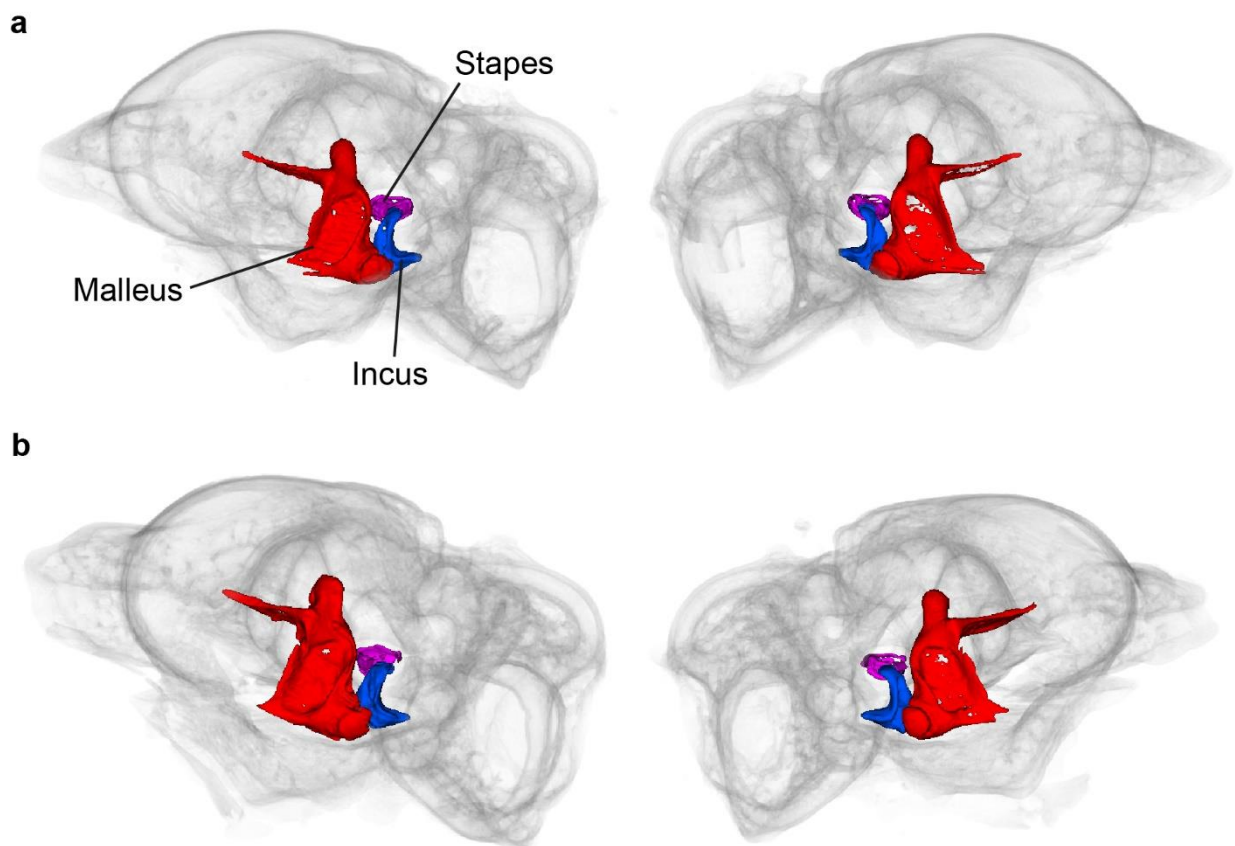


**Figure 3.6. Micro-computed tomography (microCT) images of the middle ear ossicles.** Images show the morphology of the ossicles in both ears of (a) a WT mouse and (b) a Dp5Tyb mouse. All mice were two-months-old. The malleus (red), incus (blue) and stapes (pink) are shown within the middle ear cavity of the bulla (grey). WT n = 8 (four mice), Dp5Tyb n = 8 (four mice). Images created by Zsombor Szoke-Kovacs.

### 3.2.6.2. No tympanic membrane perforations were observed at two-months-old

Another potential cause of conductive hearing loss is a perforation of the tympanic membrane (eardrum). After removing and skinning the head, the tympanic membranes were observed under a microscope and photographs were taken (*Figure 3.7*). No perforations were seen in any of the 9 Dp5Tyb mice or 14 WT littermates, suggesting this is not the cause of the conductive hearing loss found in Dp5Tyb mice.

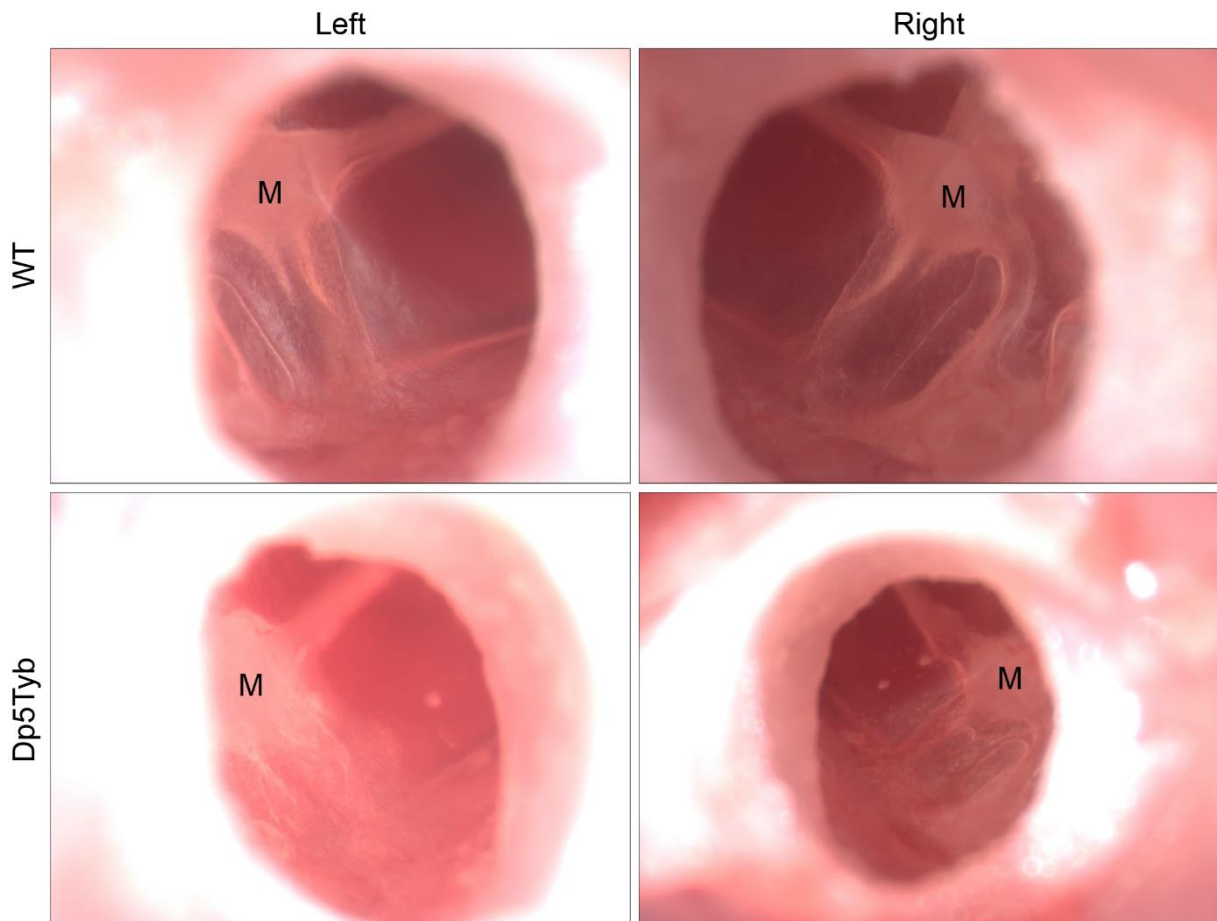


**Figure 3.7. Photographs of tympanic membranes.** Both tympanic membranes of two-month-old WT and Dp5Tyb mice were observed for any perforations. M = malleus bone, behind the tympanic membrane. No perforations were seen in either ear (WT: n = 14 mice, Dp5Tyb: n = 9 mice).

### 3.2.7. Dp5Tyb mice have a mild lung phenotype

The lungs are of interest as alveoli are air-filled spaces surrounded by epithelial cells, similar to the middle ear cavity (Takahashi, 2001). Also, the epithelial lining of the airways and middle ear are a continuous surface, connected via the Eustachian tube. Non-Down syndrome mouse models of OME (*Jeff* and *edison*) were found to have a lung phenotype (Tateossian et al., 2009, Crompton et al., 2017). For both mutants, the embryos had smaller airways with compact tissue surrounding them, leading to an emphysema phenotype in adulthood whereby they had larger alveolar spaces than WT littermates. As Dp5Tyb mice have OM, I wanted to check if they also have this lung phenotype.

Dp5Tyb alveolar size was quantified using the mean linear intercept (Lm) calculation, a concept first introduced in the 1940s as a measure of surface area (Tomkeieff, 1945), and later applied to studying lung morphology (Campbell and Tomkeieff, 1952). The Lm calculation now involves counting how many times the alveolar walls cross a superimposed grid on ImageJ software, taking into account the number and length of the lines, and scale of the image. This method was described previously (Andersen et al., 2012). The fewer times the alveolar walls cross the grid the larger the Lm value becomes, indicating a larger alveolar size (although not a direct measurement). The images used were from transverse H&E sections of the left lung of Dp5Tyb mice (n = 10) and WT littermates (n = 9). Nine images were analysed per mouse, and each data point on the graph is an average of these nine measurements. There was a significant increase in alveolar size in the Dp5Tyb mice compared to WT littermates (mean linear intercept: WT = 28.53  $\mu\text{m}$ , Dp5Tyb = 30.51  $\mu\text{m}$ ,  $p = 0.0395$ ) (*Figure 3.8*).

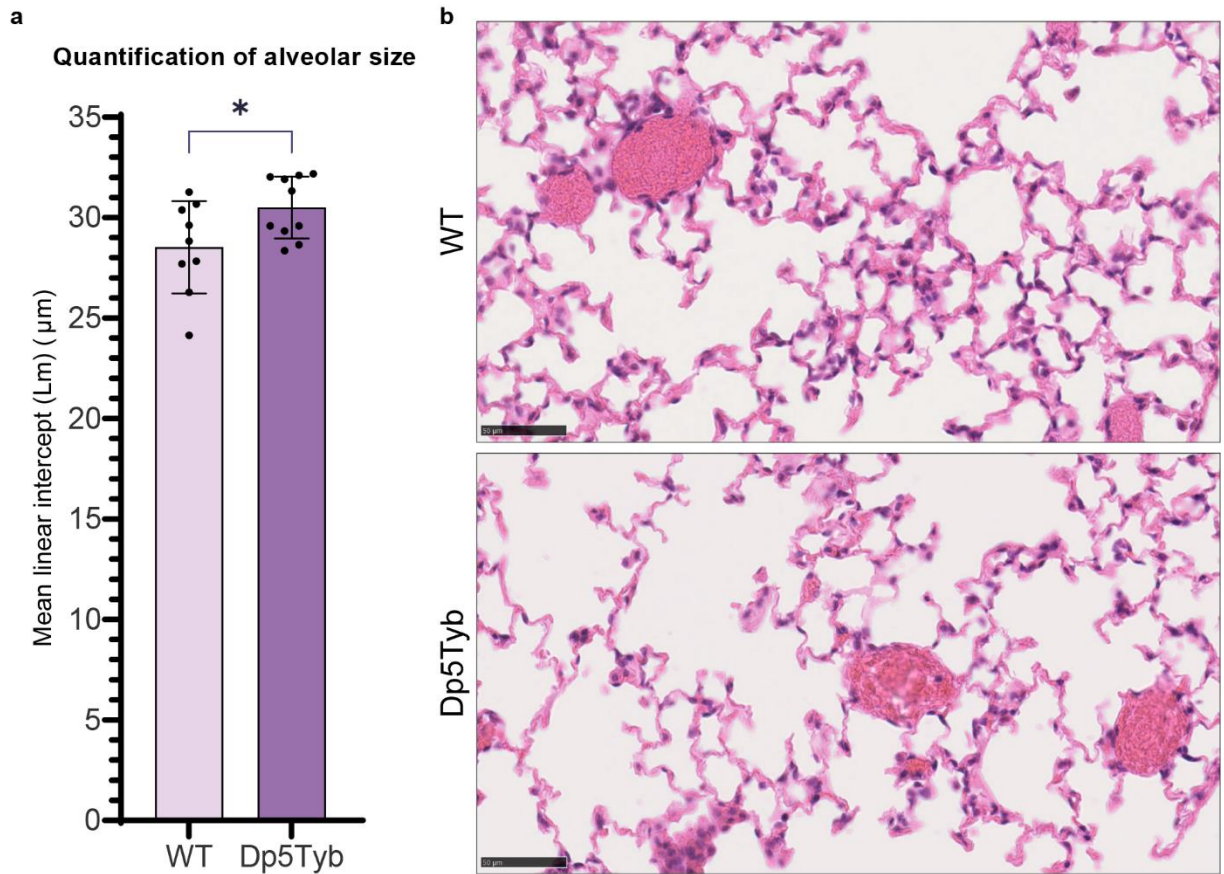


**Figure 3.8. Mean linear intercept (Lm) graph and images of the lungs.** Mean linear intercept is a representation of alveolar size. A larger Lm value corresponds to larger alveoli. (a) Error bars show mean  $\pm$  standard deviation. WT  $n = 9$ , Dp5Tyb  $n = 10$ ,  $p = 0.0395$  (Unpaired two-tailed t-test). (b) Examples of the H&E stained lung sections used to measure Lm. Scale bar = 50  $\mu\text{m}$ .

## 3.2.8. Mild craniofacial defect in Dp5Tyb mice

Craniofacial defects are one of the risk factors for chronic OME, even in children without DS (Hardisty et al., 2003). Human patients with DS have visible facial differences (Rodrigues et al., 2019), and the same was found in Dp1Tyb mice – they had significantly wider frontal bone width than their WT littermates ( $p = 0.0016$ ) (Tateossian et al., 2022). There was also a trend towards Dp1Tyb mice having a shorter frontal bone length, but the data were not significant. Through visual observation they found that Dp1Tyb ear pinnae are more rounded and sit lower on the head, their neck appears shorter, and their head is more domed in shape (Figure 3.9a).

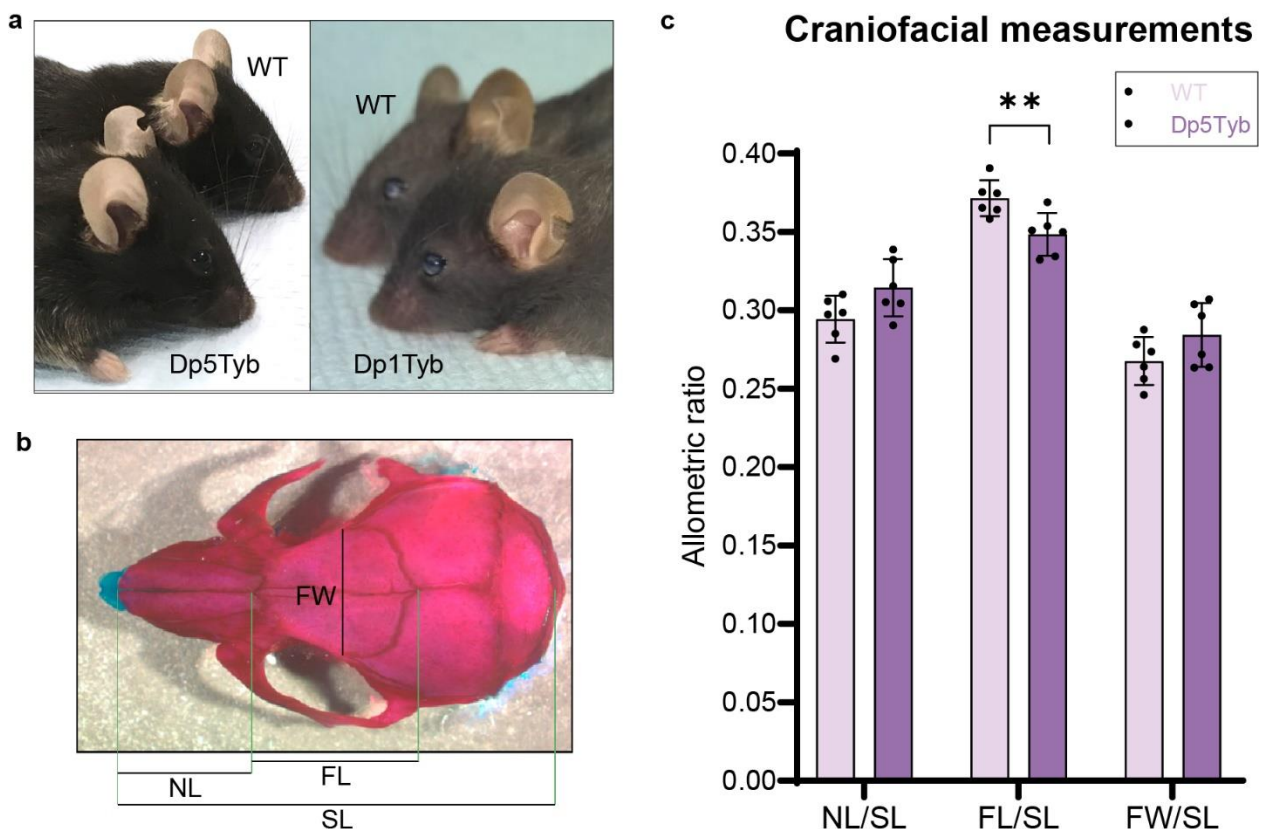


**Figure 3.9. Craniofacial measurements carried out on WT and Dp5Tyb skulls following bone preparation.** (a) Photographs of Dp5Tyb and Dp1Tyb heads alongside their respective WT littermate. (b) Diagram of the skull measurements taken. Bone preparation causes bone to be stained pink and cartilage light blue. NL = nasal bone length; FL = frontal bone length; FW = frontal bone width; SL = skull length. (c) Graph of the allometric ratios calculated from skull measurements. Allometric ratios were calculated by comparing each measurement back to the skull length (SL). Error bars show mean  $\pm$  standard deviation. WT  $n = 6$ , Dp5Tyb  $n = 6$ . NL/SL  $p = 0.0640$ , FL/SL  $p = 0.0099$ , FW/SL  $p = 0.1381$ . All unpaired two-tailed t-tests.

### CHAPTER 3: Phenotypic characterisation of Dp5Tyb mice

The Dp5Tyb mice don't have a visible defect, but a difference in skull shape did emerge after analysis of skull measurements. Dp5Tyb and WT skulls underwent bone preparation to distinguish bone (pink) from cartilage (blue). ImageJ software was then used to measure the frontal bone length (FL) and width (FW), nasal bone length (NL) and skull length (SL) (*Figure 3.9b*). Allometric ratios were then calculated, normalising each skull measurement to the overall length of skull (*Figure 3.9c*).

Dp5Tyb mice have significantly shorter frontal bones than their WT littermates (Mean WT FL/SL = 0.37, mean Dp5Tyb FL/SL = 0.35,  $p = 0.0099$ ) (*Figure 3.9c*). There was also a trend towards Dp5Tyb mice having wider frontal bones, but the data were not significant (Mean WT FW/SL = 0.27, mean Dp5Tyb FW/SL = 0.28,  $p = 0.1381$ ).

The same trend of wider and shorter frontal bones was seen in both Dp1Tyb and Dp5Tyb mice compared to their respective WT littermates.

### 3.3. Discussion

Initial investigations of the DpTyb panel identified a major locus for OME within the Dp5Tyb region. As a first step to identifying and characterising the locus involved, a detailed phenotypic analysis of the Dp5Tyb mouse was undertaken focusing on the nature of the hearing loss, as well as lung and craniofacial phenotypes.

The literature shows that fewer Dp1Tyb and Dp3Tyb mice survive to weaning age compared to their WT littermates, but that Dp5Tyb litters show the expected Mendelian ratios (Lana-Elola et al., 2016). My findings also suggest that Dp5Tyb mice do not have decreased survival compared to their WT littermates. Lana-Elola observed that the Dp1Tyb and Dp3Tyb mice were dying between E14.5 and weaning age, and attributed this, at least in part, to the prevalence of severe congenital heart defects (CHDs) in these mice. Dp5Tyb mice do not show significantly increased rates of CHDs (Lana-Elola et al., 2016), which could help explain why the expected number survive to weaning age. Others have also confirmed that fewer Dp1Tyb mice survive to weaning age compared to WT littermates (Lana-Elola et al., 2021, Tateossian et al., 2022). Their reduced viability could also be affected by other dosage-sensitive genes on Mmu16 as Dp1Tyb mice have a much larger duplication compared to Dp5Tyb mice.

At two-months-old there was no significant difference in weight between Dp5Tyb mice and their WT littermates. Dp1Tyb mice weighed less than WT littermates initially, but by two-months-old they were not significantly different (Tateossian et al., 2022). Another study found male Dp1Tyb mice to be lighter at four-weeks-old but by two months there was no significant difference in weight between the genotypes for males or females (Lana-Elola et al., 2021). An explanation for the Dp5Tyb mice appearing smaller but weighing the same as WT littermates could be related to

### CHAPTER 3: Phenotypic characterisation of Dp5Tyb mice

altered bone density or body composition. People with DS are often shorter than the general population, and tend to have a lower bone mineral density and increased body fat (LaCombe and Roper, 2020, Gutierrez-Hervas et al., 2020). No measurements were taken from Dp5Tyb mice other than weight, but future work could involve echo-MRI to establish the fat and water mass present in the mice, or a dual energy X-ray absorptiometry (DEXA) scan to study bone density. Total body length or bone length (such as the tibia) could also be measured to ascertain whether Dp5Tyb mice are smaller than WT littermates. These measurements were taken for Dp1Tyb mice, and the results showed that Dp1Tyb mice have shorter tibia bones and reduced bone mineral density, but no change in fat or lean mass compared to WT littermates (Lana-Elola et al., 2021).

When OME develops, the mucoperiosteum thickens with epithelial cell proliferation and polyp formation at the leading edge (proximal to the middle ear cavity). As the lining grows, white blood cells and plasma enter the middle ear cavity through vascular leakage. The Dp1Tyb mucoperiosteum was measured from three weeks to four months of age and it was significantly thicker than the mucoperiosteum of WT littermates at all time points (Tateossian et al., 2022). The mucoperiosteal thickening seen in the Dp5Tyb middle ear was similar to that of Dp1Tyb mice. Moreover, from four weeks of age there was significant middle ear effusion in both Dp1Tyb and Dp5Tyb mice. Overall, the data confirm that trisomy of Dp5Tyb region is sufficient to cause OME.

The conductive hearing loss indicated by elevated click ABR thresholds in Dp5Tyb was replicated in Dp1Tyb twice (Lana-Elola et al., 2021, Tateossian et al., 2022). Both sets of Dp1Tyb mice had thresholds almost 30 dB above their WT littermates, which is moderately more severe than the 22 dB increase observed in Dp5Tyb mice.

These findings correlate with the OME incidence in these mice – Dp1Tyb have fully penetrant bilateral OME, whereas Dp5Tyb mice have unilateral or bilateral OME (*Figure 3.1*). When children develop OME they can lose 35-40 dB of hearing ability compared to their peers (Fortnum et al., 2014). A loss of only 16-25 dB is sufficient to negatively affect the development of a child with DS (Sacks and Wood, 2003).

The time points for ABR started a week later than epithelial measurements to allow time for the litter to be weaned before undergoing this procedure. The ABRs weren't carried out at one-year-old as mice on a C57BL/6 background are known to have age-related sensorineural hearing loss (Jeng et al., 2021), which would likely skew the data.

The investigation of cochlear hair cell morphology indicated that it is unlikely that Dp5Tyb mice have sensorineural hearing loss. Cochlear hair cells of four-week-old Dp1Tyb mice were examined with the same methods as two-month-old Dp5Tyb mice, and normal hair cell morphology was also found in Dp1Tyb mice (Tateossian et al., 2022). The combination of moderately raised ABR thresholds, no issues with hair cell morphology, and the presence of OME in both Dp5Tyb and Dp1Tyb supports the conclusion that these mice have conductive hearing loss. However, sensorineural hearing loss cannot be ruled out solely based on the experiments performed. A more informative test of cochlear function would be to record distortion product otoacoustic emissions (DPOAEs) (Abdala and Visser-Dumont, 2001).

Although 83% of hearing loss in children with DS has been attributed to conductive hearing loss (Balkany et al., 1979), the remainder must be caused by issues with the inner ear. The findings in this thesis suggest that Dp5Tyb mice are a good model for OME in DS, but may not fully recapitulate the mixed hearing loss seen in humans with DS.

### CHAPTER 3: Phenotypic characterisation of Dp5Tyb mice

One approach to further test this conclusion would be to quantify spiral ganglion neuron (SGN) density. These neurons relay signals from the cochlear hair cells to the brain, but after the onset of sensorineural hearing loss the neurons degenerate irreversibly (Otte et al., 1978). If the SGN density of Dp5Tyb mice is not significantly different to WT it would support the hypothesis that there is no sensorineural component to the reduced hearing seen in Dp5Tyb mice.

The middle ear ossicles and tympanic membranes of Dp5Tyb mice are indistinguishable from WT. This suggests that the conductive hearing loss is due to the fluid in the middle ear cavity associated with OME. A limitation of the microCT software used to image the ossicles is that it doesn't offer the ability to measure the volume or density of the bones. Although from visual inspection of the three-dimensional images the WT and Dp5Tyb ossicles look the same, there could be a difference in size or composition that we are unable to detect with this method. Some have used Mimics software for 3D volume measuring of the ossicles after microCT (Shin, 2021). Others have used the same software as us to reconstruct the image slices (Skyscan NRecon), but then used additional programmes (Skyscan CTAn and Skyscan CTVol) to carry out morphometric analysis and volumetric mineral density of the ossicle bones (Chen et al., 2016b). This analysis is outside of the timescale available for this DPhil project, but would likely be required for publication of the microCT data. Histological analysis of the joints between the ossicles could also be performed, as studies have found the cartilage to be thicker in people with DS (Fausch and Roosli, 2015).

The Deafness lab found that Dp1Tyb mice had larger alveoli than their WT littermates (mean linear intercept: WT males = 28.54  $\mu\text{m}$ , Dp1Tyb males = 32.22  $\mu\text{m}$ ,  $p < 0.05$ ; WT females = 28.38  $\mu\text{m}$ , Dp1Tyb females = 31.22  $\mu\text{m}$ ,  $p < 0.05$ ; data not

published). This lung phenotype was replicated in Dp5Tyb mice, although not quite as severe. With sexes combined, the mean Lm value for Dp1Tyb is 3.26  $\mu\text{m}$  higher than WT littermates. For Dp5Tyb the mean Lm value is 1.98  $\mu\text{m}$  higher than WT. Both p values are  $< 0.05$ . Emphysema was previously found in non-DS models for OME suggesting widespread issues with the epithelial lining. A limitation of this experiment could be the type of measurements carried out. The Lm calculation is not a direct measurement of alveolar size, instead it gives the “mean free distance in the air spaces” (Knudsen et al., 2010). It could be more informative to study the size and number of alveoli *in situ* using non-invasive propagation-based phase contrast x-ray (PB-PCX) imaging (Leong et al., 2014).

Many have noted the impact of trisomy on the craniofacial morphology of both humans and mice with DS (Richtsmeier et al., 2000, Starbuck et al., 2011). Dp5Tyb mice have a significantly shorter frontal bone length, and a trend of narrower frontal bone width compared to WT littermates. Dp1Tyb mice follow the same trend of shorter frontal bone length, and also have significantly wider frontal bones than WT littermates (Tateossian et al., 2022). Others have also measured the skull shape of Dp1Tyb mice and found abnormalities (Toussaint et al., 2021, Lana-Elola et al., 2021). TcMAC21 mice (duplication of Hsa21 long arm) have shorter and wider faces than WT littermates, and a more rounded head (Kazuki et al., 2020). These are similar phenotypes to those seen in Dp1Tyb mice (*Figure 3.9a*) (Tateossian et al., 2022). The method I used to measure the skull was fairly limited in the amount of information provided. Although this method allowed direct comparison with the Dp1Tyb data collected by the Deafness lab, it didn't provide the three-dimensional volumetric analysis needed to study the differences between Dp5Tyb and WT skulls in detail. Others have used microCT imaging overlaid with three-dimensional coordinates of anatomical landmarks to study craniofacial morphology in more detail

(Singh et al., 2016). A more in-depth analysis might have identified craniofacial abnormalities which could alter Eustachian tube drainage. Craniofacial defects and hypotonia are thought to contribute to Eustachian tube dysfunction in children with DS, which likely hinders drainage of middle ear fluid (Ghadersohi et al., 2018). Measurements were taken of the bony part of the Eustachian tube of Dp1Tyb mice, but no significant differences in size were noted between Dp1Tyb and WT littermates (Tateossian et al., 2022). However, a more informative study might be to measure the angle of the Eustachian tubes within the skull. The craniofacial defects associated with DS could cause the Eustachian tubes to develop at a shallower angle, thereby impeding drainage of fluid from the middle ear. Anatomical features of the Eustachian tube were recently studied in sheep using histological sectioning, cone-beam computed tomography and 3Dslicer software to generate a three-dimensional model (Schuon et al., 2021). It would be interesting to carry out this analysis on Dp1Tyb and Dp5Tyb mice in the future.

In summary, the DS phenotypes seen in Dp1Tyb are also present in Dp5Tyb. Some phenotypes, such as raised hearing thresholds, the lung phenotype and craniofacial defects are more moderate than in Dp1Tyb. In addition, while Dp1Tyb shows fully penetrant OME, there is a mixture of bilateral and unilateral OME in Dp5Tyb. Thus a major locus contributing to OME is present within the Dp5Tyb region. This locus accompanied by a minor locus present in Dp9Tyb presumably contribute to the fully penetrant phenotype seen in Dp1Tyb.

The next steps for this project will be to further investigate the OME phenotype of Dp5Tyb mice, examining the cellular composition of the middle ear effusion, evaluating whether the middle ear environment is hypoxic, and investigating whether trisomy of the Dp5Tyb genes affects ciliogenesis.

# CHAPTER 4: Further exploration of the Dp5Tyb otitis media phenotype

---

## 4.1. Introduction

Otitis media (OM) is a term used to describe inflammation of the middle ear, and consists of thickening of the epithelial lining (mucoperiosteum) and the accumulation of fluid (effusion) in the middle ear cavity, usually containing white blood cells (Bhutta et al., 2019). OME occurs without the presence of a pathogen (Rosenfeld et al., 2016), and is a very common disease in children, with around 80% suffering from OME at least once by the age of 10 (Schilder et al., 2016). Incidence amongst children with DS is even higher, with up to 93% experiencing conductive hearing loss at some point, mainly due to OME (Fortnum et al., 2014).

The middle ear is lined with ciliated epithelium and goblet cells (Luo et al., 2017). The goblet cells secrete mucins (the main component of mucus). The mucus traps dust and airborne pathogens which the ciliated epithelial cells then waft down the Eustachian tube towards the nasopharynx. As for mucociliary clearance of the airways, the mucus is then expelled from the body (by coughing or sneezing) or swallowed so any pathogens are neutralised by the stomach acid (Bustamante-Marin and Ostrowski, 2017). The ciliated epithelium of the middle ear is derived from two distinct developmental origins. The neural crest epithelium lines the dorsal surface, and the endoderm epithelium covers the ventral surface and the Eustachian tube (Thompson and Tucker, 2013). The dorsal region is littered sparsely with bundles of cilia, whereas the ventral region is covered with a lawn of cilia. The motile cilia in the ventral region are orientated towards the Eustachian tube entrance, and waft debris down the Eustachian tube to the nasopharynx. When OME is present, mucociliary

clearance is not fully functional as cellular fluid accumulates in the middle ear (Luo et al., 2017).

The contents of the cellular fluid provides information about the processes that are happening during OME. The balance of macrophages and neutrophils is indicative of the stage of inflammatory response. Leukocytes, such as neutrophils, are recruited to the site of inflammation first, then macrophages arrive later (Butterfield et al., 2006). Once neutrophils have performed their roles in resolving inflammation (Rosales, 2018) they become apoptotic and are engulfed by macrophages (Kourtzelis et al., 2017). Markers for proliferation (such as Ki67) offer insight into how the mucoperiosteum thickens, and apoptosis markers (such as cleaved caspase 3) could indicate that the cause of inflammation is under control by the immune system.

The blockage of the middle ear cavity with fluid prevents oxygen from reaching the mucoperiosteum, leading to a hypoxic environment (Huang et al., 2012). Hypoxia causes the stabilisation of HIF-1 $\alpha$  (hypoxia-inducible factor 1 $\alpha$ ), which is degraded under normoxic conditions. HIF-1 $\alpha$  is a transcription factor which goes on to activate the downstream genes *Il1 $\beta$*  (interleukin 1 $\beta$ ), *Tnfa* (tumour necrosis factor  $\alpha$ ) and *Vegfa* (vascular endothelial growth factor A). The protein products of these genes are involved in promoting inflammation and enhancing blood vessel endothelium permeability to serum and immune cells (Huang et al., 2012), which leads to fluid accumulation in OME.

This chapter will continue from Chapter 3 by further investigating the middle ear environment of Dp5Tyb mice. I will observe the cellular composition of the middle ear effusion, investigate the expression of hypoxia markers, and evaluate whether trisomy of the Dp5Tyb genes affects middle ear ciliogenesis.

## 4.2. Results

## 4.2.1. Incidence of OME in DS mouse lines relative to WT littermates

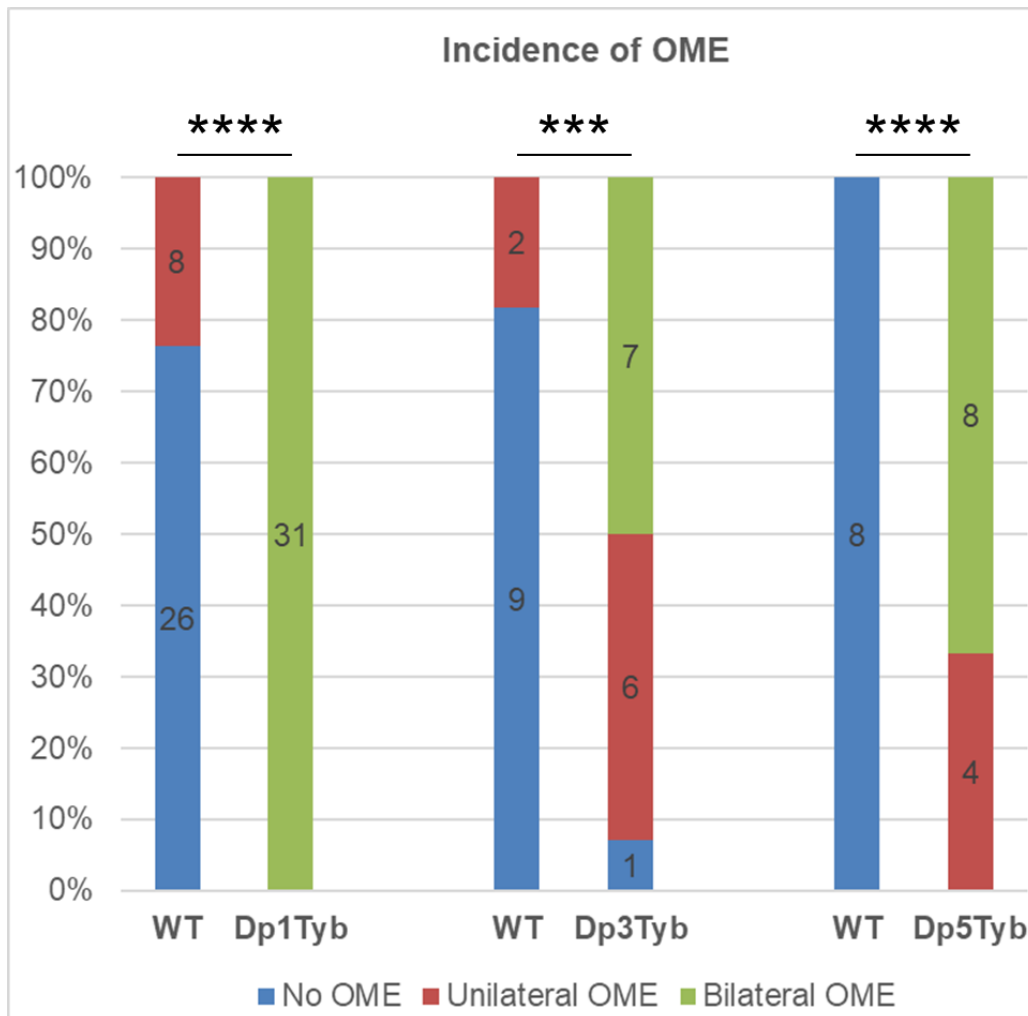


**Figure 4.1. Incidence of OME in Dp1Tyb, Dp3Tyb and Dp5Tyb compared to their respective WT littermates.** These were the main DpTyb lines used for this project. Data sourced from an extended data table in our recent publication, which also reports the OME incidence in the other DpTyb lines (Tateossian et al., 2022). Sample numbers are indicated on the bars. Dp1Tyb  $p < 0.0001$ ; Dp3Tyb  $p = 0.0002$ ; Dp5Tyb  $p < 0.0001$  (two-tailed unpaired t tests).

The OME incidence in all available DpTyb mouse strains was established in the Deafness lab before the start of my DPhil project. All Dp1Tyb mice had fully penetrant bilateral OME, and most Dp3Tyb mice had OME in at least one ear (Figure 4.1). To establish incidence of OME in two-month-old Dp5Tyb mice, histological sections from Dp5Tyb and WT mice were observed for the presence of thickened

epithelial lining in the middle ear. All Dp5Tyb mice had OME in one or both ears. This finding is included in a manuscript in preparation alongside the OME incidence found in other DpTyb mice (Tateossian et al., 2022) and the most relevant data for this project are presented here (*Figure 4.1*). Examples of Dp5Tyb sections with and without OME can be seen in Chapter 3 in *Figure 3.3*.

#### 4.2.2. Dp5Tyb mice do not appear to have more goblet cells than WT littermates at two-months-old

The epithelial lining of the middle ears contains goblet cells, which secrete mucins, the main component of mucus (Liu et al., 2017). As Dp5Tyb mice have OME, I investigated whether an increased presence of goblet cells was responsible for the accumulation of fluid in the middle ear. Goblet cells are mainly found at the entrance to the Eustachian tube (Thompson and Tucker, 2013, Liu et al., 2017). The literature suggests that more goblet cells are found in areas densely populated with cilia, such as within the bony part of the Eustachian tube, and amongst the ventral lawn of cilia around the entrance to the tube (Lim et al., 1973).

Histological sections of each mouse's head were cut in the transverse plane, at several depths to allow the whole middle ear cavity to be observed (see *Figure 2.2* in methods chapter). As goblet cells are usually concentrated around the Eustachian tube deeper sections were selected for this study. Sections were stained by the Histology department with Alcian Blue Periodic Acid Schiff (AB-PAS) to visualise mucins. The stain colours acidic mucins blue and neutral mucins magenta. The main function of goblet cells is to secrete mucins and therefore this staining method was used to highlight the goblet cells in the middle ear epithelium. Visual observation of

the sections (*Figure 4.2*) found no marked increase in goblet cells in Dp5Tyb middle ears compared to those of WT littermates.

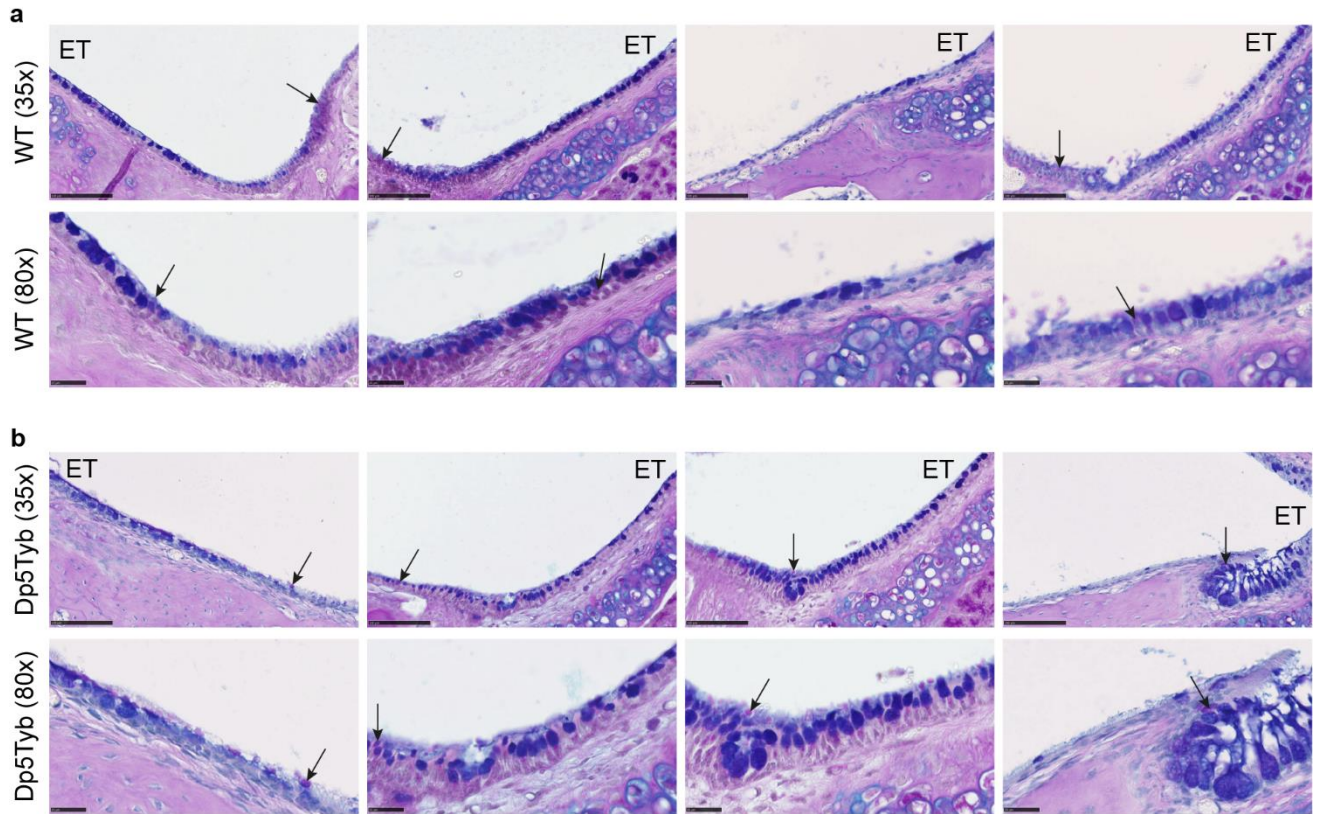


**Figure 4.2. Alcian Blue Periodic Acid Schiff (AB-PAS) staining of the middle ear epithelial lining near the Eustachian tube entrance.** (a) WT sections (n = 5) and (b) Dp5Tyb sections (n = 8) at 35x and 80x magnification. Scale bars = 100  $\mu$ m for 35x magnification and 25  $\mu$ m for 80x magnification images. AB-PAS stains mucins, which are secreted by goblet cells. Acidic mucins are stained dark blue, and neutral mucins are stained magenta. Arrows are positioned to aid with identifying some of the neutral mucins. ET = Eustachian tube, text positioned to indicate the direction of the tube in relation to the section. All mice were two-months-old. AB-PAS staining was performed by the Histology department at MRC Harwell.

### 4.2.3. Dp5Tyb and Dp3Tyb mice have impaired middle ear cilia maintenance at two months of age

To discover whether duplication of the Dp5Tyb or Dp3Tyb region leads to a developmental defect regarding middle ear ciliogenesis scanning electron microscopy (SEM) images of the middle ears of Dp3Tyb, Dp5Tyb and WT mice were observed. Due to the two distinct developmental origins of the ciliated epithelium (Thompson and Tucker, 2013), the dorsal and ventral regions of the middle ear were imaged separately. Visual observations were used to draw conclusions about cilia morphology and number, and representative images from each region, age and genotype are presented in *Figure 4.3* and *Figure 4.4*.

The images indicate that the cilia in both the dorsal and ventral regions initially develop normally, as the Dp5Tyb and Dp3Tyb cilia are indistinguishable from WT at two weeks old (*Figure 4.3a*, *Figure 4.4a*). However, it appears that the DS mouse models have problems with cilia maintenance by two months old. For both the Dp5Tyb and Dp3Tyb mice the ventral lawn of cilia has extensive cilia loss, and some inflammation of the epithelial lining is present in both the dorsal and ventral regions (*Figure 4.3b*, *Figure 4.4b*). Some signs of inflammation are already present in the dorsal region of Dp5Tyb and Dp3Tyb mice at two weeks old, but this doesn't appear to affect ciliogenesis.

To ascertain the desired magnification, lower magnification images were taken of the two-month-old Dp5Tyb and WT middle ear. We then decided that 2500x magnification was optimum as it allowed individual cilia to be seen whilst still showing enough cilia to be representative of the whole region. Images at 350x magnification can be found in the Appendix. No images were taken for Dp3Tyb mice, or for either mouse line at two weeks old.

## CHAPTER 4: Further exploration of the Dp5Tyb otitis media phenotype

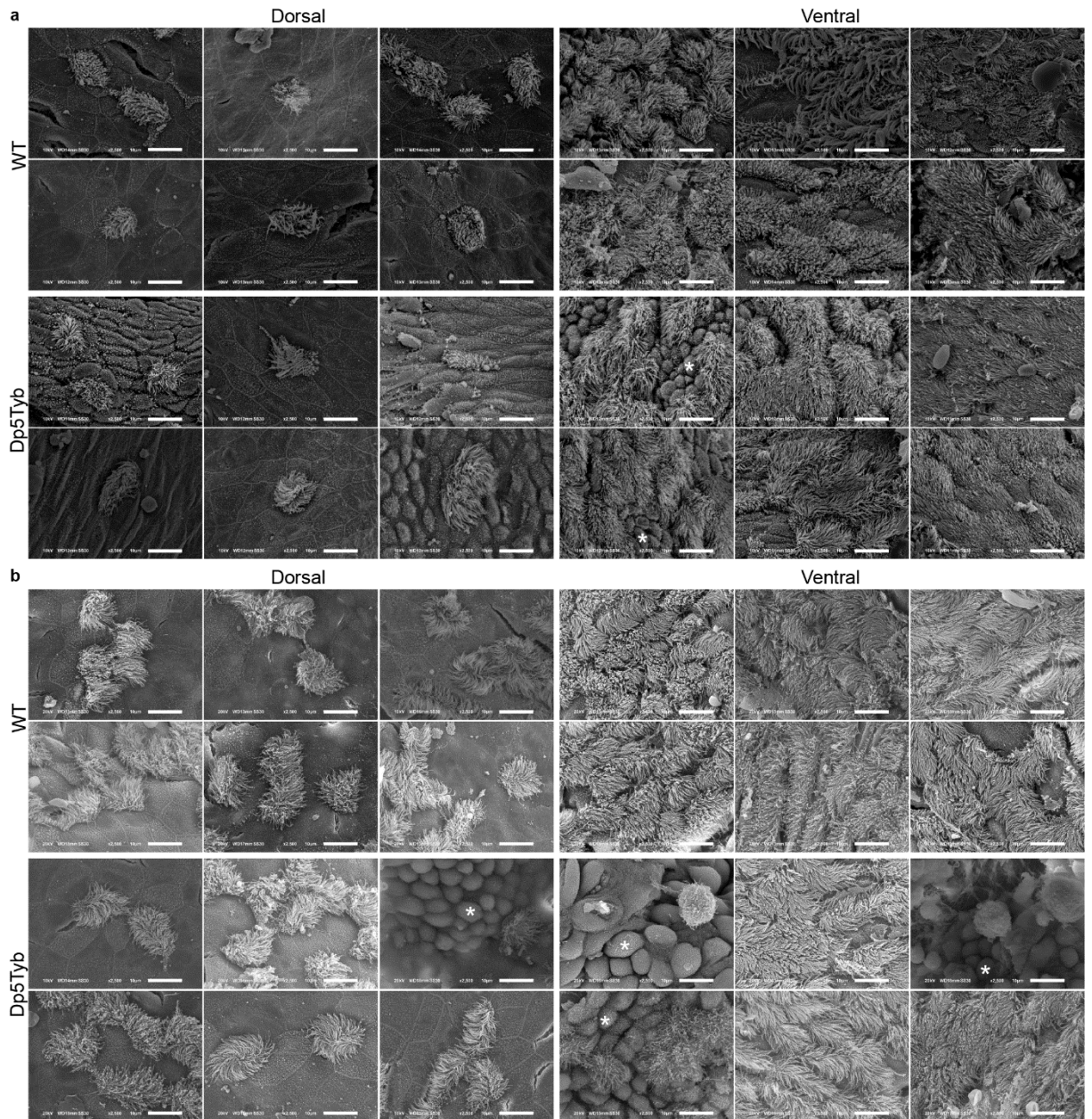


**Figure 4.3. Dp5Tyb middle ear cilia from the dorsal and ventral regions.** Scanning electron microscopy images of the middle ear cilia of (a) two-week-old and (b) two-month-old Dp5Tyb mice and WT littermates. Two-week-old: WT  $n = 3$ , Dp5Tyb  $n = 3$ ; two-month-old: WT  $n = 4$ , Dp5Tyb  $n = 6$ . Both ears of each mouse were explored, and the six images chosen for each panel are representative of the overall environment seen across that region. Asterisks indicate inflammation, seen as thickening of the epithelial lining. Magnification =  $\times 2500$ . Scale bar =  $10 \mu\text{m}$ . I shadowed Andy Parker while he took the two-month-old images, and then took the two-week-old images myself. Representative 350x magnification images of 2-month-old Dp5Tyb and WT middle ears are available in the Appendix.

## CHAPTER 4: Further exploration of the Dp5Tyb otitis media phenotype

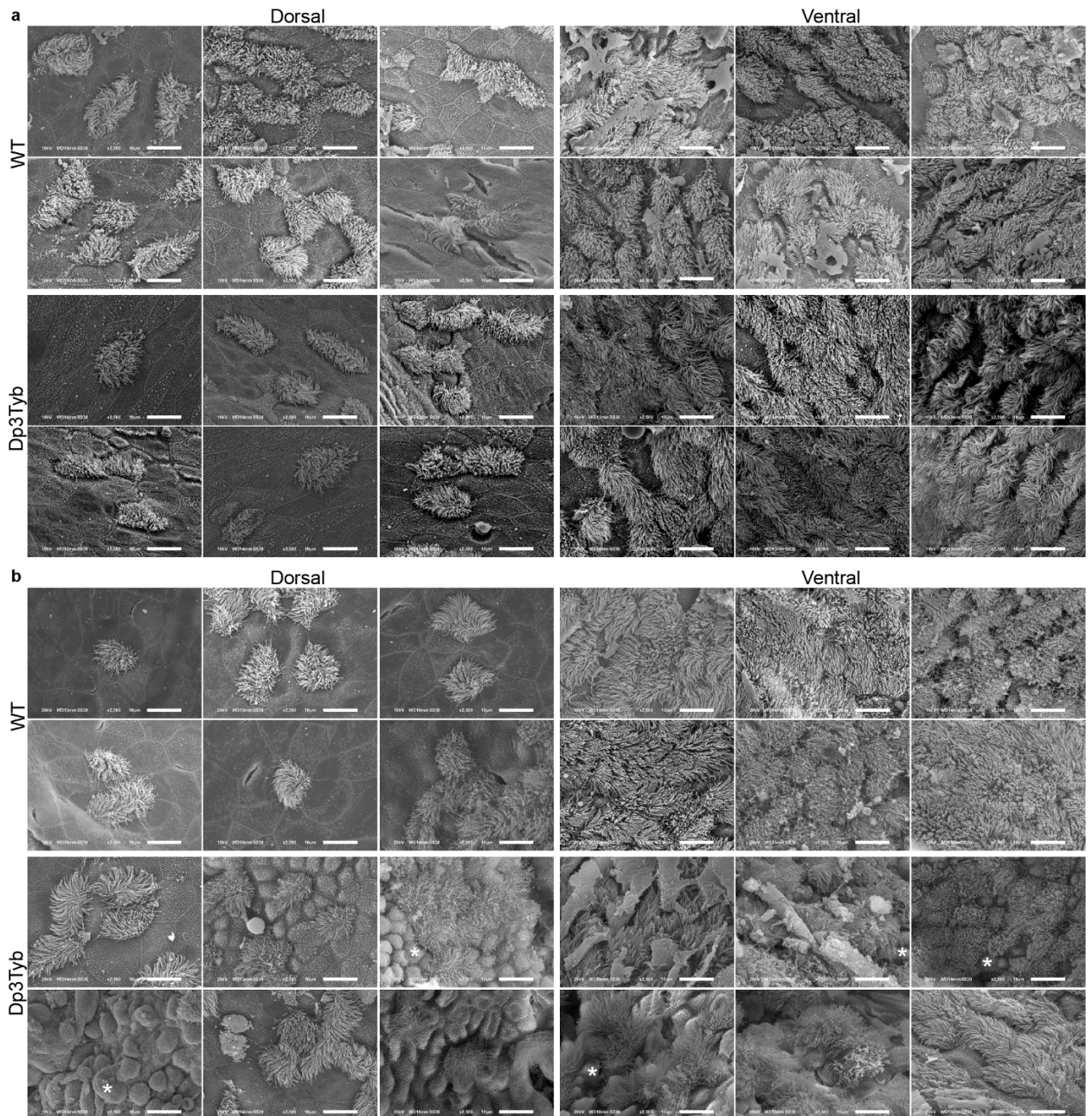


**Figure 4.4. Dp3Tyb middle ear cilia from the dorsal and ventral regions.** Scanning electron microscopy images of the middle ear cilia of (a) two-week-old and (b) two-month-old Dp3Tyb mice and WT littermates. Two-week-old: WT n = 3, Dp3Tyb n = 3; two-month-old: WT n = 3, Dp3Tyb n = 6. Both ears of each mouse were explored, and the six images chosen for each panel are representative of the overall environment seen across that region. Asterisks indicate inflammation, seen as thickening of the epithelial lining. Magnification = x2500. Scale bar = 10 μm. I shadowed Andy Parker while he took the two-month-old images, and then took the two-week-old images myself.

#### 4.2.4. Hypoxia and inflammation markers are upregulated in the middle ear of Dp5Tyb mice

In humans, hypoxia and inflammation-related genes are upregulated in the middle ear during an episode of OME (Bhutta et al., 2019, Juhn et al., 2008). The middle ears of non-DS mouse models of OME have been examined for hypoxia and inflammation markers, and the findings confirmed that hypoxia signalling is a common feature of chronic OME. The hypoxia inducible factor (*Hif1 $\alpha$* ) gene and downstream HIF-response genes *Tnfa* and *Vegfa* were upregulated in the middle ear fluid of *Jeff*, *Junbo* (Cheeseman et al., 2011) and *edison* (Crompton et al., 2017) mice. In addition, the protein levels of VEGF, TNF- $\alpha$  and IL-1 $\beta$  in ear effusions were found to be elevated in *Jeff*, *Junbo* and *Tgif1* knockout mice (Cheeseman et al., 2011, Tateossian et al., 2013). The DS mouse model Dp1Tyb also had elevated levels of these hypoxia and inflammation markers (Tateossian et al., 2022), so the expression of these genes in the Dp5Tyb middle ear at the transcript and protein level was investigated.

##### 4.2.4.1. Real time quantitative polymerase chain reaction (RT-qPCR)

To observe expression of hypoxia and inflammation markers at the transcript level, RNA was extracted from white blood cells (WBCs) and immune cells in the middle ear fluid of Dp5Tyb mice, and from the WBCs of their WT littermates. RT-qPCR was undertaken with primers for *Hif1 $\alpha$* , *Il1 $\beta$* , *Tnfa* and *Vegfa* (plus *Ppia* as the endogenous control). The expression levels in WT WBCs were used as a baseline control to which expression in Dp5Tyb WBCs and middle ear fluid was compared. It was not possible to collect WT middle ear fluid samples as WT mice have clear middle ears with no inflammation or fluid. WBCs were deemed a suitable control as

#### CHAPTER 4: Further exploration of the Dp5Tyb otitis media phenotype

the middle ear fluid comes from vascular leakage so the fluid should have a similar composition to blood serum. The key difference is that the Dp5Tyb middle ear is an inflamed and likely hypoxic environment so immune cells will have been recruited to the area. This can then be compared back to the gene expression occurring in the WBCs in circulation under normoxic and non-inflamed conditions.

The RT-qPCR dataset was inputted into R Software by a colleague at MRC Harwell, Heena Lad. The relative quantification (RQ) values were Tukey transformed based on the normality of the dataset. The p-values were calculated by multiple comparisons ANOVA with Tukey honest significant difference (HSD) using delta cycle threshold (Ct) mean values. The results showed that in Dp5Tyb middle ear fluid *Hif1 $\alpha$*  (11-fold,  $p < 0.0001$ ), *Tnfa* (59-fold,  $p < 0.0001$ ) and *Vegfa* (251-fold,  $p < 0.0001$ ) were all significantly upregulated compared to in WT WBCs, but the increase in *Il1 $\beta$*  was not significant (2-fold,  $p = 0.8830$ ). There was no difference in expression of any of the four genes between WT and Dp5Tyb WBCs (*Figure 4.5a*).

I also analysed the RT-qPCR data myself using GraphPad Prism software. Normality and descriptive statistics tests were used to ascertain whether the data were normally distributed and had equal standard deviations (SD). A one-way ANOVA was then performed on the data for each gene. Significantly more *Hif1 $\alpha$* , *Tnfa* and *Vegfa* was expressed in Dp5Tyb middle ear fluid compared to WT WBCs ( $p = 0.0025$ ;  $p = 0.0005$ ;  $p = 0.0005$ ) and also compared to Dp5Tyb WBCs ( $p = 0.0028$ ;  $p = 0.0001$ ;  $p < 0.0001$ ). There was no significant difference in *Il1 $\beta$*  expression regardless of tissue or genotype. No differences in expression were seen between WT and Dp5Tyb WBCs (*Figure 4.5b*). The experimental protocol used for Dp5Tyb mice was the same as the one used by others for Dp1Tyb mice. Their findings were very similar to the Dp5Tyb results (Tateossian et al., 2022).

CHAPTER 4: Further exploration of the Dp5Tyb otitis media phenotype

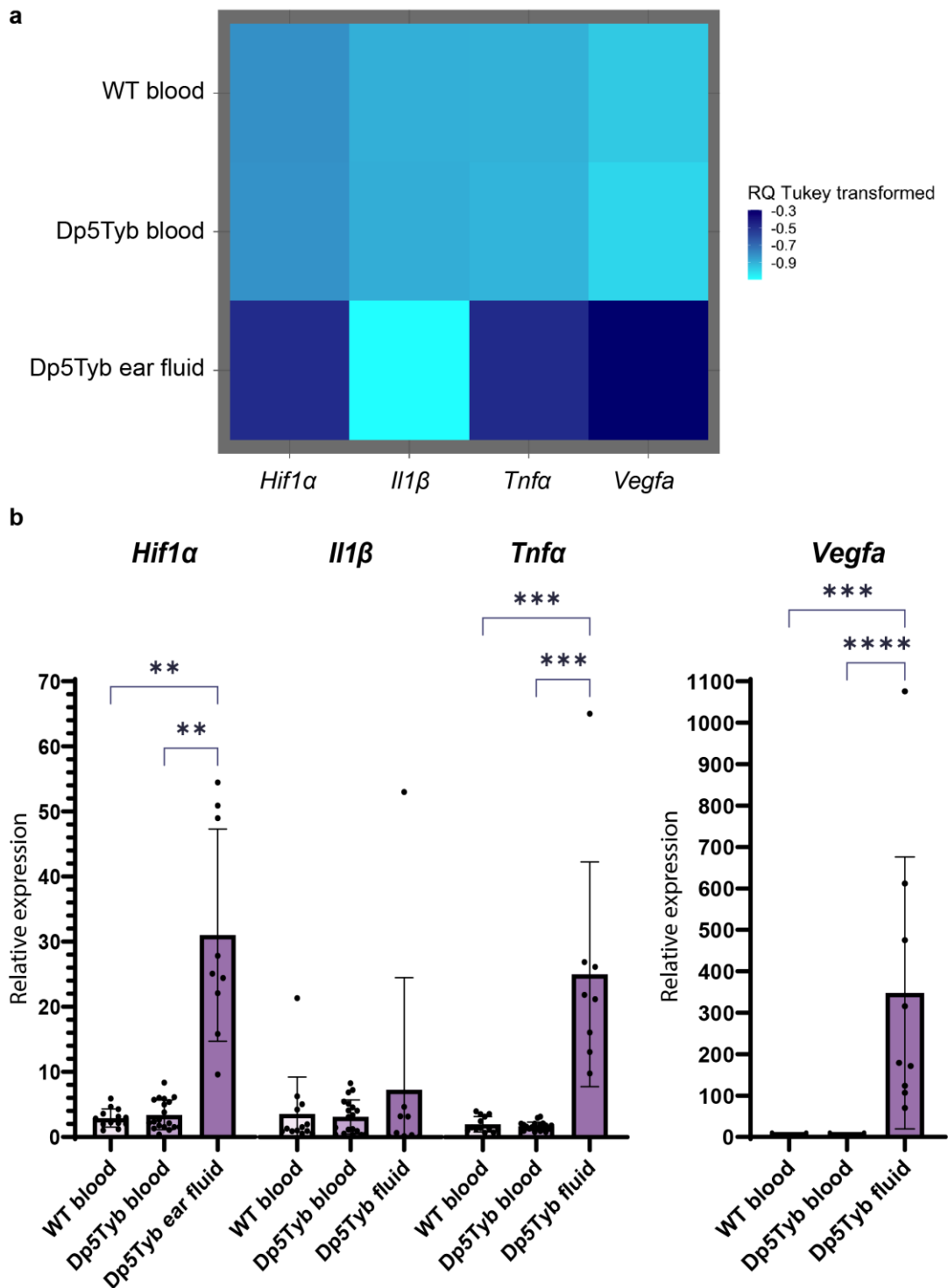


**Figure 4.5. RT-qPCR data from Dp5Tyb blood and middle ear fluid using primers for *Hif1a* and downstream genes.** Blood samples from Dp5Tyb and WT littermates were analysed alongside middle ear fluid from Dp5Tyb mice. (a) Tukey transformed RQ values represented as a heat map, with darker blue indicating higher expression. (b) Bar charts of the relative quantification (RQ) values. One data point per sample, which is an average of three technical replicates. Error bars show mean  $\pm$  standard deviation. WT blood n = 13; Dp5Tyb blood n = 19; Dp5Tyb ear fluid n = 9. P-values calculated using delta Ct values, and denoted according to: \*\*\*\*  $\leq$  0.0001, \*\*\* < 0.001, \*\* < 0.01, \* < 0.05. The RT-qPCR was performed with the support of Debbie Williams. The data were analysed and heat map generated by Heena Lad using R software. This heat map was included as extended data for our manuscript in preparation (Tateossian et al., 2022). GraphPad Prism software was used for the bar graphs and statistical analyses. A Brown-Forsythe and Welch ANOVA was performed for *Hif1a* as the data were normally distributed but had unequal SDs. A Kruskal-Wallis test (ANOVA) was performed for the other three as the data were not normally distributed.

## 4.2.4.2. Meso Scale Discovery (MSD) immunoassay

I then analysed expression of the hypoxia and inflammation markers at the protein level in WT and Dp5Tyb blood serum and Dp5Tyb ear fluid using a Meso Scale Discovery (MSD) immunoassay. An MSD plate measures the level of several proteins in the same sample using antibodies with fluorescent tags. The antibody for HIF-1 $\alpha$  was unavailable, but I proceeded with the antibodies for the downstream proteins IL-1 $\beta$ , TNF- $\alpha$  and VEGF-A.

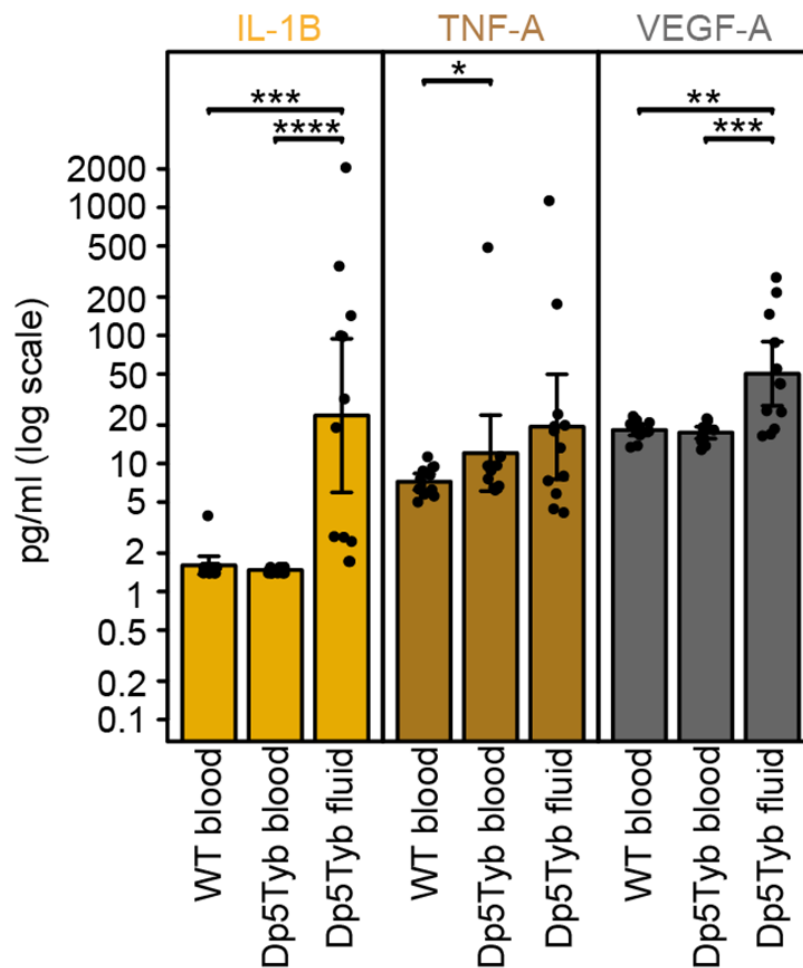


**Figure 4.6. Meso Scale Discovery (MSD) assay on WT and Dp5Tyb blood serum, and Dp5Tyb middle ear fluid.** Antibodies were used against IL-1 $\beta$ , TNF- $\alpha$  and VEGF-A, and the MSD plate reader quantified protein level in each sample. Technical replicates were averaged so each sample is represented as one data point on the graph. Error bars show mean  $\pm$  2 SEM (standard error of the mean). Mice were two months old. P-values denoted according to: \*\*\*\*  $\leq$  0.0001, \*\*\* < 0.001, \*\* < 0.01, \* < 0.05. WT blood n = 12; Dp5Tyb blood n = 12; Dp5Tyb fluid n = 12.

## CHAPTER 4: Further exploration of the Dp5Tyb otitis media phenotype

The results showed a significant upregulation of IL-1 $\beta$  ( $p = 0.0001$ ,  $p < 0.0001$ ) and VEGF-A ( $p = 0.0056$ ,  $p = 0.0009$ ) in Dp5Tyb fluid compared to WT blood serum and Dp5Tyb blood serum. TNF- $\alpha$  was expressed significantly more in Dp5Tyb serum compared to WT serum ( $p = 0.0205$ ) but the trend of increased expression of TNF- $\alpha$  in Dp5Tyb fluid was not significantly different to either WT ( $p = 0.1005$ ) or Dp5Tyb serum ( $p = 0.4776$ ) (*Figure 4.6*).

### 4.2.5. Macrophages and neutrophils are present in the inflamed Dp5Tyb middle ear, and there is widespread proliferation and cell death

To further study the middle ear environment, paraffin-embedded head sections from Dp5Tyb mice at three-weeks, four-weeks, two-months and four-months-old were stained for inflammatory markers using immunohistochemistry (IHC). The antibodies used were against F4/80 (macrophages), myeloperoxidase (MPO) (neutrophils), cleaved caspase-3 (CC-3) (apoptosis) and Ki67 (proliferation).

Histological examination of the Dp5Tyb sections (*Figure 4.7*) shows that the middle ear fluid of three- and four-week-old mice is more cellular than that of two- and four-month-old mice. This is likely due to the inflammation and recruitment of immune cells at the early stages of OME development. The epithelial lining gets thicker until two months, and then decreases slightly by four months of age. This is supported by the proliferation marker (Ki67) as positive cells are present at all time points, but more of the epithelial lining is stained brown (positive) at the earlier ages. The Ki67 staining suggests that proliferation happens mostly from the leading edge of the mucoperiosteum (proximal to the middle ear cavity) (*Figure 4.7*). Apoptotic cells (CC-3) are also present at all ages, with widespread cell death in the epithelial lining and fluid at three and four weeks, shifting to more apoptosis occurring in immune cells by two and four months.

## CHAPTER 4: Further exploration of the Dp5Tyb otitis media phenotype

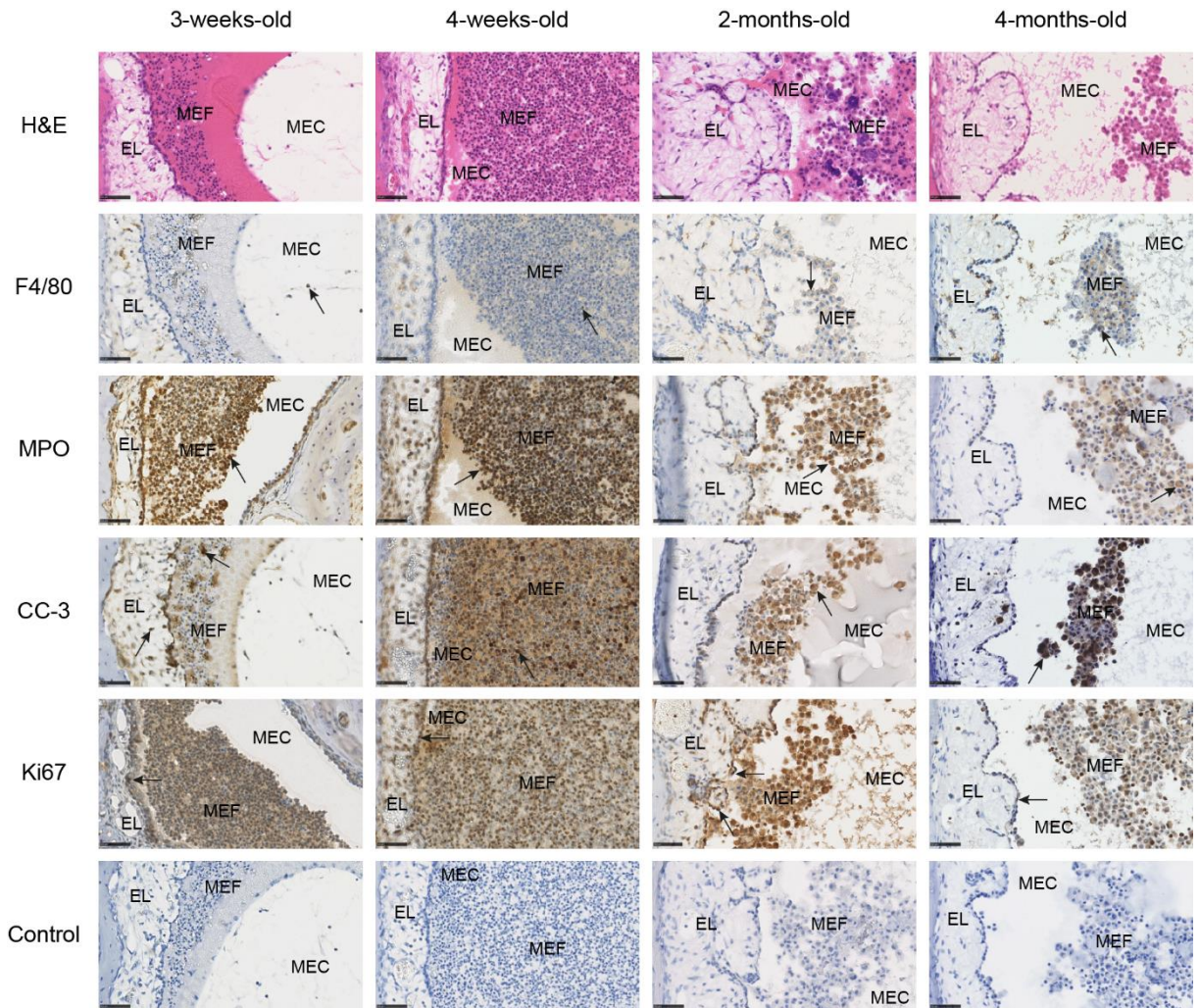


**Figure 4.7. Immunohistochemistry of proteins present in Dp5Tyb middle ear fluid.** Transverse head sections of Dp5Tyb mice were stained with haematoxylin and eosin (H&E) or antibodies against F4/80 (macrophages), MPO (neutrophils), CC-3 (apoptosis) or Ki67 (proliferation). Positive cells are stained brown, and examples are highlighted with arrows. All antibodies were raised in rabbit, apart from F4/80 which was raised in rat. Control sections underwent the same staining process but without a primary antibody to check for non-specific binding of the secondary antibody. A separate control section was used for the anti-rat secondary and no staining was seen (data not shown). Three weeks n = 1; four weeks n = 1; two months n = 3; four months n = 2. H&E = haematoxylin and eosin; MPO = myeloperoxidase; CC-3 = cleaved caspase-3; EL = epithelial lining; MEF = middle ear fluid; MEC = middle ear cavity. Scale bar = 50  $\mu$ m.

The IHC suggests that more neutrophils than macrophages are present in the fluid at all time points. Neutrophils are one of the first leukocytes to be recruited to the site of inflammation. Once they have coordinated the immune response they become apoptotic and are phagocytosed by macrophages (Kourtzelis et al., 2017). The

stained sections suggest that the proportion of neutrophils decreases as the mice age whilst the proportion of macrophages increases.

WT middle ear sections were also stained with the same antibodies, but unfortunately as they only have a single cell layer of middle ear epithelium the sections lifted during antigen retrieval and I was unable to obtain images. Examples of H&E stained WT middle ears can be seen in *Figure 3.3* in Chapter 3.

### 4.3. Discussion

The fully penetrant bilateral OME seen in Dp1Tyb mice is likely to be caused by two or more dosage-sensitive genes on Mmu16, including a major locus in the Dp5Tyb region. This is because although OME is highly penetrant in Dp5Tyb mice, some Dp5Tyb mice only present with unilateral OME. A minor locus maps to the Dp9Tyb region. Around half of Dp9Tyb mice present with OME (see *Figure 3.1* in Chapter 3). The Dp9Tyb region contains 76 protein coding genes, of which 45 are orthologous to genes on Hsa21 (Lana-Elola et al., 2016). The Tybulewicz lab have been working on dividing the Dp9Tyb region into three further lines - Dp10Tyb, Dp11Tyb and Dp12Tyb. Dp12Tyb is now available and analysis of middle ears demonstrates that they do not develop OME. This suggests the minor locus is located in the Dp10Tyb or Dp11Tyb regions. Dp10Tyb mice are currently being genetically engineered at the Francis Crick Institute.

Whilst further exploring the OME phenotype of Dp5Tyb mice, AB-PAS stained middle ear sections were examined to see if increased numbers of goblet cells were responsible for the chronic middle ear effusion. No quantification was performed, but through visual observation no obvious increase in goblet cells was found at the entrance to the Eustachian tube in Dp5Tyb mice compared to WT littermates. This

#### CHAPTER 4: Further exploration of the Dp5Tyb otitis media phenotype

was unexpected, as the literature suggests that during OME in humans middle ear basal epithelial cells differentiate into goblet cells, which proliferate throughout the mucoperiosteum and secrete mucins - the main component of middle ear fluid (Smirnova et al., 2002). Goblet cells were found to respond to TNF- $\alpha$  and IL-1 $\beta$  by secreting pro-inflammatory IL-8, which then stimulates the goblet cells to secrete mucins (Smirnova et al., 2002). Although increased goblet cell proliferation was not observed in the Dp5Tyb mucoperiosteum, there may be increased mucin secretion from goblet cells in response to the upregulated TNF- $\alpha$  and IL-1 $\beta$  present in the middle ear. Future work could include quantifying the results from the AB-PAS staining. Quantification wasn't carried out due to difficulty distinguishing between some of the neutral mucins and the unstained epithelial cells.

Motile cilia play an important role in keeping the middle ear and airways clear of mucus and debris (Luo et al., 2017). SEM images of the middle ear cilia of Dp5Tyb and Dp3Tyb mice were examined for altered cilia morphology. At two months old, Dp5Tyb and Dp3Tyb middle ears had extensive cilia loss, mainly in the ventral region. Both DS lines had dorsal and ventral cilia indistinguishable from their WT littermates at two weeks old, indicating no developmental defect regarding ciliogenesis. Therefore, impaired cilia development is not the cause of their chronic OME. It is possible that the subsequent cilia loss is a secondary effect of the developing OME. No experiments were carried out to observe the motile function of cilia in both DpTyb lines. However, studying cilia function both before and after the onset of OME would be an interesting avenue for future work, employing for example high speed video microscopy of live cilia, as described by (Rumman et al., 2017). In conclusion, as cilia appear normal at two weeks of age, it seems unlikely that impaired ciliary function caused by duplication of the Dp5Tyb genes is primarily responsible for the development of chronic OME in these mice.

#### CHAPTER 4: Further exploration of the Dp5Tyb otitis media phenotype

Hypoxia induces the stabilisation of HIF-1 $\alpha$ , which then upregulates the downstream genes *Il1 $\beta$* , *Tnfa* and *Vegfa* (Huang et al., 2012). Upregulation of these inflammation and hypoxia markers at the transcript and protein level were observed in Dp5Tyb mice, although some results were not statistically significant (*Il1 $\beta$*  at the transcript level, and TNF- $\alpha$  at the protein level). These data are very similar to what was found in Dp1Tyb mice (Tateossian et al., 2022).

The hypoxic middle ear environment has also been observed in other mouse models of OME. RT-qPCR with samples from *Jeff* and *Junbo* mice found that transcript levels of *Hif1 $\alpha$* , *Il1 $\beta$* , *Tnfa* and *Vegfa* were all significantly upregulated in the white blood cells (WBCs) of bulla fluid compared to WBCs from blood serum (Cheeseman et al., 2011). Similar findings were reported for the *edison* mouse model (Crompton et al., 2017). As with the Dp5Tyb mice, *Vegfa* was the most upregulated and *Il1 $\beta$*  the least upregulated transcript in *edison* bulla fluid (Crompton et al., 2017). Moreover, it was recently reported that three of these key genes were significantly upregulated in Dp1Tyb middle ear fluid compared to WT WBCs (*Hif1 $\alpha$* : 30-fold,  $p < 0.0001$ ; *Tnfa*: 16-fold,  $p < 0.0001$ ; *Vegfa*: 260-fold,  $p < 0.0001$ ) (Tateossian et al., 2022). There was no significant increase in *Il1 $\beta$*  expression (2-fold,  $p = 1$ ).

At the protein level, *Junbo* mice had upregulated IL-1 $\beta$ , TNF- $\alpha$  and VEGF-A in their middle ear fluid compared to blood (Cheeseman et al., 2011). The same protein assays were performed on *Jeff* samples, but the results for IL-1 $\beta$  and TNF- $\alpha$  were inconclusive as most samples were below detection threshold. However, VEGF-A was significantly upregulated in bulla fluid compared to blood (Cheeseman et al., 2011). *Tgif1* homozygous knockout mice demonstrate OME and showed elevated expression of VEGF, TNF- $\alpha$  and IL-1 $\beta$  proteins in their middle ear fluid compared to blood serum of the same mice (Tateossian et al., 2013). Dp5Tyb mice had

#### CHAPTER 4: Further exploration of the Dp5Tyb otitis media phenotype

significantly upregulated IL-1 $\beta$  and VEGF-A in their middle ear fluid compared to blood of the same animals and WT littermates. The increased expression of TNF- $\alpha$  was not statistically significant.

It has also been shown that artificially inducing hypoxia in the middle ear (by blocking the Eustachian tubes of rats) leads to OME (Huang et al., 2012). Transcript levels of *Hif1 $\alpha$* , *Il1 $\beta$* , *Tnfa* and *Vegfa*, and protein levels of HIF-1 $\alpha$  and VEGF were measured in the middle ear fluid of rats with OME and control rats with functional Eustachian tubes (Huang et al., 2012). They found that all of the genes were significantly upregulated in the rats with OME, which supports our findings in mice. A hypoxic middle ear environment has also been reported in humans with OME (Sekiyama et al., 2011).

Human studies have confirmed the presence of VEGF at both the transcript and protein level in middle ear fluid (Jung et al., 1999, Val et al., 2018). Others have also found VEGF levels to be higher in the middle ear fluid than in blood serum (Sekiyama et al., 2011) suggesting that the VEGF is being produced locally in the middle ear. VEGF has been shown to induce the formation of new blood vessels (angiogenesis) and increase vascular permeability (Sekiyama et al., 2011, Kim et al., 2005, Nagy et al., 2008). This allows blood serum, neutrophils and lymphocytes to enter the middle ear cavity and form the characteristic middle ear fluid of OME (Husseman et al., 2012).

Hypoxia and the presence of pro-inflammatory cytokines, such as TNF- $\alpha$ , lead to increased release of VEGF by epithelial cells (Sun et al., 2005). The hypoxic conditions caused by the accumulation of fluid in OME could therefore be exacerbating the condition as VEGF activation will further enhance vascular leakage of fluid and immune cells into the middle ear cavity (Sekiyama et al., 2011). The

#### CHAPTER 4: Further exploration of the Dp5Tyb otitis media phenotype

hypoxia marker pimonidazole has been used to demonstrate that the middle ear environment of *Junbo* mice was hypoxic (Cheeseman et al., 2011). Moreover, they showed that systemic administration of VEGF receptor inhibitors ameliorated the OME phenotype of *Junbo* mice as demonstrated by improved hearing, reduced angiogenesis and reduced middle ear fluid levels.

The cell types in the ear fluids were analysed histologically and by fluorescence-activated cell sorting (FACS) analysis in our lab. Granulocytes, monocytes and macrophages were found in the fluid from *Tgif1* knock out mice (Tateossian et al., 2013). Granulocytes, such as neutrophils, were the first to be recruited to the inflamed middle ear of *edison* mice at four weeks of age. By two months macrophages were also present (Crompton et al., 2017). Monocytes, neutrophils, lymphocytes and macrophages were detected in *Junbo* mice ear fluid (Vikhe et al., 2019). Neutrophils, monocytes and lymphocytes were found in Dp1Tyb mice (unpublished data). Lymphocytes and neutrophils produce VEGF (Sekiyama et al., 2011), and also release cytokines (IL-1 $\beta$ , IL-6 and TNF- $\alpha$ ) which upregulate VEGF production (Angelo and Kurzrock, 2007).

In Dp5Tyb mice, neutrophils were more common at three and four weeks old, and macrophages increased in number from two months onwards. This is in line with the literature that shows neutrophils arrive at the site of inflammation first, then become apoptotic and are engulfed by macrophages (Kourtzellis et al., 2017). In Dp5Tyb middle ear fluid IL-1 $\beta$  was significantly upregulated at the protein level, and TNF- $\alpha$  at the transcript level. These inflammatory cytokines enhance the differentiation of naïve T cells into pro-inflammatory IL-17-producing helper T cells (Th17), which promote neutrophil accumulation (Veldhoen et al., 2006).

#### CHAPTER 4: Further exploration of the Dp5Tyb otitis media phenotype

In summary, Dp5Tyb mice, like other mouse models of chronic OME, demonstrate upregulation of pro-inflammatory cytokines, Il-1 $\beta$  and TNF- $\alpha$ , either at the transcript or protein level. In addition, there are raised levels of *Hif-1a* (at the transcript level) and VEGF-A reflecting a hypoxic middle ear environment, and in the case of VEGF-A contributing to enhanced angiogenesis and vascular leakage, exacerbating the accumulation of fluid in the middle ear. The development of middle ear goblet cells appears normal. In addition, the middle ear ciliated epithelium appears to develop normally, but as Dp5Tyb and Dp3Tyb mice age there is loss of ciliated cells. It is possible that this loss of ciliated cells is secondary to the development of OME but is a contributory factor to the ongoing condition.

This chapter concludes the investigation into the first aim of this thesis – phenotypic characterisation of Dp5Tyb mice. The next aim is to study the expression of the 12 genes in the Dp5Tyb region at transcript and protein level, to better understand which gene(s) may be involved in OME pathogenesis. In the next chapter I will also address the third aim of this thesis – generation and phenotypic analysis of double mutants.

# CHAPTER 5: Middle ear expression of the 12 genes in the Dp5Tyb region, and analysis of double mutants

---

## 5.1. Introduction

Otitis media with effusion (OME) is a very common Down syndrome (DS) phenotype, affecting up to 93% of one-year-olds with DS (Barr et al., 2011). To identify the genetic cause of this predisposition to chronic middle ear inflammation, previous members of the Deafness lab (Harwell) used mice with segmental duplications of human chromosome 21 (Hsa21) orthologues on mouse chromosome 16 (Mmu16) (Tateossian et al., 2022). Using a mapping panel and DS mouse models engineered by the Tybulewicz lab (Lana-Elola et al., 2016), the duplication required to cause OME was narrowed down to Dp5Tyb, a region which contains only 12 genes. All mice with a duplication of the Dp5Tyb region have OME in one or both ears (see Introduction, *Figure 1.3*). This suggests that there are dosage-sensitive gene(s) in the Dp5Tyb region that, when present in three copies, play a role in OME pathogenesis. Investigating the expression of the Dp5Tyb genes at the mRNA and protein level in the middle ear could offer insight into the mechanisms involved.

The 12 genes in the Dp5Tyb region are: *Dyrk1a*, *Kcnj6*, *Kcnj15*, *Erg*, *Ets2*, *Psmg1*, *Brwd1*, *Hmgn1*, *Get1*, *Lca5l*, *Sh3bgr* and *B3galt5*. The University of Maryland gene expression analysis resource (gEAR) (<https://umgear.org/>) confirms expression of all 12 genes in murine cochlear sensory epithelium.

### 5.1.1. *Dual-specificity tyrosine-regulated kinase 1A (Dyrk1a)*

*Dyrk1a* encodes a protein kinase, a class of enzymes that phosphorylate proteins to alter their activity (Atas-Ozcan et al., 2021). The DYRK family of protein kinases are

CHAPTER 5: Middle ear expression of the 12 Dp5Tyb genes, and analysis of double mutants involved in cellular processes such as communication, growth and cell cycle regulation (Varjosalo et al., 2013).

Trisomy of *Dyrk1a* has been implicated in several DS phenotypes, including locomotor dysfunction (Watson-Scales et al., 2018) and craniofacial defects (McElyea et al., 2016). When *Dyrk1a* dosage was reduced to two copies in Ts65Dn mice the Alzheimer's disease phenotype was rescued (Garcia-Cerro et al., 2017), adding evidence to this conclusion.

The *Drosophila* homolog of murine *Dyrk1a* is *minibrain* (Tejedor et al., 1995).

Research using the *minibrain* mutant has identified that DYRK1A plays a role in neuronal development, as *minibrain* mutants have reduced neuronal proliferation (Atas-Ozcan et al., 2021). Overdose of *Dyrk1a* is thought to cause intellectual disability in DS (Courcet et al., 2012). Targeting this overdose with DYRK1A inhibitors has shown that the neurodevelopmental defects associated with DS could potentially be treated (Atas-Ozcan et al., 2021). Research has shown that DYRK1A inhibitors can be applied as a preventative measure in utero and also as a treatment in adult mouse models of DS (Atas-Ozcan et al., 2021).

### 5.1.2. Potassium Inwardly Rectifying Channel Subfamily J Member 6 (*Kcnj6*)

*Kcnj6* encodes the GABAB R-coupled G protein-coupled inward rectifying potassium channel subunit 2 (GIRK2). Overdose of this gene has been associated with infantile spasms in DS, as the phenotype was rescued when disomy of *Kcnj6* was restored (Joshi et al., 2016), but recently trisomy of *Kcnj6* alone was found to be insufficient to cause the seizures in Ts65Dn mice (Joshi et al., 2018).

Dosage of *Kcnj6* has been implicated in cognitive dysfunction in DS, as in Ts65Dn with restored disomy of *Kcnj6* short term and long term memory were improved

CHAPTER 5: Middle ear expression of the 12 Dp5Tyb genes, and analysis of double mutants (Kleschevnikov et al., 2017). Overdose of GIRK2 in the brain has also been linked to learning and behavioural deficits in Ts65Dn mice (Harashima et al., 2006).

### *5.1.3. Potassium Inwardly Rectifying Channel Subfamily J Member 15 (Kcnj15)*

*Kcnj15* encodes the potassium channel protein KCNJ15. Overexpression of *Kcnj15* (and *Kcnj6*) results in more inward rectifying potassium channels, reducing neuronal network activity in Ts65Dn and Tc1 mice, likely contributing to the cognitive defects seen in DS (Stern et al., 2015).

### *5.1.4. Erythroblast transformation-specific (ETS)-related gene (Erg)*

*Erg* encodes the transcription factor ERG. Ts1Cje mice have a Mmu16 duplication between *Sod1* and *Mx1*, which is slightly smaller than the duplication in Ts65Dn mice (Sago et al., 1998). Duplication of *Erg* leads to impaired neurogenesis and increased production of neutrophils in Ts1Cje DS mouse models, as these phenotypes were rescued when *Erg* dosage was reduced to two copies (Ishihara et al., 2020). Overexpression of ERG has also been linked to increased platelet production (Stankiewicz and Crispino, 2013).

### *5.1.5. Erythroblast transformation-specific (ETS) Proto-Oncogene 2 (Ets2)*

*Ets2* encodes the transcription factor ETS2. Activation of ETS2 plays a role in inflammation by promoting macrophage survival and the expression of inflammatory genes (Wei et al., 2004). Overexpression of *Ets2* in mice mirrors the DS phenotypes of increased apoptosis and an imbalance of lymphocytes (Wolvetang et al., 2003, Kusters et al., 2009). *Ets2* has also been linked to neurodegeneration in DS (Rueda et al., 2013). ETS2 activates the mitochondrial death pathway, and is upregulated in primary neurons in DS (Rueda et al., 2013). Overexpression of *Ets2* (and *Erg*) during cardiac development may contribute to the congenital heart defects commonly seen

CHAPTER 5: Middle ear expression of the 12 Dp5Tyb genes, and analysis of double mutants in children with DS (Bosman et al., 2015). Another member of the ETS family, *Ets1*, has been associated with craniofacial abnormalities and OM in heterozygous mice (Carpinelli et al., 2015).

#### *5.1.6. Proteasome Assembly Chaperone 1 (Psmg1)*

Little is known of the effects of an additional copy of *Psmg1* in DS. *Psmg1* may contribute to longevity in some rodent species, as it was a positively selected gene when the genomes of long-lived and short-lived rodents were compared (Sahm et al., 2018). *Psmg1* plays a role in proteasome assembly, ensuring correct protein folding and preventing the accumulation of misfolded proteins that lead to Alzheimer's disease (Sahm et al., 2018).

#### *5.1.7. Bromodomain and WD Repeat Domain Containing 1 (Brwd1)*

*Brwd1* encodes the nuclear protein BRWD1, which plays a role in regulating the transcription of many different genes (Huang et al., 2003). *Brwd1* was found to be upregulated in the brain of the Ts1Cje mouse model compared to WT mice (Ling et al., 2014).

#### *5.1.8. High Mobility Group Nucleosome Binding Domain 1 (Hmgn1)*

*Hmgn1* encodes HMGN1; a chromatin binding protein which modifies histone proteins and chromatin structure (Ling et al., 2014). HMGN1 negatively regulates methyl CpG-binding protein 2 (MeCP2) which influences gene expression in the brain (Abuhatzira et al., 2011). Overexpression of HMGN1 is likely to negatively affect normal brain development (Ling et al., 2014). *Hmgn1* was found to be expressed more in the Ts1Cje mouse brain than in WT mice, and this finding is in agreement with other literature (Ling et al., 2014, Pash et al., 1990, Dauphinot et al., 2005, Potier et al., 2006).

CHAPTER 5: Middle ear expression of the 12 Dp5Tyb genes, and analysis of double mutants

HMGN1 overexpression has also been linked to the increased incidence of acute lymphoblastic leukaemia (ALL) in people with DS, as it causes widespread transcriptional changes by promoting chromatin accessibility (Mowery et al., 2018). An inhibitor of HMGN1 has been suggested as a therapeutic target for ALL in DS, as knocking out *Hmgn1* halted the proliferation of the cancer cells in xenograft mouse models (Page et al., 2022).

#### 5.1.9. *Guided Entry of Tail-Anchored Proteins Factor 1 (Get1)*

This gene is also known as Tryptophan rich basic protein (*Wrb*). The protein produced has several common names, including WRB, GET1, and Congenital Heart Disease Protein 5 (CHD5). This protein is expressed in foetal hearts, and *Xenopus* research suggests it plays a role in cardiac development (Sojka et al., 2014). Congenital heart defects are common in DS, and the extra copy of *Wrb* could be involved (Sojka et al., 2014), although current mammalian research is limited. *Wrb* was also found to be upregulated in the Ts1Cje mouse brain compared to WT mice (Ling et al., 2014).

#### 5.1.10. *Leber Congenital Amaurosis 5-Like (Lca5l)*

*Lca5l* encodes the LCA5L protein, which is expressed in the cell cytoskeleton and is thought to be involved in intraciliary transport (Alliance of Genome Resources, 2022). A mutation in *Lca5l* leads to an autosomal recessive eye disease known as Leber Congenital Amaurosis 5 (Online Mendelian Inheritance in Man®, 2019). This gene has not been associated with any DS phenotypes.

#### 5.1.11. *SH3 Domain Binding Glutamate Rich Protein (Sh3bgr)*

SH3BGR is expressed mostly in cardiac and skeletal muscle, and is important for cardiomyocyte integrity and viability *in vitro* (Deshpande et al., 2021). SH3BGR was upregulated during cardiac hypertrophy in humans, and is hypothesised to play a role in congenital heart defects in DS (Deshpande et al., 2021).

### 5.1.12. *Beta-1,3-Galactosyltransferase 5 (B3galt5)*

*B3galt5* encodes B3GALT5, which glycosylates several protein and lipid targets (Hildebrandt et al., 2021). B3GALT5 promotes cell migration and tumour growth in cancer, with recent research being carried out on its role in breast cancer (Liao et al., 2021).

In addition to studying the expression of these genes, heterozygous mice for each Dp5Tyb gene were sourced from other mouse facilities. These knockouts only had one functional copy of the gene of interest due to a null or mutant allele. The knockouts were crossed to Dp5Tyb mice to create double mutant offspring. The exception is *Dyrk1a*<sup>+/-</sup>, which had instead been crossed to Dp3Tyb at the Francis Crick Institute. The double mutants have two copies of the gene of interest and three copies of the other Dp5Tyb (or Dp3Tyb) genes. If the OME phenotype seen in Dp5/3Tyb mice persists in the double mutants it will indicate that the dosage of the gene of interest is not involved in OME development. However, if the OME phenotype is rescued in the double mutants it will demonstrate that the gene of interest is dosage-sensitive and was contributing to OME pathogenesis when present in three copies in Dp5/3Tyb mice.

This chapter will address the second and third aims of this thesis. Firstly, studying expression of the 12 Dp5Tyb genes and their protein products in the middle ear. RT-qPCR will be used to observe changes in gene expression at the transcript level between WT and Dp5Tyb blood, WT and Dp5Tyb middle ear epithelium, and Dp5Tyb ear fluid. Expression at the protein level in the middle ear epithelium will then be quantified using immunohistochemistry. Finally, I will discuss the generation and phenotypic analysis of double mutants. If the OME phenotype of Dp5Tyb mice is rescued in the double mutants, this should identify the dosage-sensitive gene(s) responsible for causing OME in DS.

## 5.2. Results

### 5.2.1. Expression of the 12 Dp5Tyb genes at the RNA level

RNA was extracted from Dp5Tyb and WT white blood cells, Dp5Tyb and WT middle ear epithelium, and Dp5Tyb middle ear fluid. After checking the quality and quantity of RNA using a Bioanalyzer and NanoDrop respectively, the RNA was converted to cDNA and then RT-qPCR carried out with primers for the 12 Dp5Tyb genes plus an endogenous control gene, *Ppia*. The RT-qPCR and initial analysis were performed with the help of Debbie Williams from MRC Harwell. Analysis and visualisation of this large dataset was performed with the help of another colleague at MRC Harwell, Heena Lad. R software was used to perform statistical analysis, transform the data, and generate a heat map (*Figure 5.1a*). I also created a bar chart of the dataset to allow the statistical significance to be observed (*Figure 5.1b*).

Multiple ANOVA comparisons were carried out for each gene using delta Ct mean values. Initially male and female data were kept separate. But no significant difference in expression was found between male and female mice, so the data were combined and analysed together.

CHAPTER 5: Middle ear expression of the 12 Dp5Tyb genes, and analysis of double mutants

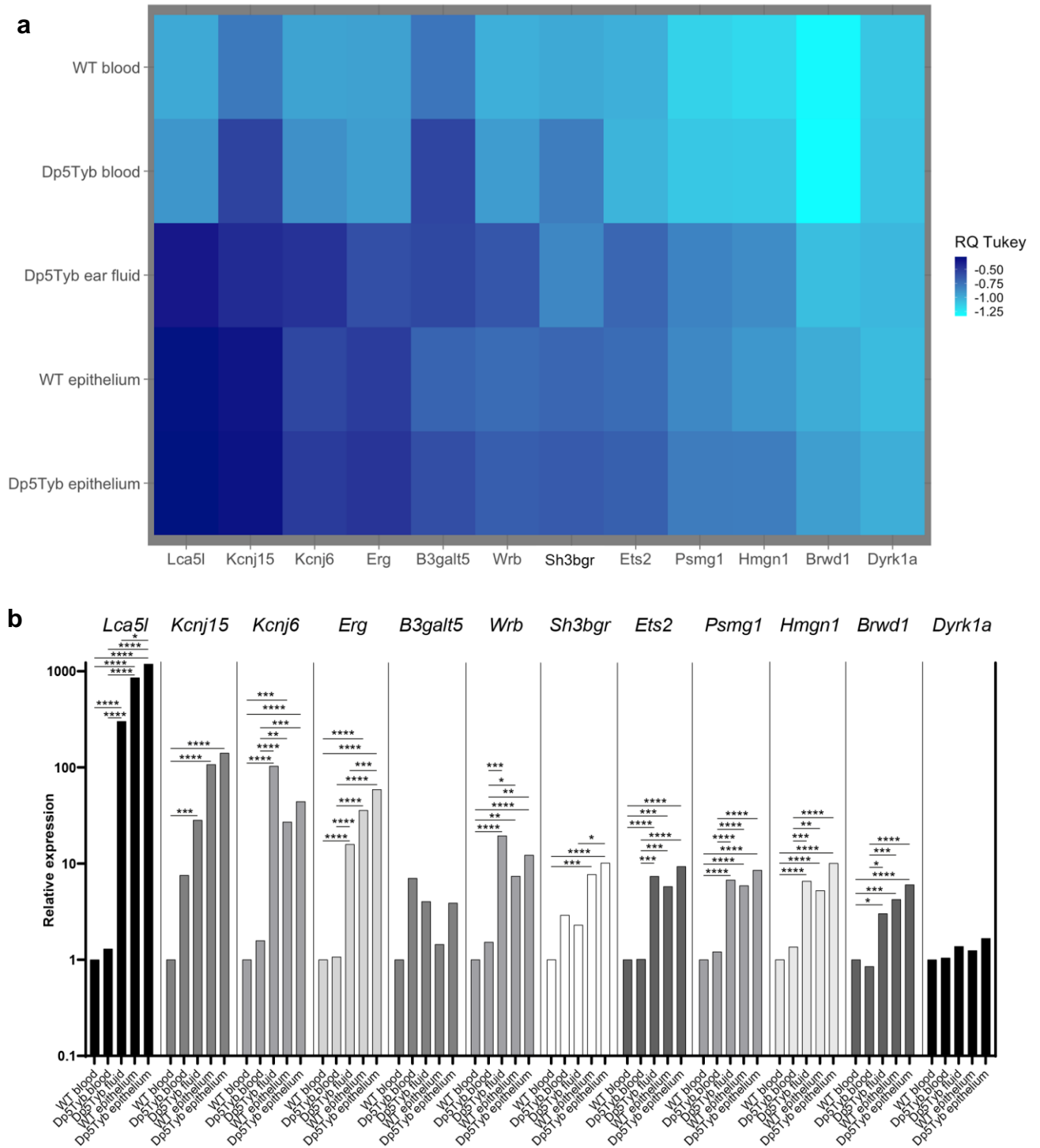


**Figure 5.1. RT-qPCR data showing expression of the 12 Dp5Tyb genes in Dp5Tyb and WT white blood cells and middle ear epithelium, and Dp5Tyb middle ear fluid.** (a) A heat map of the data, analysed and created by Heena Lad using R software. The relative quantification (RQ) values were Tukey transformed based on the normality of the dataset. P-values were calculated by multiple comparisons ANOVA with Tukey honest significant difference (HSD) using delta cycle threshold (Ct) mean values. A darker blue indicates a higher level of expression. (b) A bar chart of the data, created using GraphPad Prism software. The bars represent the mean RQ value per 'bio group'. The p-values were calculated using delta Ct mean values, and are denoted according to: \*\*\*\*  $\leq 0.0001$ , \*\*\*  $< 0.001$ , \*\*  $< 0.01$ , \*  $< 0.05$ . *Ppia* was the endogenous control gene. The relative quantification (RQ) values were calculated by normalising to this endogenous control. WT blood n = 10; Dp5Tyb blood n = 7; Dp5Tyb fluid n = 10; WT epithelium n = 10; Dp5Tyb epithelium n = 10. Genes are ordered by expression level in Dp5Tyb epithelium.

All genes, apart from *B3galt5* and *Dyrk1a*, were expressed significantly higher in WT middle ear epithelium than in WT blood: *Lca5l* ( $p < 0.0001$ ), *Kcnj15* ( $p < 0.0001$ ), *Kcnj6* ( $p = 0.0002$ ), *Erg* ( $p < 0.0001$ ), *Wrb* ( $p = 0.0014$ ), *Sh3bgr* ( $p = 0.0002$ ), *Ets2* ( $p = 0.0004$ ), *Psmg1* ( $p < 0.0001$ ), *Hmgn1* ( $p < 0.0001$ ), and *Brwd1* ( $p = 0.0007$ ).

Most of the genes were expressed more in Dp5Tyb middle ear epithelium than in Dp5Tyb blood: *Lca5l* ( $p < 0.0001$ ), *Kcnj6* ( $p = 0.0005$ ), *Erg* ( $p < 0.0001$ ), *Wrb* ( $p = 0.0028$ ), *Ets2* ( $p < 0.0001$ ), *Psmg1* ( $p < 0.0001$ ), *Hmgn1* ( $p < 0.0001$ ), and *Brwd1* ( $p < 0.0001$ ).

The same genes were also more highly expressed in Dp5Tyb middle ear fluid than in Dp5Tyb blood: *Lca5l* ( $p < 0.0001$ ), *Kcnj6* ( $p < 0.0001$ ), *Erg* ( $p < 0.0001$ ), *Wrb* ( $p = 0.0002$ ), *Ets2* ( $p = 0.0001$ ), *Psmg1* ( $p < 0.0001$ ), *Hmgn1* ( $p = 0.0002$ ), and *Brwd1* ( $p = 0.0154$ ).

No significant differences in expression were seen between WT and Dp5Tyb blood, or between WT and Dp5Tyb middle ear epithelium. However, when fold changes were calculated, 6/12 genes were upregulated more than 1.5-fold in Dp5Tyb epithelium compared to WT epithelium (*Kcnj6* 1.63-fold, *Erg* 1.65-fold, *Ets2* 1.61-fold, *Hmgn1* 1.92-fold, *Wrb* 1.66-fold, *B3galt5* 2.69-fold).

Interestingly, no significant differences were seen between any of the samples or genotypes for *B3galt5* or *Dyrk1a*, although they were both expressed more in Dp5Tyb epithelium compared to WT epithelium, 2.69 and 1.34-fold respectively. This is due to fold changes and statistical analysis measuring different criteria (McCarthy and Smyth, 2009). A true upregulation requires a fold change  $>1.5$  and a  $p$ -value  $<0.05$ . None of the 12 genes met these criteria, so none were significantly upregulated in Dp5Tyb epithelium compared to WT epithelium.

### 5.2.1.1. Further analysis of RT-qPCR data

To investigate whether there was a sex difference, any variation between the batches of RNA extractions, or whether gene expression was correlated with the RIN (RNA integrity number), the delta Ct values were sent to a statistician in Oxford (George Nicholson). George created graphs of the data split by gene, individual mouse, sex, genotype, RNA batch and RIN (RNA integrity number). This visualised the data in a way that any trends can be more easily observed (*Figure 5.2*).

The analysis shows that for half of the genes (*B3galt5*, *Brwd1*, *Dyrk1a*, *Ets2*, *Kcnj15* and *Psmg1*) the RNA batch did affect the delta Ct value, although it wasn't always consistent which batch gave the higher values.

The RNA integrity number (RIN) did not have an effect on delta Ct within sample sets, but the graphs do indicate that blood samples had higher RINs than ear fluid and epithelium.

No obvious sex differences can be seen, which correlates with the analysis carried out by Heena Lad (*Figure 5.1*).

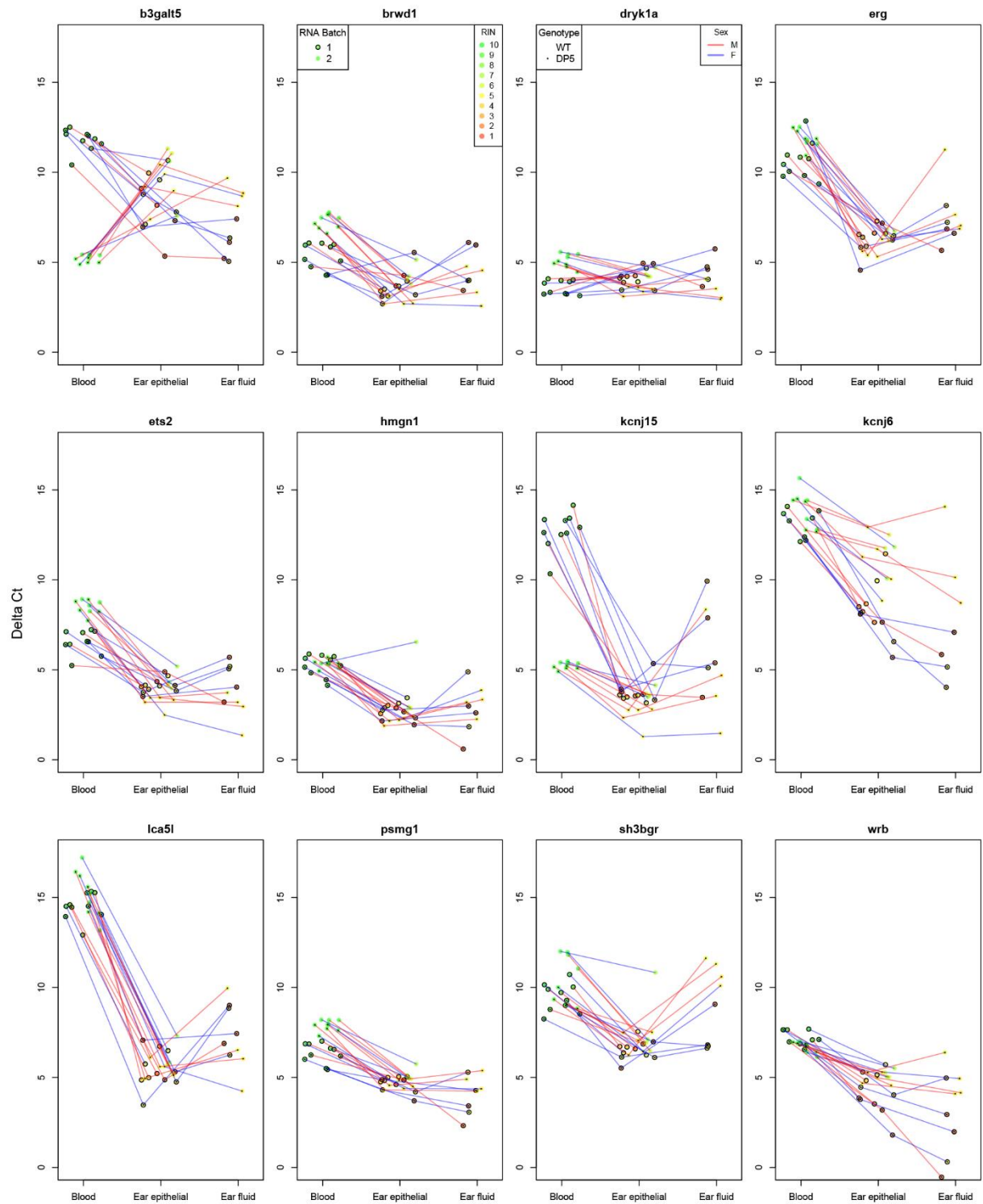


**Figure 5.2. Exploration of RT-qPCR data.** RNA was extracted from white blood cells (blood), middle ear epithelial cells and middle ear fluid. Coloured dots correlate to the RIN (RNA integrity number), which is an indication of the quality of RNA extracted. The data points for each animal are joined by lines. Lines are red for males and blue for females. Dp5Tyb data have a black dot in the centre, and WT points are just the coloured dot. A black circle around the coloured dot shows that the RNA was extracted in Batch 1, no outer circle means it was extracted in Batch 2. RNA was extracted in two batches due to the high number of samples and the need to work quickly to prevent degradation and maintain a high RIN. Delta Ct values are calculated by subtracting the Ct values from the endogenous control gene (*Ppia*) from the Ct values of the other genes. Graphs generated by George Nicholson using R software.

### 5.2.2. Human saliva qPCR data found differential expression of *DYRK1A* and *KCNJ6* in children with DS compared to their non-DS mothers

Paired saliva samples from children with DS and their mothers without DS were collected by our collaborator in Colorado, Professor Regie Santos-Cortez. The 12 Dp5Tyb genes were analysed in these samples by qPCR using human-specific primers based on the mouse-specific primers used previously (Figure 5.1). Professor Santos-Cortez then provided a summary of the data, including an average RQ (relative quantification) per gene, which normalised expression in the six children to control saliva from their six mothers. Fold changes were then calculated from these RQ values (Figure 5.3).

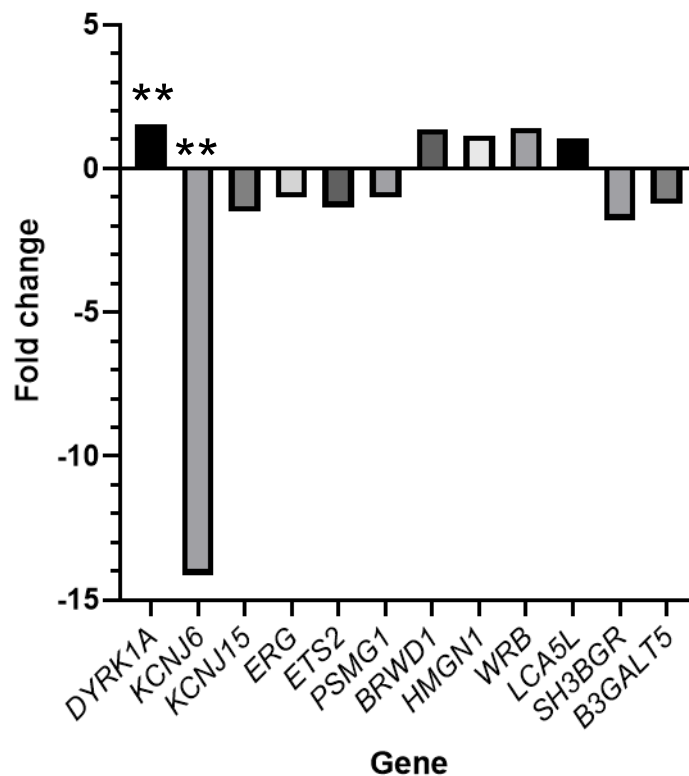


**Figure 5.3. Gene expression in the saliva of children with DS, relative to the saliva of their non-DS mothers.** If the RQ value was above 1, the fold change is the RQ value. If the RQ value was below 1, fold change is 1/RQ. Negative fold changes indicate that the child with DS expressed less of the gene than their mother. *DYRK1A* fold change = 1.54,  $p = 0.0044$ . *KCNJ6* fold change = -14,  $p = 0.0075$ . Children with DS:  $n = 6$ ; Non-DS mothers:  $n = 6$ .

If the RQ was above 1, that value was used as the positive fold change and the gene was upregulated in the children. If the RQ was below 1, the gene was downregulated compared to the mothers, and the negative fold change was calculated by  $1/RQ$  (Figure 5.3).

The only significant increase in gene expression in children with DS compared to their non-DS mothers was for *DYRK1A*. Children with DS expressed 1.54x more *DYRK1A* than their mothers ( $p = 0.0044$ ). The only significant downregulation was in *KCNJ6*, which was expressed 14x less in the saliva of the children than in their mothers ( $p = 0.0075$ ).

The rationale for this experiment was to observe whether the extra 1.5x gene dosage in DS leads to 1.5x gene expression. Blood and middle ear samples were not available from the children visiting Professor Santos-Cortez's clinic, but saliva collection is non-invasive and it contains white blood cells and epithelial cells from which genetic information can be extracted (Garbieri et al., 2017).

The DNA sequences of the 12 Dp5Tyb genes were very similar in humans and mice but sometimes there were nucleotide substitutions, including in the regions where the primers were designed to bind in mice. These single nucleotide polymorphisms meant that new primers needed to be designed to bind successfully and specifically in human samples.

### 5.2.3. Expression of the 12 Dp5Tyb genes at the protein level

The expression of the 12 Dp5Tyb genes in the middle ear at the protein level was studied using immunohistochemistry (IHC). IHC was performed on paraffin-embedded head sections, which were cut in the transverse plane so both middle ears could be seen on the same section (see methods *Figure 2.2*). The process was optimised before proceeding with data collection (see methods), as lifting of the sections was observed during heat mediated antigen retrieval. Briefly, I asked the histology department to try two different decalcification methods, and several different coatings on the glass slides. We found that decalcification with EDTA (Ethylenediaminetetraacetic acid), followed by Series 2 Adhesive microscope slides (TRAJAN, 472042491) was the best method available for keeping the epithelial lining adhered, but the success rate still wasn't 100%. The concentration of each antibody was also optimised, and some required heat mediated antigen retrieval to achieve the clearest staining.

The staining in one middle ear was quantified per mouse. The ear with the thickest epithelial lining was chosen for all WT and Dp5Tyb mice, although sometimes only one middle ear lining was available for analysis due to damage during antigen retrieval or the sectioning process. Positive cells are stained brown, and a blue counterstain (haematoxylin) was used. As a positive control, and to determine the concentration required, the antibodies were first tested on lung sections (data not shown). Lung tissue was chosen as it is epithelial tissue, similar to the middle ear, and heart tissue is also present on transverse lung sections. Of the 12 Dp5Tyb proteins, 11 were known to be expressed in adult lung or heart according to the Mouse Genome Informatics (MGI) database from the Jackson Laboratory. The B3GALT5 antibody was tested on gut sections as B3GALT5 is not known to be expressed in lung or heart. As a negative control, each antibody was tested on a

CHAPTER 5: Middle ear expression of the 12 Dp5Tyb genes, and analysis of double mutants tissue in which the protein is not expressed, commonly the thymus, but brain, pancreas, cartilage and lung were also used. No staining was seen on the negative controls (see Appendix).

Protein localisation information was sourced from <https://www.genecards.org/>.

GeneCards® provides known expression data for each protein and a confidence score for expression in each sub-cellular compartment.

### 5.2.3.1. DYRK1A

GeneCards® reports that this protein is localised to the nucleus, and can appear as speckles. Significantly more cells expressed DYRK1A in the middle ear epithelium of Dp5Tyb mice compared to WT littermates ( $p = 0.0464$ ) (Figure 5.4).

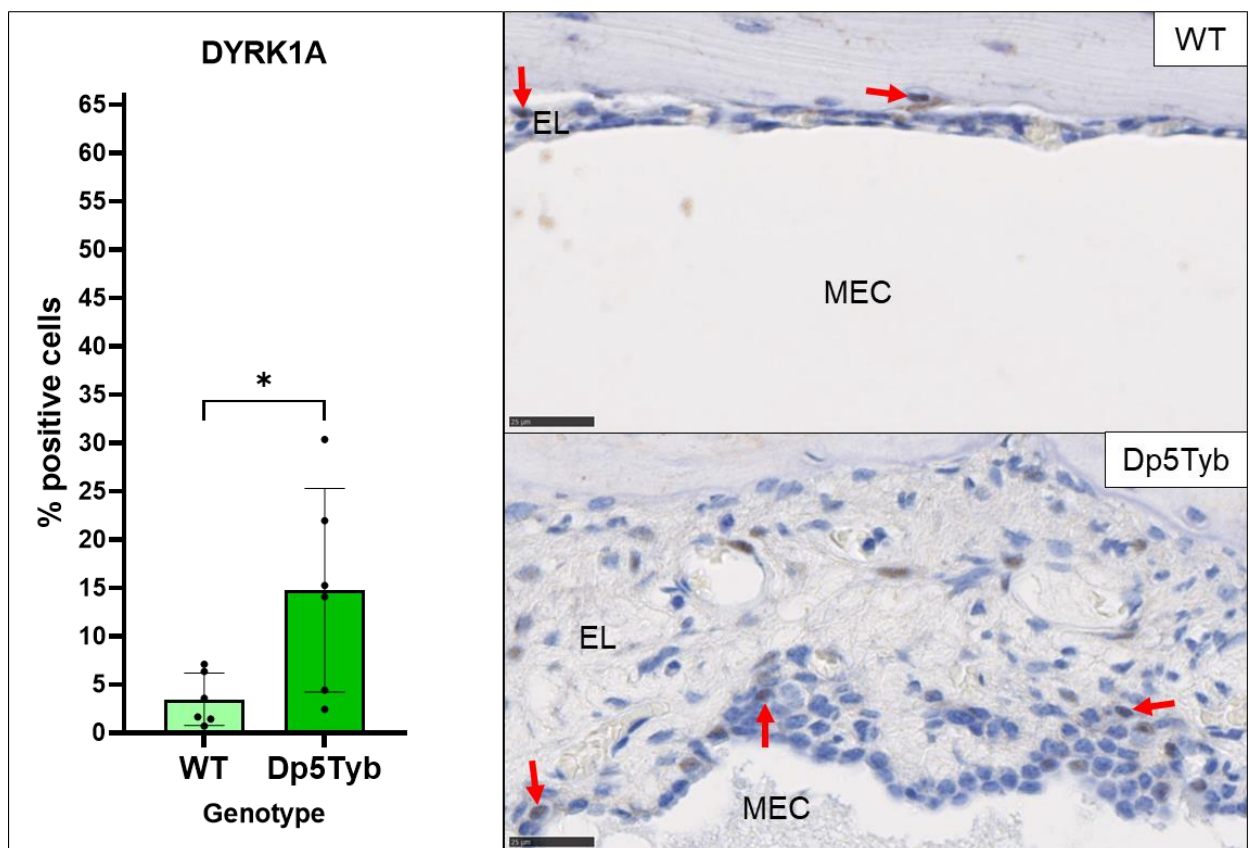


**Figure 5.4. Immunohistochemistry with antibody against DYRK1A.** Graph of quantified staining alongside example images of stained WT and Dp5Tyb middle ear epithelium. Paraffin-embedded transverse head sections from WT ( $n = 6$ ) and Dp5Tyb ( $n = 6$ ) mice were stained with anti-DYRK1A antibody (1:100, abcam, ab65220). Red arrows indicate examples of nuclei with positive staining. The staining was quantified by counting 200 cells, then counting how many of those were positive, and calculating a percentage.  $P = 0.0464$  (Welch's t test). Error bars show mean  $\pm$  standard deviation. EL = epithelial lining; MEC = middle ear cavity; MEF = middle ear fluid. Scale bar = 25  $\mu\text{m}$ .

### 5.2.3.2. GIRK2 (KCNJ6)

*Kcnj6* encodes a protein known as GIRK2. This is a transmembrane protein, mainly expressed in the plasma membrane and golgi apparatus. GeneCards® also has medium confidence in expression showing across the nucleus and cytoplasm. The nuclear staining was quantified, and no significant difference in GIRK2 staining was seen between WT and Dp5Tyb middle ear epithelium ( $p = 0.8855$ ) (Figure 5.5).

The anti-GIRK2 antibody was raised in goat, so rabbit serum (instead of goat) and an anti-goat secondary antibody were used for the IHC.

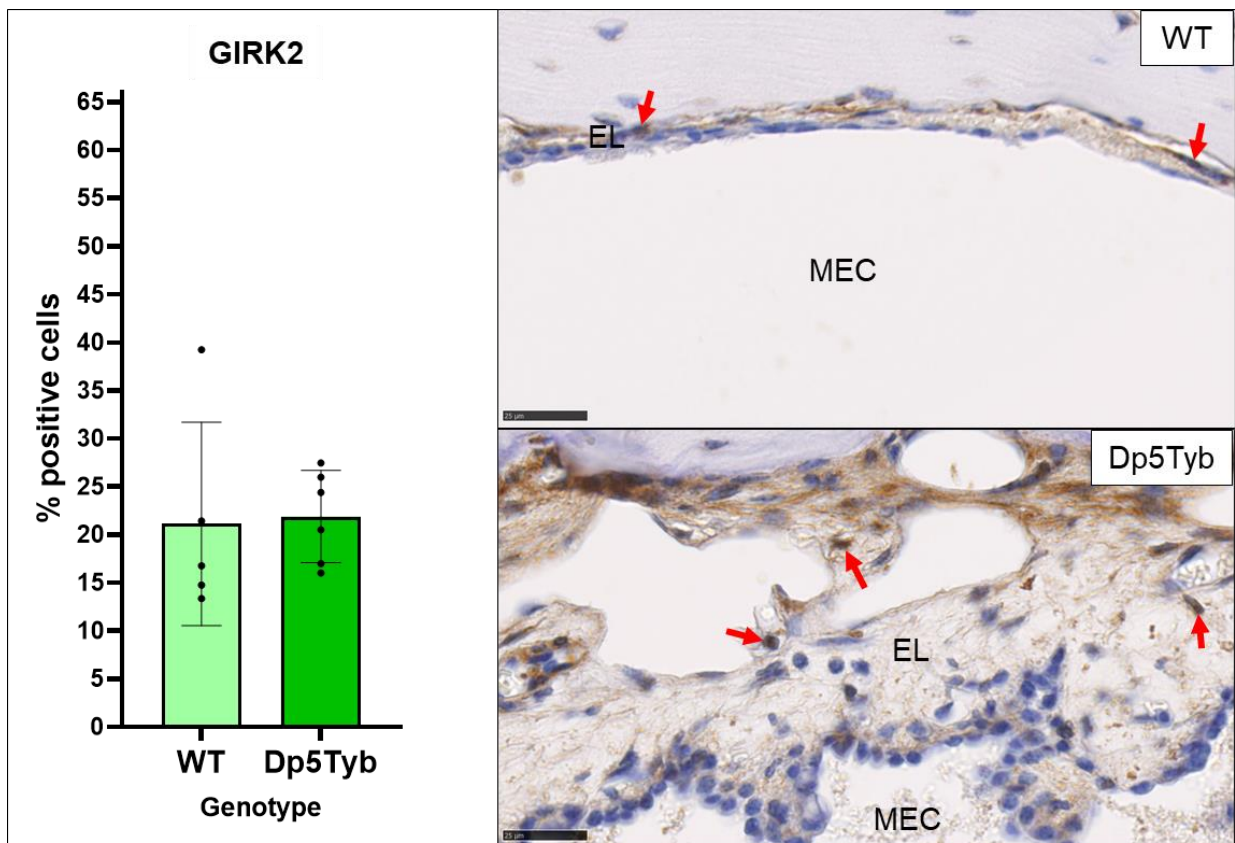


**Figure 5.5. Immunohistochemistry with antibody against GIRK2 (KCNJ6).** Graph of quantified staining alongside example images of stained WT and Dp5Tyb middle ear epithelium. Paraffin-embedded transverse head sections from WT ( $n = 5$ ) and Dp5Tyb ( $n = 6$ ) mice were stained with anti-GIRK2 antibody (1:500, abcam, ab65096). Red arrows highlight examples of nuclei with positive staining. The staining was quantified by counting 200 cells, then counting how many of those were positive, and calculating a percentage.  $P = 0.8855$  (Welch's t test). Error bars show mean  $\pm$  standard deviation. EL = epithelial lining; MEC = middle ear cavity; MEF = middle ear fluid. Scale bar = 25  $\mu$ m.

### 5.2.3.3. KCNJ15

This is a transmembrane protein, with expression only expected in the plasma membrane (GeneCards®). The staining observed is therefore likely to be non-specific as it appears in the nuclei, and no statistical analysis was performed (Figure 5.6).

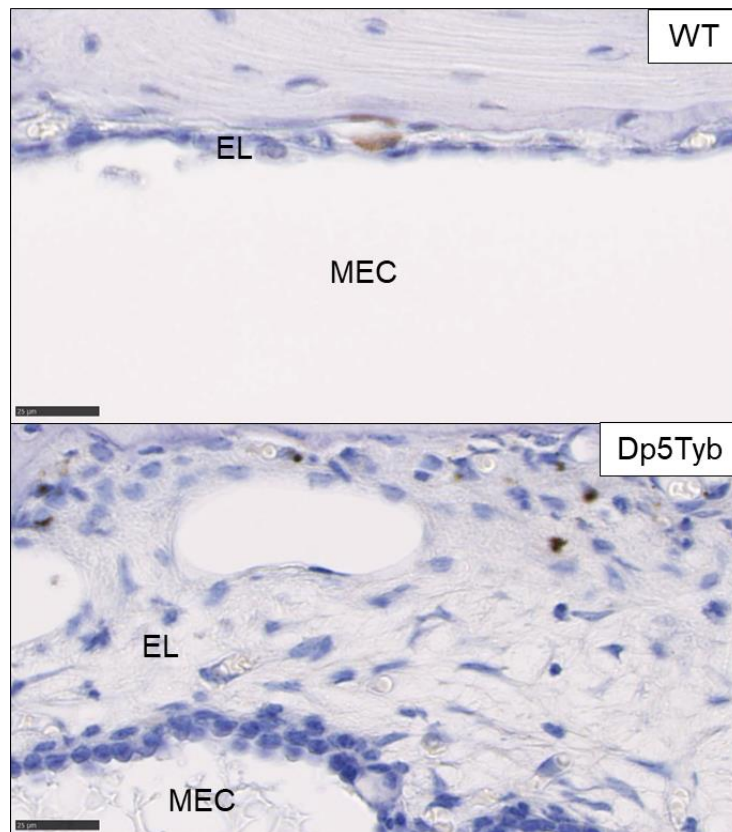


*Figure 5.6. Immunohistochemistry with antibody against KCNJ15.* Example images of stained WT and Dp5Tyb middle ear epithelium. Paraffin-embedded transverse head sections from WT (n = 5) and Dp5Tyb (n = 6) mice were stained with anti-KCNJ15 antibody (1:100, abcam, ab200397). EL = epithelial lining; MEC = middle ear cavity; MEF = middle ear fluid. Scale bar = 25 µm.

### 5.2.3.4. ERG

This protein is mainly expressed in the nucleus, but can also be found in the cytoplasm (GeneCards®). The nuclear staining was quantified, and no significant difference in the percentage of cells expressing the ERG protein was seen between WT and Dp5Tyb middle ear epithelium ( $p = 0.3041$ ) (Figure 5.7).

Heat mediated antigen retrieval was used on these sections (see methods).

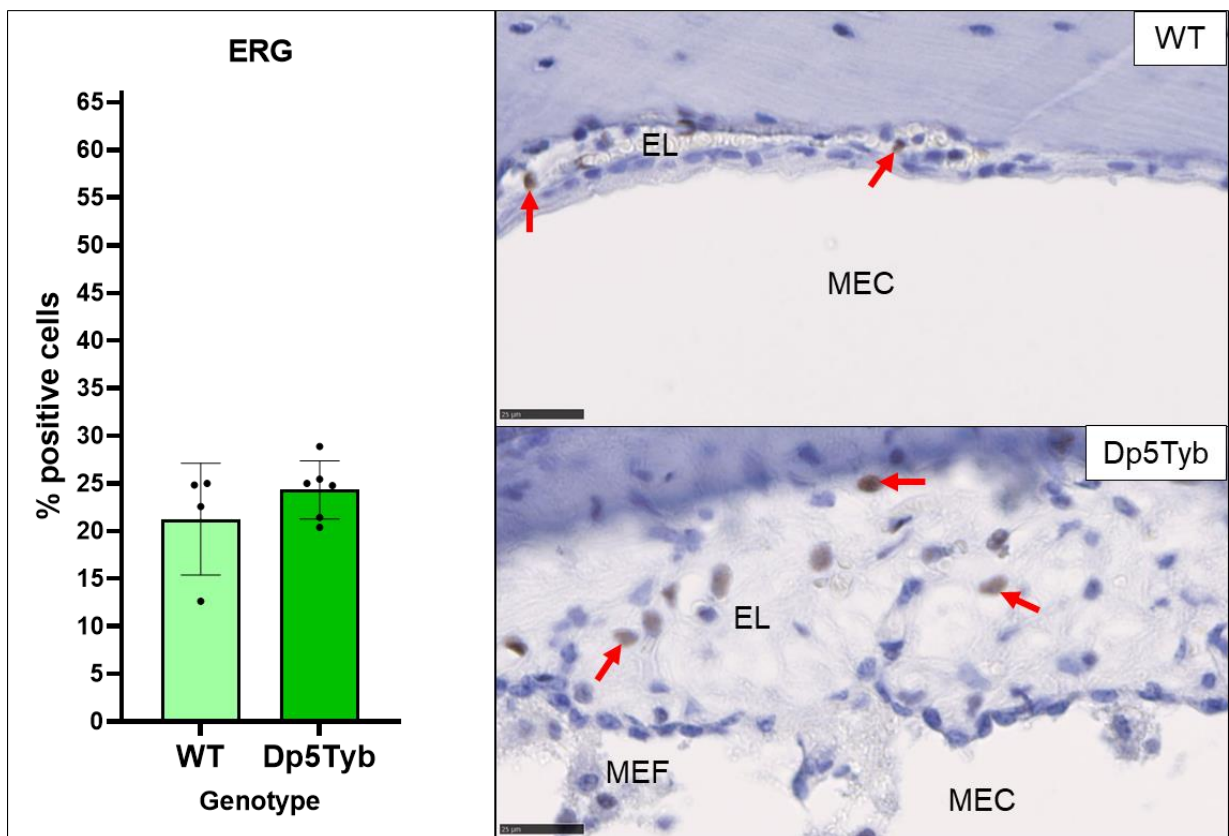


**Figure 5.7. Immunohistochemistry with antibody against ERG.** Graph of quantified staining alongside example images of stained WT and Dp5Tyb middle ear epithelium. Paraffin-embedded transverse head sections from WT ( $n = 4$ ) and Dp5Tyb ( $n = 6$ ) mice were stained with anti-ERG antibody (1:500, abcam, ab92513). Red arrows highlight examples of nuclei with positive staining. The staining was quantified by counting 200 cells, then counting how many of those were positive, and calculating a percentage.  $P = 0.3041$  (unpaired t test). Error bars show mean  $\pm$  standard deviation. EL = epithelial lining; MEC = middle ear cavity; MEF = middle ear fluid. Scale bar = 25  $\mu$ m.

### 5.2.3.5. ETS2

The ETS2 protein is mainly localised to the nucleus, but can also be found in the cytoplasm (GeneCards®). Verification of the phosphorylated ETS2 antibody showed that the staining was localised to the nucleus in mouse liver, human thymus and human T-cell lymphoma tissue (ThermoFisher). The nuclear staining was quantified and there was no significant difference in the percentage of cells expressing the phosphorylated ETS2 protein between WT and Dp5Tyb middle ear epithelium ( $p = 0.9170$ ) (Figure 5.8). Heat mediated antigen retrieval was used for these sections.

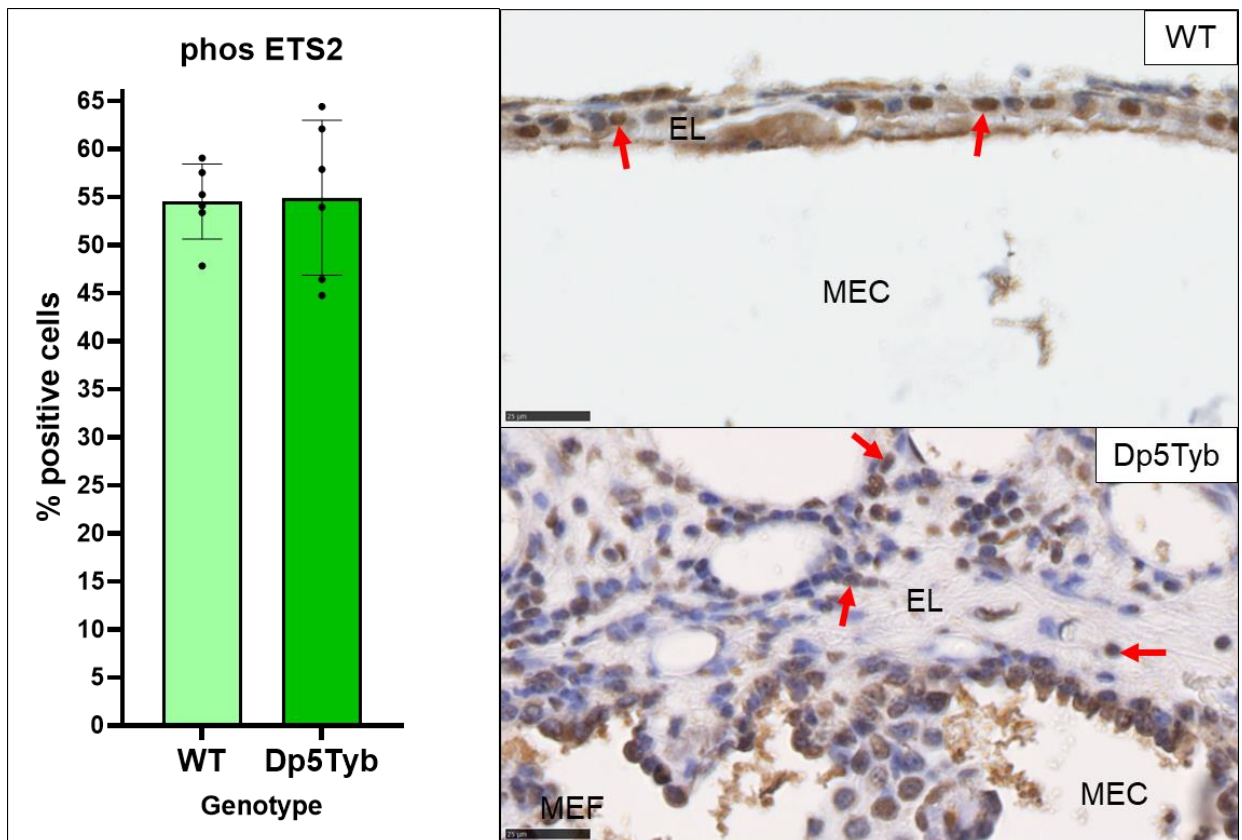


**Figure 5.8. Immunohistochemistry with antibody against phosphorylated ETS2.** Graph of quantified staining alongside example images of stained WT and Dp5Tyb middle ear epithelium. Paraffin-embedded transverse head sections from WT ( $n = 6$ ) and Dp5Tyb ( $n = 6$ ) mice were stained with anti-phosETS2 antibody (1:500, ThermoFisher, 44-1105G). Red arrows highlight examples of nuclei with positive staining. The staining was quantified by counting 200 cells, then counting how many of those were positive, and calculating a percentage.  $P = 0.9170$  (unpaired t test). Error bars show mean  $\pm$  standard deviation. EL = epithelial lining; MEC = middle ear cavity; MEF = middle ear fluid. Scale bar = 25  $\mu$ m.

### 5.2.3.6. PSMG1

Expression of this protein can be expected across the cell, but particularly in the cytoplasm, endoplasmic reticulum, golgi apparatus and nucleus (GeneCards®).

The nuclear staining was quantified, and there was no significant difference in the percentage of cells expressing the PSMG1 protein between WT and Dp5Tyb middle ear epithelium ( $p = 0.9449$ ) (Figure 5.9).

Heat mediated antigen retrieval was used for this staining.

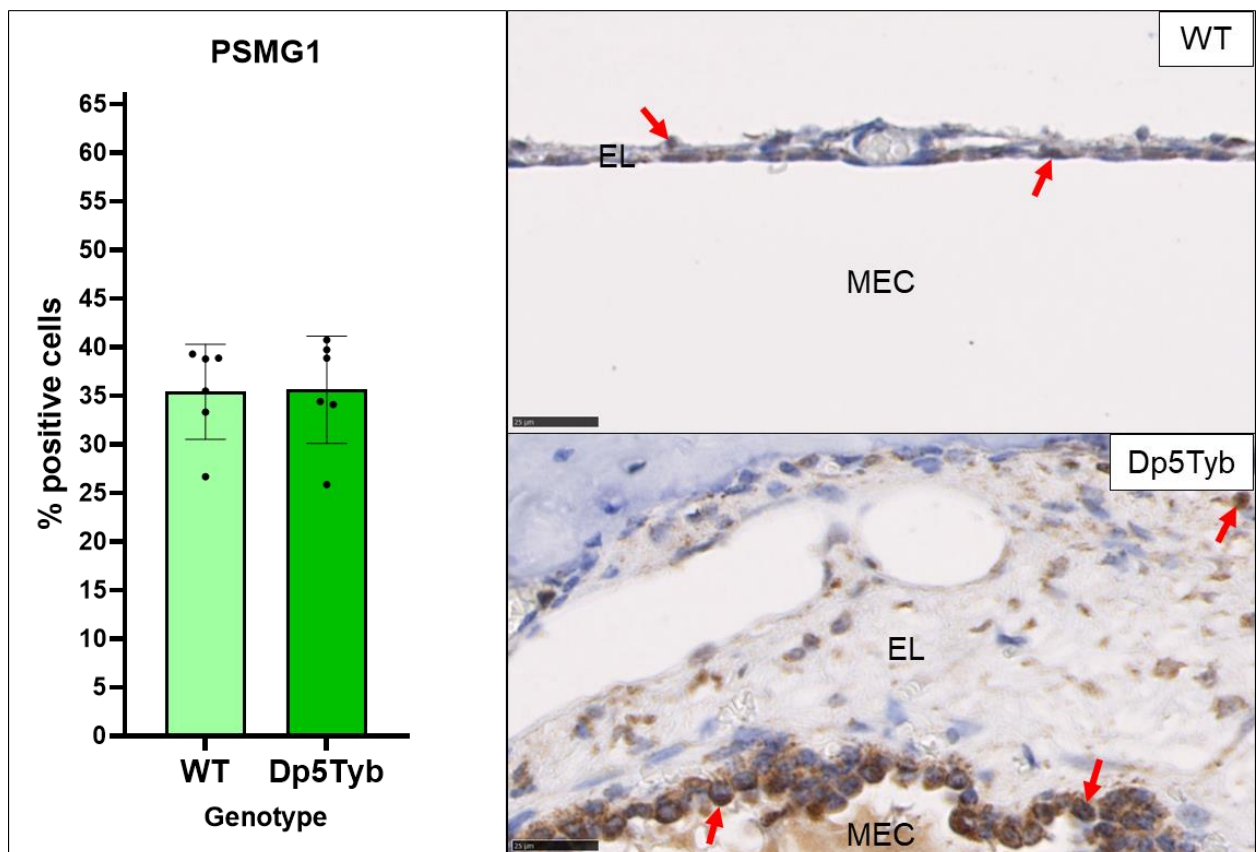


**Figure 5.9. Immunohistochemistry with antibody against PSMG1.** Graph of quantified staining alongside example images of stained WT and Dp5Tyb middle ear epithelium. Paraffin-embedded transverse head sections from WT ( $n = 6$ ) and Dp5Tyb ( $n = 6$ ) mice were stained with anti-PSMG1 antibody (1:1000, abcam, ab167396). Red arrows highlight examples of positively stained nuclei. The staining was quantified by counting 200 cells, then counting how many of those were positive, and calculating a percentage.  $P = 0.9449$  (unpaired t test). Error bars show mean  $\pm$  standard deviation. EL = epithelial lining; MEC = middle ear cavity; MEF = middle ear fluid. Scale bar = 25  $\mu\text{m}$ .

### 5.2.3.7. BRWD1

This protein is expressed in the nucleus and cytoplasm (GeneCards®). This staining is intense, indicating that the antibody concentration was likely too high causing considerably background staining. However, the nuclear staining was still quantified. No significant difference in the percentage of cells expressing the BRWD1 protein was seen between WT and Dp5Tyb middle ear epithelium ( $p = 0.0513$ ) (Figure 5.10).

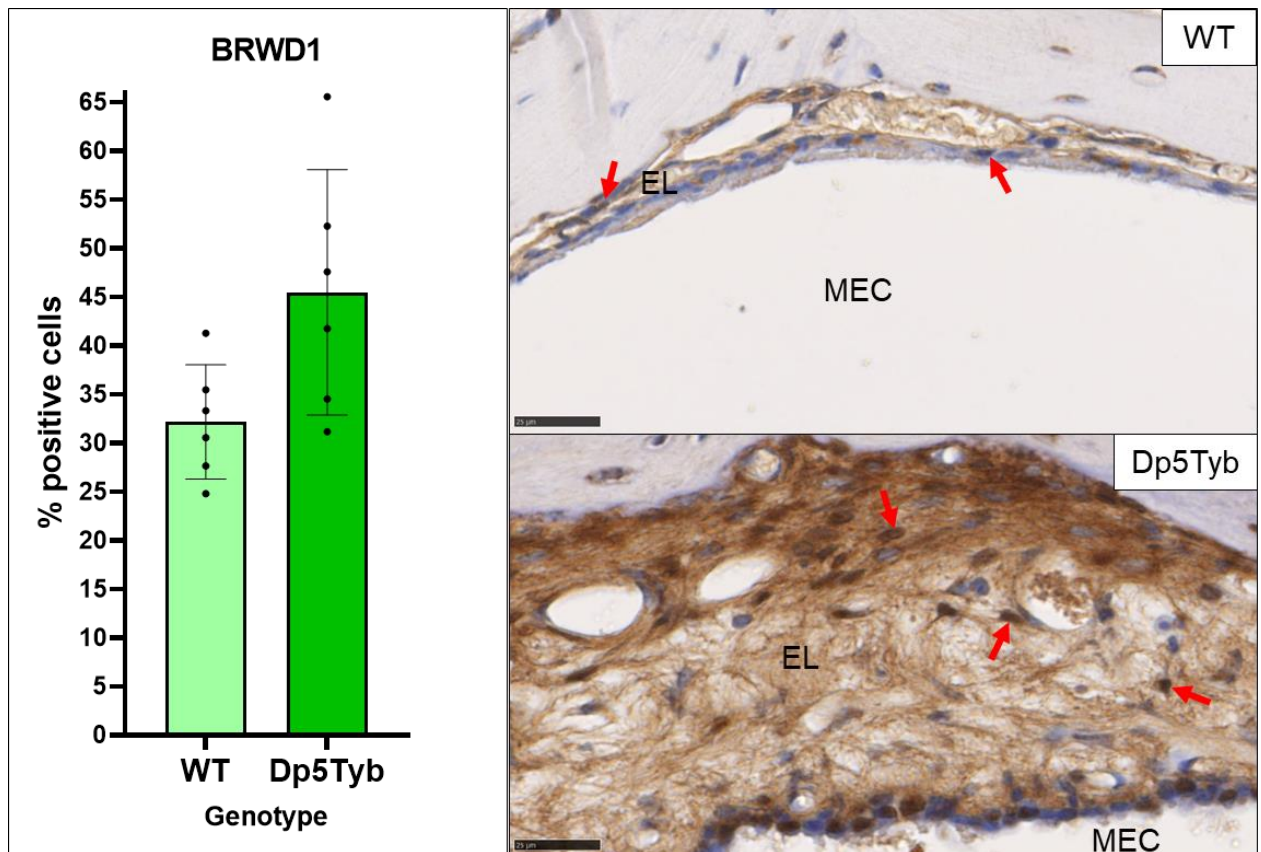


**Figure 5.10. Immunohistochemistry with antibody against BRWD1.** Graph of quantified staining alongside example images of stained WT and Dp5Tyb middle ear epithelium. Paraffin-embedded transverse head sections from WT ( $n = 6$ ) and Dp5Tyb ( $n = 6$ ) mice were stained with anti-BRWD1 antibody (1:100, Elabscience, E-AB-17567). Red arrows highlight examples of positively stained nuclei. The staining was quantified by counting 200 cells, then counting how many of those were positive, and calculating a percentage.  $P = 0.0513$  (Welch's t test). Error bars show mean  $\pm$  standard deviation. EL = epithelial lining; MEC = middle ear cavity; MEF = middle ear fluid. Scale bar = 25  $\mu\text{m}$ .

### 5.2.3.8. HMGN1

The HMGN1 protein is mainly expressed in the nucleus but also the cytoplasm (GeneCards®). Some faint nuclear stain can be seen, but unfortunately the staining is very weak despite being diluted only 1:40. Analysis of HMGN1 would likely have benefitted from antigen retrieval. The current staining shows no significant difference in the percentage of cells expressing the HMGN1 protein between WT and Dp5Tyb middle ear epithelium ( $p = 0.9967$ ) (Figure 5.11).

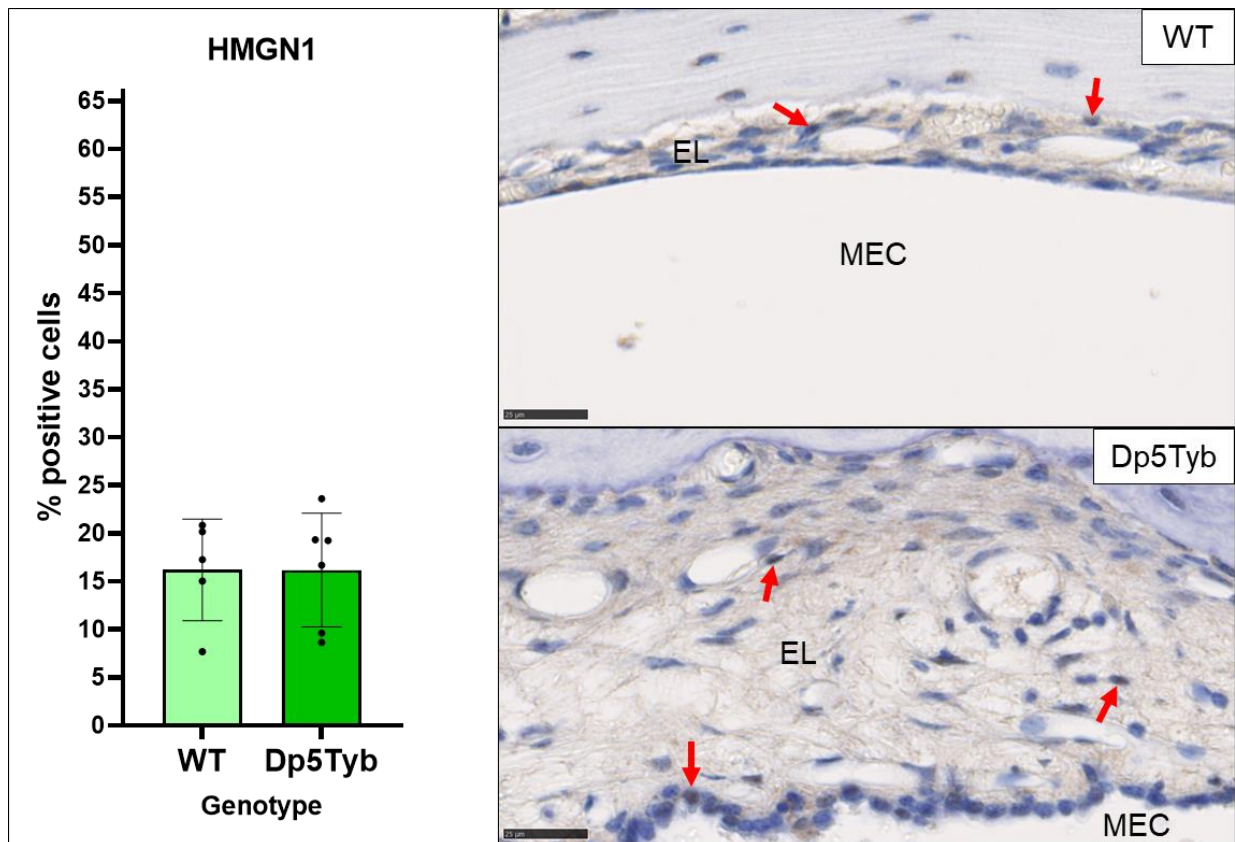


**Figure 5.11. Immunohistochemistry with antibody against HMGN1.** Graph of quantified staining alongside example images of stained WT and Dp5Tyb middle ear epithelium. Paraffin-embedded transverse head sections from WT ( $n = 5$ ) and Dp5Tyb ( $n = 6$ ) mice were stained with anti-HMGN1 antibody (1:40, Invitrogen, PA5-76859). Red arrows highlight some of the positively stained nuclei. The staining was quantified by counting 200 cells, then counting how many of those were positive, and calculating a percentage.  $P = 0.9967$  (unpaired t test). Error bars show mean  $\pm$  standard deviation. EL = epithelial lining; MEC = middle ear cavity; MEF = middle ear fluid. Scale bar = 25  $\mu\text{m}$ .

### 5.2.3.9. GET1 (WRB)

The GET1 protein is expressed in the endoplasmic reticulum and nucleus (GeneCards®). Some expression can also be expected in the cytoplasm but with a much lower confidence score. Staining of the endoplasmic reticulum appears as dots around the nucleus. The nuclear stain was quantified and there was no significant difference in the percentage of cells expressing the GET1 protein between WT and Dp5Tyb middle ear epithelium ( $p = 0.2110$ ) (Figure 5.12).

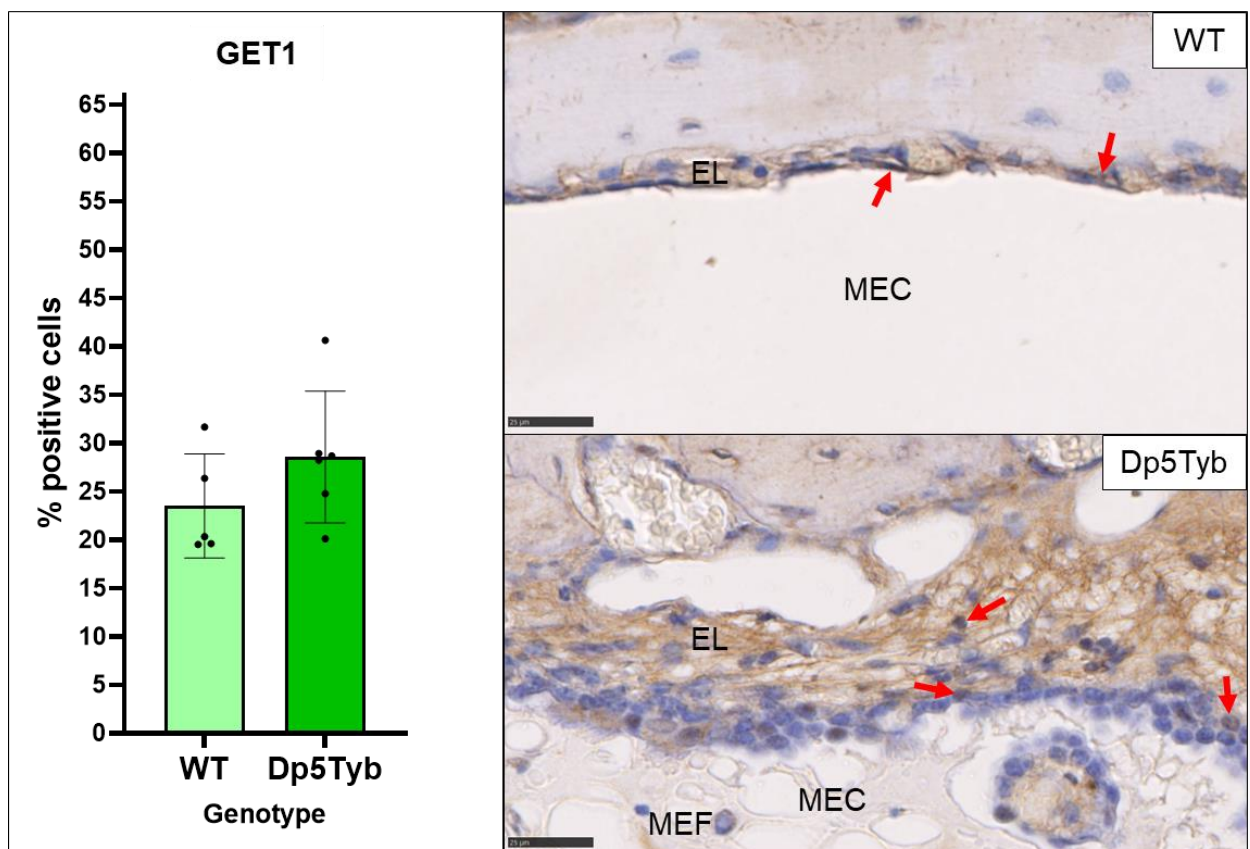


**Figure 5.12. Immunohistochemistry with antibody against GET1 (WRB).** Graph of quantified staining alongside example images of stained WT and Dp5Tyb middle ear epithelium. Paraffin-embedded transverse head sections from WT ( $n = 5$ ) and Dp5Tyb ( $n = 6$ ) mice were stained with anti-GET1 antibody (1:100, Bioss antibodies, bs-11774R). Red arrows indicate some of the positively stained nuclei. The staining was quantified by counting 200 cells, then counting how many of those were positive, and calculating a percentage.  $P = 0.2110$  (unpaired t test). Error bars show mean  $\pm$  standard deviation. EL = epithelial lining; MEC = middle ear cavity; MEF = middle ear fluid. Scale bar = 25  $\mu$ m.

### 5.2.3.10. LCA5L

The LCA5L protein is localised to the cytoskeleton and nucleus. Some expression may also be in the cytoplasm, but the confidence level on GeneCards® is fairly low.

The nuclear staining was quantified, and there was no significant difference in the percentage of cells expressing the LCA5L protein between WT and Dp5Tyb middle ear epithelium ( $p = 0.4024$ ) (Figure 5.13).

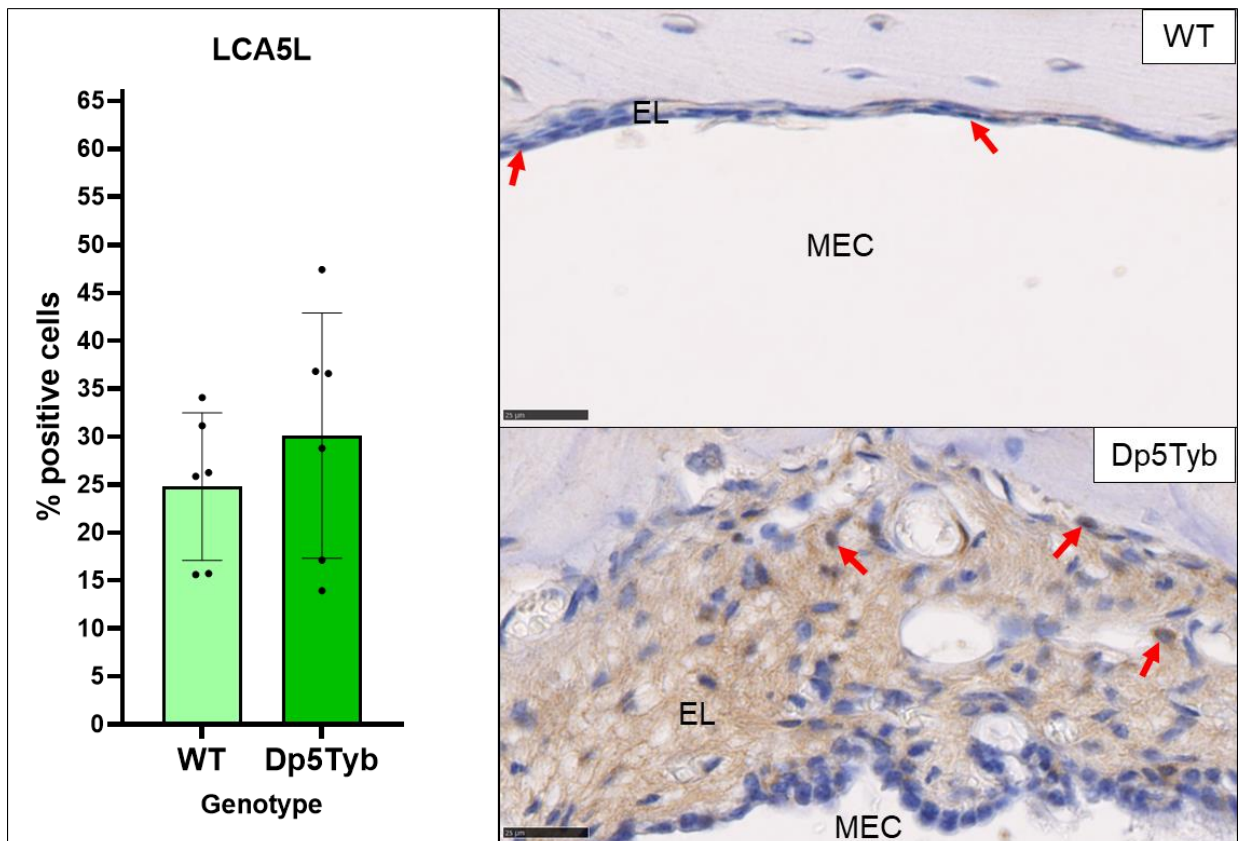


**Figure 5.13. Immunohistochemistry with antibody against LCA5L.** Graph of quantified staining alongside example images of stained WT and Dp5Tyb middle ear epithelium. Paraffin-embedded transverse head sections from WT ( $n = 6$ ) and Dp5Tyb ( $n = 6$ ) mice were stained with anti-LCA5L antibody (1:1000, Bioss antibodies, bs-9972R). Red arrows highlight examples of the nuclei with positive staining. The staining was quantified by counting 200 cells, then counting how many of those were positive, and calculating a percentage.  $P = 0.4024$  (unpaired t test). Error bars show mean  $\pm$  standard deviation. EL = epithelial lining; MEC = middle ear cavity; MEF = middle ear fluid. Scale bar = 25  $\mu\text{m}$ .

### 5.2.3.11. SH3BGR

The SH3BGR protein is mainly expressed in the cytoplasm (GeneCards®). A low confidence score is also given to expression in the nucleus. The nuclear staining seen was therefore non-specific and could not be quantified (*Figure 5.14*).

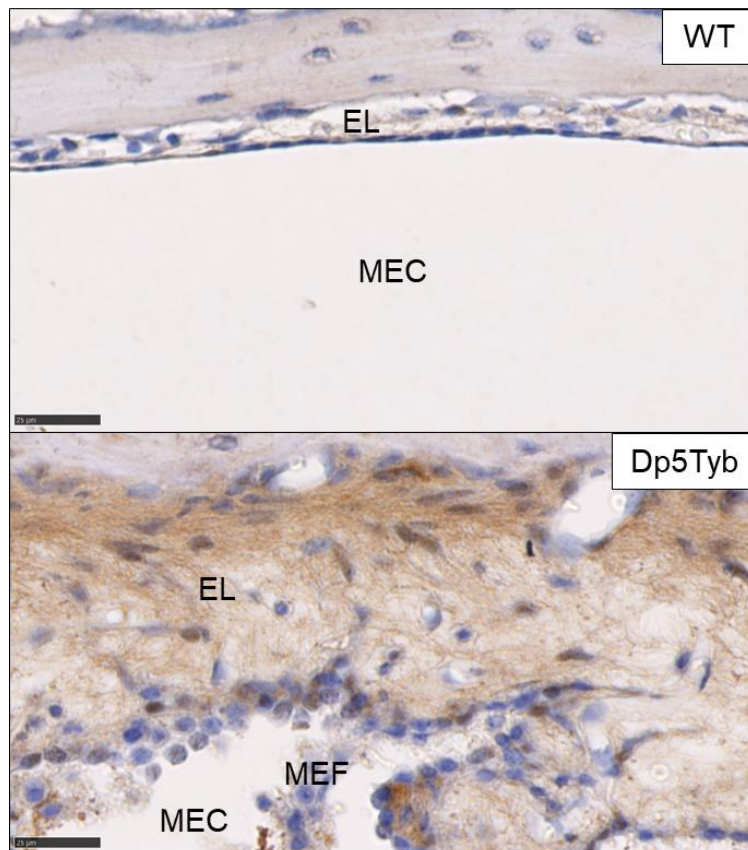


*Figure 5.14. Immunohistochemistry with antibody against SH3BGR.* Example images of stained WT and Dp5Tyb middle ear epithelium. Paraffin-embedded transverse head sections from WT (n = 6) and Dp5Tyb (n = 6) mice were stained with anti-SH3BGR antibody (1:200, Proteintech, 21161-1-AP). EL = epithelial lining; MEC = middle ear cavity; MEF = middle ear fluid. Scale bar = 25  $\mu$ m.

### 5.2.3.12. B3GALT5

The B3GALT5 protein is localised to the endoplasmic reticulum, golgi apparatus and membrane proteins (GeneCards®). The staining in *Figure 5.15* is distinct from the blue haematoxylin nuclear stain, so is likely to be the Golgi apparatus. The Golgi staining was quantified, and no significant difference in the percentage of cells expressing the B3GALT5 protein was found between WT and Dp5Tyb middle ear epithelium ( $p = 0.8842$ ) (*Figure 5.15*). The B3GALT5 antibody was raised in rat so anti-rat secondary antibody was used for this IHC. Heat mediated antigen retrieval was performed on the histological sections.

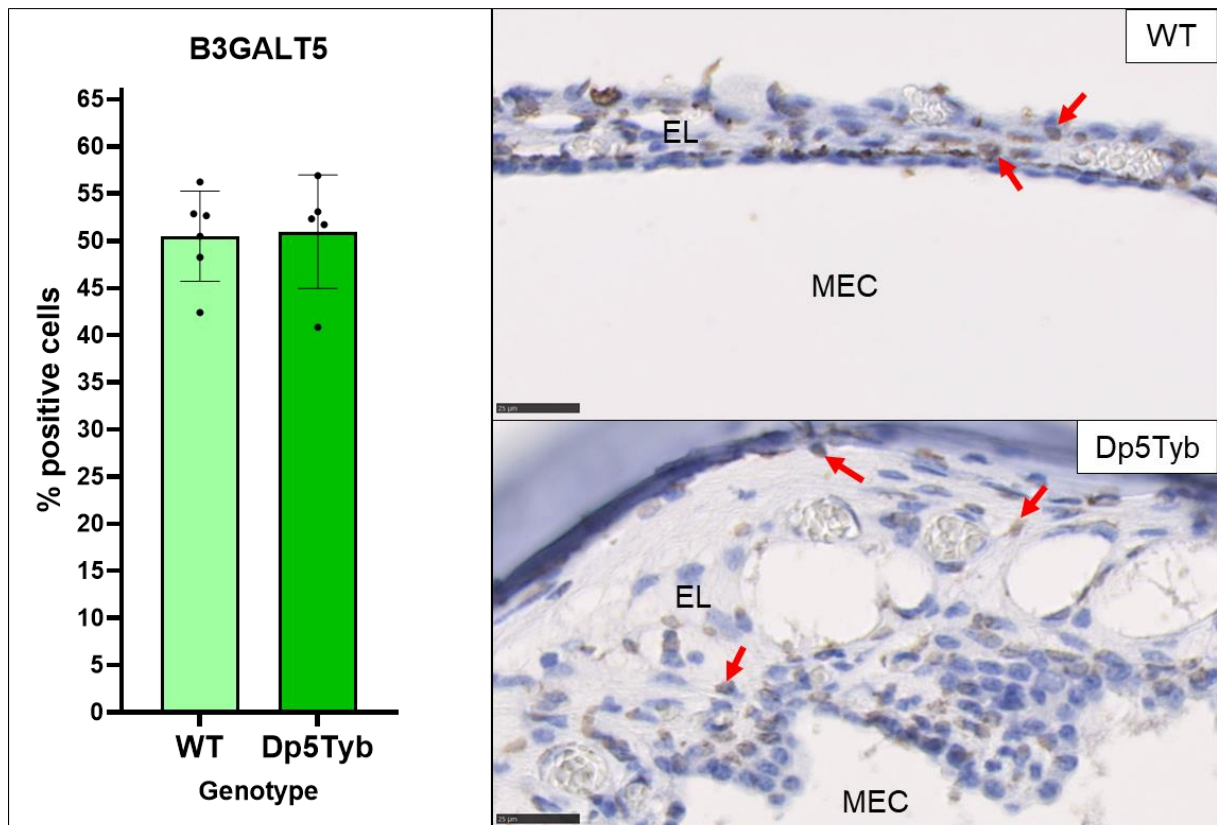


*Figure 5.15. Immunohistochemistry with antibody against B3GALT5.* Graph of quantified staining alongside example images of stained WT and Dp5Tyb middle ear epithelium. Paraffin-embedded transverse head sections from WT ( $n = 6$ ) and Dp5Tyb ( $n = 5$ ) mice were stained with anti-B3GALT5 antibody (1:10, Origene, TA336273). Red arrows highlight some of the positively stained Golgi apparatus. The staining was quantified by counting 200 cells, then counting how many of those were positive, and calculating a percentage.  $P = 0.8842$  (unpaired t test). Error bars show mean  $\pm$  standard deviation. EL = epithelial lining; MEC = middle ear cavity; MEF = middle ear fluid. Scale bar = 25  $\mu\text{m}$ .

CHAPTER 5: Middle ear expression of the 12 Dp5Tyb genes, and analysis of double mutants  
Western blots were also run with WT and Dp5Tyb epithelial cells and antibodies for the 12 Dp5Tyb proteins. Examples of these can be found in the Appendix.  
Unfortunately the results were inconsistent between the replicates so western blot analysis was omitted from this thesis.

#### 5.2.4. Generation and phenotypic analysis of double mutants

Knockouts for 8 of the 12 Dp5Tyb genes were imported from other mouse facilities. Although referred to as a knockout for simplicity, the *Ets2* mutant imported has a missense point mutation, leading to a non-functional copy of the gene (European Mouse Mutant Archive, EM:07468). *Hmgn1* knockout mice were crossed to Dp5Tyb mice at the Francis Crick Institute and the heads were sent to MRC Harwell. A *Kcnj6* knockout was already available at the Mary Lyon Centre (MLC), and a *Kcnj15* knockout was unavailable. The MLC were unable to produce viable Dp5Tyb *Dyrk1a*<sup>+/-</sup> mice. However, our collaborators at the Francis Crick Institute had created Dp3Tyb *Dyrk1a*<sup>+/-</sup> mice and shipped the heads to MRC Harwell in formalin, along with heads from WT and Dp3Tyb littermates. No spare *Dyrk1a*<sup>+/-</sup> heads were available for comparison.

For the other crosses, heads from WT, knockout, Dp5Tyb and double mutant mice were given to the histology department for fixing, sectioning and H&E staining (see methods). Each mouse was then scored as having zero, one or two ears with OME. This is represented on the graphs as no OM (blue), unilateral OM (red), and bilateral OM (green) (*Figure 5.16*). Sections from the single gene knockouts were also observed to determine whether knocking the gene out predisposes the mice to OME. None of the knockouts had a higher OME incidence than would be expected for the general WT population. The knockouts were not included in the statistical analysis as

CHAPTER 5: Middle ear expression of the 12 Dp5Tyb genes, and analysis of double mutants  
the research question was whether the OME incidence in double mutants is significantly different from WT or DS littermates.

I was unable to analyse all sections from all of the crosses before the submission deadline. For this reason, no statistical analysis was performed on some of the datasets as the sample size was too low.

For each cross we expect WT mice to show little evidence of OME, though occasionally WT mice ears will show OME (around 1 in 10 WT mice develop spontaneous unilateral OME (Deafness lab, unpublished)). In contrast, we expect Dp5Tyb mice to show significant unilateral and bilateral OME. We aim to examine if in the double mutant there is a reduction in the number of ears with OME that differs significantly from the DpTyb mice and, importantly, is now no longer significantly different from WT mice that indicates that the WT phenotype has been restored and OME rescued. For several lines – *Erg*, *Ets2*, *Psmg1*, and *Sh3bgr* – the sample numbers did not allow us to make an assessment of whether or not the restoration of disomy led to rescue of the OME phenotype.

CHAPTER 5: Middle ear expression of the 12 Dp5Tyb genes, and analysis of double mutants

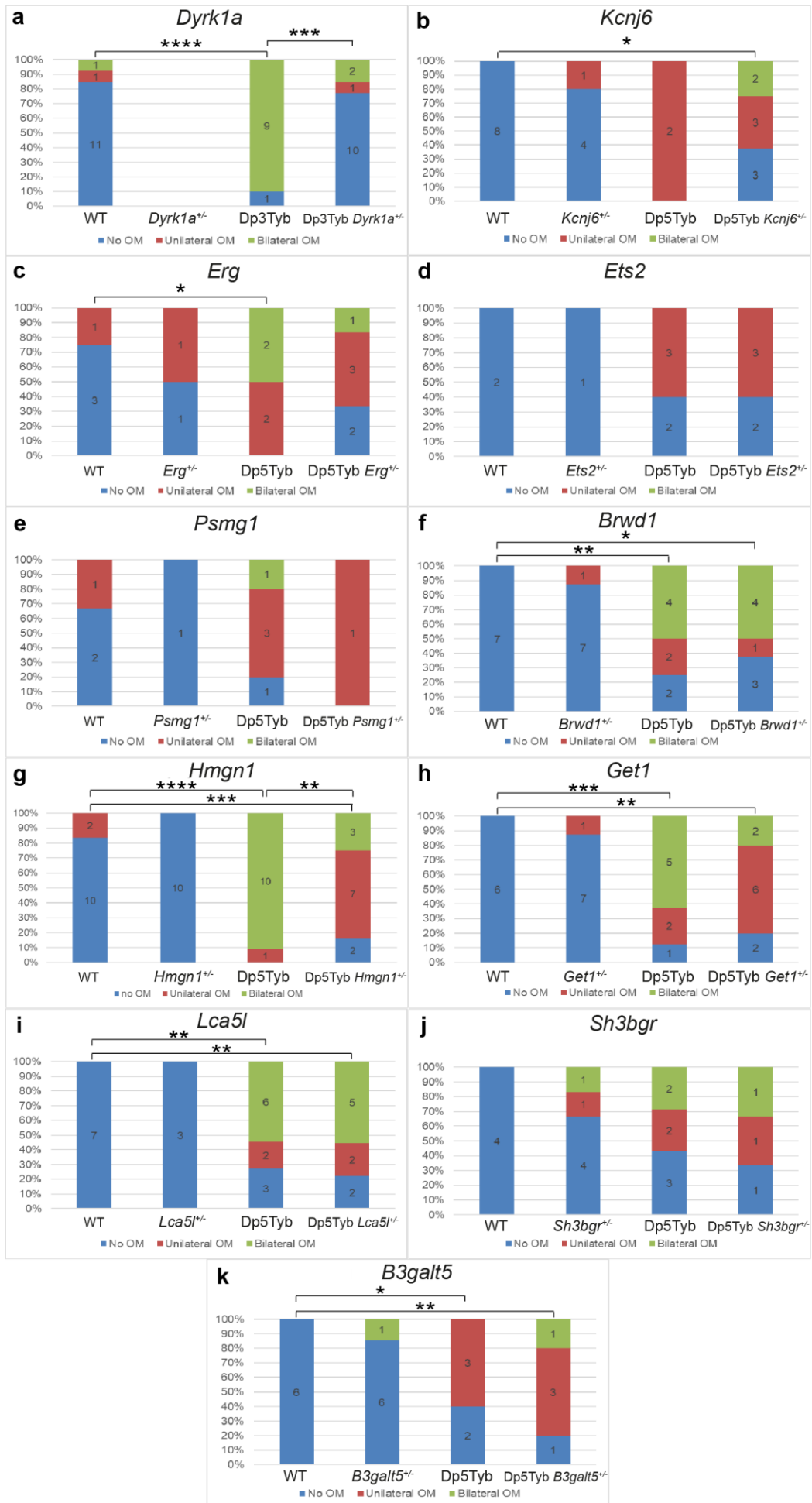


**Figure 5.16. Percentage of mice with OME when knockouts of single genes in the Dp5Tyb region were crossed to Dp3Tyb or Dp5Tyb mice to create double mutants.** Double mutants have two copies of the gene of interest. Bars represent the proportion of each genotype with no OM (blue), unilateral OM (red) and bilateral OM (green). Statistical analysis consisted of two-tailed unpaired t tests. P values denoted according to: \*\*\*\*  $\leq 0.0001$ , \*\*\*  $\leq 0.001$ , \*\*  $\leq 0.01$ , \*  $\leq 0.05$ . Sample numbers are shown on the bars. Note that no *Kcnj15* knockout mouse strain was available so there are only 11 crosses. Heads from the Dp5Tyb *Hmgn1*<sup>+/-</sup> cross came from the Francis Crick Institute. Heads from the Dp3Tyb *Dyrk1a*<sup>+/-</sup> cross were also sent from the Francis Crick Institute, but no *Dyrk1a*<sup>+/-</sup> heads were available so the OME phenotype of these mice is unknown.

#### 5.2.4.1. Dp3Tyb *Dyrk1a*<sup>+/-</sup>

The majority of Dp3Tyb mice had OME and, as expected, the WT littermates had a much lower incidence ( $p < 0.0001$ ) (Figure 5.16a). Significantly fewer Dp3Tyb *Dyrk1a*<sup>+/-</sup> mice had OME compared to Dp3Tyb littermates ( $p = 0.0001$ ), and importantly, there was no significant difference in OME incidence between Dp3Tyb *Dyrk1a*<sup>+/-</sup> mice and WT littermates ( $p = 0.5743$ ). This means that restoring disomy of *Dyrk1a*<sup>+/-</sup> in Dp3Tyb mice rescued the OME phenotype and restored it to WT level.

#### 5.2.4.2. Dp5Tyb *Kcnj6*<sup>+/-</sup>

The sample number for Dp5Tyb mice from this cohort was too low to be included in the statistical analysis. However, the double mutants (Dp5Tyb *Kcnj6*<sup>+/-</sup>) had significantly more OME than the WT littermates ( $p = 0.0102$ ) (Figure 5.16b), so *Kcnj6* is not likely to be the causative gene for OME in Dp5Tyb mice.

#### 5.2.4.3. Dp5Tyb *Erg*<sup>+/-</sup>

WT mice had significantly less OME than Dp5Tyb littermates ( $p = 0.0169$ ). There was no significant difference between the OME incidence in WT mice and double mutants (Dp5Tyb *Erg*<sup>+/-</sup>) ( $p = 0.2139$ ). This would suggest a partial rescue of the Dp5Tyb OME phenotype, however the double mutants do not have significantly less OME than Dp5Tyb mice ( $p = 0.1740$ ) (Figure 5.16c). The low sample numbers must be

CHAPTER 5: Middle ear expression of the 12 Dp5Tyb genes, and analysis of double mutants taken into account, and more sections need to be analysed to determine whether *Erg* is involved in OME pathogenesis.

#### 5.2.4.4. Dp5Tyb *Ets2*<sup>+/-</sup>

The sample number for this cross was too low for statistical analysis (*Figure 5.16d*).

#### 5.2.4.5. Dp5Tyb *Psmg1*<sup>+/-</sup>

There is currently no significant difference in OME incidence between WT and Dp5Tyb mice ( $p = 0.2199$ ) (*Figure 5.16e*), but this is likely due to low sample numbers. No conclusions can be drawn yet about the involvement of *Psmg1* in OME.

#### 5.2.4.6. Dp5Tyb *Brwd1*<sup>+/-</sup>

The OME incidence was the same in Dp5Tyb and double mutant mice ( $p = 0.7942$ ), and WT mice had significantly less OME than Dp5Tyb and double mutants ( $p = 0.0026$ ,  $p = 0.0105$ ) (*Figure 5.16f*). These results indicate that *Brwd1* is not likely to be the causative gene.

#### 5.2.4.7. Dp5Tyb *Hmgn1*<sup>+/-</sup>

The *Hmgn1*<sup>+/-</sup> mice had no OME, and Dp5Tyb mice had significantly more OME than the WT littermates ( $p < 0.0001$ ) (*Figure 5.16g*). Significantly fewer Dp5Tyb *Hmgn1*<sup>+/-</sup> mice had OME compared to Dp5Tyb littermates ( $p = 0.0012$ ), but the OME incidence in double mutants was still significantly higher than in WT littermates ( $p = 0.0005$ ). This suggests that *Hmgn1* is not a key gene, but the partial rescue of the Dp5Tyb OME phenotype suggests *Hmgn1* may be involved in OME pathogenesis.

#### 5.2.4.8. Dp5Tyb *Get1*<sup>+/-</sup>

*Get1* is also known as *Wrb*. For this cross, Dp5Tyb mice had significantly more OME than their WT littermates ( $p = 0.0004$ ). *Get1* is not believed to be the dosage-sensitive gene as Dp5Tyb and double mutant (Dp5Tyb *Get1*<sup>+/-</sup>) mice have a similar

CHAPTER 5: Middle ear expression of the 12 Dp5Tyb genes, and analysis of double mutants OME incidence ( $p = 0.1555$ ), and double mutants have significantly more OME than WT mice ( $p = 0.0028$ ) (*Figure 5.16h*).

#### 5.2.4.9. Dp5Tyb *Lca5*<sup>+/-</sup>

*Lca5* is also not thought to be the causative gene as Dp5Tyb and double mutant mice have an almost identical OME incidence ( $p = 0.8810$ ), and double mutants are much more affected by OME than their WT littermates ( $p = 0.0012$ ). Dp5Tyb mice have significantly more OME than WT mice as expected ( $p = 0.0020$ ) (*Figure 5.16i*).

#### 5.2.4.10. Dp5Tyb *Sh3bgr*<sup>+/-</sup>

Currently there are no significant differences in OME incidence between WT and Dp5Tyb ( $p = 0.0956$ ), or WT and double mutant mice ( $p = 0.0932$ ). This is likely due to the low sample number rather than an indication that *Sh3bgr* is involved in OME, as the double mutants currently have the same OME incidence as Dp5Tyb mice ( $p = 0.8287$ ) (*Figure 5.16j*).

#### 5.2.4.11. Dp5Tyb *B3galt5*<sup>+/-</sup>

As expected, Dp5Tyb had a higher incidence of OME than WT mice ( $p = 0.0239$ ). Dp5Tyb and double mutant mice had a similar incidence ( $p = 0.3466$ ), with double mutant mice affected more severely. WT mice had a significantly lower OME incidence than double mutants ( $p = 0.0067$ ), indicating that the dosage of *B3galt5* has no effect on the Dp5Tyb OME phenotype.

### 5.3. Discussion

The first aim of this chapter was to determine the expression of the 12 Dp5Tyb genes in the middle ear epithelium of WT and Dp5Tyb mice. This was investigated at both the transcript and protein level through RT-qPCR and immunohistochemistry respectively. The second aim was to cross single gene knockout mice to Dp3Tyb or Dp5Tyb mice and observe whether the OME phenotype is rescued.

#### 5.3.1. Expression of the Dp5Tyb genes at the transcript level

RT-qPCR showed that gene expression is generally highest in the Dp5Tyb fluid, followed by the epithelial samples, followed by the blood. Surprisingly the Dp5Tyb samples did not have significantly higher gene expression than their equivalent WT samples (*Figure 5.1*). *Dyrk1a* and *B3galt5* were not significantly upregulated in Dp5Tyb mice at the transcript level, despite their fold changes being 1.34 and 2.69-fold respectively.

The in-depth analysis by George Nicholson highlighted that the majority of the ear fluid and epithelial cell samples had low RNA integrity numbers (RIN) (*Figure 5.2*). This is likely due to the length of time taken to collect the samples, as blood samples were taken via retro-orbital bleed immediately after death, whereas collection of middle ear fluid and epithelial cells required dissection under a microscope, during which time the RNA will have degraded slightly. Overall, this additional analysis and graphical representation offers a deeper insight into the RNA expression data as any trends can be clearly observed. The data suggest that for future experiments the collection of samples from the middle ear needs to be performed on ice to preserve the RNA integrity, and the RNA should be extracted in one batch if possible to avoid batch variation.

CHAPTER 5: Middle ear expression of the 12 Dp5Tyb genes, and analysis of double mutants

The human data generated by Regie Santos-Cortez highlighted *DYRK1A* as a gene that was expressed significantly more in children with DS than in their non-DS mothers (*Figure 5.3*). Although this doesn't correlate to the data from mice, it does correlate with the gene dosage of *DYRK1A* in these individuals. In Dp5Tyb mice, gene expression in the white blood cells of the middle ear fluid and epithelial cells of the middle ear lining was investigated. These samples were not available from the children with DS, but saliva was the best alternative available. Saliva collection is a non-invasive process, and the sample contains white blood cells and epithelial cells from which genetic information can be extracted (Garbieri et al., 2017).

### 5.3.2. Expression of the Dp5Tyb genes at protein level

Quantification of the proteins KCNJ15 and SH3BGR was not possible as although nuclear staining was present, this was likely non-specific according to localisation data on GeneCards®. Only the proteins that were expressed in the nucleus could be analysed as staining in other subcellular compartments is much harder to quantify. The exception was B3GALT5, as although not localised to the nucleus, the golgi apparatus staining was clear and quantifiable. The protein HMGN1 is expressed in the nucleus according to GeneCards®, but only faint nuclear staining was observed. This staining was still quantified, but heat-mediated antigen retrieval likely would have increased the strength of the staining.

Quantification of the successful IHC showed that only *DYRK1A* was expressed in significantly more Dp5Tyb than WT epithelial cells (*Figure 5.4*). All other proteins showed the trend of being expressed in a slightly higher percentage of Dp5Tyb epithelial cells, or exactly the same in WT and Dp5Tyb epithelium. No proteins were expressed more in WT epithelium than Dp5Tyb.

There was evidence for some proteins (KCNJ15 and SH3BGR) of non-specific staining. For future experiments a blocking peptide could be used. These are peptides that perfectly match the epitope that the antibody was designed to bind to. The antibody is incubated with an excess of the peptide before adding them to the histological sections. They should bind to each other (instead of the antibody binding to the protein in the sample) and the tissue should show no staining when compared to sections incubated with the antibody alone. If staining is still seen it indicates that non-specific binding is taking place.

Additional future work would be to repeat the IHC for GIRK2, KCNJ15, HMGN1 and SH3BGR. Blocking peptides would be used to highlight any non-specific staining, and the protocols would be further optimised regarding antigen retrieval and antibody concentrations to ensure the staining is clearer. The DAB chromogen used for visualisation can spread to give a background stain. More precise staining could be obtained using fluorescence IHC combined with confocal or super resolution microscopy to accurately observe sub-cellular localisation of the staining. This could also be used to quantify protein expression per cell.

The phenotypes associated with DS are mostly attributed to overexpression of the genes present in trisomy (Antonarakis et al., 2004). Between 29-62% of trisomic genes are overexpressed at the expected level of 1.5-fold, as reviewed by (Duchon and Herault, 2016). My RT-qPCR data showed that 50% of the Dp5Tyb genes were at least 1.5-fold upregulated in Dp5Tyb middle ear epithelium, relative to a baseline of WT middle ear epithelium. However my IHC data (for the 10 proteins successfully quantified) indicated that most of the Dp5Tyb proteins were expressed quite equally in WT and Dp5Tyb epithelium, apart from *DYRK1A* which was expressed 3-fold more. Others have found that *DYRK1A* is expressed 1.5-fold higher at both the mRNA and protein level in foetal and adult brain samples (Demuro et al., 2021).

CHAPTER 5: Middle ear expression of the 12 Dp5Tyb genes, and analysis of double mutants  
Another group found *DYRK1A* to be overexpressed 1.5-fold in the brain of all human patients and mouse models of DS, but not children under three (Dowjat et al., 2007). The human data from collaborators showed a 1.5x increase in *DYRK1A* expression in the saliva of children with DS compared to their mothers (Figure 5.3).

### 5.3.3. Restoring disomy of each Dp5Tyb gene to find the dosage-sensitive gene(s) causing OME

The second aim of this chapter was to cross single gene knockout mice to Dp5Tyb (or Dp3Tyb mice) and observe the OME phenotype of the double mutant offspring. The hypothesis being that there is a dosage-sensitive gene in the Dp5Tyb region that, when present in three copies, is driving OME pathogenesis.

*Dyrk1a* is involved with several cellular processes which may play a role in epithelial inflammation, so *Dyrk1a* dosage was investigated to see if it influences OME development in DS. *Dyrk1a*<sup>+/-</sup> mice were crossed to Dp1Tyb mice at both the Francis Crick Institute and the MLC at MRC Harwell. At the Francis Crick Institute, Dp1Tyb *Dyrk1a*<sup>+/-</sup> mice had significantly less OME than Dp1Tyb littermates ( $p = 0.0021$ ), but the OME incidence was still significantly higher than WT littermates ( $p = 0.0022$ ) (Tateossian et al., 2022). This means that the WT phenotype was not completely restored in Dp1Tyb *Dyrk1a*<sup>+/-</sup> mice. In the MLC, the results were similar to the Francis Crick Institute. Dp1Tyb *Dyrk1a*<sup>+/-</sup> mice had significantly less OME than Dp1Tyb littermates ( $p = 0.0110$ ) and significantly more OME than WT littermates ( $p = 0.0096$ ) (Tateossian et al., 2022). Histological analysis of *Dyrk1a*<sup>+/-</sup> mice from both locations showed no OME. The incomplete rescue of the WT OME phenotype in Dp1Tyb *Dyrk1a*<sup>+/-</sup> mice is likely due to the influence of other genes on Mmu16.

In contrast, restoring *Dyrk1a* to two copies in Dp3Tyb mice rescued the OME phenotype to WT levels. This finding indicates that *Dyrk1a* is involved in the development of OME in Dp3Tyb mice, and therefore Dp5Tyb mice too as *Dyrk1a* is in the Dp5Tyb region within Dp3Tyb (see Introduction, *Figure 1.3*). The rest of the Dp3Tyb region consists of the Dp4Tyb and Dp6Tyb regions, and mice with duplications of these regions don't have OME (see Introduction, *Figure 1.3*). Thus, the dosage-sensitive causative gene must be in the Dp5Tyb region.

The crosses highlighted another dosage-sensitive gene that may be involved in OME pathogenesis – *Hmgn1*. Dp5Tyb *Hmgn1*<sup>+/-</sup> mice had significantly less OME than Dp5Tyb mice, but still significantly more than WT littermates. The phenotype was therefore partially rescued.

All other crosses either had sample numbers that were too low, or the incidence of OME in Dp5Tyb mice and double mutants was not significantly different. It is important to note that some of the single gene knockout mice had unilateral OME, but the OME incidence was very similar to their WT littermates. This indicates that knocking out the genes did not predispose the mice to OME, and it was the Dp5Tyb OME that was being displayed in the double mutants.

Future work would be to analyse the rest of the histological sections from the crosses. The COVID-19 lockdowns delayed the import of mouse lines from other facilities. The lockdowns also caused the MLC to downsize mouse colonies (including Dp5Tyb) to reduce the workload for their staff while they were social distancing and had reduced staffing levels. In addition to this, the MRC Harwell histology department has only had one member of staff since July, which has slowed output dramatically.

CHAPTER 5: Middle ear expression of the 12 Dp5Tyb genes, and analysis of double mutants

This chapter addressed the second and third aims of this thesis – studying expression of the 12 Dp5Tyb genes and their protein products in the middle ear, and phenotypic analysis of double mutants. The next chapter will address the fourth and final aim – investigating the mechanism of DYRK1A involvement in OME pathogenesis.

## CHAPTER 6: Investigating the role of DYRK1A in otitis media

---

### 6.1. Introduction

Dual-specificity tyrosine-(Y)-phosphorylation regulated kinase 1a (DYRK1A) is involved with several cellular processes which may play a role in inflammation (Kim et al., 2023). In Chapter 5 I investigated whether *Dyrk1a* dosage influences OME development in DS. Normalizing *Dyrk1a* gene dosage in Dp3Tyb mice reduced the incidence of OME to a level that was not significantly different from the WT littermates. This demonstrates that *Dyrk1a* is a major gene involved in OME pathogenesis in DS.

Several pathways are thought to crosstalk with DYRK1A, such as Hedgehog (Hh) signalling, which interacts with Transforming Growth Factor (TGF)- $\beta$  signalling (Singh and Lauth, 2017, Pelullo et al., 2019). DYRK1A has also been shown to crosstalk with TGF- $\beta$ /SMAD signalling (Li et al., 2022). This is of interest as TGF- $\beta$  signalling is known to be involved in OME (Tateossian et al., 2009, Tateossian et al., 2013).

The potential involvement of DYRK1A in the T cell response and its role in OME also merits consideration. T cells are white blood cells (lymphocytes) that are part of the immune response to an invading pathogen. Broadly they can be categorised into CD8<sup>+</sup> (which includes cytotoxic T cells) and CD4<sup>+</sup> (which includes helper and regulatory T cells) (Dutta et al., 2021). T cells patrol the body looking for foreign antigens, and are particularly numerous in lymphoid tissues and mucosal surfaces (Ganusov and De Boer, 2007). Once activated by a foreign antigen, helper T (Th) cells secrete pro-inflammatory cytokines to coordinate an immune response from other cells, such as B cells (Cosmi et al., 2014). The role of cytotoxic T cells is to kill infected cells (Nolz, 2015). Regulatory T cells (Treg) are anti-inflammatory and act to

## CHAPTER 6: Investigating the role of DYRK1A in otitis media

calm the immune response once the pathogen is no longer a threat (Oukka, 2008). As naïve CD4<sup>+</sup> T cells are maturing in the thymus they differentiate into either pro-inflammatory Th cells, or anti-inflammatory Treg cells (Cosmi et al., 2014). Types of Th cells include Th1, Th2, and Th17 (Annunziato et al., 2012). For this project I focused on Th17 cells as they appear to be the key driver of disease pathogenesis in other inflammatory disorders (Tesmer et al., 2008). Th17 cells are known to recruit leukocytes (such as neutrophils) to sites of inflammation (Tesmer et al., 2008), and also secrete TNF- $\alpha$  to enhance neutrophil recruitment (Annunziato et al., 2012). Many neutrophils were seen in the middle ear fluid associated with OME (see Chapter 4 *Figure 4.7*). Another potential link between Th17 cells and OME is that IL-17 (secreted by Th17 cells) and IL-6 together have been shown to stimulate the production of mucins by airway epithelial cells (Chen et al., 2003). Increased production of mucins is a hallmark of OME (Smirnova et al., 2002).

DYRK1A may be involved in deciding the fate of naïve CD4<sup>+</sup> T cell pre-cursors (Khor et al., 2015). An imbalance of pro-inflammatory helper T cells (Th17) and anti-inflammatory regulatory T cells (Treg) cells has been documented in patients with OM and in OM mouse models (Tang et al., 2020). The initial differentiation of naïve CD4<sup>+</sup> T cells is coordinated by TGF- $\beta$ , which promotes the development of protective Treg cells. However, in the presence of pro-inflammatory cytokines such as IL-6, TGF- $\beta$  will induce the production of pathogenic Th17 cells instead (Bettelli et al., 2006, Veldhoen et al., 2006). DYRK1A has been found to play a role in the process of T cell differentiation, as inhibition of DYRK1A both promotes Treg cell production and suppresses Th17 cells (Khor et al., 2015). This places DYRK1A at the branch point where the lineage is chosen for a naïve CD4<sup>+</sup> T cell pre-cursor. Th17 cells release cytokines such as IL-17 and IL-21 (Oukka, 2008), and Treg cells secrete IL-10. HIF-1 $\alpha$  has also been implicated in T cell differentiation (McNamee et al., 2013),

## CHAPTER 6: Investigating the role of DYRK1A in otitis media

with several studies suggesting that HIF-1 $\alpha$  promotes Th17 production and inhibits Treg cells (Dang et al., 2011, Shi et al., 2011).

Hypoxia-inducible factor (HIF) transcription factors control the cellular changes that occur due to low oxygen availability (Palazon et al., 2014). One of these transcription factors is HIF-1 $\alpha$ , which is degraded under normoxic conditions. Inflammation and hypoxia induce the expression of HIF-1 $\alpha$  by immune cells and stabilise the HIF-1 $\alpha$  protein (Palazon et al., 2014). This then activates the transcription of genes involved in the formation of new blood vessels, such as *Vegfa* (Palazon et al., 2014), and pro-inflammatory cytokines, such as *Tnfa* and *Il1 $\beta$*  (Mancino et al., 2008). Vascular endothelial growth factors (VEGFs) and their receptors promote growth of new blood vessels (angiogenesis) both during normal development and in disease (Lohela et al., 2009). Elevated VEGF has been shown to increase vascular leakage and effusion in OME (Cheeseman et al., 2011). DYRK1A is likely to be involved in the VEGF signalling pathway, as reduced vasculature was found in *Dyrk1a*<sup>+/-</sup> mice compared to WT littermates (Rozen et al., 2018). DYRK1A was also found to be positively regulating VEGF-dependent nuclear factor of activated T cells (NFAT) activation, which is a key part of endothelial cell angiogenesis (Rozen et al., 2018). It will thus be important to investigate the potentially diverse mechanisms by which *Dyrk1a* is involved in OME pathogenesis. This chapter will explore this final aim of this thesis. The expression of DYRK1A and other associated proteins in the middle ear epithelium of mouse models of DS will be compared to WT littermates and mice with two copies of *Dyrk1a* (Dp3Tyb *Dyrk1a*<sup>+/-</sup>). Expression of downstream proteins in Dp5Tyb middle ear fluid will be compared to expression in the uninfamed environment of Dp5Tyb and WT blood. These experiments should offer insight into how an extra copy of *Dyrk1a* could be driving the development of OME in DS.

## 6.2. Results

### 6.2.1. DYRK1A, SMAD proteins, VEGF-A and IL-6 were restored to WT levels when *Dyrk1a* copy number was normalised

After identifying that increased *Dyrk1a* dosage is involved in OME in DS, the expression of DYRK1A in the middle ear epithelium was studied. The expression of other proteins in pathways related to DYRK1A, such as phospho-SMAD2 (pSMAD2), SMAD3, VEGF-A, IL-6 and IL-10 were also investigated. Paraffin-embedded sections from the middle ear of mice with three copies (Dp3Tyb and Dp5Tyb) and two copies of the *Dyrk1a* gene (Dp3Tyb *Dyrk1a*<sup>+/-</sup> and WT littermates) were used for the immunohistochemistry (IHC).

IHC shows DYRK1A localised in the middle ear epithelium (*Figure 6.1a*). A 50% increase in the number of cells positive for DYRK1A was detected in Dp3Tyb and Dp5Tyb mice compared to their WT littermates and Dp3Tyb *Dyrk1a*<sup>+/-</sup> mice, which correlates with their *Dyrk1a* copy number (*Figure 6.1b*).

Phospho-SMAD2 (pSMAD2) and SMAD3 are involved in TGF- $\beta$  signalling, which may crosstalk with DYRK1A. IHC showed that pSMAD2 and SMAD3 were expressed in a significantly higher percentage of epithelial cells in the middle ear epithelium of the DS lines (Dp3Tyb and Dp5Tyb) compared to WT littermates (for Dp3Tyb:  $p = 0.0001$  and  $p = 0.0007$ ; for Dp5Tyb:  $p = 0.0011$  and  $p = 0.0093$ ). Interestingly, expression of pSMAD2 and SMAD3 was restored to WT level in Dp3Tyb *Dyrk1a*<sup>+/-</sup> epithelium ( $p = 0.6171$ ,  $p = 0.8413$ ) (*Figure 6.1b*).

DYRK1A may be involved in naïve T cell differentiation, along with TGF- $\beta$  and IL-6. The absence of IL-6 causes production of Treg cells (Bettelli et al., 2006), and so does the inhibition of DYRK1A (Khor et al., 2015). IHC showed that IL-6 expression

## CHAPTER 6: Investigating the role of DYRK1A in otitis media

was upregulated in the DS lines (Dp3Tyb  $p = 0.0013$ ; Dp5Tyb  $p = 0.0041$ ) compared to WT littermates, and restored to WT level in Dp3Tyb *Dyrk1a*<sup>+/-</sup> ( $p = 0.2159$ ). IL-10 is secreted by the anti-inflammatory Treg cells, and there was no significant difference in IL-10 expression across any of the genotypes (*Figure 6.1b*).

VEGF-A is involved in vascular leakage, which is believed to be the cause of increased effusion in OM. Significantly more cells were expressing VEGF-A in the DS lines compared to WT littermates (Dp3Tyb  $p < 0.0001$ ; Dp5Tyb  $p < 0.0001$ ), and expression of VEGF-A in Dp3Tyb *Dyrk1a*<sup>+/-</sup> mice was indistinguishable from WT ( $p = 0.9542$ ). VEGF was found by others to be expressed in ciliated epithelial cells and some inflammatory cells (Jung et al., 1999). This corresponds with the staining seen in *Figure 6.1a*.

Mice from two litters were used for this staining. Both litters were from crosses produced at the Francis Crick Institute. The first litter were from a cross between Dp3Tyb and *Dyrk1a*<sup>+/-</sup> mice, these are the WT, Dp3Tyb and Dp3Tyb *Dyrk1a*<sup>+/-</sup> mice on the left side of each bar graph. The second litter was from a Dp5Tyb *Hmgn1*<sup>+/-</sup> cross. These are the WT and Dp5Tyb mice on the right side of each bar graph.

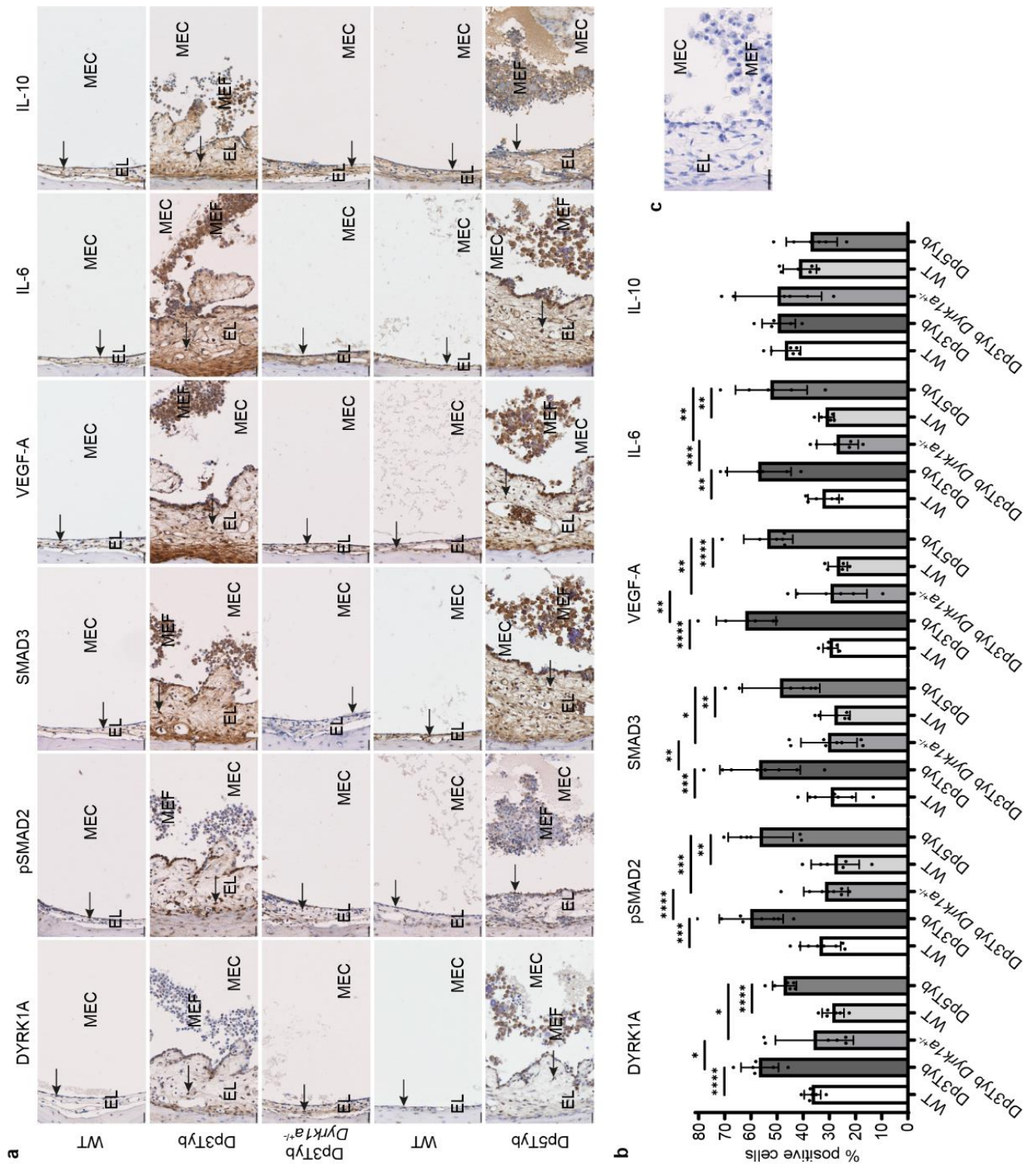


**Figure 6.1. Immunohistochemistry showing expression of DYRK1A and associated proteins.** (a) Immunohistochemistry (IHC) on paraffin-embedded transverse middle ear sections, with antibodies against DYRK1A, phospho-SMAD2 (pSMAD2), SMAD3, VEGF-A, IL-6 and IL-10. The positive cells are stained brown, against a blue Haematoxylin counterstain. Arrows highlight examples of positive cells. EL = epithelial lining; MEC = middle ear cavity; MEF = middle ear fluid. Scale bar = 25  $\mu$ m. (b) Bar graphs of the IHC data, quantified by manually counting the cells, and represented as a percentage of the epithelial cells that are expressing the protein. For WT, Dp3Tyb and Dp3Tyb *Dyrk1a*<sup>+/+</sup>, n = 6 per genotype for DYRK1A, VEGF-A, IL-6 and IL-10, and n = 8 per genotype for pSMAD2 and SMAD3. For WT and Dp5Tyb, n = 6 per genotype on all graphs. Significance levels are represented by \* = p $\leq$ 0.05, \*\* = p $\leq$ 0.01, \*\*\* = p $\leq$ 0.001, \*\*\*\* = p $\leq$ 0.0001 and were calculated using two-tailed unpaired t-tests. Error bars: mean  $\pm$  standard deviation. (c) Negative control (no primary antibody) for the IHC to check for non-specific secondary antibody binding. Scale bar = 25  $\mu$ m. Mice were two-months-old. Figure modified from one included in our manuscript in preparation (Tateossian et al., 2022).

### 6.2.2. The pro-inflammatory Th17 lineage is activated in Dp5Tyb mice, and hypoxia-related proteins are upregulated in Dp5Tyb middle ear fluid

Expression of T cell-related cytokines and hypoxia-related proteins in the middle ear fluid of Dp5Tyb mice was compared to expression in blood from the same animals and blood from WT littermates (*Figure 6.2*). The rationale being that the white blood cells (WBCs) present in the blood are in a non-inflamed environment compared to those in the Dp5Tyb middle ear fluid.

An imbalance of regulatory T cells (Treg) and helper T cells (Th17) is reported in OME patients (Tang et al., 2020). A Meso Scale Discovery (MSD) immunoassay was used to investigate whether more Th17 or Treg cells were present in Dp5Tyb middle ear fluid, and whether this varied between the middle ear and blood from Dp5Tyb or WT mice.

DYRK1A is believed to be at the branch point where naïve T cells enter one of these lineages (Khor et al., 2015). TGF- $\beta$  and IL-6 together promote the Th17 lineage (Bettelli et al., 2006). Th17 cells secrete IL-17A and IL-21, which were significantly upregulated in Dp5Tyb middle ear fluid compared to Dp5Tyb serum ( $p = 0.0120$ ,  $p = 0.0142$ ) and also WT serum ( $p = 0.0043$ ,  $p = 0.0143$ ). IL-6 expression follows the same pattern, with significantly more IL-6 being expressed in Dp5Tyb fluid compared to blood serum from Dp5Tyb and WT mice ( $p = 0.0042$ ,  $p = 0.0019$ ).

IL-10 is secreted by the anti-inflammatory Treg cells. Expression of IL-10 was consistent in blood serum and fluid. No significant difference was seen in IL-10 expression between Dp5Tyb fluid and Dp5Tyb or WT blood ( $p = 0.1244$ ,  $p = 0.7497$ ).

The HIF signalling pathway promotes production of pro-inflammatory cytokines, such as IL-1 $\beta$  and TNF- $\alpha$ , and VEGF-A expression is also enhanced by HIF (Malkov et al., 2021). We can therefore expect higher expression of these proteins under hypoxic

## CHAPTER 6: Investigating the role of DYRK1A in otitis media

conditions. IL-1 $\beta$  and VEGF-A were significantly upregulated in Dp5Tyb fluid compared to Dp5Tyb blood ( $p < 0.0001$ ,  $p = 0.0009$ ) and WT blood ( $p = 0.0001$ ,  $p = 0.0056$ ). TNF- $\alpha$  followed the trend of increased expression in Dp5Tyb fluid, but was not significantly increased compared to Dp5Tyb or WT blood ( $p = 0.4776$ ,  $p = 0.1005$ ).

No significant difference in expression was seen between WT and Dp5Tyb blood for any proteins measured, apart from TNF- $\alpha$ , which was expressed more in Dp5Tyb blood ( $p = 0.0205$ ).

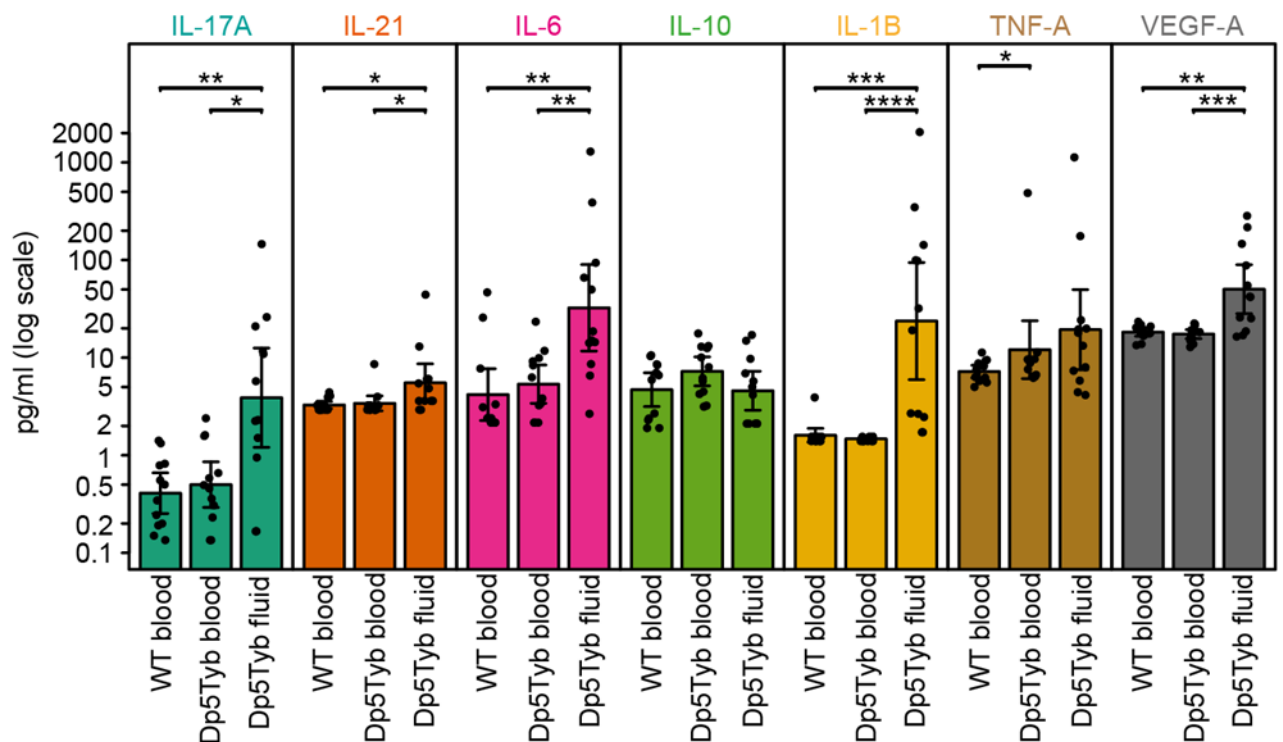


**Figure 6.2. Meso Scale Discovery (MSD) assay to quantify protein levels in WT and Dp5Tyb blood serum, and Dp5Tyb middle ear fluid.** Antibodies were used against IL-17A, IL-21, IL-6, IL-10, IL-1 $\beta$ , TNF- $\alpha$ , and VEGF-A. Each point corresponds to a single sample which was measured repeatedly and averaged (see data pre-processing in Methods). For each group in each panel the height of the coloured bar indicates the mean and error bars extend to  $\pm 2$  SEM (standard error of the mean). For each pairwise comparison in a panel a two-sided Mann–Whitney–Wilcoxon (MWW) test was performed and raw p-values are denoted according to: \*\*\*\*  $< 0.0001$ , \*\*\*  $< 0.001$ , \*\*  $< 0.01$ , \*  $< 0.05$ . In order to control for multiple testing, we applied the Benjamini-Hochberg procedure to the complete set of 24 p-values arising from all the MWW tests across all assays and pairs of groups. Rejecting the null in all starred cases (\*, \*\*, \*\*\* and \*\*\*\*) controlled the false discovery rate (FDR) below 5%. WT blood serum  $n = 12$ ; Dp5Tyb blood serum  $n = 12$ ; Dp5Tyb fluid  $n = 12$ . Mice were two-months-old. Data were analysed and graph created by George Nicholson. This figure was included in our manuscript in preparation (Tateossian et al., 2022).

N.B. The IL-1 $\beta$ , TNF- $\alpha$ , and VEGF-A data were previously shown in Chapter 4 when discussing hypoxia signalling.

### 6.3. Discussion

After establishing that *Dyrk1a* is a major gene involved in OME in DS, I began to investigate how this gene may be involved in the pathogenesis of this disease.

DYRK1A has been reported to both positively and negatively regulate Hh signalling (Larsen and Møller, 2020). Hh signalling induces the expression of members of the TGF- $\beta$  signalling pathway (Pelullo et al., 2019), and TGF- $\beta$  signalling is known to be involved in OME (Tateossian et al., 2009, Tateossian et al., 2013). This implies there may be cross-talk between TGF- $\beta$  and DYRK1A, and this could be a mechanism by which DYRK1A is driving OME development. From analysing expression levels of TGF- $\beta$  pathway members (pSMAD2 and SMAD3), relative to WT littermates, these proteins were significantly upregulated in Dp3Tyb middle ear epithelium, however expression in Dp3Tyb *Dyrk1a*<sup>+/-</sup> mice was not significantly different to WT. This suggests that there is a positive correlation between TGF- $\beta$  signalling and *Dyrk1a* dosage.

TGF- $\beta$  signalling has been linked to hypoxia signalling (Cheeseman et al., 2011). Hypoxia causes the stabilisation of HIF-1 $\alpha$ , which works in combination with TGF- $\beta$  and SMAD3 to upregulate VEGF (Sánchez-Elsner et al., 2001, Jeon et al., 2007). Increased VEGF expression causes increased vascular leakage, leading to increased accumulation of middle ear fluid in OME (Sekiyama et al., 2011, Cheeseman et al., 2011). The hypoxic and inflamed middle ear environment created by fluid accumulation and inflammation could be activating TGF- $\beta$  signalling (Crompton et al., 2017), creating a positive feedback loop. The OME mouse model *Jeff* shows upregulated pSMAD2 in epithelial cells, a protein which is known to activate downstream genes in the TGF- $\beta$  signalling pathway (Tateossian et al., 2009). Macrophages are recruited to the middle ear during OME (see Chapter 4 *Figure 4.7*) and are known to produce TGF- $\beta$  in the resolution phase of inflammation

## CHAPTER 6: Investigating the role of DYRK1A in otitis media

(Kourtzelis et al., 2017). This could further explain why high levels of TGF- $\beta$ -related proteins (pSMAD2 and SMAD3) were seen in the inflamed middle ear.

TGF- $\beta$  signalling is also involved in the differentiation of naïve CD4<sup>+</sup> T cells. In the presence of IL-6, the pro-inflammatory helper T cell (Th17) pathway is induced (Veldhoen et al., 2006). However when IL-6 is absent, the anti-inflammatory regulatory T cell (Treg) pathway is chosen (Bettelli et al., 2006). DYRK1A is also thought to sit at this branch point of T cell differentiation and can suppress the development of Treg cells (Khor et al., 2015). The IHC data showed increased levels of IL-6 in DS middle ear epithelium, and the MSD data showed increased IL-6 in Dp5Tyb middle ear fluid compared to Dp5Tyb and WT blood. Both experiments found IL-10 to be expressed at a similar level regardless of tissue or genotype. These findings suggest that the T cells in the middle ear fluid are pro-inflammatory Th17 cells.

DYRK1A, pSMAD2, SMAD3, VEGF-A and IL-6 followed the pattern of being upregulated in mice with three copies of *Dyrk1a* (Dp3Tyb and Dp5Tyb mice), but were expressed at a WT level in mice with two copies of *Dyrk1a* (Dp3Tyb *Dyrk1a*<sup>+/-</sup>). IL-10 was expressed very similarly in all epithelium regardless of genotype. The unchanging IL-10 expression is important as it indicates that there is unlikely to be a Treg response happening in the DS middle ear. No significant difference in expression was seen between double mutants and WT mice for any of the proteins. This suggests that increased *Dyrk1a* dosage is affecting TGF- $\beta$  signalling, T cell differentiation, and VEGF signalling.

Using MSD immunoassays to compare protein levels in WBCs from Dp5Tyb middle ear fluid to WBCs from Dp5Tyb and WT blood, showed markers for Th17 cells were significantly upregulated in the fluid and so were hypoxia markers. IL-17A is secreted

## CHAPTER 6: Investigating the role of DYRK1A in otitis media

by Th17 cells and was found to be significantly upregulated in Dp5Tyb middle ear fluid compared to blood. Overexpression of IL-17 in lung epithelium has been shown to trigger an immune response and inflammation, similar to the functions of TNF and IL-1 (Park et al., 2005). IL-21 promotes differentiation of naïve CD4<sup>+</sup> cells into Th17 cells, which then release more IL-21 (Annunziato et al., 2012). The finding of increased IL-21 expression is therefore supportive of the hypothesis that the Th17 lineage is being chosen. The marker for Treg cells, IL-10, was expressed fairly equally in blood and fluid, with a slightly decreased expression in middle ear fluid (although not significant). IL-6 expression was significantly increased in the Dp5Tyb fluid, and IL-6 (alongside TGF- $\beta$ ) is known to promote Th17 differentiation. These findings lead me to conclude that the activated T cells of the middle ear fluid are pro-inflammatory Th17 cells. This is supported by the IHC data showing upregulation of IL-6, combined with no change in the expression of IL-10, suggesting that increased *Dyrk1a* dosage may be causing naïve CD4<sup>+</sup> T cells to follow the pro-inflammatory Th17 lineage rather than the anti-inflammatory Treg lineage.

The MSD data also showed upregulation of IL-1 $\beta$ , TNF- $\alpha$  and VEGF-A in middle ear fluid compared to blood (although TNF- $\alpha$  was not statistically significant). IHC also showed increased VEGF-A expression in DS middle ear epithelium compared to WT. This is likely due to the hypoxia signalling and inflammation in the middle ear. These genes were also upregulated at the transcript level (see Chapter 4 *Figure 4.5*). Both Dp5Tyb and Dp1Tyb mice had significantly upregulated *Hif1 $\alpha$* , *Tnfa*, and *Vegfa* in the middle ear fluid compared to blood from the same animal and also WT littermates. The upregulation of *Il1 $\beta$*  at transcript level was not statistically significant (Tateossian et al., 2022). The increased *Hif1 $\alpha$*  mRNA could be at least partly due to the increased presence of Th17 cells, as ligation of their T cell receptor causes stabilisation and

CHAPTER 6: Investigating the role of DYRK1A in otitis media  
accumulation of *Hif1α* at the transcript and protein level (reviewed in (Palazon et al., 2014)).

Trisomy of *Dyrk1a* has been shown to cause other DS comorbidities, such as the motor dysfunction phenotype of Ts1Rhr mice (Watson-Scales et al., 2018). When the dosage of *Dyrk1a* was reduced to two copies (Ts1Rhr *Dyrk1a*<sup>+/-</sup>) the mice no longer had a locomotor deficit. However the authors did note that there could be several dosage-sensitive genes on Mmu16 contributing to the motor dysfunction, likely in the region duplicated in the Dp5Tyb, Ts1Rhr and Dp4Tyb mouse lines (Watson-Scales et al., 2018). Another group found that normalising *Dyrk1a* dosage also improves learning and memory deficits in Ts65Dn mice (García-Cerro et al., 2014)

DYRK1A inhibitors, such as harmine, have been shown to counteract the pro-inflammatory role of DYRK1A regarding T cell differentiation (Khor et al., 2015). The introduction of harmine reduced the inflammation seen in the epithelial lining of the gut and airways. Another DYRK1A inhibitor, Leucettine L41, has shown potential as a drug to treat the intellectual disability associated with DS after ameliorating memory deficits in three different mouse models of DS (Nguyen et al., 2018). Several other DYRK1A inhibitors are also available and their efficacy at rescuing various DS phenotypes is being tested in animal models of DS, for example: PST-001 (Zhu et al., 2022), Epigallocatechin-3-gallate (EGCG) (McElyea et al., 2016, Souchet et al., 2019), aristolactam BIII (Choi et al., 2021) and F-DANDY derivative 5a (3-(4-fluorophenyl)-5-(3,4-dihydroxyphenyl)-1H-pyrrolo[2,3-b]pyridine, 5a) (Neumann et al., 2018). Future work for this project would be to test one or more of these inhibitors in Dp3Tyb or Dp5Tyb mice to determine whether the OME phenotype can be rescued. The ideal inhibitor would be applied topically to the tympanic membrane to have a targeted effect on the middle ear, rather than a tablet or injection which would affect the mouse systemically.

## CHAPTER 6: Investigating the role of DYRK1A in otitis media

This chapter addressed the final aim of this thesis, which was to investigate the mechanism of *Dyrk1a* involvement in OME pathogenesis. In summary I believe that the accumulation of middle ear fluid is creating hypoxic conditions, which is causing a positive feedback loop as HIF-1 $\alpha$  upregulates VEGF, which increases angiogenesis and vascular leakage (Sekiyama et al., 2011, Cheeseman et al., 2011), adding to the middle ear effusion. Hypoxia could also be activating TGF- $\beta$  signalling which interacts with Hh signalling – a pathway known to cross talk with DYRK1A (Singh and Lauth, 2017). This suggests cross talk is possible between TGF- $\beta$  signalling and DYRK1A. This hypothesis is supported by the IHC results as mice with three copies of *Dyrk1a* (Dp3Tyb and Dp5Tyb) express more pSMAD2 and SMAD3 than mice with two copies of *Dyrk1a*. TGF- $\beta$ , in the presence of IL-6, triggers the differentiation of naïve T cells into pro-inflammatory Th17 cells (Bettelli et al., 2006). The additional copy of *Dyrk1a* could also be enhancing Th17 cell differentiation as DYRK1A sits at the branch point where this decision is made (Khor et al., 2015). Investigating the downstream pathways of DYRK1A has uncovered numerous ways that trisomy of *Dyrk1a* may be leading to the development and maintenance of OME in mice. This makes DYRK1A an excellent therapeutic target for OME in children with DS.

## CHAPTER 7: Discussion

---

### 7.1. Project overview

Children with Down syndrome (DS) are particularly susceptible to otitis media with effusion (OME) due to an unknown genetic component (Bhutta et al., 2013). The hearing loss caused by OME greatly affects the child's ability to develop their speech and language skills, particularly as children with DS already have learning difficulties (Nightengale et al., 2017). Finding the genetic cause of OME in DS could lead to the development of therapies to prevent the occurrence of, or help resolve, the middle ear fluid associated with OME.

The genes on human chromosome 21 (Hsa21) have orthologues on mouse chromosome 16 (Mmu16), Mmu17 and Mmu10. Research using mouse models with duplications of these chromosomes identified that only mice with a duplication of Mmu16 had OME, and this was a severe phenotype with all mice having bilateral OME (Tateossian et al., 2022). A mapping panel of the duplicated regions in DpTyb mice (Lana-Elola et al., 2016) was used to narrow down the causative genes from being in the Dp1Tyb region (duplication of Mmu16), to being in the Dp5Tyb region (duplication of 12 genes on Mmu16) (Tateossian et al., 2022). All Dp5Tyb mice had OME in one or both ears, but as this doesn't fully recapitulate the severe phenotype of Dp1Tyb mice, there is likely a second minor locus in the Dp10Tyb or Dp11Tyb region contributing to the OME phenotype of Dp1Tyb mice.

Using mouse models of DS, this project aimed to find the gene(s) which, when present in three copies, leads to the development of OME. Once the gene(s) were identified, their involvement in the pathological mechanisms of OME was investigated.

## CHAPTER 7: Discussion

The hypothesis for my PhD project was that there is a major locus in the Dp5Tyb region that, when present in three copies, leads to OME. To investigate this, I established the following research aims:

- 1) Phenotypic characterisation of Dp5Tyb mice
- 2) Studying expression of the 12 Dp5Tyb genes and their protein products in the middle ear
- 3) Generation and phenotypic analysis of double mutants
- 4) Investigating the mechanism of DYRK1A involvement in OME pathogenesis

### 7.2. Summary of results

#### 7.2.1. Dp5Tyb as a mouse model of DS

As part of the phenotypic analysis of Dp5Tyb mice, it was investigated whether they have the same craniofacial defects as the Dp1Tyb mouse model of DS (Tateossian et al., 2022). The same trend of a shorter and wider frontal bone was seen in Dp1Tyb and Dp5Tyb mice. This is similar to the wider and flatter face shape often seen in people with DS (Tornali et al., 2021). This finding indicates that Dp5Tyb mice recapitulate one of the common phenotypes seen in people with DS, supporting their use as a mouse model of DS.

#### 7.2.2. Dp5Tyb as a mouse model of OME in DS

The ABR thresholds show that Dp5Tyb have reduced hearing for the whole time course measured (one-six months). Dp5Tyb mice all had OME in one or both ears, and the effusion was persistent for up to a year, indicating that it was chronic OME. The prolonged inflammation and hearing loss mirrors the condition seen in children with DS (Fortnum et al., 2014).

## CHAPTER 7: Discussion

Further study of the deafness phenotype of Dp5Tyb mice found that they likely had no sensorineural element to their hearing loss, as histological analysis and scanning electron microscopy imaging of the cochlea showed healthy hair cell morphology. However, more experiments would be required to rule out sensorineural hearing loss completely, such as distortion product otoacoustic emissions (DPOAEs) to test cochlear function (Abdala and Visser-Dumont, 2001). Dp5Tyb mice also do not appear to have any other cause for the conductive hearing loss detected by ABR. The ossicles have the same morphology as in WT mice, and no perforations were seen in the tympanic membranes. This leaves OME as the cause of the reduced hearing.

To investigate whether Dp5Tyb mice have altered middle ear epithelial lining, the goblet cells and cilia in the middle ear were studied. Other studies report a marked increase in the number of goblet cells present in the middle ear during an OME episode (Smirnova et al., 2002). However the AB-PAS stained sections that I observed appeared to show a similar number of goblet cells around the Eustachian tubes of WT and Dp5Tyb mice, although no quantification was performed. The ciliated epithelial cells in the Dp5Tyb middle ear appeared indistinguishable from WT at two weeks of age, this indicates that impaired ciliary function is not responsible for the development of OME at three weeks of age. Although Dp5Tyb mice may not have a ciliogenesis defect, they have impaired cilia maintenance as by two-months-old gaps are present in the lawn of cilia in the ventral region of the middle ear. This may be a secondary effect of the OME.

The middle ear fluid that accumulates during an episode of OME contains white blood cells that have entered the middle ear cavity from the surrounding blood vessels. Looking deeper into the composition of the Dp5Tyb middle ear fluid, neutrophils predominated the fluid at three weeks of age, followed by the arrival of

## CHAPTER 7: Discussion

more macrophages as the OME progressed. Neutrophils are the first leukocytes to be recruited to sites of inflammation. Their recruitment is enhanced by Th17 cells (Tesmer et al., 2008) and also by TNF- $\alpha$  which is secreted by Th17 cells (Annunziato et al., 2012).

During an episode of OME the epithelial lining becomes thickened. Staining showed that apoptosis and proliferation were occurring across the middle ear epithelium and fluid, with proliferation particularly prevalent in the epithelial cells at the leading edge (proximal to the middle ear cavity), highlighting the way in which the lining is expanding.

### 7.2.3. Expression of the 12 genes in the Dp5Tyb region

RT-qPCR data on middle ear epithelial cells showed that half of the Dp5Tyb genes are expressed 1.5-fold more or greater in Dp5Tyb than in WT epithelium (*Kcnj6* 1.63-fold, *Erg* 1.65-fold, *Ets2* 1.61-fold, *Hmgn1* 1.92-fold, *Wrb* 1.66-fold, *B3galt5* 2.69-fold). *Dyrk1a* was expressed 1.34-fold higher. However, the increased expression measured by RT-qPCR was not statistically significant for any gene. This can be explained by fold change and statistical significance measuring different parameters, as fold changes do not take variability or reproducibility into account. Statistical analysis can identify significant differences between values with very small fold changes which are not biologically relevant. It is therefore good practice to require a fold change of  $>1.5$  in addition to a p-value  $<0.05$  to confer a true difference in gene expression (McCarthy and Smyth, 2009). None of the 12 Dp5Tyb genes satisfied both the fold change and statistical significance criteria.

As a pilot study to observe whether humans with DS have differential expression of the Dp5Tyb genes, an RT-qPCR was performed with human saliva samples by our collaborators in Colorado. Middle ear tissue was not available from the children at the

## CHAPTER 7: Discussion

clinic, so saliva was chosen as a suitable alternative. Saliva sample collection is a non-invasive procedure, and saliva contains white blood cells and epithelial cells, which correlates to the middle ear fluid and epithelium samples taken from Dp5Tyb mice. *DYRK1A* was expressed 1.5-fold higher in children with DS compared to their non-DS mothers ( $p = 0.0044$ ). This correlates with *DYRK1A* gene dosage in DS. The other significant finding was a 14-fold downregulation in *KCNJ6* in children compared to their mothers ( $p = 0.0075$ ).

The immunohistochemistry data was quantifiable for 10 of the 12 Dp5Tyb proteins. Of these, the only protein expressed significantly more in Dp5Tyb epithelium compared to WT epithelium was *DYRK1A*, which was expressed 3-fold more in Dp5Tyb mice ( $p = 0.0464$ ).

### 7.2.4. Crossing single gene knockouts to Dp5Tyb or Dp3Tyb mice

The hypothesis was that one of the genes in the Dp5Tyb region, when present in three copies, is leading to the development of OME. By restoring disomy of the gene, the OME phenotype should be rescued to a WT level. Thus single gene knockout mice were crossed to Dp3Tyb or Dp5Tyb mice to produce double mutant offspring carrying two copies of the gene of interest. Double mutant mice were analysed for evidence of OME. When *Dyrk1a*<sup>+/-</sup> mice were crossed to Dp3Tyb, the Dp3Tyb *Dyrk1a*<sup>+/-</sup> offspring had significantly less OME than Dp3Tyb littermates, and the same OME incidence as WT littermates. This indicates that *Dyrk1a* is required in three copies for Dp3Tyb mice to have OME. Dp3Tyb is comprised of the Dp4Tyb, Dp5Tyb and Dp6Tyb regions, and of these only Dp5Tyb mice have OME. *Dyrk1a* is in the Dp5Tyb region. This demonstrates that *Dyrk1a* is the key dosage-sensitive gene causing the Dp5Tyb OME phenotype.

## CHAPTER 7: Discussion

The crosses highlighted another dosage-sensitive gene that could contribute to OME pathogenesis – *Hmgn1*. Dp5Tyb *Hmgn1*<sup>+/-</sup> mice had significantly less OME than Dp5Tyb mice, but still significantly more than WT littermates. The phenotype was therefore only partially rescued and the WT phenotype was not restored. It is possible that the role of *Hmgn1* in promoting chromatin accessibility, causing widespread transcriptional changes (Mowery et al., 2018), increases the susceptibility to OME in Dp5Tyb mice. This will require further investigation.

### 7.2.5. Hypoxia signalling in the Dp5Tyb middle ear

The epithelial lining of the airways is continuous with the middle ear mucoperiosteum via the Eustachian tube, meaning that the epithelial cells are usually in contact with oxygenated air. During an episode of OME, the fluid that accumulates in the middle ear prevents oxygen from reaching the middle ear cavity. This creates a hypoxic environment, which stabilises the Hypoxia Inducible Factor protein HIF-1 $\alpha$ . HIF-1 $\alpha$  then upregulates a wide range of downstream genes, including *Il1 $\beta$*  (*interleukin 1 $\beta$* ), *Tnfa* (*tumour necrosis factor  $\alpha$* ) and *Vegfa* (*vascular endothelial growth factor A*). Upregulation of these genes at the transcript and protein level was observed in Dp5Tyb middle ear fluid compared to Dp5Tyb and WT blood (although the increase in *Il1 $\beta$*  at transcript level and TNF- $\alpha$  at the protein level were not statistically significant). This is similar to findings in other mouse models of OME, as *Hif1 $\alpha$* , *Tnfa* and *Vegfa* were upregulated at the transcript level in the middle ear fluid of *Jeff*, *Junbo* (Cheeseman et al., 2011) and *edison* mice (Crompton et al., 2017), and the protein levels of VEGF, TNF- $\alpha$  and IL-1 $\beta$  were upregulated in the middle ear fluid of *Jeff*, *Junbo* (Cheeseman et al., 2011) and *Tgif1* knockout mice (Tateossian et al., 2013). These findings also mirror the trends of the transcript and protein expression of these four genes in the Dp1Tyb middle ear (Tateossian et al., 2022). The

reproducibility of these findings in several mouse models supports the theory that hypoxia signalling is involved in OME pathogenesis.

### 7.2.6. Mechanisms for *Dyrk1a* involvement in OME pathogenesis

Normalising *Dyrk1a* dosage rescued the OME phenotype of Dp3Tyb mice, and the hypoxia data described above provides mechanistic links to *Dyrk1a*. VEGF signalling promotes angiogenesis (Sekiyama et al., 2011). DYRK1A could be involved in the VEGF pathway as *Dyrk1a*<sup>+/-</sup> mice had reduced vasculature compared to WT mice (Rozen et al., 2018). DYRK1A was also found to enhance activation of VEGF-dependent Nuclear Factor of Activated T cells (NFAT), which plays a key role in angiogenesis (Rozen et al., 2018). VEGF-A was found to be upregulated in the middle ear epithelium of mice with three copies of *Dyrk1a*, compared to those with two copies - Dp3Tyb *Dyrk1a*<sup>+/-</sup> mice and WT mice. Elevated VEGF levels have been linked to increased vascular leakage, contributing to the accumulation of fluid in the middle ear cavity (Cheeseman et al., 2011). VEGF receptor inhibitors delivered to *Junbo* mice ameliorated the OME phenotype by reducing angiogenesis and vascular leakage (Cheeseman et al., 2011). These findings suggest that VEGF is playing a key role in OME pathogenesis, the effects of which could be enhanced in Dp5Tyb mice by the increased dosage of *Dyrk1a*.

*Dyrk1a* both positively and negatively regulates Hh signalling (Larsen and Møller, 2020), which in turn induces the expression of TGF- $\beta$  pathway proteins (Pelullo et al., 2019). TGF- $\beta$  has long been known to play a role in OME development in non-DS mouse models (Tateossian et al., 2009). The TGF- $\beta$  pathway proteins pSMAD2 and SMAD3 showed increased expression in mice with three copies of *Dyrk1a* (Dp3Tyb) compared to double mutant mice with two copies (Dp3Tyb *Dyrk1a*<sup>+/-</sup>) and WT mice. In *Jeff* mice pSMAD2 is upregulated in epithelial tissues (Tateossian et al., 2009).

## CHAPTER 7: Discussion

These findings suggest that TGF- $\beta$  is involved in OME pathogenesis, and in DS the expression of TGF- $\beta$  pathway members is influenced by *Dyrk1a* dosage.

*Dyrk1a* and TGF- $\beta$  are both involved in the differentiation of naïve CD4<sup>+</sup> T cells (Khor et al., 2015, Bettelli et al., 2006). TGF- $\beta$  promotes the development of anti-inflammatory Treg cells, unless IL-6 is also present, in which case the pro-inflammatory Th17 lineage is chosen (Veldhoen et al., 2006). Inhibition of DYRK1A favours the development of Treg cells over Th17 cells (Khor et al., 2015). One can therefore deduce that overexpression of DYRK1A likely has a pro-inflammatory effect. This is supported by the MSD data, which show markers for Th17 cells (IL-17A, IL-21) and IL-6 to be upregulated in the middle ear fluid of Dp5Tyb mice compared to Dp5Tyb and WT blood serum. The IHC data also supports the presence of Th17 cells over Treg cells as IL-6 expression mirrors DYRK1A expression - more *Dyrk1a* copies leads to more DYRK1A and IL-6 expressed in the middle ear epithelium - whereas expression of IL-10 (secreted by Treg cells) remains fairly constant regardless of *Dyrk1a* copy number.

However, it must be noted that discriminating between the effects of *Dyrk1a* trisomy and the secondary effects of OME is challenging. Some of the phenotypes seen may be caused by the Dp5Tyb middle ear being an inflamed environment, such as the issues with cilia maintenance. More in-depth experiments must be carried out to determine the true effects of *Dyrk1a* trisomy in the Dp5Tyb middle ear.

### 7.3. Wider impact and contribution to the field

Dp5Tyb mice recapitulate the OME phenotype seen in OME mouse models, and the DS phenotypes seen in DS mouse models. The OME is present from three weeks of age, and persists for many months – making Dp5Tyb a good model of the chronic OME affecting toddlers with DS.

## CHAPTER 7: Discussion

Recently a child was identified as carrying a 2.56 Mb mosaic micro-duplication of Hsa21, encompassing an extra copy of only 15 genes, including 11 of the Dp5Tyb genes (not *LCA5L*), in approximately half of his cells. *DYRK1A* is therefore present in three copies. The child was said to have several common DS phenotypes including craniofacial defects, intellectual disability, muscle hypotonia, and a developmental delay regarding speech and auditory perception (Schnabel et al., 2018). This finding suggests that the key dosage-sensitive genes responsible for many common DS phenotypes must be in this region. The OME phenotype of this child was not investigated. Therefore the link between duplication of the Dp5Tyb region, particularly *Dyrk1a*, and the increased incidence of OME is still a completely novel discovery.

*Dyrk1a* has been identified as a key driver of many common DS phenotypes, and now due to the research presented in this thesis, increased dosage of *Dyrk1a* is also thought to drive OME pathogenesis in DS.

### 7.4. Future directions

There are a number of additional experiments and avenues that would merit consideration and investigation.

#### 7.4.1. Hearing loss

Dp5Tyb mice have conductive hearing loss due to chronic OME. Other causes of conductive hearing loss, such as abnormal ossicle morphology or tympanic membrane perforations, and causes of sensorineural hearing loss, such as defects in cochlear hair cell morphology, have been ruled out. However, to further investigate any sensorineural contribution to hearing loss in Dp5Tyb mice, spiral ganglion neuron (SGN) density could be quantified. SGNs degenerate after the onset of sensorineural hearing loss so no longer convey information from the cochlea to the brain (Otte et

al., 1978). If no significant difference in density is found between WT and Dp5Tyb SGNs, there is unlikely to be a sensorineural element to the hearing loss, supporting the hypothesis that Dp5Tyb mice have conductive hearing loss due to OME. To confirm that no other defect is contributing to the conductive hearing loss, in-depth morphometric analysis and volumetric mineral density of ossicles could be performed (Chen et al., 2016b). Currently they have only been compared by eye, but this analysis would quantify any differences in shape or composition of Dp5Tyb ossicles compared to WT.

### 7.4.2. Craniofacial defects

Detailed analysis could also be carried out for the craniofacial defects seen in Dp5Tyb mice. Current analysis involved measuring the bones of the skull and calculating allometric ratios. Imaging using microCT and three-dimensional coordinates of anatomical landmarks would offer quantification of all aspects of the skull (Singh et al., 2016), allowing a true comparison of WT and Dp5Tyb skull shape and size. Investigation of the Eustachian tube angle within the skull would also be beneficial (Schuon et al., 2021), as a shallow angle could be exacerbating fluid accumulation in the middle ear.

### 7.4.3. Cilia morphology

Using scanning electron microscopy to image the middle ear cilia allowed detailed cilia morphology to be observed, but it doesn't offer insight into their functionality. Future work could include harvesting epithelial cells from the middle ear and growing them in air-liquid interface culture to recapitulate the middle ear environment (Mulay et al., 2016). High speed video microscopy of the cilia could then be performed to check their beat pattern and frequency (Rumman et al., 2017).

#### 7.4.4. Hypoxia

The upregulation of the HIF-response genes *Vegfa*, *IL 1 $\beta$*  and *Tnfa* were assumed to indicate that the middle ear of Dp5Tyb mice is hypoxic, although no hypoxia test was performed. Pimonidazole is a hypoxia marker that was used to demonstrate that the *Junbo* middle ear was hypoxic (Cheeseman et al., 2011). Future work should include the same experiment but with Dp5Tyb mice.

#### 7.4.5. DYRK1A inhibitors

Due to the findings that *Dyrk1a* dosage plays a critical role in OME pathogenesis, it would be important to investigate the effects of a DYRK1A inhibitor on Dp5Tyb mice. DYRK1A inhibitors could be delivered systemically to Dp5Tyb mice and the onset and chronicity of OME examined. DYRK1A inhibitors have already been shown to prevent the promotion of the pro-inflammatory Th17 lineage, and reduce inflammation of the epithelial lining of the gut and airways (Khor et al., 2015).

Demonstration of the efficacy of DYRK1A inhibitors in ameliorating OME in Dp5Tyb mice would provide support for their use as a therapy for OME in DS. Other common DS phenotypes may also be alleviated by the administration of a DYRK1A inhibitor, such as motor dysfunction in Ts1Rhr mice (Watson-Scales et al., 2018) and learning and memory deficits in Ts65Dn mice (García-Cerro et al., 2014). In particular, it would be important to consider investigating the opportunity to deliver DYRK1A inhibitors topically across the tympanic membrane, and the Dp5Tyb model would be a suitable model for investigating this route of delivery. As it stands, none of the available DYRK1A inhibitors are in a liquid form to use as ear drops.

#### 7.4.6. Additional genetic loci involved in OME

Although the *Dyrk1a* findings are compelling, it would also be important to investigate the minor OME locus in the Dp10Tyb or Dp11Tyb region. Half of Dp9Tyb mice have

## CHAPTER 7: Discussion

OME, and the fully penetrant bilateral OME seen in Dp1Tyb mice is not fully replicated in Dp5Tyb mice. This suggests that in Dp1Tyb mice *Dyrk1a* could be interacting with other gene(s). The identification of this locus remains of continuing interest in providing a fuller account of loci across the genome predisposing to OME.

### 7.5. Conclusion

Overall, the data presented in this thesis demonstrate that there is a major locus in the Dp5Tyb region which, when present in three copies, is driving OME pathogenesis. The restoration of the WT phenotype in double mutants (Dp3Tyb *Dyrk1a*<sup>+/+</sup>) shows that *Dyrk1a* is the likely candidate gene. There is also likely to be a minor locus in the Dp10Tyb or Dp11Tyb region, which remains to be discovered. Together these two dosage-sensitive loci are responsible for the fully penetrant bilateral OME seen in Dp1Tyb mice. *Dyrk1a* interacts with many signalling pathways, but in the particular case of OME in DS, overexpression of DYRK1A is likely enhancing middle ear inflammation through promoting TGF- $\beta$  and VEGF signalling, and by driving the differentiation of naïve CD4<sup>+</sup> T cells into pro-inflammatory Th17 cells. DYRK1A inhibitors are available and successfully ameliorate other DS phenotypes in animal models. It would be interesting to explore the efficacy of DYRK1A inhibitors in Dp5Tyb mice, both applied systemically and also topically to the eardrum. The identification of *Dyrk1a* as a key gene involved in the pathogenesis of OME in DS opens up a number of novel avenues for treatment of hearing loss in DS. For children with DS this would be a huge step forward - helping with communication and learning, so they are better able to thrive and achieve independence.

## References

---

- ABDALA, C. & VISSER-DUMONT, L. 2001. Distortion Product Otoacoustic Emissions: A Tool for Hearing Assessment and Scientific Study. *Volta Rev*, 103, 281-302.
- ABDULLAH, S. N., ZAKARIA, M. N., SALIM, R., MD DAUD, M. K. & NIK OTHMAN, N. A. 2022. Comparing the diagnostic accuracy of audiometric Weber test and tuning fork Weber test in patients with conductive hearing loss. *Laryngoscope Investig Otolaryngol*, 7, 523-529.
- ABUHATZIRA, L., SHAMIR, A., SCHONES, D. E., SCHÄFFER, A. A. & BUSTIN, M. 2011. The chromatin-binding protein HMGN1 regulates the expression of methyl CpG-binding protein 2 (MECP2) and affects the behavior of mice. *J Biol Chem*, 286, 42051-42062.
- ANDERSEN, M. P., PARHAM, A. R., WALDREP, J. C., MCKENZIE, W. N. & DHAND, R. 2012. Alveolar fractal box dimension inversely correlates with mean linear intercept in mice with elastase-induced emphysema. *Int J Chron Obstruct Pulmon Dis*, 7, 235-43.
- ANGELO, L. S. & KURZROCK, R. 2007. Vascular endothelial growth factor and its relationship to inflammatory mediators. *Clin Cancer Res*, 13, 2825-30.
- ANNUNZIATO, F., COSMI, L., LIOTTA, F., MAGGI, E. & ROMAGNANI, S. 2012. Defining the human T helper 17 cell phenotype. *Trends Immunol*, 33, 505-12.
- ANTHWAL, N. & THOMPSON, H. 2016. The development of the mammalian outer and middle ear. *J Anat*, 228, 217-32.
- ANTONARAKIS, S. E. 2017. Down syndrome and the complexity of genome dosage imbalance. *Nature Reviews Genetics*, 18, 147-163.
- ANTONARAKIS, S. E., LYLE, R., DERMITZAKIS, E. T., REYMOND, A. & DEUTSCH, S. 2004. Chromosome 21 and down syndrome: from genomics to pathophysiology. *Nat Rev Genet*, 5, 725-38.
- ANTONARAKIS, S. E., SKOTKO, B. G., RAFII, M. S., STRYDOM, A., PAPE, S. E., BIANCHI, D. W., SHERMAN, S. L. & REEVES, R. H. 2020. Down syndrome. *Nat Rev Dis Primers*, 6, 9.
- ATAS-OZCAN, H., BRAULT, V., DUCHON, A. & HERAULT, Y. 2021. Dyrk1a from Gene Function in Development and Physiology to Dosage Correction across Life Span in Down Syndrome. *Genes (Basel)*, 12.
- BALKANY, T. J., DOWNS, M. P., JAFEK, B. W. & KRAJICEK, M. J. 1979. Hearing loss in Down's syndrome. A treatable handicap more common than generally recognized. *Clin Pediatr (Phila)*, 18, 116-8.
- BARR, E., DUNGWORTH, J., HUNTER, K., MCFARLANE, M. & KUBBA, H. 2011. The prevalence of ear, nose and throat disorders in preschool children with Down's syndrome in Glasgow. *Scott Med J*, 56, 98-103.
- BETTELLI, E., CARRIER, Y., GAO, W., KORN, T., STROM, T. B., OUKKA, M., WEINER, H. L. & KUCHROO, V. K. 2006. Reciprocal developmental pathways for the generation of pathogenic effector TH17 and regulatory T cells. *Nature*, 441, 235-8.
- BHUTTA, M. F. 2012. Mouse models of otitis media: strengths and limitations. *Otolaryngol Head Neck Surg*, 147, 611-4.
- BHUTTA, M. F., CHEESEMAN, M. T., HERAULT, Y., YU, Y. E. & BROWN, S. D. 2013. Surveying the Down syndrome mouse model resource identifies critical regions responsible for chronic otitis media. *Mamm Genome*, 24, 439-45.
- BHUTTA, M. F., LAMBIE, J., HOBSON, L., GOEL, A., HAFRÉN, L., EINARSDOTTIR, E., MATTILA, P. S., FARRALL, M., BROWN, S. & BURTON,

## References

- M. J. 2017a. A mouse-to-man candidate gene study identifies association of chronic otitis media with the loci TGIF1 and FBXO11. *Sci Rep*, 7, 12496.
- BHUTTA, M. F., LAMBIE, J., HOBSON, L., WILLIAMS, D., TYRER, H. E., NICHOLSON, G., BROWN, S. D. M., BROWN, H., PICCINELLI, C., DEVAILLY, G., RAMSDEN, J. & CHEESEMAN, M. T. 2019. Transcript Analysis Reveals a Hypoxic Inflammatory Environment in Human Chronic Otitis Media With Effusion. *Front Genet*, 10, 1327.
- BHUTTA, M. F., THORNTON, R. B., KIRKHAM, L. S., KERSCHNER, J. E. & CHEESEMAN, M. T. 2017b. Understanding the aetiology and resolution of chronic otitis media from animal and human studies. *Dis Model Mech*, 10, 1289-1300.
- BLANC, F., AYACHE, D., CALMELS, M. N., DEGUINE, O., FRANCOIS, M., LÉBOULANGER, N., LESCANNE, E., MARIANOWSKI, R., NEVOUX, J., NICOLLAS, R., TRINGALI, S., TESSIER, N., FRANCO-VIDAL, V., BORDURE, P. & MONDAIN, M. 2018. Management of otitis media with effusion in children. Societe francaise d'ORL et de chirurgie cervico-faciale clinical practice guidelines. *Eur Ann Otorhinolaryngol Head Neck Dis*, 135, 269-273.
- BOSMAN, A., LETOURNEAU, A., SARTIANI, L., DEL LUNGO, M., RONZONI, F., KUZIYAKIV, R., TOHONEN, V., ZUCCHELLI, M., SANTONI, F., GUIPPONI, M., DUMEVSKA, B., HOVATTA, O., ANTONARAKIS, S. E. & JACONI, M. E. 2015. Perturbations of heart development and function in cardiomyocytes from human embryonic stem cells with trisomy 21. *Stem Cells*, 33, 1434-46.
- BOWL, M. R. & DAWSON, S. J. 2019. Age-Related Hearing Loss. *Cold Spring Harb Perspect Med*, 9.
- BROWN, S. D., HARDISTY-HUGHES, R. E. & MBURU, P. 2008. Quiet as a mouse: dissecting the molecular and genetic basis of hearing. *Nat Rev Genet*, 9, 277-90.
- BROWN, S. D. M. 2021. Advances in mouse genetics for the study of human disease. *Hum Mol Genet*, 30, R274-r284.
- BUSTAMANTE-MARIN, X. M. & OSTROWSKI, L. E. 2017. Cilia and Mucociliary Clearance. *Cold Spring Harb Perspect Biol*, 9.
- BUTTERFIELD, T. A., BEST, T. M. & MERRICK, M. A. 2006. The dual roles of neutrophils and macrophages in inflammation: a critical balance between tissue damage and repair. *J Athl Train*, 41, 457-65.
- CAMPBELL, H. & TOMKEIEFF, S. I. 1952. Calculation of the Internal Surface of a Lung. *Nature*, 170, 117-117.
- CARPINELLI, M. R., KRUSE, E. A., ARHATARI, B. D., DEBRINCAT, M. A., OGIER, J. M., BORIES, J. C., KILE, B. T. & BURT, R. A. 2015. Mice Haploinsufficient for Ets1 and Fli1 Display Middle Ear Abnormalities and Model Aspects of Jacobsen Syndrome. *Am J Pathol*, 185, 1867-76.
- CASSELBRANT, M. L., MANDEL, E. M., ROCKETTE, H. E., KURS-LASKY, M., FALL, P. A., BLUESTONE, C. D. & FERRELL, R. E. 2004. The genetic component of middle ear disease in the first 5 years of life. *Arch Otolaryngol Head Neck Surg*, 130, 273-8.
- CHEESEMAN, M. T., TYRER, H. E., WILLIAMS, D., HOUGH, T. A., PATHAK, P., ROMERO, M. R., HILTON, H., BALI, S., PARKER, A., VIZOR, L., PURNELL, T., VOWELL, K., WELLS, S., BHUTTA, M. F., POTTER, P. K. & BROWN, S. D. 2011. HIF-VEGF pathways are critical for chronic otitis media in Junbo and Jeff mouse mutants. *PLoS Genet*, 7, e1002336.

## References

- CHEN, G. D., LI, L., MCCALL, A., DING, D., XING, Z., YU, Y. E. & SALVI, R. 2022. Hearing impairment in murine model of Down syndrome. *Front Genet*, 13, 936128.
- CHEN, R., SCHWANDER, M., BARBE, M. F. & CHAN, M. M. 2016. Ossicular Bone Damage and Hearing Loss in Rheumatoid Arthritis: A Correlated Functional and High Resolution Morphometric Study in Collagen-Induced Arthritic Mice. *PLoS One*, 11, e0164078.
- CHEN, Y., THAI, P., ZHAO, Y. H., HO, Y. S., DESOUZA, M. M. & WU, R. 2003. Stimulation of airway mucin gene expression by interleukin (IL)-17 through IL-6 paracrine/autocrine loop. *J Biol Chem*, 278, 17036-43.
- CHITTKA, L. & BROCKMANN, A. 2005. Perception space--the final frontier. *PLoS Biol*, 3, e137.
- CHOI, M., KIM, A. K., HAM, Y., LEE, J. Y., KIM, D., YANG, A., JO, M. J., YOON, E., HEO, J. N., HAN, S. B., KI, M. H., LEE, K. S. & CHO, S. 2021. Aristolactam BIII, a naturally derived DYRK1A inhibitor, rescues Down syndrome-related phenotypes. *Phytomedicine*, 92, 153695.
- COSMI, L., MAGGI, L., SANTARLASCI, V., LIOTTA, F. & ANNUNZIATO, F. 2014. T helper cells plasticity in inflammation. *Cytometry A*, 85, 36-42.
- COURCET, J.-B., FAIVRE, L., MALZAC, P., MASUREL-PAULET, A., LOPEZ, E., CALLIER, P., LAMBERT, L., LEMESLE, M., THEVENON, J., GIGOT, N., DUPLOMB, L., RAGON, C., MARLE, N., MOSCA-BOIDRON, A.-L., HUET, F., PHILIPPE, C., MONCLA, A. & THAUVIN-ROBINET, C. 2012. The DYRK1A gene is a cause of syndromic intellectual disability with severe microcephaly and epilepsy. *Journal of Medical Genetics*, 49, 731.
- CROMPTON, M., PURNELL, T., TYRER, H. E., PARKER, A., BALL, G., HARDISTY-HUGHES, R. E., GALE, R., WILLIAMS, D., DEAN, C. H., SIMON, M. M., MALLON, A. M., WELLS, S., BHUTTA, M. F., BURTON, M. J., TATEOSSIAN, H. & BROWN, S. D. M. 2017. A mutation in Nischarin causes otitis media via LIMK1 and NF-kappaB pathways. *PLoS Genet*, 13, e1006969.
- DANG, E. V., BARBI, J., YANG, H. Y., JINASENA, D., YU, H., ZHENG, Y., BORDMAN, Z., FU, J., KIM, Y., YEN, H. R., LUO, W., ZELLER, K., SHIMODA, L., TOPALIAN, S. L., SEMENZA, G. L., DANG, C. V., PARDOLL, D. M. & PAN, F. 2011. Control of T(H)17/T(reg) balance by hypoxia-inducible factor 1. *Cell*, 146, 772-84.
- DAUPHINOT, L., LYLE, R., RIVALS, I., DANG, M. T., MOLDRICH, R. X., GOLFIER, G., ETTWILLER, L., TOYAMA, K., ROSSIER, J., PERSONNAZ, L., ANTONARAKIS, S. E., EPSTEIN, C. J., SINET, P. M. & POTIER, M. C. 2005. The cerebellar transcriptome during postnatal development of the Ts1Cje mouse, a segmental trisomy model for Down syndrome. *Hum Mol Genet*, 14, 373-84.
- DAVISSON, M. T., SCHMIDT, C. & AKESON, E. C. 1990. Segmental trisomy of murine chromosome 16: a new model system for studying Down syndrome. *Prog Clin Biol Res*, 360, 263-80.
- DE SCHRIJVER, L., TOPSAKAL, V., WOJCIECHOWSKI, M., VAN DE HEYNING, P. & BOUDEWYNS, A. 2019. Prevalence and etiology of sensorineural hearing loss in children with down syndrome: A cross-sectional study. *Int J Pediatr Otorhinolaryngol*, 116, 168-172.
- DEMURO, S., DI MARTINO, R. M. C., ORTEGA, J. A. & CAVALLI, A. 2021. GSK-3 $\beta$ , FYN, and DYRK1A: Master Regulators in Neurodegenerative Pathways. *Int J Mol Sci*, 22.

## References

- DESHPANDE, A., BORLEPAWAR, A., ROSSKOPF, A., FRANK, D., FREY, N. & RANGREZ, A. Y. 2021. SH3-Binding Glutamic Acid Rich-Deficiency Augments Apoptosis in Neonatal Rat Cardiomyocytes. *Int J Mol Sci*, 22.
- DOWJAT, W. K., ADAYEV, T., KUCHNA, I., NOWICKI, K., PALMINIELLO, S., HWANG, Y. W. & WEGIEL, J. 2007. Trisomy-driven overexpression of DYRK1A kinase in the brain of subjects with Down syndrome. *Neurosci Lett*, 413, 77-81.
- DUCHON, A. & HERAULT, Y. 2016. DYRK1A, a Dosage-Sensitive Gene Involved in Neurodevelopmental Disorders, Is a Target for Drug Development in Down Syndrome. *Front Behav Neurosci*, 10, 104.
- DUCHON, A., RAVEAU, M., CHEVALIER, C., NALESSO, V., SHARP, A. J. & HERAULT, Y. 2011. Identification of the translocation breakpoints in the Ts65Dn and Ts1Cje mouse lines: relevance for modeling Down syndrome. *Mamm Genome*, 22, 674-84.
- DUNLEVY, L., BENNETT, M., SLENDER, A., LANA-ELOLA, E., TYBULEWICZ, V. L., FISHER, E. M. & MOHUN, T. 2010. Down's syndrome-like cardiac developmental defects in embryos of the transchromosomal Tc1 mouse. *Cardiovasc Res*, 88, 287-95.
- DUTTA, A., VENKATAGANESH, H. & LOVE, P. E. 2021. New Insights into Epigenetic Regulation of T Cell Differentiation. *Cells*, 10, 3459.
- FAUSCH, C. & ROOSLI, C. 2015. The incudomalleolar articulation in Down syndrome (trisomy 21): a temporal bone study. *Otol Neurotol*, 36, 348-53.
- FORTNUM, H., LEIGHTON, P., SMITH, M. D., BROWN, L., JONES, M., BENTON, C., MARDER, E., MARSHALL, A. & SUTTON, K. 2014. Assessment of the feasibility and clinical value of further research to evaluate the management options for children with Down syndrome and otitis media with effusion: a feasibility study. *Health Technol Assess*, 18, 1-147, v-vi.
- FUCHS, J. C. & TUCKER, A. S. 2015. Chapter Nine - Development and Integration of the Ear. In: CHAI, Y. (ed.) *Current Topics in Developmental Biology*. Academic Press.
- GALANTE, M., JANI, H., VANES, L., DANIEL, H., FISHER, E. M., TYBULEWICZ, V. L., BLISS, T. V. & MORICE, E. 2009. Impairments in motor coordination without major changes in cerebellar plasticity in the Tc1 mouse model of Down syndrome. *Hum Mol Genet*, 18, 1449-63.
- GANUSOV, V. V. & DE BOER, R. J. 2007. Do most lymphocytes in humans really reside in the gut? *Trends in Immunology*, 28, 514-518.
- GARBIERI, T. F., BROZOSKI, D. T., DIONÍSIO, T. J., SANTOS, C. F. & NEVES, L. T. 2017. Human DNA extraction from whole saliva that was fresh or stored for 3, 6 or 12 months using five different protocols. *J Appl Oral Sci*, 25, 147-158.
- GARCÍA-CERRO, S., MARTÍNEZ, P., VIDAL, V., CORRALES, A., FLÓREZ, J., VIDAL, R., RUEDA, N., ARBONÉS, M. L. & MARTÍNEZ-CUÉ, C. 2014. Overexpression of Dyrk1A is implicated in several cognitive, electrophysiological and neuromorphological alterations found in a mouse model of Down syndrome. *PLoS One*, 9, e106572.
- GARCIA-CERRO, S., RUEDA, N., VIDAL, V., LANTIGUA, S. & MARTINEZ-CUE, C. 2017. Normalizing the gene dosage of Dyrk1A in a mouse model of Down syndrome rescues several Alzheimer's disease phenotypes. *Neurobiol Dis*, 106, 76-88.
- GHADERSOHI, S., BHUSHAN, B. & BILLINGS, K. R. 2018. Challenges and outcomes of cholesteatoma management in children with Down syndrome. *Int J Pediatr Otorhinolaryngol*, 106, 80-84.

## References

- GRIBBLE, S. M., WISEMAN, F. K., CLAYTON, S., PRIGMORE, E., LANGLEY, E., YANG, F., MAGUIRE, S., FU, B., RAJAN, D., SHEPPARD, O., SCOTT, C., HAUSER, H., STEPHENS, P. J., STEBBINGS, L. A., NG, B. L., FITZGERALD, T., QUAIL, M. A., BANERJEE, R., ROTHKAMM, K., TYBULEWICZ, V. L., FISHER, E. M. & CARTER, N. P. 2013. Massively parallel sequencing reveals the complex structure of an irradiated human chromosome on a mouse background in the Tc1 model of Down syndrome. *PLoS One*, 8, e60482.
- GUTIERREZ-HERVAS, A., GOMEZ-MARTINEZ, S., IZQUIERDO-GOMEZ, R., VEIGA, O. L., PEREZ-BEY, A., CASTRO-PINERO, J. & MARCOS, A. 2020. Inflammation and fatness in adolescents with and without Down syndrome: UP & DOWN study. *J Intellect Disabil Res*, 64, 170-179.
- HAN, F., YU, H., ZHANG, J., TIAN, C., SCHMIDT, C., NAVA, C., DAVISSON, M. T. & ZHENG, Q. Y. 2009. Otitis media in a mouse model for Down syndrome. *Int J Exp Pathol*, 90, 480-8.
- HARASHIMA, C., JACOBOWITZ, D. M., WITTA, J., BORKE, R. C., BEST, T. K., SIAREY, R. J. & GALDZICKI, Z. 2006. Abnormal expression of the G-protein-activated inwardly rectifying potassium channel 2 (GIRK2) in hippocampus, frontal cortex, and substantia nigra of Ts65Dn mouse: a model of Down syndrome. *J Comp Neurol*, 494, 815-33.
- HARDISTY-HUGHES, R. E., TATEOSSIAN, H., MORSE, S. A., ROMERO, M. R., MIDDLETON, A., TYMOWSKA-LALANNE, Z., HUNTER, A. J., CHEESEMAN, M. & BROWN, S. D. 2006. A mutation in the F-box gene, *Fbxo11*, causes otitis media in the Jeff mouse. *Hum Mol Genet*, 15, 3273-9.
- HARDISTY, R. E., ERVEN, A., LOGAN, K., MORSE, S., GUIONAUD, S., SANCHO-OLIVER, S., HUNTER, A. J., BROWN, S. D. & STEEL, K. P. 2003. The deaf mouse mutant Jeff (Jf) is a single gene model of otitis media. *J Assoc Res Otolaryngol*, 4, 130-8.
- HILDEBRANDT, C., FULTON, A. & RODAN, L. H. 2021. Homozygous deletion of 21q22.2 in a patient with hypotonia, developmental delay, cortical visual impairment, and retinopathy. *Am J Med Genet A*, 185, 555-560.
- HUANG, H., RAMBALDI, I., DANIELS, E. & FEATHERSTONE, M. 2003. Expression of the *Wdr9* gene and protein products during mouse development. *Dev Dyn*, 227, 608-14.
- HUANG, Q., ZHANG, Z., ZHENG, Y., ZHENG, Q., CHEN, S., XU, Y., OU, Y. & QIU, Z. 2012. Hypoxia-inducible factor and vascular endothelial growth factor pathway for the study of hypoxia in a new model of otitis media with effusion. *Audiol Neurootol*, 17, 349-56.
- HUSSEMAN, J., PALACIOS, S. D., RIVKIN, A. Z., OEHL, H. & RYAN, A. F. 2012. The role of vascular endothelial growth factors and fibroblast growth factors in angiogenesis during otitis media. *Audiol Neurootol*, 17, 148-54.
- ISHIHARA, K., SHIMIZU, R., TAKATA, K., KAWASHITA, E., AMANO, K., SHIMOHATA, A., LOW, D., NABE, T., SAGO, H., ALEXANDER, W. S., GINHOUX, F., YAMAKAWA, K. & AKIBA, S. 2020. Perturbation of the immune cells and prenatal neurogenesis by the triplication of the *Erg* gene in mouse models of Down syndrome. *Brain Pathol*, 30, 75-91.
- JACKSON, S. J., ANDREWS, N., BALL, D., BELLANTUONO, I., GRAY, J., HACHOUMI, L., HOLMES, A., LATCHAM, J., PETRIE, A., POTTER, P., RICE, A., RITCHIE, A., STEWART, M., STREPKA, C., YEOMAN, M. & CHAPMAN, K. 2017. Does age matter? The impact of rodent age on study outcomes. *Lab Anim*, 51, 160-169.

## References

- JENG, J. Y., CARLTON, A. J., JOHNSON, S. L., BROWN, S. D. M., HOLLEY, M. C., BOWL, M. R. & MARCOTTI, W. 2021. Biophysical and morphological changes in inner hair cells and their efferent innervation in the ageing mouse cochlea. *J Physiol*, 599, 269-287.
- JEON, S. H., CHAE, B. C., KIM, H. A., SEO, G. Y., SEO, D. W., CHUN, G. T., KIM, N. S., YIE, S. W., BYEON, W. H., EOM, S. H., HA, K. S., KIM, Y. M. & KIM, P. H. 2007. Mechanisms underlying TGF-beta1-induced expression of VEGF and Flk-1 in mouse macrophages and their implications for angiogenesis. *J Leukoc Biol*, 81, 557-66.
- JIANG, L., KERCHBERGER, V. E., SHAFFER, C., DICKSON, A. L., ORMSETH, M. J., DANIEL, L. L., LEON, B. G. C., COX, N. J., CHUNG, C. P., WEI, W. Q., STEIN, C. M. & FENG, Q. 2022. Genome-wide association analyses of common infections in a large practice-based biobank. *BMC Genomics*, 23, 672.
- JOSHI, K., SHEN, L., CAO, F., DONG, S., JIA, Z., CORTEZ, M. A. & SNEAD, O. C. 2018. Kcnj6(GIRK2) trisomy is not sufficient for conferring the susceptibility to infantile spasms seen in the Ts65Dn mouse model of down syndrome. *Epilepsy Research*, 145, 82-88.
- JOSHI, K., SHEN, L., MICHAELI, A., SALTER, M., THIBAUT-MESSIER, G., HASHMI, S., EUBANKS, J. H., CORTEZ, M. A. & SNEAD, O. C. 2016. Infantile spasms in down syndrome: Rescue by knockdown of the GIRK2 channel. *Ann Neurol*, 80, 511-21.
- JUHN, S. K., JUNG, M.-K., HOFFMAN, M. D., DREW, B. R., PRECIADO, D. A., SAUSEN, N. J., JUNG, T. T. K., KIM, B. H., PARK, S.-Y., LIN, J., ONDREY, F. G., MAINS, D. R. & HUANG, T. 2008. The role of inflammatory mediators in the pathogenesis of otitis media and sequelae. *Clinical and experimental otorhinolaryngology*, 1, 117-138.
- JUNG, H. H., KIM, M. W., LEE, J. H., KIM, Y. T., KIM, N. H., CHANG, B. A., CHOI, J. O. & LIM, H. H. 1999. Expression of vascular endothelial growth factor in otitis media. *Acta Otolaryngol*, 119, 801-8.
- KAZUKI, Y., GAO, F. J., LI, Y., MOYER, A. J., DEVENNEY, B., HIRAMATSU, K., MIYAGAWA-TOMITA, S., ABE, S., KAZUKI, K., KAJITANI, N., UNO, N., TAKEHARA, S., TAKIGUCHI, M., YAMAKAWA, M., HASEGAWA, A., SHIMIZU, R., MATSUKURA, S., NODA, N., Ogonuki, N., INOUE, K., MATOBA, S., OGURA, A., FLOREA, L. D., SAVONENKO, A., XIAO, M., WU, D., BATISTA, D. A., YANG, J., QIU, Z., SINGH, N., RICHTSMEIER, J. T., TAKEUCHI, T., OSHIMURA, M. & REEVES, R. H. 2020. A non-mosaic transchromosomal mouse model of down syndrome carrying the long arm of human chromosome 21. *Elife*, 9.
- KHOR, B., GAGNON, J. D., GOEL, G., ROCHE, M. I., CONWAY, K. L., TRAN, K., ALDRICH, L. N., SUNDBERG, T. B., PATERSON, A. M., MORDECAL, S., DOMBKOWSKI, D., SCHIRMER, M., TAN, P. H., BHAN, A. K., ROYCHOUDHURI, R., RESTIFO, N. P., O'SHEA, J. J., MEDOFF, B. D., SHAMJI, A. F., SCHREIBER, S. L., SHARPE, A. H., SHAW, S. Y. & XAVIER, R. J. 2015. The kinase DYRK1A reciprocally regulates the differentiation of Th17 and regulatory T cells. *Elife*, 4.
- KIM, T. H., CHAE, S. W., KIM, H. J. & JUNG, H. H. 2005. Effect of recombinant vascular endothelial growth factor on experimental otitis media with effusion. *Acta Otolaryngol*, 125, 256-9.
- KLESCHCHEVNIKOV, A. M., YU, J., KIM, J., LYSSENKO, L. V., ZENG, Z., YU, Y. E. & MOBLEY, W. C. 2017. Evidence that increased Kcnj6 gene dose is necessary

## References

- for deficits in behavior and dentate gyrus synaptic plasticity in the Ts65Dn mouse model of Down syndrome. *Neurobiol Dis*, 103, 1-10.
- KNUDSEN, L., WEIBEL, E. R., GUNDERSEN, H. J., WEINSTEIN, F. V. & OCHS, M. 2010. Assessment of air space size characteristics by intercept (chord) measurement: an accurate and efficient stereological approach. *J Appl Physiol* (1985), 108, 412-21.
- KOURTZELIS, I., MITROULIS, I., VON RENESSE, J., HAJISHENGALLIS, G. & CHAVAKIS, T. 2017. From leukocyte recruitment to resolution of inflammation: the cardinal role of integrins. *J Leukoc Biol*, 102, 677-683.
- KREICHER, K. L., WEIR, F. W., NGUYEN, S. A. & MEYER, T. A. 2018. Characteristics and Progression of Hearing Loss in Children with Down Syndrome. *J Pediatr*, 193, 27-33 e2.
- KUBINYEZ, O., VIKHE, P. P., PURNELL, T., BROWN, S. D. M. & TATEOSSIAN, H. 2020. The Jeff Mouse Mutant Model for Chronic Otitis Media Manifests Gain-of-Function as Well as Loss-of-Function Effects. *Front Genet*, 11, 498.
- KUHN, S., INGHAM, N., PEARSON, S., GRIBBLE, S. M., CLAYTON, S., STEEL, K. P. & MARCOTTI, W. 2012. Auditory function in the Tc1 mouse model of down syndrome suggests a limited region of human chromosome 21 involved in otitis media. *PLoS One*, 7, e31433.
- KUROKAWA, M., MITANI, K., IRIE, K., MATSUYAMA, T., TAKAHASHI, T., CHIBA, S., YAZAKI, Y., MATSUMOTO, K. & HIRAI, H. 1998. The oncoprotein Evi-1 represses TGF-beta signalling by inhibiting Smad3. *Nature*, 394, 92-6.
- KUSTERS, M. A., VERSTEGEN, R. H., GEMEN, E. F. & DE VRIES, E. 2009. Intrinsic defect of the immune system in children with Down syndrome: a review. *Clin Exp Immunol*, 156, 189-93.
- LACOMBE, J. M. & ROPER, R. J. 2020. Skeletal dynamics of Down syndrome: A developing perspective. *Bone*, 133, 115215.
- LANA-ELOLA, E., CATER, H., WATSON-SCALES, S., GREENAWAY, S., MULLER-WINKLER, J., GIBBINS, D., NEMES, M., SLENDER, A., HOUGH, T., KESKIVALI-BOND, P., SCUDAMORE, C. L., HERBERT, E., BANKS, G. T., MOBBS, H., CANONICA, T., TOSH, J., NOY, S., LLORIAN, M., NOLAN, P. M., GRIFFIN, J. L., GOOD, M., SIMON, M., MALLON, A. M., WELLS, S., FISHER, E. M. C. & TYBULEWICZ, V. L. J. 2021. Comprehensive phenotypic analysis of the Dp1Tyb mouse strain reveals a broad range of Down syndrome-related phenotypes. *Dis Model Mech*, 14.
- LANA-ELOLA, E., WATSON-SCALES, S., SLENDER, A., GIBBINS, D., MARTINEAU, A., DOUGLAS, C., MOHUN, T., FISHER, E. M. & TYBULEWICZ, V. 2016. Genetic dissection of Down syndrome-associated congenital heart defects using a new mouse mapping panel. *Elife*, 5.
- LARSEN, L. J. & MØLLER, L. B. 2020. Crosstalk of Hedgehog and mTORC1 Pathways. *Cells*, 9.
- LEONG, A. F., BUCKLEY, G. A., PAGANIN, D. M., HOOPER, S. B., WALLACE, M. J. & KITCHEN, M. J. 2014. Real-time measurement of alveolar size and population using phase contrast x-ray imaging. *Biomed Opt Express*, 5, 4024-38.
- LI, H., HELPARD, L., EKEROOT, J., ROHANI, S. A., ZHU, N., RASK-ANDERSEN, H., LADAK, H. M. & AGRAWAL, S. 2021. Three-dimensional tonotopic mapping of the human cochlea based on synchrotron radiation phase-contrast imaging. *Sci Rep*, 11, 4437.
- LI, Y. L., ZHANG, M. M., WU, L. W., LIU, Y. H., ZHANG, Z. Y., ZENG, L. H., LIN, N. M. & ZHANG, C. 2022. DYRK1A reinforces epithelial-mesenchymal transition

## References

- and metastasis of hepatocellular carcinoma via cooperatively activating STAT3 and SMAD. *J Biomed Sci*, 29, 34.
- LIAO, Y. M., WANG, Y. H., HUNG, J. T., LIN, Y. J., HUANG, Y. L., LIAO, G. S., HSU, Y. L., WU, J. C. & YU, A. L. 2021. High B3GALT5 expression confers poor clinical outcome and contributes to tumor progression and metastasis in breast cancer. *Breast Cancer Res*, 23, 5.
- LIM, D. J., SHIMADA, T. & YODER, M. 1973. Distribution of mucus-secreting cells in normal middle ear mucosa. *Arch Otolaryngol*, 98, 2-9.
- LIN, J. J., GILLAM, L., SMITH, L., CAREW, P., KING, A., CHING, T. Y. C. & SUNG, V. 2022. Mild matters: parental insights into the conundrums of managing mild congenital hearing loss. *Int J Audiol*, 61, 500-506.
- LING, K. H., HEWITT, C. A., TAN, K. L., CHEAH, P. S., VIDYADARAN, S., LAI, M. I., LEE, H. C., SIMPSON, K., HYDE, L., PRITCHARD, M. A., SMYTH, G. K., THOMAS, T. & SCOTT, H. S. 2014. Functional transcriptome analysis of the postnatal brain of the Ts1Cje mouse model for Down syndrome reveals global disruption of interferon-related molecular networks. *BMC Genomics*, 15, 624.
- LIU, X., CONG, N., CHENG, X., MA, R., WANG, J., HUANG, Y. B., ZHAO, M., WANG, X. W., CHI, F. L. & REN, D. D. 2017. The Role of the Notch Signal Pathway in Mucosal Cell Metaplasia in Mouse Acute Otitis Media. *Sci Rep*, 7, 4588.
- LOHELA, M., BRY, M., TAMMELA, T. & ALITALO, K. 2009. VEGFs and receptors involved in angiogenesis versus lymphangiogenesis. *Curr Opin Cell Biol*, 21, 154-65.
- LUO, W., YI, H., TAYLOR, J., LI, J. D., CHI, F., TODD, N. W., LIN, X., REN, D. & CHEN, P. 2017. Cilia distribution and polarity in the epithelial lining of the mouse middle ear cavity. *Sci Rep*, 7, 45870.
- MALKOV, M. I., LEE, C. T. & TAYLOR, C. T. 2021. Regulation of the Hypoxia-Inducible Factor (HIF) by Pro-Inflammatory Cytokines. *Cells*, 10.
- MANCINO, A., SCHIOPPA, T., LARGHI, P., PASQUALINI, F., NEBULONI, M., CHEN, I. H., SOZZANI, S., AUSTYN, J. M., MANTOVANI, A. & SICA, A. 2008. Divergent effects of hypoxia on dendritic cell functions. *Blood*, 112, 3723-34.
- MANICKAM, V., SHOTT, G. S., HEITHAUS, D. & SHOTT, S. R. 2016. Hearing loss in Down Syndrome revisited - 15 years later. *Int J Pediatr Otorhinolaryngol*, 88, 203-7.
- MANN, Z. F., THIEDE, B. R., CHANG, W., SHIN, J. B., MAY-SIMERA, H. L., LOVETT, M., CORWIN, J. T. & KELLEY, M. W. 2014. A gradient of Bmp7 specifies the tonotopic axis in the developing inner ear. *Nat Commun*, 5, 3839.
- MARIS, M., WOJCIECHOWSKI, M., VAN DE HEYNING, P. & BOUDEWYNS, A. 2014. A cross-sectional analysis of otitis media with effusion in children with Down syndrome. *Eur J Pediatr*, 173, 1319-25.
- MAZZONI, D. S., ACKLEY, R. S. & NASH, D. J. 1994. Abnormal pinna type and hearing loss correlations in Down's syndrome. *J Intellect Disabil Res*, 38 ( Pt 6), 549-60.
- MCCARTHY, D. J. & SMYTH, G. K. 2009. Testing significance relative to a fold-change threshold is a TREAT. *Bioinformatics*, 25, 765-71.
- MCELYEA, S. D., STARBUCK, J. M., TUMBLESON-BRINK, D. M., HARRINGTON, E., BLAZEK, J. D., GHONEIMA, A., KULA, K. & ROPER, R. J. 2016. Influence of prenatal EGCG treatment and Dyrk1a dosage reduction on craniofacial features associated with Down syndrome. *Hum Mol Genet*, 25, 4856-4869.
- MCNAMEE, E. N., KORNS JOHNSON, D., HOMANN, D. & CLAMBEY, E. T. 2013. Hypoxia and hypoxia-inducible factors as regulators of T cell development, differentiation, and function. *Immunol Res*, 55, 58-70.

## References

- MICHELS, T. C., DUFFY, M. T. & ROGERS, D. J. 2019. Hearing Loss in Adults: Differential Diagnosis and Treatment. *Am Fam Physician*, 100, 98-108.
- MITWALLI, M., WAHBA, Y., SHALTOU, A. & GOUIDA, M. 2018. Lymphocyte subgroups and recurrent infections in children with Down syndrome - a prospective case control study. *Cent Eur J Immunol*, 43, 248-254.
- MORICE, E., ANDREAE, L. C., COOKE, S. F., VANES, L., FISHER, E. M., TYBULEWICZ, V. L. & BLISS, T. V. 2008. Preservation of long-term memory and synaptic plasticity despite short-term impairments in the Tc1 mouse model of Down syndrome. *Learn Mem*, 15, 492-500.
- MOWERY, C. T., REYES, J. M., CABAL-HIERRO, L., HIGBY, K. J., KARLIN, K. L., WANG, J. H., KIMMERLING, R. J., CEJAS, P., LIM, K., LI, H., FURUSAWA, T., LONG, H. W., PELLMAN, D., CHAPUY, B., BUSTIN, M., MANALIS, S. R., WESTBROOK, T. F., LIN, C. Y. & LANE, A. A. 2018. Trisomy of a Down Syndrome Critical Region Globally Amplifies Transcription via HMGN1 Overexpression. *Cell Rep*, 25, 1898-1911.e5.
- MOZZI, A., PONTREMOLI, C. & SIRONI, M. 2018. Genetic susceptibility to infectious diseases: Current status and future perspectives from genome-wide approaches. *Infect Genet Evol*, 66, 286-307.
- MULAY, A., AKRAM, K. M., WILLIAMS, D., ARMES, H., RUSSELL, C., HOOD, D., ARMSTRONG, S., STEWART, J. P., BROWN, S. D., BINGLE, L. & BINGLE, C. D. 2016. An in vitro model of murine middle ear epithelium. *Dis Model Mech*, 9, 1405-1417.
- NAGY, J. A., BENJAMIN, L., ZENG, H., DVORAK, A. M. & DVORAK, H. F. 2008. Vascular permeability, vascular hyperpermeability and angiogenesis. *Angiogenesis*, 11, 109-19.
- NEUMANN, F., GOURDAIN, S., ALBAC, C., DEKKER, A. D., BUI, L. C., DAIROU, J., SCHMITZ-AFONSO, I., HUE, N., RODRIGUES-LIMA, F., DELABAR, J. M., POTIER, M. C., LE CAËR, J. P., TOUBOUL, D., DELATOUR, B., CARIOU, K. & DODD, R. H. 2018. DYRK1A inhibition and cognitive rescue in a Down syndrome mouse model are induced by new fluoro-DANDY derivatives. *Sci Rep*, 8, 2859.
- NGUYEN, T. L., DUCHON, A., MANOUSOPOULOU, A., LOAEC, N., VILLIERS, B., PANI, G., KARATAS, M., MECHLING, A. E., HARSAN, L. A., LIMANTON, E., BAZUREAU, J. P., CARREAUX, F., GARBIS, S. D., MEIJER, L. & HERAULT, Y. 2018. Correction of cognitive deficits in mouse models of Down syndrome by a pharmacological inhibitor of DYRK1A. *Dis Model Mech*, 11.
- NICE 2008. Surgical management of otitis media with effusion in children. *Surgical Management of Otitis Media with Effusion in Children*. London.
- NIGHTENGALE, E., YOON, P., WOLTER-WARMERDAM, K., DANIELS, D. & HICKEY, F. 2017. Understanding Hearing and Hearing Loss in Children With Down Syndrome. *Am J Audiol*, 26, 301-308.
- NOLAN, P. M., PETERS, J., STRIVENS, M., ROGERS, D., HAGAN, J., SPURR, N., GRAY, I. C., VIZOR, L., BROOKER, D., WHITEHILL, E., WASHBOURNE, R., HOUGH, T., GREENAWAY, S., HEWITT, M., LIU, X., MCCORMACK, S., PICKFORD, K., SELLEY, R., WELLS, C., TYMOWSKA-LALANNE, Z., ROBY, P., GLENISTER, P., THORNTON, C., THAUNG, C., STEVENSON, J. A., ARKELL, R., MBURU, P., HARDISTY, R., KIERNAN, A., ERVEN, A., STEEL, K. P., VOEGELING, S., GUENET, J. L., NICKOLS, C., SADRI, R., NASSE, M., ISAACS, A., DAVIES, K., BROWNE, M., FISHER, E. M., MARTIN, J., RASTAN, S., BROWN, S. D. & HUNTER, J. 2000. A systematic, genome-wide, phenotype-driven mutagenesis programme for gene function studies in the mouse. *Nat Genet*, 25, 440-3.

## References

- NOLZ, J. C. 2015. Molecular mechanisms of CD8(+) T cell trafficking and localization. *Cell Mol Life Sci*, 72, 2461-73.
- O'DOHERTY, A., RUF, S., MULLIGAN, C., HILDRETH, V., ERRINGTON, M. L., COOKE, S., SESAY, A., MODINO, S., VANES, L., HERNANDEZ, D., LINEHAN, J. M., SHARPE, P. T., BRANDNER, S., BLISS, T. V., HENDERSON, D. J., NIZETIC, D., TYBULEWICZ, V. L. & FISHER, E. M. 2005. An aneuploid mouse strain carrying human chromosome 21 with Down syndrome phenotypes. *Science*, 309, 2033-7.
- OLSON, L. E., RICHTSMIEIER, J. T., LESZL, J. & REEVES, R. H. 2004. A chromosome 21 critical region does not cause specific Down syndrome phenotypes. *Science*, 306, 687-90.
- OTTE, J., SCHUNKNECHT, H. F. & KERR, A. G. 1978. Ganglion cell populations in normal and pathological human cochleae. Implications for cochlear implantation. *Laryngoscope*, 88, 1231-46.
- OUKKA, M. 2008. Th17 cells in immunity and autoimmunity. *Annals of the rheumatic diseases*, 67, iii26-iii29.
- PAGE, E. C., HEATLEY, S. L., EADIE, L. N., MCCLURE, B. J., DE BOCK, C. E., OMARI, S., YEUNG, D. T., HUGHES, T. P., THOMAS, P. Q. & WHITE, D. L. 2022. HMGN1 plays a significant role in CRLF2 driven Down Syndrome leukemia and provides a potential therapeutic target in this high-risk cohort. *Oncogene*, 41, 797-808.
- PALAZON, A., GOLDRATH, A. W., NIZET, V. & JOHNSON, R. S. 2014. HIF transcription factors, inflammation, and immunity. *Immunity*, 41, 518-28.
- PARK, A. H., WILSON, M. A., STEVENS, P. T., HARWARD, R. & HOHLER, N. 2012. Identification of hearing loss in pediatric patients with Down syndrome. *Otolaryngol Head Neck Surg*, 146, 135-40.
- PARK, H., LI, Z., YANG, X. O., CHANG, S. H., NURIEVA, R., WANG, Y. H., WANG, Y., HOOD, L., ZHU, Z., TIAN, Q. & DONG, C. 2005. A distinct lineage of CD4 T cells regulates tissue inflammation by producing interleukin 17. *Nat Immunol*, 6, 1133-41.
- PARKINSON, N., HARDISTY-HUGHES, R. E., TATEOSSIAN, H., TSAI, H. T., BROOKER, D., MORSE, S., LALANE, Z., MACKENZIE, F., FRAY, M., GLENISTER, P., WOODWARD, A. M., POLLEY, S., BARBARIC, I., DEAR, N., HOUGH, T. A., HUNTER, A. J., CHEESEMAN, M. T. & BROWN, S. D. 2006. Mutation at the Evi1 locus in Junbo mice causes susceptibility to otitis media. *PLoS Genet*, 2, e149.
- PASH, J., POPESCU, N., MATOCHA, M., RAPOPORT, S. & BUSTIN, M. 1990. Chromosomal protein HMG-14 gene maps to the Down syndrome region of human chromosome 21 and is overexpressed in mouse trisomy 16. *Proc Natl Acad Sci U S A*, 87, 3836-40.
- PATTERSON, D. 2009. Molecular genetic analysis of Down syndrome. *Hum Genet*, 126, 195-214.
- PAULSON, L. M., WEAVER, T. S. & MACARTHUR, C. J. 2014. Outcomes of tympanostomy tube placement in children with Down syndrome--a retrospective review. *Int J Pediatr Otorhinolaryngol*, 78, 223-6.
- PELULLO, M., ZEMA, S., NARDOZZA, F., CHECQUOLO, S., SCREPANTI, I. & BELLAVIA, D. 2019. Wnt, Notch, and TGF-beta Pathways Impinge on Hedgehog Signaling Complexity: An Open Window on Cancer. *Front Genet*, 10, 711.
- PLETCHER, M. T., WILTSHIRE, T., CABIN, D. E., VILLANUEVA, M. & REEVES, R. H. 2001. Use of comparative physical and sequence mapping to annotate mouse chromosome 16 and human chromosome 21. *Genomics*, 74, 45-54.

## References

- POTIER, M. C., RIVALS, I., MERCIER, G., ETTWILLER, L., MOLDRICH, R. X., LAFFAIRE, J., PERSONNAZ, L., ROSSIER, J. & DAUPHINOT, L. 2006. Transcriptional disruptions in Down syndrome: a case study in the Ts1Cje mouse cerebellum during post-natal development. *J Neurochem*, 97 Suppl 1, 104-9.
- RAVEL, A., MIRCHER, C., REBILLAT, A. S., CIEUTA-WALTI, C. & MEGARBANE, A. 2020. Feeding problems and gastrointestinal diseases in Down syndrome. *Arch Pediatr*, 27, 53-60.
- REINHOLDT, L. G., DING, Y., GILBERT, G. J., CZECHANSKI, A., SOLZAK, J. P., ROPER, R. J., JOHNSON, M. T., DONAHUE, L. R., LUTZ, C. & DAVISSON, M. T. 2011. Molecular characterization of the translocation breakpoints in the Down syndrome mouse model Ts65Dn. *Mamm Genome*, 22, 685-91.
- REYNOLDS, L. E., WATSON, A. R., BAKER, M., JONES, T. A., D'AMICO, G., ROBINSON, S. D., JOFFRE, C., GARRIDO-URBANI, S., RODRIGUEZ-MANZANEQUE, J. C., MARTINO-ECHARRI, E., AURRAND-LIONS, M., SHEER, D., DAGNA-BRICARELLI, F., NIZETIC, D., MCCABE, C. J., TURNELL, A. S., KERMORGANT, S., IMHOF, B. A., ADAMS, R., FISHER, E. M., TYBULEWICZ, V. L., HART, I. R. & HODIVALA-DILKE, K. M. 2010. Tumour angiogenesis is reduced in the Tc1 mouse model of Down's syndrome. *Nature*, 465, 813-7.
- RICHTSMEIER, J. T., BAXTER, L. L. & REEVES, R. H. 2000. Parallels of craniofacial maldevelopment in Down syndrome and Ts65Dn mice. *Dev Dyn*, 217, 137-45.
- RODRIGUES, M., NUNES, J., FIGUEIREDO, S., MARTINS DE CAMPOS, A. & GERALDO, A. F. 2019. Neuroimaging assessment in Down syndrome: a pictorial review. *Insights Imaging*, 10, 52.
- ROSALES, C. 2018. Neutrophil: A Cell with Many Roles in Inflammation or Several Cell Types? *Front Physiol*, 9, 113.
- ROSENFELD, R. M., SHIN, J. J., SCHWARTZ, S. R., COGGINS, R., GAGNON, L., HACKELL, J. M., HOELTING, D., HUNTER, L. L., KUMMER, A. W., PAYNE, S. C., POE, D. S., VELING, M., VILA, P. M., WALSH, S. A. & CORRIGAN, M. D. 2016. Clinical Practice Guideline: Otitis Media with Effusion (Update). *Otolaryngol Head Neck Surg*, 154, S1-S41.
- ROZEN, E. J., ROEWENSTRUNK, J., BARALLOBRE, M. J., DI VONA, C., JUNG, C., FIGUEIREDO, A. F., LUNA, J., FILLAT, C., ARBONES, M. L., GRAUPERA, M., VALVERDE, M. A. & DE LA LUNA, S. 2018. DYRK1A Kinase Positively Regulates Angiogenic Responses in Endothelial Cells. *Cell Rep*, 23, 1867-1878.
- RUEDA, N., FLÓREZ, J. & MARTÍNEZ-CUÉ, C. 2013. Apoptosis in Down's syndrome: lessons from studies of human and mouse models. *Apoptosis*, 18, 121-34.
- RUMMAN, N., JACKSON, C., COLLINS, S., GOGGIN, P., COLES, J. & LUCAS, J. S. 2017. Diagnosis of primary ciliary dyskinesia: potential options for resource-limited countries. *Eur Respir Rev*, 26.
- RYE, M. S., BHUTTA, M. F., CHEESEMAN, M. T., BURGNER, D., BLACKWELL, J. M., BROWN, S. D. & JAMIESON, S. E. 2011. Unraveling the genetics of otitis media: from mouse to human and back again. *Mamm Genome*, 22, 66-82.
- SACKS, B. & WOOD, A. Hearing disorders in children with Down syndrome. 2003.
- SAGO, H., CARLSON, E. J., SMITH, D. J., KILBRIDGE, J., RUBIN, E. M., MOBLEY, W. C., EPSTEIN, C. J. & HUANG, T. T. 1998. Ts1Cje, a partial trisomy 16 mouse model for Down syndrome, exhibits learning and behavioral abnormalities. *Proc Natl Acad Sci U S A*, 95, 6256-61.

## References

- SAHM, A., BENS, M., SZAFRANSKI, K., HOLTZE, S., GROTH, M., GÖRLACH, M., CALKHOVEN, C., MÜLLER, C., SCHWAB, M., KRAUS, J., KESTLER, H. A., CELLERINO, A., BURDA, H., HILDEBRANDT, T., DAMMANN, P. & PLATZER, M. 2018. Long-lived rodents reveal signatures of positive selection in genes associated with lifespan. *PLoS Genet*, 14, e1007272.
- SÁNCHEZ-ELSNER, T., BOTELLA, L. M., VELASCO, B., CORBÍ, A., ATTISANO, L. & BERNABÉU, C. 2001. Synergistic cooperation between hypoxia and transforming growth factor-beta pathways on human vascular endothelial growth factor gene expression. *J Biol Chem*, 276, 38527-35.
- SCHILDER, A. G., CHONMAITREE, T., CRIPPS, A. W., ROSENFELD, R. M., CASSELBRANT, M. L., HAGGARD, M. P. & VENEKAMP, R. P. 2016. Otitis media. *Nat Rev Dis Primers*, 2, 16063.
- SCHNABEL, F., SMOGAVEC, M., FUNKE, R., PAULI, S., BURFEIND, P. & BARTELS, I. 2018. Down syndrome phenotype in a boy with a mosaic microduplication of chromosome 21q22. *Mol Cytogenet*, 11, 62.
- SCHUON, R., SCHWARZENSTEINER, J., PAASCHE, G., LENARZ, T. & JOHN, S. 2021. Functional aspects of the Eustachian tube by means of 3D-modeling. *PLoS One*, 16, e0244909.
- SCHWARTZ, D. M. & SCHWARTZ, R. H. 1978. Acoustic impedance and otoscopic findings in young children with Down's syndrome. *Arch Otolaryngol*, 104, 652-6.
- SEKIYAMA, K., OHORI, J., MATSUNE, S. & KURONO, Y. 2011. The role of vascular endothelial growth factor in pediatric otitis media with effusion. *Auris Nasus Larynx*, 38, 319-24.
- SELIKOWITZ, M. 1992. Health problems and health checks in school-aged children with Down syndrome. *J Paediatr Child Health*, 28, 383-6.
- SHI, L. Z., WANG, R., HUANG, G., VOGEL, P., NEALE, G., GREEN, D. R. & CHI, H. 2011. HIF1alpha-dependent glycolytic pathway orchestrates a metabolic checkpoint for the differentiation of TH17 and Treg cells. *J Exp Med*, 208, 1367-76.
- SHIN, K. J. 2021. Navigational guidelines and positional relationships of the human auditory ossicles from three-dimensional topography for ensuring safe and effective malleostapedotomy : Stereotactic topography of the auditory ossicles and its clinical implication. *Surg Radiol Anat*, 43, 153-159.
- SHOTT, S. R., JOSEPH, A. & HEITHAUS, D. 2001. Hearing loss in children with Down syndrome. *Int J Pediatr Otorhinolaryngol*, 61, 199-205.
- SIMON, F., HAGGARD, M., ROSENFELD, R. M., JIA, H., PEER, S., CALMELS, M. N., COULOIGNER, V. & TEISSIER, N. 2018. International consensus (ICON) on management of otitis media with effusion in children. *European Annals of Otorhinolaryngology, Head and Neck Diseases*, 135, S33-S39.
- SINGH, N., DUTKA, T., REEVES, R. H. & RICHTSMEIER, J. T. 2016. Chronic up-regulation of sonic hedgehog has little effect on postnatal craniofacial morphology of euploid and trisomic mice. *Dev Dyn*, 245, 114-22.
- SINGH, R. & LAUTH, M. 2017. Emerging Roles of DYRK Kinases in Embryogenesis and Hedgehog Pathway Control. *J Dev Biol*, 5.
- SMIRNOVA, M. G., BIRCHALL, J. P. & PEARSON, J. P. 2002. In vitro study of IL-8 and goblet cells: possible role of IL-8 in the aetiology of otitis media with effusion. *Acta Otolaryngol*, 122, 146-52.
- SOJKA, S., AMIN, N. M., GIBBS, D., CHRISTINE, K. S., CHARPENTIER, M. S. & CONLON, F. L. 2014. Congenital heart disease protein 5 associates with CASZ1 to maintain myocardial tissue integrity. *Development*, 141, 3040-9.

## References

- SOUCHET, B., DUCHON, A., GU, Y., DAIROU, J., CHEVALIER, C., DAUBIGNEY, F., NALESSO, V., CRÉAU, N., YU, Y., JANEL, N., HERAULT, Y. & DELABAR, J. M. 2019. Prenatal treatment with EGCG enriched green tea extract rescues GAD67 related developmental and cognitive defects in Down syndrome mouse models. *Sci Rep*, 9, 3914.
- STANKIEWICZ, M. J. & CRISPINO, J. D. 2013. AKT collaborates with ERG and Gata1s to dysregulate megakaryopoiesis and promote AMKL. *Leukemia*, 27, 1339-47.
- STARBUCK, J., REEVES, R. H. & RICHTSMEIER, J. 2011. Morphological integration of soft-tissue facial morphology in Down Syndrome and siblings. *Am J Phys Anthropol*, 146, 560-8.
- STERN, S., SEGAL, M. & MOSES, E. 2015. Involvement of Potassium and Cation Channels in Hippocampal Abnormalities of Embryonic Ts65Dn and Tc1 Trisomic Mice. *EBioMedicine*, 2, 1048-62.
- SUN, D., MATSUNE, S., OHORI, J., FUKUIWA, T., USHIKAI, M. & KURONO, Y. 2005. TNF-alpha and endotoxin increase hypoxia-induced VEGF production by cultured human nasal fibroblasts in synergistic fashion. *Auris Nasus Larynx*, 32, 243-9.
- TAKAHASHI, H. 2001. *The Middle Ear: The Role of Ventilation in Disease and Surgery*, Japan, Springer.
- TANG, S. H., SILVA, F. J., TSARK, W. M. & MANN, J. R. 2002. A Cre/loxP-deleter transgenic line in mouse strain 129S1/SvImJ. *Genesis*, 32, 199-202.
- TANG, Z., ZENG, X., LI, J., ZHANG, H., WU, H., ZHUANG, S. & ZHENG, Y. 2020. The immune imbalance of Treg/Th17 in secretory otitis media patients may be related to PI3K/Akt/mTOR signaling activation in the middle ear mucosa. *Authorea*.
- TATEOSSIAN, H., HARDISTY-HUGHES, R. E., MORSE, S., ROMERO, M. R., HILTON, H., DEAN, C. & BROWN, S. D. 2009. Regulation of TGF-beta signalling by Fbxo11, the gene mutated in the Jeff otitis media mouse mutant. *Pathogenetics*, 2, 5.
- TATEOSSIAN, H., MORSE, S., PARKER, A., MBURU, P., WARR, N., ACEVEDO-AROZENA, A., CHEESEMAN, M., WELLS, S. & BROWN, S. D. 2013. Otitis media in the Tgif knockout mouse implicates TGFbeta signalling in chronic middle ear inflammatory disease. *Hum Mol Genet*, 22, 2553-65.
- TATEOSSIAN, H., MORSE, S., SIMON, M. M., DEAN, C. H. & BROWN, S. D. 2015. Interactions between the otitis media gene, Fbxo11, and p53 in the mouse embryonic lung. *Dis Model Mech*, 8, 1531-42.
- TATEOSSIAN, H., SOUTHERN, A., VIKHE, P., LANA-ELOLA, E., WATSON-SCALES, S., GIBBINS, D., WILLIAMS, D., PURNELL, T., MBURU, P., PARKER, A., NORRIS, D. P., SANTOS-CORTEZ, R., WELLS, S., LAD, H. V., FISHER, E. M. C., TYBULEWICZ, V. L. J. & BROWN, S. D. M. 2022. DYRK1A kinase trisomy is the major cause of Otitis Media in Down Syndrome.
- TEJEDOR, F., ZHU, X. R., KALTENBACH, E., ACKERMANN, A., BAUMANN, A., CANAL, I., HEISENBERG, M., FISCHBACH, K. F. & PONGS, O. 1995. minibrain: a new protein kinase family involved in postembryonic neurogenesis in Drosophila. *Neuron*, 14, 287-301.
- TESMER, L. A., LUNDY, S. K., SARKAR, S. & FOX, D. A. 2008. Th17 cells in human disease. *Immunol Rev*, 223, 87-113.
- THOMPSON, H. & TUCKER, A. S. 2013. Dual origin of the epithelium of the mammalian middle ear. *Science*, 339, 1453-6.
- TIAN, C., HROMATKA, B. S., KIEFER, A. K., ERIKSSON, N., NOBLE, S. M., TUNG, J. Y. & HINDS, D. A. 2017. Genome-wide association and HLA region fine-

## References

- mapping studies identify susceptibility loci for multiple common infections. *Nat Commun*, 8, 599.
- TOMKEIEFF, S. I. 1945. Linear Intercepts, Areas and Volumes. *Nature*, 155, 24-24.
- TORNALI, C., MIGLIORE, M., POLIZZI, A., BRAGAZZI, N. L., MARTINI, M., RUGGIERI, M., PRATICÒ, A. D. & VECCHIO, I. 2021. Reconstructive Surgery in Children with Down Syndrome: Bioethical Implications. *Journal of pediatric neurology*, 19, 001-006.
- TOUSSAINT, N., REDHEAD, Y., VIDAL-GARCÍA, M., LO VERCIO, L., LIU, W., FISHER, E. M. C., HALLGRÍMSSON, B., TYBULEWICZ, V. L. J., SCHNABEL, J. A. & GREEN, J. B. A. 2021. A landmark-free morphometrics pipeline for high-resolution phenotyping: application to a mouse model of Down syndrome. *Development*, 148.
- TYRER, H. E., CROMPTON, M. & BHUTTA, M. F. 2013. What Have We Learned from Murine Models of Otitis Media? *Current Allergy and Asthma Reports*, 13, 501-511.
- UGAZIO, A. G., MACCARIO, R., NOTARANGELO, L. D. & BURGIO, G. R. 1990. Immunology of Down syndrome: a review. *Am J Med Genet Suppl*, 7, 204-12.
- VAL, S., POLEY, M., ANNA, K., NINO, G., BROWN, K., PEREZ-LOSADA, M., GORDISH-DRESSMAN, H. & PRECIADO, D. 2018. Characterization of mucoid and serous middle ear effusions from patients with chronic otitis media: implication of different biological mechanisms? *Pediatr Res*, 84, 296-305.
- VARJOSALO, M., KESKITALO, S., VAN DROGEN, A., NURKKALA, H., VICHALKOVSKI, A., AEBERSOLD, R. & GSTAIGER, M. 2013. The Protein Interaction Landscape of the Human CMGC Kinase Group. *Cell Reports*, 3, 1306-1320.
- VELDHOEN, M., HOCKING, R. J., ATKINS, C. J., LOCKSLEY, R. M. & STOCKINGER, B. 2006. TGFbeta in the context of an inflammatory cytokine milieu supports de novo differentiation of IL-17-producing T cells. *Immunity*, 24, 179-89.
- VIKHE, P. P., PURNELL, T., BROWN, S. D. M. & HOOD, D. W. 2019. Cellular content plays a crucial role in Non-typeable Haemophilus influenzae infection of preinflamed Junbo mouse middle ear. *Cell Microbiol*, 21, e12960.
- VIKHE, P. P., TATEOSSIAN, H., BHARJ, G., BROWN, S. D. M. & HOOD, D. W. 2020. Mutation in Fbxo11 Leads to Altered Immune Cell Content in Jeff Mouse Model of Otitis Media. *Front Genet*, 11, 50.
- WATSON-SCALES, S., KALMAR, B., LANA-ELOLA, E., GIBBINS, D., LA RUSSA, F., WISEMAN, F., WILLIAMSON, M., SACCON, R., SLENDER, A., OLERINYOVA, A., MAHMOOD, R., NYE, E., CATER, H., WELLS, S., YU, Y. E., BENNETT, D. L. H., GREENSMITH, L., FISHER, E. M. C. & TYBULEWICZ, V. L. J. 2018. Analysis of motor dysfunction in Down Syndrome reveals motor neuron degeneration. *PLoS Genet*, 14, e1007383.
- WATSON, D. R., MCCLELLAND, R. J. & ADAMS, D. A. 1996. Auditory brainstem response screening for hearing loss in high risk neonates. *Int J Pediatr Otorhinolaryngol*, 36, 147-83.
- WEI, G., GUO, J., DOSEFF, A. I., KUSEWITT, D. F., MAN, A. K., OSHIMA, R. G. & OSTROWSKI, M. C. 2004. Activated Ets2 is required for persistent inflammatory responses in the mouse heat shock model. *J Immunol*, 173, 1374-9.
- WOLVETANG, E. J., WILSON, T. J., SANIJ, E., BUSCIGLIO, J., HATZISTAVROU, T., SETH, A., HERTZOG, P. J. & KOLA, I. 2003. ETS2 overexpression in

## References

- transgenic models and in Down syndrome predisposes to apoptosis via the p53 pathway. *Hum Mol Genet*, 12, 247-55.
- XU, X., WOO, C.-H., STEERE, R. R., LEE, B. C., HUANG, Y., WU, J., PANG, J., LIM, J. H., XU, H., ZHANG, W., KONDURU, A. S., YAN, C., CHEESEMAN, M. T., BROWN, S. D. M. & LI, J.-D. 2012. EVI1 Acts as an Inducible Negative-Feedback Regulator of NF- $\kappa$ B by Inhibiting p65 Acetylation. *The Journal of Immunology*, 188, 6371-6380.
- YU, T., LI, Z., JIA, Z., CLAPCOTE, S. J., LIU, C., LI, S., ASRAR, S., PAO, A., CHEN, R., FAN, N., CARATTINI-RIVERA, S., BECHARD, A. R., SPRING, S., HENKELMAN, R. M., STOICA, G., MATSUI, S., NOWAK, N. J., RODER, J. C., CHEN, C., BRADLEY, A. & YU, Y. E. 2010. A mouse model of Down syndrome trisomic for all human chromosome 21 syntenic regions. *Hum Mol Genet*, 19, 2780-91.
- ZAITOUN, M., RAWASHDEH, M., ALQUDAH, S., H, A. L., NUSEIR, A. & AL-TAMIMI, F. 2021. Knowledge and Practice of Hearing Screening and Hearing Loss Management among Ear, Nose, and Throat Physicians in Jordan. *Int Arch Otorhinolaryngol*, 25, e98-e107.
- ZHU, B., PARSONS, T., STENSEN, W., MJØEN SVENDSEN, J. S., FUGELLI, A. & HODGE, J. J. L. 2022. DYRK1a Inhibitor Mediated Rescue of Drosophila Models of Alzheimer's Disease-Down Syndrome Phenotypes. *Front Pharmacol*, 13, 881385.

## Appendix

### 8.1. Primary antibodies

**Table 8.1. Primary antibodies used for immunohistochemistry (IHC).** The table details the supplier and catalogue number, and the animal species that the antibody was raised in. Also shown are the antibody concentrations used, and whether heat mediated antigen retrieval was required.

Antibody	Supplier	Catalogue number	Host species	Concentration	Antigen retrieval
DYRK1A	Abcam	ab65220	Rabbit	1:100	No
KCNJ6 (GIRK2)	Abcam	ab65096	Goat	1:500	No
KCNJ15	Abcam	ab200397	Rabbit	1:100	No
ERG	Abcam	ab92513	Rabbit	1:500	Yes
phosETS2	ThermoFisher	44-1105G	Rabbit	1:500	Yes
PSMG1	Abcam	ab167396	Rabbit	1:1000	Yes
BRWD1	Elabscience	E-AB-17567	Rabbit	1:100	No
HMG1	Invitrogen	PA5-76859	Rabbit	1:40	No
GET1	Bioss antibodies	bs-11774R	Rabbit	1:100	No
LCA5L	Bioss antibodies	bs-9972R	Rabbit	1:1000	No
SH3BGR	Proteintech	21161-1-AP	Rabbit	1:200	No
B3GALT5	Origene	TA336273	Rat	1:10	Yes
F4/80	Invitrogen	MF48005	Rat	1:100	Yes
MPO	Abcam	ab208670	Rabbit	1:200	Yes
Cleaved Caspase-3	Cell Signaling Technology	9664S	Rabbit	1:1000	Yes
Ki67	Abcam	ab15580	Rabbit	1:1000	Yes
phospho SMAD2	Merck Millipore	AB3849-I	Rabbit	1:100	No
SMAD3	Merck Millipore	06-920	Rabbit	1:100	No
VEGF-A	Merck Millipore	AB1876-I	Rabbit	1:200	No
IL-6	Abcam	ab6672	Rabbit	1:100	No
IL-10	Abcam	ab217941	Rabbit	1:100	No

### 8.2. Secondary antibodies

For immunohistochemistry, the primary antibodies raised in rabbit were followed by the secondary and tertiary antibodies from the VECTASTAIN® Elite® ABC HRP kit (PK-6101). Those raised in goat or rat were followed by a HRP secondary and no tertiary antibody.

**Table 8.2. Secondary antibodies used for immunohistochemistry.** The secondary antibody corresponded to the host species of the primary antibody.

Antibody	Supplier	Catalogue number	Concentration
Rabbit anti-goat IgG (H+L)-HRP	Invitrogen	81-1620	1:200
Goat anti-rat HRP	Cell Signaling Technology	7077S	1:200

### 8.3. Lower magnification images for cilia SEM

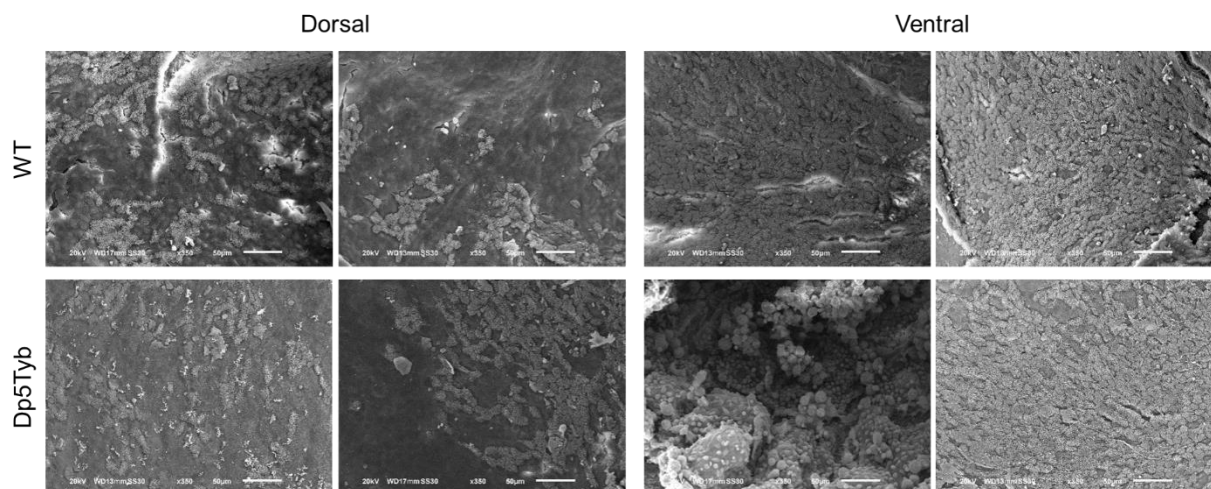


**Figure 8.1. Lower magnification images of the middle ear of two-month-old Dp5Tyb and WT mice.** Images taken by Andy Parker using a scanning electron microscope. Magnification = x350. Scale bar = 50 µm.

### 8.4. RT-qPCR primers for Dp5Tyb genes

Gene	Forward exon	Reverse exon	Forward primer	Reverse primer
<i>Dyrk1a</i>	3	4	TGACCAGATTCAGCAACCTCTAAC	CCGCCTCTGTAACATGACAATG
<i>Kcnj6</i>	3	4	GAGGAACCTGGAGATTGTGGTCAT	GGGCTTGGCACGTCATTTC
<i>Kcnj15</i>	4	4	CAACCGTCATCGACATGAAGTG	ATCACAAAGGTGGCAGCAAAT
<i>Erg</i>	4	5	GCAACCCTAGTCAGGTGAATGG	CATCTTCCCACCTTTGTTTACA
<i>Ets2</i>	3	4	CCTGGATTCTGTCTCCCATGA	TGCAGGGAGTGAGCAAAGG
<i>Psmg1</i>	2	3	TAGGAAGCAACGCAACAGCAT	TTCCCAGACTCCCGAGTTCA
<i>Brwd1</i>	14	15	CCTACACTGGACAGCTGCTTCA	TGTGTCTCCAAAACAACACTTCA
<i>Hmgn1</i>	4	5	CGCGAAGCCGAAAAAGG	ATCTGCACTTTTTGTCTGATGCT
<i>Wrb (Get1)</i>	4	4-5	TGCCAGCAAGTGGATCAC	GTGATTCCAATCCACCTGCTACT
<i>Lca5l</i>	4	5	AAAAGGAAGTACAACGCTGGTAAAC	CTCAGCTGGGATGTCCTTCTG
<i>Sh3bgr</i>	2	3	GCCCCCTCAGATCTTCAATG	GCCAGACCAAGGAATGAATAAATAA
<i>B3galt5</i>	4	4	CATGGCCATCCGCAAGAC	GGTCCCCAGAAGGAAGAAGGT

**Figure 8.2. Primers for all 12 genes in the Dp5Tyb region.** Primers were designed using Primer Express 3. The table details the exons in which the forward and reverse primers will bind.

## 8.5. Negative controls for immunohistochemistry

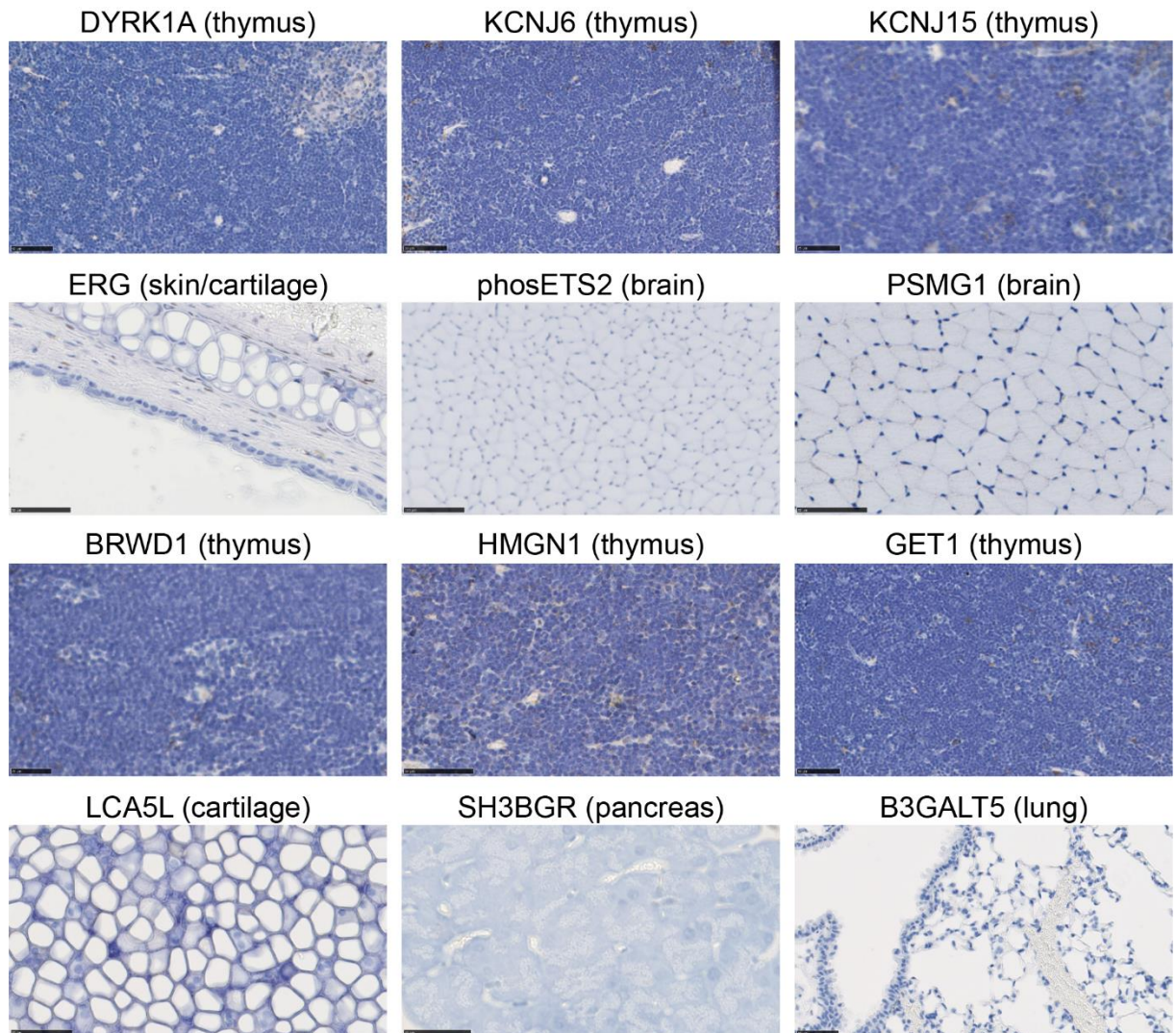


*Figure 8.3. Negative controls for immunohistochemistry.* Sections underwent the same staining process but without the primary antibody. Counterstained with haematoxylin (blue).

## 8.6. Examples of western blots for the 12 Dp5Tyb proteins

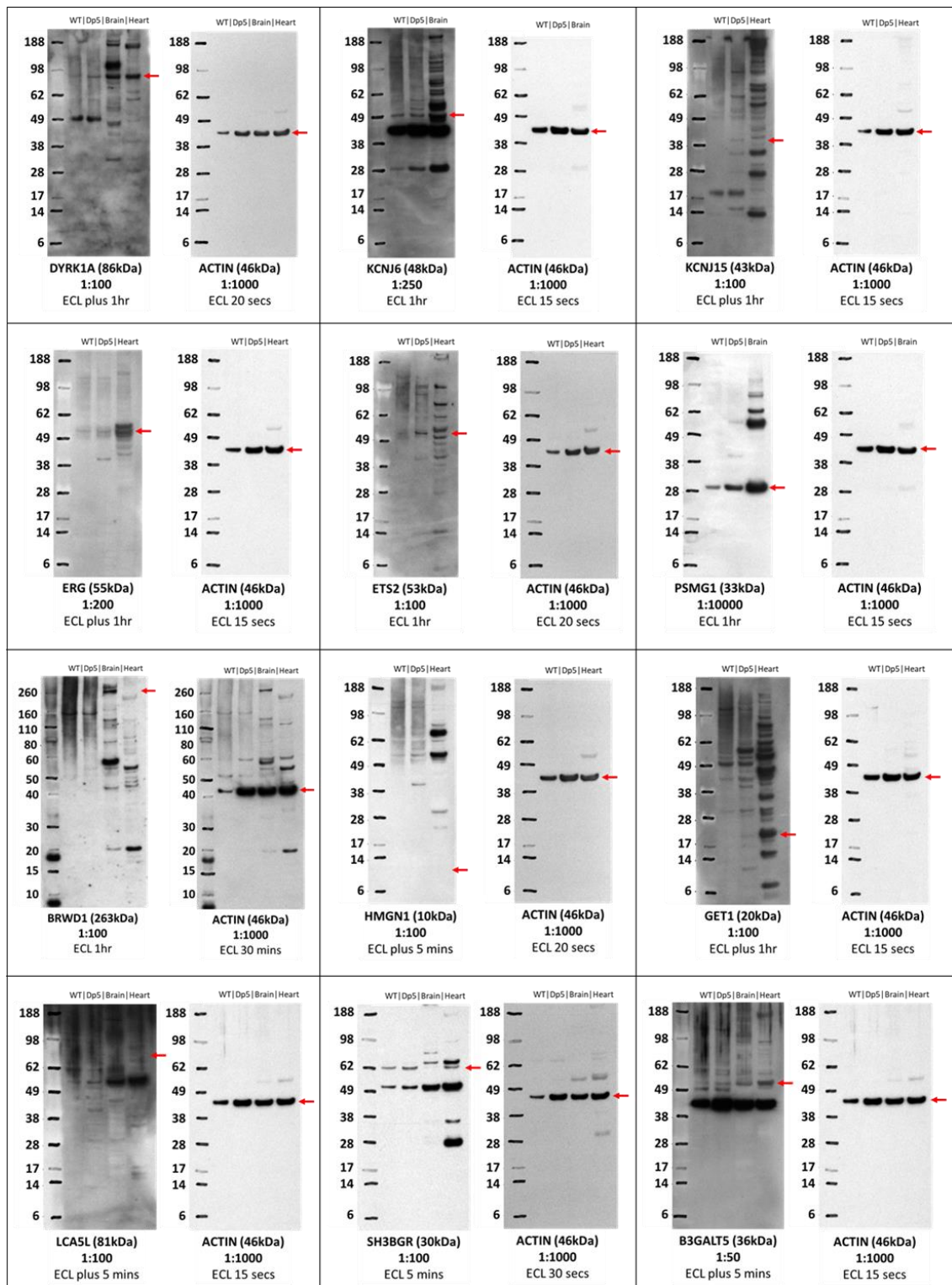


**Figure 8.4. Examples of western blots with antibodies against the 12 Dp5Tyb proteins.** Middle ear epithelial cell lysate from WT and Dp5Tyb mice was run alongside WT brain or heart lysate as a positive control. The protein concentration was calculated using a BCA assay, and then 15  $\mu$ g of protein was added per well. Each blot is shown alongside the same membrane incubated with anti-ACTIN antibody as a loading control. The protocol used NuPAGE® MES buffer with 4-12% bis-tris gels. SeeBlue® Plus2 Pre-Stained Standard (Invitrogen) was used for all blots except BRWD1 which used the Novex™ Sharp Pre-Stained Standard (Invitrogen). Red arrows highlight bands of interest due to molecular weight of known isoforms). The molecular weight of the protein of interest can be found under each blot, along with the antibody concentration, exposure time and type of ECL substrate used.

## 8.7. Genotyping

All genotyping was performed by the Genotyping team at MRC Harwell, and their methods are as follows.

### 8.7.1. Genotyping of Dp lines

Dp(16Lipi-Zbtb21)1TybEmcf (Dp1Tyb), Dp(16Mir802-Zbtb21)3TybEmcf (Dp3Tyb) and Dp(16Dyrk1a-B3galt5)5TybEmcf (Dp5Tyb) were the main DS lines used for this project. All were genotyped using qPCR with Taqman probes and copy counting.

The qPCRs involved amplification of DNA between two primers whilst monitoring the progress of DNA replication using a probe. The Taqman probes used were short DNA oligos complimentary to a section of DNA between the forward and reverse primers. At the 5' end of the probe was a fluorescent reporter and at the 3' end there was a quencher (*Figure 8.5*). As the forward primer was extended the reporter was cleaved from the probe, resulting in a fluorescent signal. As the DNA replication continued the quencher was cleaved, which stopped the fluorescent signal.

The amount of DNA doubles with every cycle, and the number of cycles taken to reach the threshold is known as the CT value. The higher the CT value the lower the amount of template DNA in the sample. The CT value was used to determine how many copies of a particular allele the samples had (e.g. CT 25 = 2 x template DNA, CT 26 = 1 x template DNA, CT 30+ = no template DNA). Multiple qPCR assays can be multiplexed and run together if probes with different fluorescent signals are used. In this case, a FAM-labelled genotyping assay was run in multiplex with a VIC-labelled internal control (*Dot1l*) (*Figure 8.6*). All qPCR genotyping assays were run in duplicate.

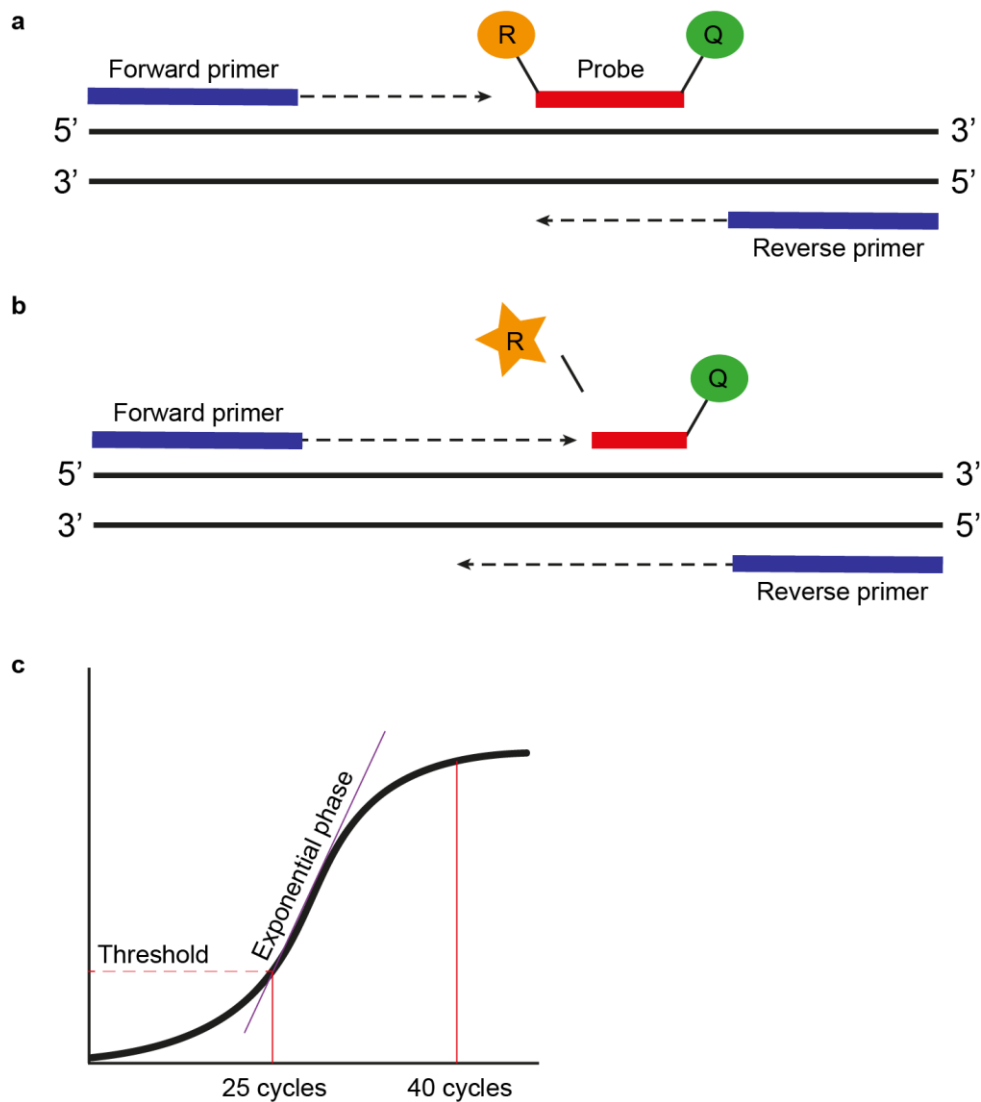


**Figure 8.5. Genotyping using quantitative PCR (qPCR).** A qPCR amplifies the DNA between two primers whilst monitoring the progress of DNA synthesis using a probe. The probe is complementary to a sequence situated between the forward and reverse primers, and is attached to a fluorescent reporter (R) and a quencher (Q). Whilst they remain attached no signal is produced.

(a) The primers and probes are attached to the DNA sequence and replication is beginning.

(b) As the forward primer is extended the reporter is cleaved from the probe and a fluorescent signal is produced. The primers will continue extending and eventually the forward primer will cleave the quencher, which stops the fluorescent signal.

(c) Each doubling of DNA content is one cycle. The number of cycles taken to reach a set threshold is called the CT value, and is inversely proportional to the amount of DNA in the sample. Whilst in the exponential phase of DNA replication there are no limiting factors. This PCR reaction plot shows the typical S-shaped curve. If a sample gives a CT value of above 30 it's deemed that there's no template present in the sample.

The Dp lines all have an insertion mutation (duplication of all/part of Mmu16) (Figure 8.7). The inserted region creates a new mutant breakpoint sequence. The mutant allele was defined as the presence of both mutant breakpoints, and the WT allele was defined as the absence of both.

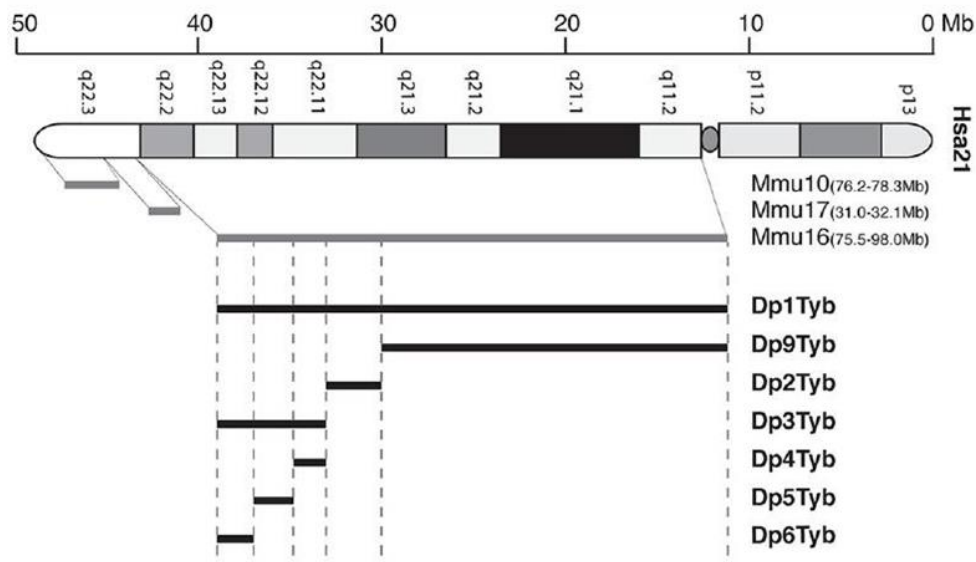


Figure 8.7. **Duplicated regions present in the DpTyb mouse lines.** The lines used for this project were Dp1Tyb, Dp3Tyb and Dp5Tyb. Each line has an insertion mutation of all/part of Mmu16. Genotyping was performed by qPCR looking for the new mutant breakpoint sequence present at either end of the inserted region.

***Dot1l* internal control (VIC-labelled)**

```
CCTAGCCATGGTGTGTTGTGTGCCAGTTCTCATGAGGCAAGCCTACAGCCTTCATCATTCTACAGTTGCCTTCAT
TACCCTACAGTCCACTTCTCCAGTGGAGCTGGGCCTGTGCAAACAGTGGGCAGTGATGTGAAGGGCAGGAAGC
TCATAGGGTGACTGGCCAACCCAGGGAAGCCGGAGTGCCTGCGTCTTCTGTTCCCTTGTTCTTTCCCTCTAGTC
GTTTTCTGTTAGTAGTTGGCATCCTTATGCTTCATCTTACAGTGGACTTGAGAGCTGGCCCTGAATGGTCGTGCT
GGGGCAAGGCTTTATTTTAGGCGTAGCACACATGGTGGCCAATGGGACTCTGTAGGATCTGCCACACCCATCAG
GTGTGCAGGGAGACAGAGCTGAGTCAGGCTCCAGCTCTGGGGAATATGTTGAGTCACCACCTCTGTAGGGTGGTT
GTGCATCATAGAACAAGAGGACTTTGGGGTGTCACTGTGGTGTGGTGGTCCAACCTGTGCATCTTTTCTCTTCAG
GACAAGCACCATGATGCTG
```

Primer 1 = GCCCCAGCACGACCATT  
 Primer 2 = TAGTTGGCATCCTTATGCTTCATC  
 Probe = CCAGCTCTCAAGTCG

Figure 8.6. **Primers and probe sequences for the VIC-labelled internal control, *Dot1l*.**

The assays for Dp5Tyb were 5b18 and 3c09, for Dp1Tyb were Zfp295-1KO and Zfp295-3KO, and for Dp3Tyb the assays were Zfp295-1KO and Ms2Tyb-2KO. The forward and reverse primers, and the FAM-labelled probes are detailed below (Figure 8.8).

<p><u>5b18-BP-LOA-Mut1 (FAM labelled probe)</u></p> <p>TAGTATTCTACTTCTGGGCGGTCTGAGGTGCTACCTGTTCAATTATTTTGGCTCCGGTGAAAGACCCAGAGCG  AACAACTCAAGGGAGGAAGATCCGGCGCGCCAAGCTTTAATTCAAGAACTATTCTCTAGAAGTTTAAACAA  CTGCTATTCTGCTCTCTATGACTCTTAAACA</p> <p>TCCGGTGAAAGACCCAGA  AGAAGAGCAGAATAGCAGTTGTTTA  AAGATCCGGCGCGCCAAGCT</p> <p><u>3c09-BP-LOA-Mut1 (FAM labelled probe)</u></p> <p>GCTACAGGGCGGTCCCATTCGCCATTCAGGCTGCGCAACTGTTGGGAAGGGCGATCGGTGCGGGCCTCTTC  GCTATTACGCCAGGGCGCGCCGGATCAAAGCTGTGCGCCAGCACCGCCTGGCTTGTCTTTGATTATATCAG  TGCACATAAATACAACCTGAGGAGCTCCCGAAAATCGCTTAAAAACAACTAAAAAGCTGTTGTATTTTGCTT  TTTTATACCAATGTAGGGAG</p> <p>TTCAGGCTGCGCAACTGT  CCTCAAGTTGTATTTATGTGCACTGATA  CGCCGGATCAAAGCTGTGCG</p>
<p><u>Zfp295-1KO-BP-LOA-Mut1 (FAM-labelled probe)</u></p> <p>CATTCTTCTAGTTGGATTTTAATTCTAACCCCTAACCCCTAAGTCCTTGTCCTCACAGCAGTGCAG&lt;ATCACG  GC&gt;GCGCCAAGCTTTAATTCAAGAACTATTCTCTAGAAGTTTAAACAACCTGCTATTCTGCTCTTCTATGACTCT  TTAACATGTCTCTCAAAATATGTTTCTCCAGAAAACCTCTCCTCAACTTC</p> <p>CTAACCCCTAACCCCTAAGTCCTTGTC  TGAGGAGAGTTTTCTGGGAGAA  CTCACAGCAGTGCAGATCACGGC</p> <p><u>Zfp295-3KO-BP-LOA-Mut1 (FAM-labelled probe)</u></p> <p>ACAGGGCGCGTCCCATTCGCCATTCAGGCTGCGCAACTGTTGGGAAGGGCGATCGGTGCGGGCCTCTTCGCT  ATTACGCCAGGGCGCG&lt;CCGGA&gt;TCTTTAGAGTTTGCAGCTGCTCATCTGAATGAGGAGAATGCACCTCAGGG  AGAGAG</p> <p>CGGGCCTCTTCGCTATTACG  GAGTGCATTCTCCTCATTGAGATG  AGGGCGCGCCGGATCTTTAGA</p>
<p><u>Zfp295-1KO-BP-LOA-Mut1 (FAM-labelled probe)</u></p> <p>CATTCTTCTAGTTGGATTTTAATTCTAACCCCTAACCCCTAAGTCCTTGTCCTCACAGCAGTGCAG&lt;ATCACG  GC&gt;GCGCCAAGCTTTAATTCAAGAACTATTCTCTAGAAGTTTAAACAACCTGCTATTCTGCTCTTCTATGACTCT  TTAACATGTCTCTCAAAATATGTTTCTCCAGAAAACCTCTCCTCAACTTC</p> <p>CTAACCCCTAACCCCTAAGTCCTTGTC  TGAGGAGAGTTTTCTGGGAGAA  CTCACAGCAGTGCAGATCACGGC</p>
<p><u>Ms2Tyb-2KO-BP-LOA-Mut1 (FAM-labelled probe)</u></p> <p>AGGAAGCGGAAGAGCGCCAATACGCAAACCGCCTCTCCCGCGGTTGGCCGATTATTAATGCAGGGCGC  &lt;GCCGAGT A&gt;AGGGTGTGGTTAAGTGGTACTGTTTCAATGATGTGGTGTGTCCTATGCTGCGTCTGTA  TAGTTAGATGGAGTCAACCAAGCCCTTACACACAGTGTACCCTTGTAGACTTCATACCACTGTCCAGGAA  CAAGAACCAGCAATGGAATACATGTCAAGACCACTAAAAAT</p> <p>AGCGCCAATACGCAAAC  GCGGACACACCACATCAC  ATTAATGCAGGGCGCGCCGAGT</p>

**Figure 8.8. Primer sequences and FAM-labelled probes for the Dp5Tyb, Dp1Tyb and Dp3Tyb assays, respectively.**

The master mix for each qPCR comprised of the assay primers, the relevant FAM and VIC-labelled probes, Taqman master mix, double-distilled water, and the DNA sample isolated from the mouse ear biopsy (*Figure 8.9*).

<u>qPCR master mix</u>	
ABI GTX Taqman master mix	5 $\mu$ l
Primers Dot1L_2F (20 $\mu$ M)	0.225 $\mu$ l
Primers Dot1L_R (20 $\mu$ M)	0.225 $\mu$ l
Probe DotL_2M (5 $\mu$ M)	0.2 $\mu$ l
FAM Assay (probe 5 $\mu$ M & primers 15 $\mu$ M each)	0.3 $\mu$ l
ddH <sub>2</sub> O	1.55 $\mu$ l
DNA (1/10 dilution of ABI Sample-to-SNP prep)	2.5 $\mu$ l

*Figure 8.9. Master mix for each qPCR.* ddH<sub>2</sub>O = double-distilled water.

The two replicates were then combined onto one graph for the copy counting (*Figure 8.10*).

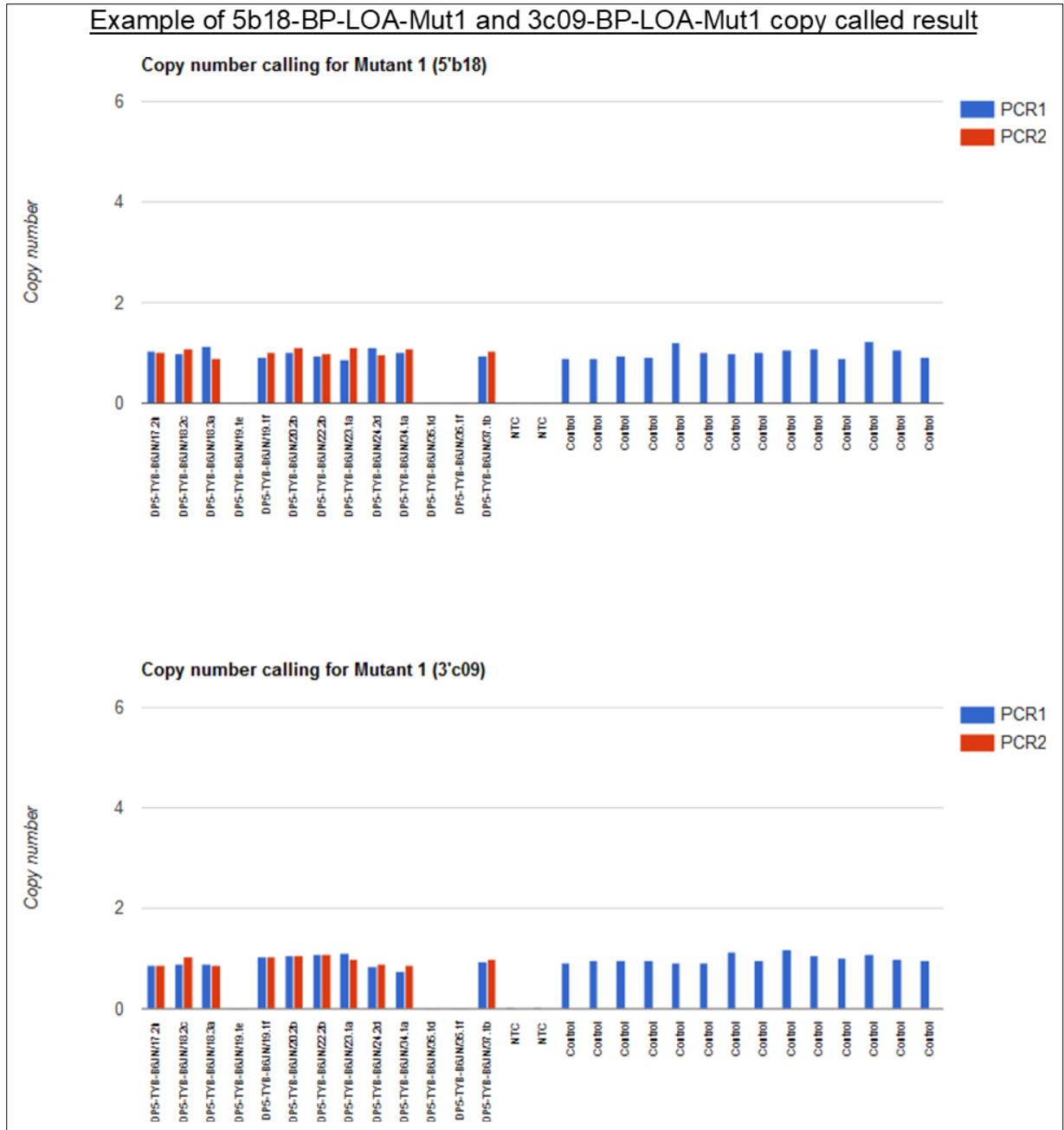


**Figure 8.10. Example of 5b18 and 3c09 assay copy calling.** The graphs show the number of copies of each breakpoint sequence in each mouse. The qPCRs were done in duplicate, so each mouse has a blue and red bar. If the mouse has one copy of both breakpoints (5'b18 and 3'c09) then the Dp5Tyb duplication is present. No copies means it's a WT mouse.

## 8.7.2. Genotyping of knockout and point mutation lines

Knockout and point mutation mouse lines were imported to cross to Dp5Tyb mice and restore disomy of one Dp5Tyb gene at a time. Of the 12 Dp5Tyb genes, 10 are listed below as they were genotyped onsite (MRC Harwell). *Hmgn1* was crossed to Dp5Tyb in a collaborators lab (Victor Tybulewicz) so genotyping was carried out there instead. We received heads in formalin pots and passed on to Histology for sectioning. A knockout for *Kcnj15* was not available on the IMPC website and due to time constraints we continued without one. For *Dyrk1a*, the Deafness lab imported a knockout to cross to Dp1Tyb so genotyping information is available. However, the Dp3Tyb *Dyrk1a*<sup>+/-</sup> mice used for this project were created in the Tybulewicz lab and the heads were shipped over in formalin.

### 8.7.2.1. Gel based genotyping

This method was performed for the following knockout mice: *Dyrk1a*<sup>tm1Mla</sup> (*Dyrk1a*<sup>+/-</sup>), C57BL/6N-*Erg*<sup>em1(IMPC)Bay/Mmucd</sup> (*Erg*<sup>+/-</sup>), C57BL/6N-CrI-*Brwd1*<sup>em1(IMPC)Tcp</sup> (*Brwd1*<sup>+/-</sup>), C57BL/6N-*Wrb*<sup>tm1.1(KOMP)Vlcg/MbpMmucd</sup> (*Wrb*<sup>+/-</sup>), *Lca5*<sup>em1(IMPC)lcs</sup> (*Lca5*<sup>+/-</sup>), *Sh3bgr*<sup>em1(IMPC)lcs</sup> (*Sh3bgr*<sup>+/-</sup>) and *B3galt5*<sup>em1(IMPC)lcs</sup> (*B3galt5*<sup>+/-</sup>). Gel based assays were run on the Qiagen QIAxcel (*Figure 8.11*), which is a capillary based system with clearer resolution and a faster running time than standard agarose gels. The ladder used was 50-800 bp and the PCR was performed using KAPA fast Taq polymerase.

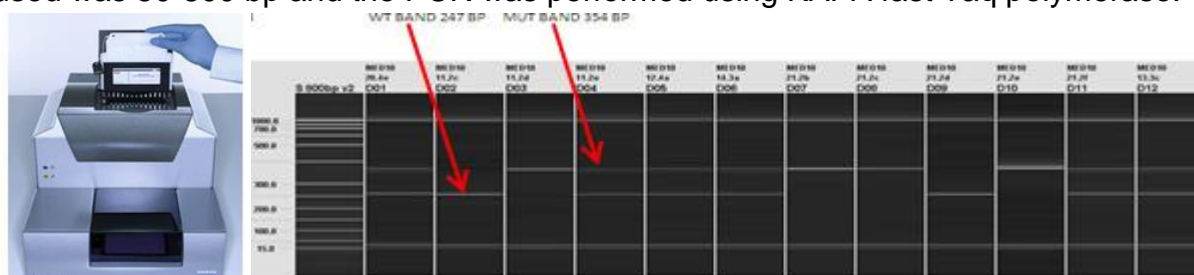


**Figure 8.11.** The Qiagen QIAxcel machine used to run the PCR, alongside an example readout showing WT and mutant bands.

The figure over the next two pages (*Figure 8.12*) details the reagents used for the PCRs. For each reaction, the specific forward and reverse primers for that gene were used. The protocol was the same for all reactions.

<u>PCR protocol</u>		<u>Erg gel based primers</u>	
1. 95°C	1 min	47583-comF	CATGATGGTCTTTCCAGGTG
2. 95°C	10 secs	47583-WtR	GTAGCTGCCGTAGCTCATCC
3. 60°C	10 secs	47583-mutR	GGAACAGTGGAGCTTACGAA
4. 72°C	1 sec	<u>PCR mix</u>	
5. Back to step 2 for 29 cycles		KAPA Taq PCR master mix	5 µl
6. 72°C	30 secs	47583-comF	0.5 µl
7. 16°C	held	47583-WtR	0.5 µl
		47583-mutR	0.5 µl
		H <sub>2</sub> O	3.0 µl
		DNA	1 µl

<u>Dyrk1a gel based primers</u>	
Dyrk1a_Neo_P1	ATTCGCAGCGCATCGCCTTCTATCGCC
Dyrk1a_P2	CTTATGACAGAGTGGAGCAA
Dyrk1a_P3	CGTGATGAGCCCTTACCTATG
<u>PCR mix</u>	
KAPA Taq PCR master mix	5 µl
Dyrk1a_Neo_P1	0.5 µl
Dyrk1a_P2	0.5 µl
Dyrk1a_P3	0.5 µl
H <sub>2</sub> O	2.5 µl
DNA	1 µl

<u>Brwd1 gel based primers</u>			
Brwd1_WTF	CTCCACTTGTTTCGCTGGTCC		
Brwd1_WTR	CAACAGCTGGAATGAGACACGAAAAG		
Brwd1_MUTF	CCAGCCAAGGAGCCACATCC		
Brwd1_MUTR	TACAGAGGAAGGGAGTACAGTACAG		
Slc40a1_sh_F	CCTTTGTAACCTCCTCTGTGTC		
Slc40a1_sh_R	CTGAAGTCTTTCATGATAACTGCATT		
<u>WT PCR mix</u>		<u>Mutant PCR mix</u>	
KAPA Taq PCR master mix	5 µl	KAPA Taq PCR master mix	5 µl
Primer_WT_F	0.5 µl	Primer_MUT_F	0.5 µl
Primer_WT_R	0.5 µl	Primer_MUT_R	0.5 µl
Slc40a1_sh_F	0.5 µl	Slc40a1_sh_F	0.5 µl
Slc40a1_sh_R	0.5 µl	Slc40a1_sh_R	0.5 µl
H <sub>2</sub> O	3.0 µl	H <sub>2</sub> O	3.0 µl
DNA	1 µl	DNA	1 µl

<u>Wrb gel based primers</u>		<u>WT PCR mix</u>	
Reg-Wrb-R	ACGTCGTCTCATGAACACATGTAGG	KAPA Taq PCR master mix	5 µl
Reg-Wrb-wtR	TGGGTTCACATGCTAGGTATTCCCC	Reg_Wrb_wtF	0.5 µl
Reg-Wrb-wtF	TTTTGCTCTGAGTTTCGTGAGCTGG	Reg_Wrb_wtR	0.5 µl
Reg-NeoF	GCAGCCTCTGTTCCACATACACTTCA	H <sub>2</sub> O	3.0 µl
Reg-LacF	ACTTGCTTTAAAAAACCTCCCACA	DNA	1 µl
Slc40a1_sh_F	CCTTTGTAACCTCCTCTGTGTC		
Slc40a1_sh_R	CTGAAGTCTTTCATGATAACTGCATT		
<u>Pre Cre PCR mix</u>		<u>Post Cre PCR mix</u>	
KAPA Taq PCR master mix	5 µl	KAPA Taq PCR master mix	5 µl
Reg-NeoF	0.5 µl	Reg-LacF	0.5 µl
Reg-Wrb-R	0.5 µl	Reg-Wrb-R	0.5 µl
Slc40a1_sh_F	0.5 µl	Slc40a1_sh_F	0.5 µl
Slc40a1_sh_R	0.5 µl	Slc40a1_sh_R	0.5 µl
H <sub>2</sub> O	3.0 µl	H <sub>2</sub> O	3.0 µl
DNA	1 µl	DNA	1 µl

<u>Lca5l gel based primers</u>	
Lca5l_Wr	GGCCATGCCTGCTGCTGGTTAG
Lca5l_Ef	GATACAGGAATGTGCCTCCACAACCTGG
Lca5l_Er	GAGCTGAAAGCAGGTGTTTCATTTCAAAG
<u>PCR mix</u>	
KAPA Taq PCR master mix	5 µl
Lca5l_Wr	0.5 µl
Lca5l_Ef	0.5 µl
Lca5l_Er	0.5 µl
H <sub>2</sub> O	3.0 µl
DNA	1 µl

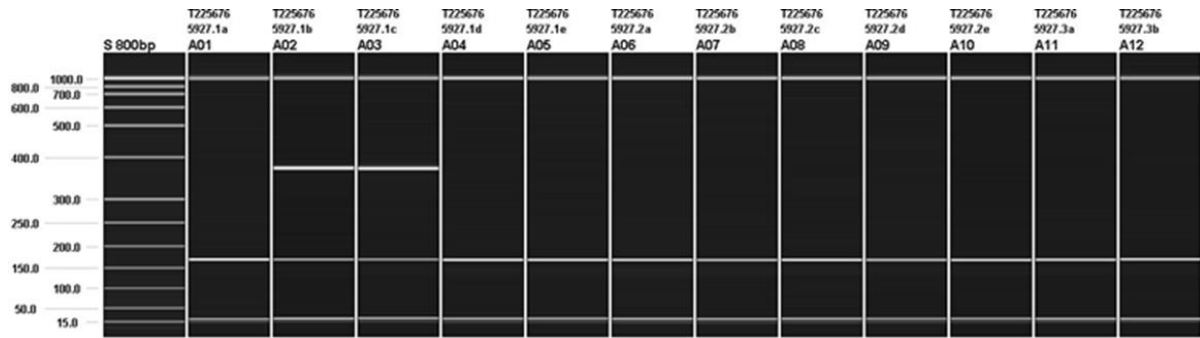
<u>Sh3bgr gel based primers</u>	
Sh3bgr_Wf	GGCCTTGTGCTTGCATGGCAAG
Sh3bgr_Ef	GTCCAAGGCCTGGTGAATCCAG
Sh3bgr_Er	GCATAAGACTACACGTCACTAGCCAGTC
<u>PCR mix</u>	
KAPA Taq PCR master mix	5 µl
Sh3bgr_Wr	0.5 µl
Sh3bgr_Ef	0.5 µl
Sh3bgr_Er	0.5 µl
H <sub>2</sub> O	3.0 µl
DNA	1 µl

<u>B3galt5 gel based primers</u>	
B3galt5_Ef	CACAGCTCCAGACCCATAGGC
B3galt5_Er	CGAGTAAGTGACCCTGGCTGC
B3galt5_Wr	GAATCGGTGCAAACACCACTCG
Slc40a1_sh_F	CCTTTGTAACCTCCTCTGTGTC
Slc40a1_sh_R	CTGAAGTCTTTCATGATAACTGCATT
<u>WT PCR mix</u>	
KAPA Taq PCR master mix	5 µl
B3galt5_Ef	0.5 µl
B3galt5_Wr	0.5 µl
Slc40a1_sh_F	0.5 µl
Slc40a1_sh_R	0.5 µl
H <sub>2</sub> O	3.0 µl
DNA	1 µl
<u>Mutant PCR mix</u>	
KAPA Taq PCR master mix	5 µl
B3galt5_Ef	0.5 µl
B3galt5_Er	0.5 µl
Slc40a1_sh_F	0.5 µl
Slc40a1_sh_R	0.5 µl
H <sub>2</sub> O	3.0 µl
DNA	1 µl

**Figure 8.12. The PCR protocol, and gel based primers and PCR master mixes for all seven mouse lines using the gel based genotyping method.** Each mouse line had a slightly different PCR mix, but all followed the same PCR protocol.

The Qiagen QIAxcel then gave a readout indicating whether the DNA contained the mutant breakpoints or only the WT sequence. An example of this is shown below for *Dyrk1a* (Figure 8.13).



WT band = 150 bp  
 Mutant band = 350 bp

Figure 8.13. Example of a *Dyrk1a* gel based assay. The results show two mice carrying the knockout mutation (wells A02 and A03).

### 8.7.2.2. CRISPR generated critical exon deletion genotyping

This method was performed for  $Kcnj6^{em1(IMPC)H}$  ( $Kcnj6^{+/-}$ ) mice.

The knockout allele was generated using CRISPR/Cas9 to delete a critical exon (Figure 8.14).

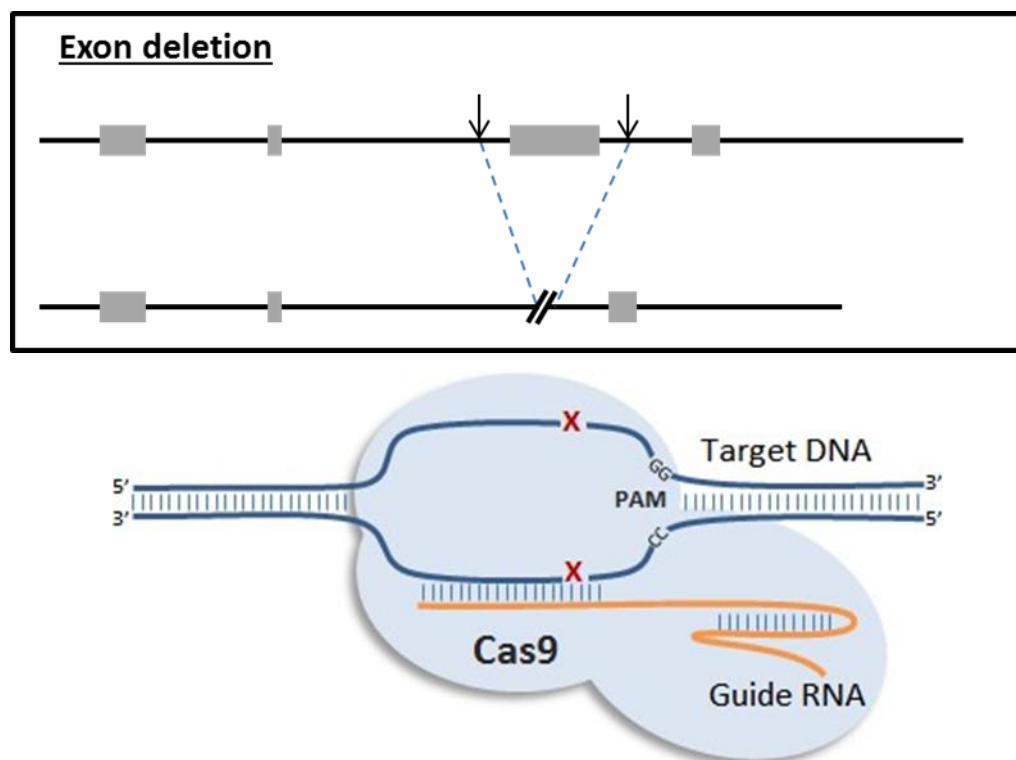
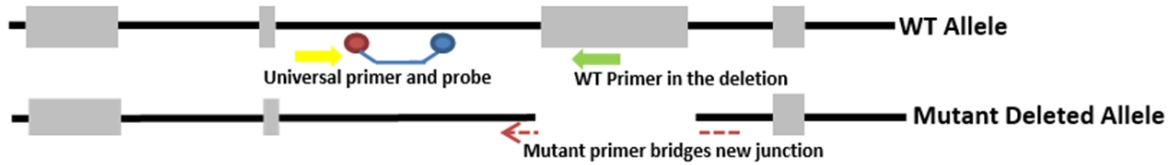


Figure 8.14. Schematics showing CRISPR/Cas9 technology removing an exon.

These mice were then genotyped using qPCR as described in section 8.7.1, specifically Figure 8.5 and Figure 8.6. The ear biopsies were genotyped with both WT and mutant assays, using the following FAM-labelled primers and probes (Figure 8.15), alongside a VIC-labelled internal control, *Dot1l* (Figure 8.6). A universal probe and universal primer were designed near the CRISPR deletion for both alleles. A WT primer was designed for the WT allele, and a mutant primer was designed that bridges the gap caused by the CRISPR deletion.



Kcnj6-DEL569 WT1 assay (FAM-labelled)

GACCAAAAGGAAAATCCAGAGGTACGTGAGGAAGGATGGGAAGTGCAACGTTACCACGGCAATGTGCGGGAGAC  
 GTACCGATACCTGACGGACATCTTACCACCCTGGTGGACCTGAAGTGGAGATTCAACCTGTTGATCTTTGTCAT  
 GGTCTACACAGTGACGTGGCTTTTCTTTGGGATGATCTGGTGGTGCAATGGCGTACATCCCGGAGATATGGACCA  
 CATAGAGGACCCCTCGTGGACTCCTTGTGTACCAACCTCAACGGGTTTGTCTCTGCTTTTTATTCTCCATAGA  
 GACAGAAACCACCATCGGTTATGGCTACCGGTTCATCAGGACAAGTGCCTGAGGGGATTATTCTCTCTTAAT  
 CCAGTCCGTGTTGGGTCCATGTCAACGCCTTCATGGTAGGATGTATGTTTGTGAAAATATCCCAACCAAGAA  
 GAGGGCAGAGACCCCTGGTCTTTTCCACCACGCGGTGATCTCCATGCGGGATGGGAAACTGTGCTTGATGTTCCG  
 GGTGGGGGACTTGAGGAATTCACATTGTGGAGGCATCCATCAGAGCCAAGTTGATCAAGTCCAACAGACTTC  
 AGAGGGGGAGTTTATCCCTCAACCAGACTGATATCAACGTGGGGTACTACACAGGGGACGACCGGCTCTTTCT  
 GGTGTCACCATTGATTATTAGCCATGAAATTAACCAACAGAGTCCC

Kcnj6-DEL569-Univ-Probe (5 nmol) TGCAACGTTACCACGGCAATG  
 Kcnj6-DEL569-WT-R (15 nmol) CCCC GGATGTACGCAATCAG  
 Kcnj6-DEL569-Univ-F (15 nmol) ACGTGAGGAAGGATGGGAAG

Kcnj6-DEL569 MUT1 assay (FAM-labelled)

GACCAAAAGGAAAATCCAGAGGTACGTGAGGAAGGATGGGAAGTGCAACGTTACCACGGCAATGTGCGGGAGAC  
 GTACCGATAC [569nt deletion]  
 AAGGGGACGACCGGCTCTTTCTGGTGTCAACATTGATTATTAGCCATGAAATTAACCAACAGAGTCCC

Kcnj6-DEL569-Univ-Probe (5 nmol) TGCAACGTTACCACGGCAATG  
 Kcnj6-DEL569-MUT-R (15 nmol) AGCCGGTCTCCCTGTA  
 Kcnj6-DEL569-Univ-F (15 nmol) ACGTGAGGAAGGATGGGAAG

**Figure 8.15. FAM-labelled primers and probes used in the genotyping of *Kcnj6*<sup>+/-</sup> mice.** These were run alongside a VIC-labelled internal control, *Dot1l*.

The primers and probes were added to the following master mix (Figure 8.16).

qPCR master mix	
ABI GTX Taqman master mix	5 µl
Primers Dot1L_2F (20 µM)	0.225 µl
Primers Dot1L_R (20 µM)	0.225 µl
Probe DotL_2M (5 µM)	0.2 µl
FAM Assay (probe 5 µM & primers 15 µM each)	0.3 µl
ddH2O	1.55 µl
DNA (1/10 dilution of ABI Sample-to-SNP prep)	2.5 µl

**Figure 8.16. Master mix used for *Kcnj6*<sup>+/-</sup> genotyping.**



### 8.7.2.3. Allelic discrimination assay

This method was performed for C3HeB/FeJ-Ets2<sup>m1Mhda/leg</sup> (*Ets2*<sup>+/-</sup>) mice, which have a point mutation. These mice were created with a missense mutation in exon 9 of *Ets2*, c.1076G-T, p.S359L. An allelic discrimination assay detects two possible variants of a Single Nucleotide Polymorphism (SNP). It is a multiplex assay, with two primer and probe pairs. The fluorescence emitted by each probe was used to determine the genotype.



Figure 8.18. Sequences of the primers and probes used for ETS2-B6JNM genotyping.

The qPCR used forward and reverse primers common to both WT and mutant alleles, a WT probe complementary to the WT base mutated in the mutant allele, and a mutant probe complementary to the SNP (*Figure 8.18*).

DNA was extracted from ear biopsies using a Taqman Sample-to-SNP kit (Applied Biosystems). The qPCR was run using a 1:10 dilution of the crude preparation. The instrument used was an Applied Biosystems 7500, and the master mix and protocol are as below (*Figure 8.19*).

<b>qPCR master mix (1X)</b>	
ABI GTX Taqman master mix	5 $\mu$ l
Assay (Probes 5 $\mu$ M each & Primers 15 $\mu$ M each)	2 $\mu$ l
ddH <sub>2</sub> O	0.5 $\mu$ l
DNA (1/10 dilution of ABI Sample-to-SNP prep)	2.5 $\mu$ l

<b>PCR protocol</b>
1. 95°C for 20 secs
2. 40 cycles of: 95°C for 3 secs, 60°C for 30 secs

*Figure 8.19. The master mix and PCR protocol for Ets2<sup>+/-</sup> genotyping.*

An example of the results from an allelic discrimination assay for *Ets2*<sup>+/-</sup> are shown below (Figure 8.20).

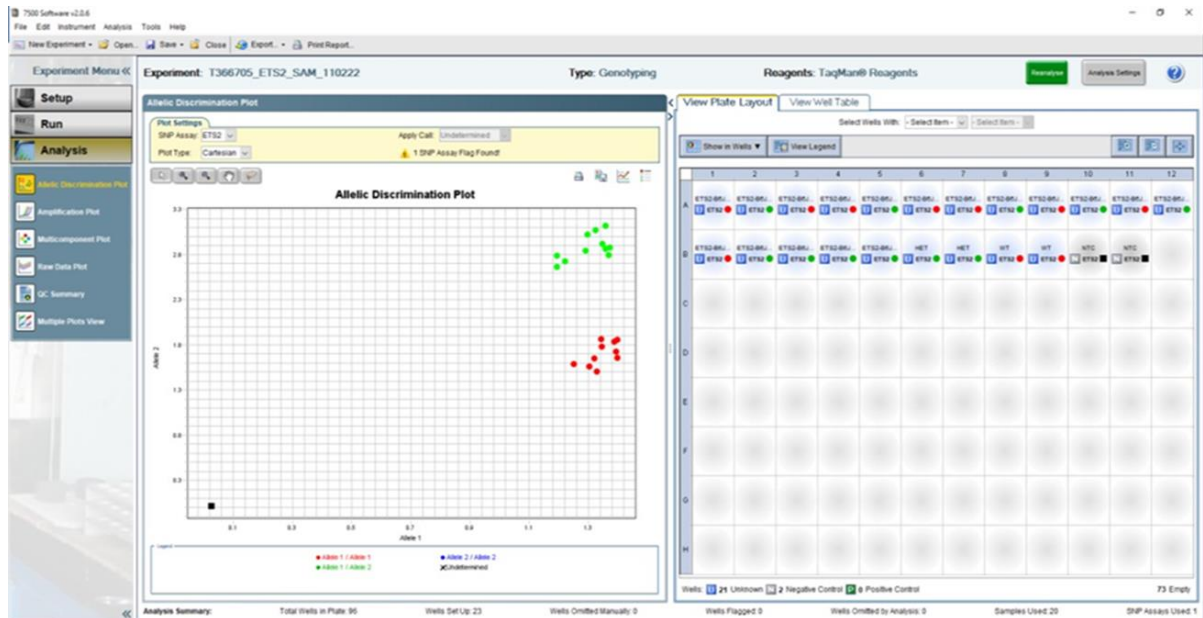


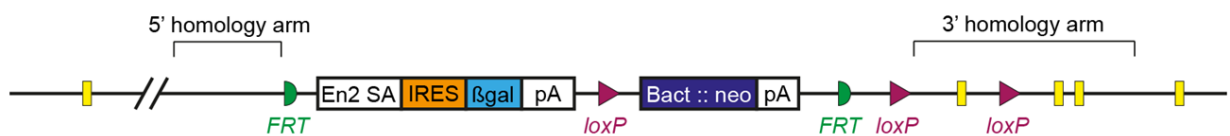
Figure 8.20. An example of *Ets2*<sup>+/-</sup> allelic discrimination assay results. The results were analysed using 7500 software v2.0.6 (Applied Biosystems).

### 8.7.2.4. Knockout first genotyping

This method was performed for C57BL/6N-*Psmg1*<sup>tm1a(KOMP)Wtsi</sup>/BayMmucd (*Psmg1*<sup>+/-</sup>) mice.

This line came from the EUCOMM/KOMP-CSD ES cell source and contained the Knockout-First-Reporter Tagged Insertion allele. The targeting cassette contained gene specific elements, as well as elements that are common to all mice given this allele (e.g. encoding beta-galactosidase (*lacZ* gene), neomycin resistance (*neo* gene), and *FRT* and *loxP* sites). The cassettes were either Promoter-driven or Promoterless (Figure 8.21).

#### Promoter driven line



#### Promoterless line



**Figure 8.21. Schematic of *Psmg1* genotyping technique.** Promoter driven describes a cassette where the *neo* gene contains its own promoter and is separated from the *lacZ* gene by a 3<sup>rd</sup> loxP site. Promoterless is where the *neo* and *lacZ* are adjacent and there are only two loxP sites.

Animals containing the full Knockout-First mutant allele (Tm1a) (Figure 8.22) were crossed to mice expressing Flp or Cre recombinase.

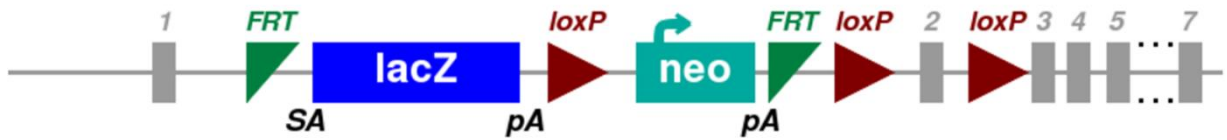


Figure 8.22. **Schematic of the full Knockout-First mutant allele (Tm1a).** Image from the IMPC website (<https://www.mousephenotype.org/data/genes/MGI:1860263>).

The progeny from this mating contained converted forms of the Tm1a allele known as Tm1b, Tm1c and Tm1d depending on the breeding strategy performed. The *Psmg1*<sup>+/-</sup> mice contained the Tm1b allele. A combination of mutant assays looking for sequences occurring in the targeting cassette and WT specific assays were performed in order to genotype them. Real time qPCR and copy counting of the various alleles were carried out by the Genotyping team.

### 8.7.3. Genotyping of double mutants

Double mutants were genotyped using the qPCR for the relevant DS line, plus the genotyping method used for the specific knockout/point mutation line. Dp5Tyb *Hmgn1*<sup>+/-</sup> and Dp3Tyb *Dyrk1a*<sup>+/-</sup> heads arrived from the Francis Crick Institute already genotyped.

## 8.8. Tateossian *et al.* 2022 – unpublished draft

### **DYRK1A kinase trisomy is the major cause of Otitis Media in Down Syndrome**

Hilda Tateossian<sup>1,\*,†</sup>, Amy Southern<sup>1,†</sup>, Pratik Vikhe<sup>1</sup>, Eva Lana-Elola<sup>2</sup>, Sheona Watson-Scales<sup>2</sup>, Dorota Gibbins<sup>2</sup>, Debbie Williams<sup>1</sup>, Thomas Purnell<sup>1</sup>, Philomena Mburu<sup>1</sup>, Andrew Parker<sup>1</sup>, Dominic P Norris<sup>1</sup>, Regie Lyn P Santos-Cortez<sup>3</sup>, Brian W Herrmann<sup>3,4</sup>, Sara Wells<sup>5</sup>, Heena V Lad<sup>1</sup>, Elizabeth MC Fisher<sup>6</sup>, Victor LJ Tybulewicz<sup>2,7</sup> and Steve DM Brown<sup>1,\*</sup>

1 Mammalian Genetics Unit, MRC Harwell Institute, Oxfordshire, UK.

2 The Francis Crick Institute, London, UK.

3 Department of Otolaryngology-Head and Neck Surgery, School of Medicine, University of Colorado Anschutz Medical Campus, Aurora, CO 80045, USA.

4 Department of Pediatric Otolaryngology, Children's Hospital Colorado, Aurora, CO, USA.

5 Mary Lyon Centre, MRC Harwell Institute, Oxfordshire, UK.

6 Department of Neuromuscular Diseases, UCL Queen Square Institute of Neurology, London, UK.

7 Department of Immunology and Inflammation, Imperial College, London, UK.

\* Corresponding authors: Hilda Tateossian, Steve DM Brown

**Email:** [h.tateossian@har.mrc.ac.uk](mailto:h.tateossian@har.mrc.ac.uk), [s.brown@har.mrc.ac.uk](mailto:s.brown@har.mrc.ac.uk)

[† Joint first authors](#)

### **Abstract**

Down syndrome (DS), which arises from trisomy of the whole or part of chromosome 21 (Hsa21), is one of the most common genetic abnormalities in humans. DS manifests as a broad spectrum of phenotypic features, including hearing loss due to otitis media with effusion (OME), affecting around 50% of children with DS. We employed a panel of mouse models of DS comprising a nested series of duplications covering the regions of the mouse genome syntenic to Hsa21 in order to define the loci involved with OME in DS. We identified a major locus on mouse chromosome 16, containing only 12 genes, which causes OME. Within this region we demonstrate that normalizing the gene dosage of *Dyrk1a* restored the wild-type phenotype. Investigation of downstream pathways of DYRK1A uncovered a number of pleiotropic mechanisms that are responsible for the OME. Thus, DYRK1A is a potential therapeutic target for OME in children with DS.

### **Introduction**

Down syndrome (DS) is a common genetic disorder caused by an extra copy of dosage-sensitive genes of human chromosome 21 (Hsa21), and a key challenge remains to determine which genes are causal for aspects of the DS phenotype – the syndrome manifests with a range of physical and intellectual disabilities. More than half of the children with DS have hearing problems as a result of the development of otitis media with effusion (OME) (Maris et al., 2014), and this may significantly impact skills such as the acquisition of language. OME is characterised by a middle ear inflammation accompanied by the presence of fluid in the middle ear cavity and thickened middle ear epithelium in the absence of an acute infection. Chronic OME (COME) may last for at least three months. In the general population COME is the most common reason for hearing loss in children and may lead to developmental delay in young children including speech and language impairment. A common treatment for COME is the placement of tympanostomy tubes by surgical procedure into the eardrum ostensibly to prevent the accumulation of fluid in the middle ear and to balance the pressure on each side of the membrane. However, the mechanisms by which tympanostomy tubes reduce inflammation and improve hearing are not clear (Vanneste and Page, 2019). For DS, the majority of patients with

## Appendix

COME require several rounds of tympanostomy tube placements each involving a surgical procedure with the added risk of complications (Paulson et al., 2014).

There is a significant genetic component to susceptibility to COME within the human population. Mouse models of COME have elucidated key genes and pathways that may be involved, as well as elaborating the molecular and pathological mechanisms (Cheeseman et al., 2011, Crompton et al., 2017, Hardisty-Hughes et al., 2006, Parkinson et al., 2006, Tateossian et al., 2009, Tateossian et al., 2013, Tateossian et al., 2015). In some cases these loci have been implicated in COME in the human population (Bhutta et al., 2017a). However, the genes on human chromosome 21 involved with susceptibility to OME are unknown. In order to identify and characterise the dosage-sensitive genetic loci involved in DS a number of mouse models of DS have been generated and analysed. The mouse orthologues to genes on Hsa21 are spread across three regions of the mouse genome on chromosomes 10 (Mmu10), 16 (Mmu16) and 17 (Mmu17).

An early model, Ts65Dn mice are trisomic for a part of Mmu16 (Davisson et al., 1990) and have been used to study different DS phenotypes, one of which is OME (Han et al., 2009). Auditory-evoked brainstem responses (ABR) were used to assess the hearing of the Ts65Dn mice, demonstrating that the mean ABR thresholds of Ts65Dn were significantly higher than those of the wild-type controls. In addition, histological examination of the ears of mutant mice, aged 3 to 4 months, revealed middle ear inflammation which correlated with the ABR threshold data (Han et al., 2009). However, Ts65Dn animals have a triplication of a large region of Mmu17 containing many genes that do not have synteny to Hsa21, potentially confounding these results (Duchon et al., 2011, Reinholdt et al., 2011). Tc1 mice are transchromosomic mice that carry an almost complete copy (75%) of human chromosome 21 (Gribble et al., 2013, O'Doherty et al., 2005). Auditory function of Tc1 mice was comparable to wild-type animals (Kuhn et al., 2012). In addition, sections of the middle ears of the mice showed no evidence of fluid in the cavities or thickened middle ear lining. One possible conclusion is that the genes which are trisomic in the Ts65Dn mice (i.e. from the Hsa21-orthologous region of Mmu16) but disomic in Tc1 mice may predispose Ts65Dn mice to OME (Kuhn et al., 2012). A more recent study (Bhutta et al., 2013) examined histological evidence of middle ear inflammation in eight mouse models of DS and found that only Dp(16)1Yey mice, which have full trisomy of the genes from Mmu16, develop significant chronic OME. Similar to the previous study, Tc1 mice

## Appendix

did not develop OME and interestingly the authors did not detect signs of middle ear inflammation in Ts65Dn mice. It was concluded that genes trisomic in the Dp(16)1Yey mouse but not in the Tc1 mouse predispose Dp(16)1Yey mice to OM (Bhutta et al., 2013).

Recently, a systematic effort has been underway to create a comprehensive set of genome duplications in the mouse covering those regions of the mouse genome syntenic to Hsa21 (Lana-Elola et al., 2016, Yu et al., 2010). A set of nested duplications is available that allows for the preliminary localisation of phenotypic effects followed by a more precise refinement of map position to small regions encompassing relatively few genes. This panel of DS mouse models includes Dp1Tyb, Dp(10)2Yey and Dp(17)3Yey encompassing all of the Hsa21-orthologous regions of Mmu16, Mmu10 and Mmu17 respectively. A whole series of smaller nested duplications provide finer resolution across the Dp1Tyb region (Lana-Elola et al., 2016). These panels of duplications have been employed already to identify regions and loci involved with the heart defects and locomotor dysfunction seen in DS (Lana-Elola et al., 2016, Watson-Scales et al., 2018, Toussaint et al., 2021).

We have employed these panels to undertake a deep genetic analysis of the loci involved with OME in DS. We localised one major locus on Mmu16 that causes the development of highly penetrant OME, and a minor locus, also on Mmu16, which results in low penetrant OME. From within the major locus we found that normalization of gene dosage of the *Dyrk1a* (Dual-specificity tyrosine phosphorylation regulated kinase 1a) gene restored the wild-type phenotype, demonstrating *Dyrk1a* as the causative gene for OME in Down syndrome.

### Results

#### **Dp1Tyb mice carrying a duplication of mouse chromosome 16 display OME**

We examined the presence of otitis media in a number of mouse lines carrying a nested series of genome duplications across chromosome segments syntenic to Hsa21. We first investigated mutants with duplication of the entire syntenic segments from Mmu10 (Dp(10)2Yey), Mmu17 (Dp(17)3Yey) and Mmu16 (Dp1Tyb) (Fig. 1a and Extended Data Fig. 1a). Histological analysis revealed no middle ear inflammation in Dp(10)2Yey or Dp(17)3Yey mice (Extended Data Fig. 1b, Extended Data Table 1). However, all Dp1Tyb mice had characteristic OME: fluid in the middle ear and thickened middle ear lining, from as early as 3 weeks (Fig. 1b). We extended the analysis to mice from different ages (3, 4, 8 and 16 weeks) and from both sexes. All 31 mice we examined had bilateral OME, significantly different from wild-type littermates which could occasionally develop unilateral OME ( $p < 0.00001$ ) (Extended Data Table 1). Further examination revealed that Dp1Tyb mice also developed a thickened middle ear mucosa. We measured the mucoperiosteal thickness of the middle ears of 3-, 4-, 8- and 16-week old Dp1Tyb and wild-type mice and found significant differences between the two genotypes at all four ages (3wk:  $p = 0.0010$ ; 4wk:  $p = 0.0026$ ; 8wk:  $p < 0.0001$ ; 16wk:  $p = 0.0006$ ) (Fig. 1c).

We further tested the Dp1Tyb mice for hearing loss by performing click-evoked auditory brainstem response (ABR). At two months of age, the Dp1Tyb carriers had elevated mean thresholds of 27.5 dB SPL compared to wild-type mice ( $p < 0.0001$ ) indicating conductive hearing loss (Fig. 1d). These findings agree with a recent comprehensive phenotyping assessment of Dp1Tyb mice, which also identified raised ABR thresholds<sup>24</sup>. We conclude that there is a locus or loci on mouse chromosome 16 which when duplicated leads to a chronic OME, which is in agreement with observations from previous partial trisomy models of mouse chromosome 16 (Han et al., 2009).

#### **Normal morphology of the cochlea and middle ear in Dp1Tyb mice**

The finding of moderately raised ABR thresholds in Dp1Tyb mice accompanied by OME suggests that hearing loss in these mice is caused by a conductive deafness and that sensorineural components in the inner ear are not involved. We sought to confirm this and undertook histological examination of sagittal sections from the cochlea of 4-week old mice, soon after the mice develop OME. Dp1Tyb mice showed no obvious abnormalities of the cochlea (Fig. 2a). In addition, scanning electron microscopy of the organ of Corti at the same

## Appendix

age showed normal hair cell and bundle morphology in both mutants and wild-type littermates (Fig. 2b). We conclude that the lack of abnormalities in the inner ear of Dp1Tyb indicates that there is no sensorineural element to the hearing loss in this line. We also assessed if there were abnormalities in the tympanic membrane and ossicles of the middle ear that might contribute to the conductive deafness in Dp1Tyb mice. Visual inspection of the tympanic membrane was used to examine if the membrane was intact. All 8-week old wild-type mice we used for this study (n = 8 mice, 16 ears) had no visible fluid behind the tympanic membrane, and the malleus (the largest of the three ossicles) was easily recognizable and the membrane was intact. All 8-week old Dp1Tyb mutants analysed (n = 5 mice, 10 ears) had cloudy ears as a result of the fluid behind the eardrum. The malleus of the mutants was obscured but the membrane was intact (Fig. 2c). MicroCT analysis of middle ear ossicles in 8-week old mice revealed no difference in the shape and the size of the bones between mutants (n = 4 mice, 8 ears) and wild-type mice (n = 4 mice, 8 ears) (Fig. 2d). In summary, we conclude that the hearing loss in Dp1Tyb mice is entirely due to OME within the middle ear.

### **Reduced body weight and craniofacial dysmorphology in Dp1Tyb mice**

We compared weights of Dp1Tyb mice to wild-type littermates at the age of 3, 4 and 8 weeks. There was a significant difference between male mutants and wild-type mice at the first two time points but not at 8 weeks (mean weight of males at: 3 weeks wild-type 10.34 g, mutants 5.13 g,  $p < 0.0001$ ; 4 weeks wild-type 17.22 g, mutants 12.65 g,  $p = 0.0376$ ; 8 weeks wild-type 26.46 g, mutants 23.33 g,  $p = 0.0901$ ) (Extended Data Fig. 2). By the age of 8 weeks the surviving Dp1Tyb male mice had an average weight not significantly different from wild-type mice. In addition, we also observed that Dp1Tyb mice have craniofacial defects. Recent reports of skeletal phenotyping in Dp1Tyb mice identified abnormally shaped skulls (Lana-Elola et al., 2021, Toussaint et al., 2021). As for other OM mouse models we also analysed the craniofacial defects of the Dp1Tyb mice. 8-week-old Dp1Tyb mice appeared to have an abnormally shaped head with short neck, low set ears and rounded pinna (Fig. 2e). To investigate the craniofacial phenotype further we compared measurements of the skulls of Dp1Tyb and wild-type littermates. We measured the length of the nasal and frontal bone, and the frontal bone width. We normalised the data to the full skull length and detected a significant difference only in the frontal bone width of Dp1Tyb mice compared to wild-type mice ( $p = 0.0016$ ) (Fig. 2f). We also investigated whether skull shape changes in Dp1Tyb mice affects Eustachian tube morphology.

## Appendix

However, measurements of the bony part of the tube did not detect any significant difference between the length or the width of the Eustachian tube (Fig. 2g).

### **Localisation of OME loci using the DpTyb mapping panel**

We next utilised the nested series of genomic duplications across the Dp1Tyb region of Mmu16 to localise the locus or loci involved with susceptibility to OME. For each line we performed histological analysis of the middle ears to assess the incidence of OME. Analysis of Dp2Tyb, Dp3Tyb and Dp9Tyb mice revealed OME in Dp3Tyb and Dp9Tyb mice (Extended Data Fig. 3a and b, Extended Data Table 1). However, no OM was observed in Dp2Tyb mice. Out of fourteen Dp3Tyb carriers one did not have OME (7%), six had unilateral (43%) and seven bilateral OME (50%). The number of Dp3Tyb mice with OME was significantly different from wild-type mice ( $p = 0.0002$ ) (Extended Data Fig. 3b, Extended Data Table 1). Out of twenty-six Dp9Tyb mice thirteen (50%) did not have middle ear inflammation, nine (34.6%) had unilateral and four (15.4%) bilateral OME (Extended Data Fig. 3b, Extended Data Table 1) significantly different from wild-type mice ( $p = 0.0339$ ). The ABR threshold of the Dp3Tyb mice compared to wild-type mice was significantly raised by 20 dB SPL ( $p = 0.0072$ ) when using the data from the mouse without OM in the calculation, or by 23.3 dB SPL ( $p = 0.0049$ ) when Dp3Tyb mice with normal middle ears are excluded (Extended Data Fig. 3c). There was no significant difference in the threshold for the Dp9Tyb mice (Extended Data Fig. 3c). Thus, the data demonstrates that there is a major locus with highly penetrant OME in the Dp3Tyb interval.

We then proceeded to further localise the major locus within the Dp3Tyb interval. Dp4Tyb, Dp5Tyb and Dp6Tyb mice have duplications of three shorter regions that together cover the entire region duplicated in Dp3Tyb mice (Fig. 3a). OME was not observed in Dp4Tyb and Dp6Tyb mice (Fig. 3b, Extended Data Table 1). However, all Dp5Tyb mice had OME, 33% of them unilateral and 67% bilateral OME (Fig. 3b, Extended Data Table 1), significantly different from wild-type mice ( $p < 0.0001$ ). In addition, we also investigated the OME phenotype of Ts1Rhr mice which have a duplication that is shorter than that in the Dp3Tyb mice by 8 genes, but encompasses all of the region duplicated in Dp5Tyb mice (Fig. 3a). All the Ts1Rhr mutants had OME, 33% of them unilateral and 67% bilateral OME (Fig. 3a and b, Extended Data Table 1), significantly different to wild-type mice ( $p = 0.0004$ ). We tested both Dp5Tyb and Ts1Rhr mice for hearing loss by performing click-evoked auditory ABR. At two months of age, the

## Appendix

Dp5Tyb carriers had elevated mean thresholds of 28.5 dB SPL ( $p = 0.0081$ ) and Ts1Rhr mice of 19 dB SPL ( $p = 0.0248$ ) compared to wild-type mice (Fig. 3c).

We carried out histological analysis on Dp7Tyb and Dp8Tyb mice that have duplications that between them cover the region duplicated in Dp2Tyb mice (Extended Data Fig. 4a) but neither, as expected, showed the presence of OME (Extended Data Fig. 4b, Extended Data Table 1). Finally, we assessed the middle ears of Dp12Tyb mice, which have a duplication of part of the region duplicated in Dp9Tyb mice, containing about half of the genes from the Dp9Tyb region (Extended Data Fig. 5a). None of the seven Dp12Tyb mice showed histological evidence of OME (Extended Data Fig. 5b, Extended Data Table 1). In conclusion, we have localised a major DS locus for OME within the Dp5Tyb region of Mmu16 (Fig. 4a and b). This region contains only 12 genes.

### **Normalisation of *Dyrk1a* dosage in Dp3Tyb mice leads to restoration of the wild-type phenotype**

The 12 genes in the Dp5Tyb region represent candidates for the major OME gene in DS. Given its pleiotropic role in a number of cellular pathways, some of which might impact on epithelial inflammatory processes, we investigated if *Dyrk1a* dosage plays a key role in the development of otitis media in Down syndrome mouse models. We crossed Dp1Tyb mice to *Dyrk1a* knockout mice establishing replicate matings in two of the facilities we used to breed mice for this study – Francis Crick Institute and MRC Harwell Institute. Out of sixteen double mutants (Dp1Tyb *Dyrk1a*<sup>+/-</sup>) produced in the Francis Crick Institute six (37%) did not have OM, eight (50%) had unilateral and two (13%) bilateral OM which was significantly different from Dp1Tyb littermates ( $p = 0.0021$ ). The wild-type phenotype was not completely restored as double mutants were significantly different from wild-type mice ( $p = 0.0022$ ). Out of eighteen double mutants (Dp1Tyb *Dyrk1a*<sup>+/-</sup>) produced in the Harwell Institute ten had no OM (55%), three unilateral (17%) and five bilateral OM (28%) significantly different from Dp1Tyb littermate mice ( $p = 0.0110$ ). Similar to the mice produced in the Francis Crick Institute there was a significant difference between the wild-type and double mutant mice ( $p = 0.0148$ ) (Fig. 4c). We also carried out middle ear histology on *Dyrk1a* heterozygote knockout mice used for this study (four from the Francis Crick Institute and four from the MRC Harwell Institute) and

## Appendix

found no evidence of OME. These findings suggest that *Dyrk1a* is one of the major genes contributing to the OM phenotype of the Dp1Tyb mice.

We next crossed *Dyrk1a* knockout mice to Dp3Tyb mice. Out of thirteen double mutants (Dp3Tyb *Dyrk1a*<sup>+/-</sup>) ten (77%) did not have OM, one (8%) had unilateral OM and two (15%) bilateral. Significantly fewer double mutant ears had OM compared to Dp3Tyb mice ( $p = 0.0001$ ) and furthermore there was no significant difference in the phenotype between double mutants and wild-type mice ( $p = 0.5743$ ) (Fig. 4c). Thus, normalising the gene dosage of *Dyrk1a* in Dp3Tyb mice showed a restoration of the wild-type phenotype demonstrating the role of *Dyrk1a* as a major gene causing the OM phenotype in Down syndrome.

In addition, we studied the candidature of the *Hmgn1* locus, which might also be expected to have pleiotropic roles impacting a number of organ systems. In this case we crossed Dp5Tyb mice to *Hmgn1* knockout mice and tested double mutants (Dp5Tyb *Hmgn1*<sup>+/-</sup>) carrying the duplication and heterozygous for the knockout allele. Out of twelve double mutants two (17%) did not have OM, seven (58%) had unilateral and three (25%) bilateral OM. We carried out histological analysis of the middle ears of the *Hmgn1* heterozygote knockout mice used for this study and found no OME. Despite a significant improvement in the frequency of OME between double mutants and Dp5Tyb mice ( $p = 0.0012$ ), there was still a highly significant difference between double mutants and wild-type littermates ( $p = 0.0005$ ) (Fig. 4c). Thus, the wild-type phenotype was not restored in the double mutants demonstrating that *Hmgn1*, unlike *Dyrk1a*, is not a major gene contributing to the OM phenotype of the Dp5Tyb mice.

### **Expression of DYRK1A and associated pathway members in middle ear epithelial cells, fluid and blood**

Following the identification of the *Dyrk1a* gene as a major locus involved in Down syndrome OME we proceeded to investigate by immunohistochemistry the expression of the protein and associated pathway members in the middle ear in order to better understand the pathological mechanisms at the middle ear epithelium. DYRK1A was localised in the middle ear epithelial cells in both wild-type and mutant tissues. We detected a one-third increase, as expected, of the number of cells positive for DYRK1A in Dp3Tyb mice (56.6%) compared to wild-type littermates (36.4%) and a similar increase in Dp5Tyb mice (47.2%) compared to 28.6% in wild-type littermates (Fig. 5a and b). Given the potential cross-talk of DYRK1A signalling to the

## Appendix

TGF $\beta$  pathway (Pelullo et al., 2019, Singh and Lauth, 2017) and the known involvement of TGF $\beta$  signalling in OME (Tateossian et al., 2009, Tateossian et al., 2013), we studied the expression of pSMAD2 and SMAD3, members of the TGF $\beta$  family, in middle ear epithelial cells. We detected a significant increase in the number of cells positive for pSMAD2 ( $p = 0.0001$ ,  $p = 0.0011$ ) and SMAD3 ( $p = 0.0007$ ,  $p = 0.0093$ ) in Dp3Tyb and Dp5Tyb mice compared to wild-type littermates. Importantly, the number of cells positive for pSMAD2 and SMAD3 was restored to wild-type levels in double mutants ( $p = 0.6171$ ,  $p = 0.8413$ ) (Fig. 5a and b). Regulatory T cells/T helper cells (Treg/Th17) imbalances are reported in OME patients and mouse models. TGF $\beta$  is required in combination with inflammatory cytokines, such as IL-6, for the initial differentiation of Th17 and Treg cells (Bettelli et al., 2006). DYRK1A is also known to regulate the differentiation of these cells (Khor et al., 2015). We therefore examined expression of IL-6 in middle ear epithelial cells and recorded a significant increase in the number of cells positive for IL-6 ( $p = 0.0013$ ,  $0.0041$ ), but not IL-10, in Dp3Tyb and Dp5Tyb mice compared to wild-type littermates ( $p = 0.4427$ ,  $p = 0.3687$ ). In addition, we found no significant difference between the number of cells positive for IL-6 in double mutants compared to wild-type mice ( $p = 0.2160$ ) (Fig 5a and b). Furthermore, we employed Meso Scale Discovery Immunoassays to analyse the levels of several of those cytokines in middle ear fluids and bloods. We detected significantly more IL-6 in ear fluid compared to both wild-type ( $p = 0.0019$ ) and mutant ( $p = 0.0042$ ) blood samples (Fig. 5d). Levels of IL-17 and IL-21 (products of Th17 cells) were higher in ear fluid compared to wild-type ( $p = 0.0043$ ,  $p = 0.0143$ ) and Dp5Tyb ( $p = 0.0120$ ,  $p = 0.0142$ ) blood. The levels of IL-10 (product of Treg cells) in ear fluid, on the other hand were not significantly different from both blood samples ( $p = 0.7497$ ,  $p = 0.1244$ ) (Fig. 5d) and this was confirmed by immunohistochemistry analysis.

We also studied the involvement of DYRK1A in the VEGF pathway as VEGF levels in the middle ear are raised in OME, contributing to vascular leak and effusion into the middle ear cavity (Cheeseman et al., 2011). There were notably more cells positive for VEGFA in the middle ear epithelial cells in Dp3Tyb and Dp5Tyb mice compared to wild-type littermates ( $p < 0.0001$ ,  $p < 0.0001$ ). Moreover, the expression of VEGF was restored to wild-type levels in double mutants ( $p = 0.9545$ ) (Fig 5a and b).

## Appendix

### **Upregulation of hypoxia and inflammatory genes in Dp1Tyb and Dp5Tyb mice**

The existence of hypoxia and elevated levels of *Hif1 $\alpha$*  and HIF responsive genes *Vegfa*, *Il-1 $\beta$*  and *Tnfa* in middle ear fluids have been previously reported for a number of mouse models of OM: *Jeff*, *Junbo* (Cheeseman et al., 2011), and *edison* mice (Crompton et al., 2017). We therefore studied expression levels of these genes in blood and ear fluid from Dp1Tyb and Dp5Tyb mice. We first examined expression by RT-qPCR in blood samples from wild-type (n = 25) and Dp1Tyb (n = 16) mice and ear fluid from Dp1Tyb mutants (n = 17). Relative to a baseline control of wild-type white blood cells, the inflammatory cells that accumulate within the middle ear fluid of Dp1Tyb mice showed elevated expression of *Hif1a* (30-fold; p <0.0001), *Vegfa* (260-fold; p <0.0001) and *Tnfa* (16-fold; p <0.0001) but not *Il-1 $\beta$*  (2-fold; p = 1) (Extended Fig. 6 and Extended Data Table 2). There was no significant difference in the expression levels between wild-type and mutant white blood cells (Extended Data Table 2). We then carried out similar analysis using wild-type (n = 13) and Dp5Tyb (n = 19) mice and ear fluid from Dp5Tyb mice (n = 9). We recorded very similar results with elevated expression of *Hif1a* (11-fold; p < 0.0001), *Vegfa* (251-fold; p <0.0001) and *Tnfa* (59-fold; p <0.0001) but not *Il-1 $\beta$*  (2-fold; p = 0.8830) in ear fluid compared to wild-type blood samples (Extended Fig. 6 and Extended Data Table 2). In addition, using Meso Scale Discovery Immunoassays we found significant increases in protein levels of VEGF-A (p = 0.0056, p = 0.0009) and IL-1 $\beta$  (p = 0.0001, p < 0.0001) in ear fluid from Dp5Tyb mice compared to wild-type and Dp5Tyb blood samples (Fig. 5c). The increased protein levels of VEGF-A are consistent with the results from immunohistochemistry described above.

### **Cilia distribution across the middle ear epithelium of Dp3Tyb and Dp5Tyb mice**

The middle ear epithelium arises during development from two distinct lineages (Thompson and Tucker, 2013). Dorsally in the middle ear cavity the epithelium is derived from neural crest, whereas ventrally and around the Eustachian tube the epithelium is endodermal in origin. The ventral epithelium develops cilia, which play a role in middle ear clearance, whereas in the dorsal region few cilia are present. DYRK1A has recently been implicated in ciliogenesis (Willsey et al., 2020), so we sought to uncover the effects of *Dyrk1a* triplication on ciliogenesis in the middle ear and the role that this pathway might play in OME. We used SEM to study cilia coverage in wild-type and Dp5Tyb mice in ventral and dorsal regions of the middle ear at 2 weeks of age, before OME develops, and also at 2 months. At 2 weeks, in Dp5Tyb mice, compared to wild-type, cilia development was normal with the expected distribution of cilia in

## Appendix

both ventral and dorsal regions (Fig. 6a). Similarly, in Dp3Tyb mice, cilia development was normal apart from one mouse which showed some evidence of cilia loss in the dorsal region (Extended Fig. 7a). In contrast, at 2 months of age in Dp5Tyb mice, in comparison with wild-type, we saw extensive cilia loss in the ventral region in one mouse, and extensive cilia loss in the dorsal region in 3 mice (Fig. 6b). A similar picture was found in Dp3Tyb mice at 2 months of age, where in the ventral region 2 mice showed extensive cilia loss, and in the dorsal region 4 mice had lost the uniform carpet of ciliated cells that characterizes the region of the middle ear (Extended Fig. 7b). The normal cilia development in both Dp5Tyb and Dp3Tyb mice at 2 weeks of age indicates that there is no direct effect of three copies of *Dyrk1a* (or any other gene in these regions) on cilia development. The extensive cilia loss observed in 2-month old Dp5Tyb and Dp3Tyb mice is thus likely secondary to the inflammatory OME that develops and is not a direct result of trisomic effects on cilia development. Nevertheless, the cilia loss that is observed may be a contributory factor to the development of OME in DS.

### **Expression of duplicated genes from the Dp5Tyb region in children with Down syndrome**

We studied the expression of the twelve genes from the Dp5Tyb region to test if their expression is increased in samples from children with DS compared to unaffected parents. qPCR results comparing saliva DNA from six paired Down syndrome children with OM and unaffected mothers revealed that out of the twelve genes tested the gene with the highest fold difference, 1.54, was *DYRK1A*. There was a significant difference in the expression of *DYRK1A* in saliva samples from children compared to their mothers ( $p = 0.004$ ) (Extended Data Table 3).

### Discussion

Otitis media with effusion is a very common middle ear disease in non-syndromic children (Vanneste and Page, 2019) but is even more common in children with Down syndrome (Maris et al., 2014). Whereas there has been significant progress using mouse models in identifying genes and genetic pathways involved in COME and that might contribute to susceptibility to the disease in the human population (Cheeseman et al., 2011, Crompton et al., 2017, Hardisty-Hughes et al., 2006, Parkinson et al., 2006, Tateossian et al., 2009, Tateossian et al., 2013), we remain ignorant of the underlying genetic loci that are involved with otitis media in DS. The localisation and identification of the genetic loci for COME in DS will enable us to develop a molecular understanding of the pathological mechanisms. Moreover, we can relate the loci involved in DS to genes and pathways identified from mouse models of COME and potential loci that are involved in susceptibility in the human population (Bhutta et al., 2017a). Collectively, insights will emerge from these studies that may lead to improved treatments of this serious and common condition.

To identify critical regions and genes that contribute to genetic susceptibility to COME in DS we used a panel of mouse lines with complete and partial duplications of the gene regions from the three mouse chromosomes that are orthologous to Hsa21. We tested each of the mouse lines for a middle ear OM phenotype and for hearing loss. We found that the Dp1Tyb line demonstrates a fully penetrant bilateral OME phenotype with a highly cellular exudate arising at weaning age. We did not observe COME in either the Dp2Yey or Dp3Yey lines demonstrating that Hsa21-orthologous genes on Mmu10 and Mmu17 are not involved. However, we employed the nested set of duplications covering Dp1Tyb to localise the COME genetic loci to the Hsa21-orthologous region of Mmu16. We identified a major highly penetrant locus predisposing to COME in Dp3Tyb, which was narrowed down by the examination of Dp4Tyb, Dp5Tyb and Dp6Tyb lines. Only Dp5Tyb mice showed COME, which is consistent with the observation of COME in the Ts1Rhr line which has a duplication of a region that encompasses and is slightly larger than that duplicated in Dp5Tyb mice. Analysis of Dp9Tyb mice suggests the presence of a minor locus on mouse chromosome 16. We suggest that the complete penetrance observed in the Dp1Tyb line may arise through additive effects of the major locus in the Dp5Tyb region and a minor locus within the Dp9Tyb region. Overall, we conclude that a major, highly penetrant locus conferring susceptibility to COME lies within the Dp5Tyb region. This small

## Appendix

region contains only 12 genes: *Dyrk1a*, *Kcnj6*, *Kcnj15*, *Erg*, *Ets2*, *Psmg1*, *Brwd1*, *Hmgn1*, *Wrb*, *Lca5l*, *Sh3bgr* and *B3galt5* (Lana-Elola et al., 2016).

Various trisomic mouse models of DS have been examined for evidence of COME (Bhutta et al., 2013, Han et al., 2009, Kuhn et al., 2012). Our finding of a major locus in the Dp1Tyb region, and localised to the Dp5Tyb region, is consistent with the COME observed in the Ts65Dn (Han et al., 2009) and Dp(16)1Yey mouse strains (Bhutta et al., 2013). Two studies have separately reported that they find no evidence of COME in Tc1 transchromosomic mice that carry an almost complete copy of human chromosome 21 (Bhutta et al., 2013, Kuhn et al., 2012). The human 21 Tc1 chromosome however, carries two deletions and it has been surmised that genes carried within these two regions may contribute to COME susceptibility. One of these regions contains five genes, *CXADR*, *BTG3*, *C21orf91*, *CHODL* and *TMPRSS15* and lies within the Dp9Tyb region. The other region is contained within Dp2Tyb and encompasses *MIS18A*, *MRAP*, *URB1*, *EVA1C*, *C21orf59*, *SYNJ1*, *PAXBPI*, *C21orf62*, *OLIG2*, *OLIG1*, *IFNGR2*, *AP00295.1*, *IL10RB*, *IFNARI*, *IFNGR2*, *TMEM50B*, *DNAJC28*, *GART*, *SON*, *DONSON*, *ATP5PO*, *CRYZL1*, *ITSN1*, *MRPS6*, *SLC5A3*, *KCNE2*, *SMIM11A*, *FAM243A*, *KCNE1*, *RCAN1*, *CLIC6* and *RUNX1*. Thus, these two deleted regions do not overlap with the Dp5Tyb region, suggesting that other factors are impacting on the development of COME in the Tc1 mouse. These factors could include genetic background and environmental effects, and a critical aspect of the current study is that all the DpTyb mouse lines are maintained on the same C57BL/6J genetic background. Moreover, our findings on the presence of COME in the different Dp lines are reproducible across two centres (Francis Crick Institute and Harwell Institute).

To identify the gene or genes within the Dp5Tyb region which are responsible for OME we crossed relevant Dp lines to gene knockouts in order to normalize gene copy number and to assess whether the wild-type phenotype was restored in progeny carrying two gene copies. Crosses of Dp1Tyb and Dp3Tyb to *Dyrk1a* knockouts demonstrated that restoring the normal copy number led to a significant reduction in OME. It is noteworthy that in the Dp3Tyb cross we saw a dramatic improvement in the middle ear phenotype such that the ‘two gene’ progeny were not significantly different from wild-type. It is possible that the improvement in Dp1Tyb double mutants was less dramatic given the continued triplication of the minor Dp9 locus in the disomic progeny from the Dp1Tyb cross. We also tested the *Hmgn1* locus and data from the

## Appendix

Dp5Tyb *Hmgn1* knockout cross suggested that although the double mutants produced from the cross have reduced incidence of OM, *Hmgn1* is not the main gene as the wild-type phenotype was not restored. Overall, the findings demonstrate that *Dyrk1a* is a major gene involved with the development of OME in DS.

In order to investigate the pathological mechanisms of *Dyrk1a* trisomy that lead to OME, we investigated the known pathways in which *Dyrk1a* is involved. This includes firstly its impact on Hedgehog (Hh) signalling (Singh and Lauth, 2017) and cross-talk with TGF $\beta$  signalling (Pelullo et al., 2019) which is already known to be involved with OME (Tateossian et al., 2009, Tateossian et al., 2013). We therefore assessed the levels of pSMAD2 and SMAD3 from the TGF $\beta$  pathway in middle ear epithelium and found that they were significantly raised in Dp3Tyb mice, but restored to normal wild-type levels in double mutants. TGF $\beta$  is a key contributing factor for the reciprocal differentiation of Th17 versus Treg cells and the fate of these cells depend on the presence of pro-inflammatory cytokines like IL-6. TGF $\beta$  in combination with IL-6, a pro-inflammatory cytokine, can induce Th17 differentiation from naïve CD4<sup>+</sup> T cells and inhibit the differentiation of Treg cells. In the absence of pro-inflammatory cytokines TGF $\beta$  induces the differentiation of Treg cells (Bettelli et al., 2006). More recently DYRK1A was also identified as part of a pathway that suppresses the development of Treg cells (Khor et al., 2015). In Dp5Tyb and Dp3Tyb mice, we recorded high levels of pSMAD2 and SMAD3 (which operate downstream of the TGF $\beta$  ligands) and high levels of IL-6 in the middle ear epithelial cells. This potential cross-talk of DYRK1A signalling and TGF $\beta$  pathway in the middle ear could result in differentiation of naïve CD4<sup>+</sup> T cells into Th17 cells. Cytokines expressed by Th17 cells are known to have a role in the pathogenesis of inflammatory disease (Singh et al., 2014). One of those cytokines is IL-17 which is reported to be overexpressed in inflamed lung endothelial cells (Park et al., 2005). For that reason, we assessed the levels of IL-17 and detected a significant increase of the protein in Dp5Tyb middle ear fluid compared to wild-type bloods.

Second, DYRK1A positively regulates VEGF-dependent NFAT transcription in endothelial cells and when silenced reduces intracellular Ca<sup>2+</sup> influx in response to VEGF along with a reduction in VEGFR2 receptors (Rozen et al., 2018). Thus, DYRK1A overexpression may enhance the VEGF response and exacerbate vascular leak from endothelial cells in the middle ear epithelium that arise from raised levels of VEGF (Cheeseman et al., 2011). Indeed, we

## Appendix

show, as for other mouse mutants with OME, that levels of VEGF in the middle ear epithelium are significantly raised in Dp3Tyb mice and levels are restored to wild-type in double mutants. Moreover, we found that the expression levels of *Hif1a* are raised in middle ear exudate in Dp1Tyb mice. These findings indicate that the middle ears of the Dp1Tyb mice are hypoxic. These results highlight similarities between the downstream molecular pathology identified in the Dp1Tyb line and previously characterised mouse mutants with OME (Cheeseman et al., 2011, Tateossian et al., 2013, Crompton et al., 2017). This hypoxic response has also been observed in human middle ear effusions by transcript analysis and the determination of VEGF protein titres that were found to be significantly raised (Bhutta et al., 2019). It has been surmised that the hypoxic response and upregulated VEGF signalling found in mouse models and humans underlie the vascular leak, angiogenesis and lymphangiogenesis that are hallmarks of OM and identifies VEGF and VEGF receptors as potential targets for the treatment of OME (Cheeseman et al., 2011).

Third, it has recently been reported that DYRK1A plays a role in ciliogenesis (Willsey et al., 2020). We therefore explored the histopathology of cilia in the middle ear, which may play a role in clearance of middle ear effusion and thus contribute to the onset and severity of OME. In Dy5Tyb and Dp3Tyb mice at 2 months of age, in both the dorsal and ventral regions of the middle ear we found in that there was significant loss of ciliated epithelium. However, this was not observed at 2 weeks of age, indicating that likely the observed cilia loss at 2 months of age is secondary to the development of OME and not a direct result of *Dyrk1a* trisomy. We had previously observed loss of ciliated epithelium in the middle ears of the *Jeff* mutant mouse, which carries a mutation in the *Fbxo11* gene and displays chronic otitis media (Hardisty et al., 2003). Other genes involved in cilia function and which are triplicated in DS have been studied for their role in DS phenotypes. Ts1Rhr mice were reported to have ventricular enlargement accompanied by ependymal cilia beating deficiency. The *Pcp4* gene (Purkinje cell protein 4) lies within the Ts1Rhr trisomic segment and regulates calmodulin and intracellular calcium concentration. Restoration of *Pcp4* to two copies rescued both phenotypes in Ts1Rhr mice (Raveau et al., 2017) suggesting a key role of *Pcp4* in cilia function. However, *Pcp4* is present in three copies in Dp6Tyb mice, which do not develop OM. Trisomy and increased levels of the Pericentrin gene (*PCNT*) have been associated with disruptions to centrosomal trafficking and cilia development (Galati et al., 2018). *Pcnt* is on Mmu10, in the Dp(10)2Yey segment and we found that Dp(10)2Yey mice do not develop middle ear inflammation ruling out the

## Appendix

involvement of Pericentrin in OME in DS. In summary, there are a variety of pathophysiological impacts of *Dyrk1a* in three copies and the evidence suggests that a number of pleiotropic phenomena are contributing to the development of OME in DS.

Three copies of *Dyrk1a* has been implicated for some of the phenotypes found in Down syndrome such as neurogenesis and brain development defects, neurodegeneration and congenital heart defects (Duchon and Herault, 2016, Ji et al., 2020). It has been reported that normalising the gene dosage of *Dyrk1a* in the Ts65Dn Down syndrome mice rescues some of the Alzheimer's disease phenotypes (Garcia-Cerro et al., 2017). Mice with *Dyrk1a* over expression were found to develop heart failure (Hille et al., 2016). We now show that *Dyrk1a* is involved in another major disease feature of DS, and it is intriguing to speculate that many phenotypes of DS emerge from a few critical genes on human chromosome 21, some of which have widespread pleiotropic impact on a number of organ systems.

A number of inhibitors of DYRK1A have been recently identified and used to study the molecular mechanisms of DYRK1A action. Harmine was used to identify DYRK1A as a regulator of Treg cell differentiation (Khor et al., 2015). The small-molecule Wnt pathway inhibitor lorecivivint (SM04690) was reported to modify the Wnt pathway through the inhibition of CLK2 and *DYRK1A* (Deshmukh et al., 2019). A recent study examining the therapeutic potential of another small-molecule Wnt pathway inhibitor, SM04755, for the treatment of tendinopathy identified DYRK1A as a target for the inhibitor (Deshmukh et al., 2021). Most recently a natural product from herbal plants, aristolactam BIII, was also identified as a novel DYRK1A inhibitor and proposed as a potential therapy for Down syndrome-related disorders (Choi et al., 2021). The middle ear is potentially directly accessible for topical treatment and the identification of *Dyrk1a* as a major gene contributing to OME in DS provides a novel route for the treatment of this condition. Suppressing the activity of DYRK1A by localized delivery of inhibitors to the middle ear cavity in Down syndrome patients should be explored as a potential strategy for future treatment of OME.

## Appendix

### Materials and Methods

#### Mice

Mice carrying the Dp(16Lipi-Zbtb21)1TybEmcf (Dp1Tyb), Dp(16Mis18a-Runx1)2TybEmcf (Dp2Tyb), Dp(16Mir802-Zbtb21)3TybEmcf (Dp3Tyb), Dp(16Mir802-Dscr3)4TybEmcf (Dp4Tyb), Dp(16Dyrk1a-B3galt5)5TybEmcf (Dp5Tyb), Dp(16Igsf5-Zbtb21)6TybEmcf (Dp6Tyb), Dp(16Lipi-Hunk)9TybEmcf (Dp9Tyb), Dp(10Prmt2-Pdxk)2Yey (Dp(10)2Yey), Dp(17Abcg1-Rrp1b)3Yey (Dp(17)3Yey), Dp(16Cbr1-Fam3b)1Rhr (Ts1Rhr) and *Dyrk1a*<sup>em1Mla</sup> (*Dyrk1a* KO) alleles have been described previously (Lana-Elola et al., 2016, Olson et al., 2004, Yu et al., 2010). The generation of mice carrying Dp(16Mis18a-Il10rb)7TybEmcf (Dp7Tyb), Dp(16Ifnar1-Runx1)8TybEmcf, Dp(16Krtap24-1-Hunk)12TybEmcf (Dp12Tyb) and *Hmgn1*<sup>em1Tyb</sup> alleles will be described elsewhere (Lana-Elola, Watson-Scales, Fisher and Tybulewicz manuscript in preparation). The *Hmgn1*<sup>em1Tyb</sup> allele has a 360 bp CRISPR/Cas9-generated deletion (16:96127399 - 16:96127758) which removes all of exon 1, intron 1 and part of exon 2. They were bred and maintained at the Mary Lyon Centre, MRC Harwell and at the Francis Crick Institute and were housed in specific-pathogen free conditions. All mouse strains were maintained on a C57BL/6JNimr background. Genotyping was carried out using custom probes (Transnetyx). The humane care and use of mice in this study was under the authority of the appropriate UK Home Office Project License.

#### Histology

Heads from 3-, 4-, 8- and 16-week old mice were collected and fixed in 10% buffered formaldehyde, decalcified and embedded in paraffin following routine procedures. 5 µm-thick sections were obtained and stained with haematoxylin and eosin for morphological observations.

#### Immunohistochemistry

Paraffin sections of mouse heads from 8- and 16-week-old mutant and wild-type mice were de-waxed and rehydrated following routine procedures. Endogenous peroxidase was blocked with 3% hydrogen peroxide and sections were incubated overnight with primary antibodies against: DYRK1A, 1:100 (ab65220, Abcam); phospho SMAD2 (Ser465/467), 1:100 (AB3849-I, Merck Millipore); SMAD3, 1:100 (06-920, Merck Millipore); VEGFA, 1:200 (AB1876-I, Merck Millipore); IL-6, 1:100 (ab6672, Abcam); and IL-10, 1:100 (ab217941, Abcam). The

## Appendix

Vectastain Elite ABC HRP kit (PK-6101, Vector Laboratories) kit was used according to the manufacturer's instructions for all of the antibodies. For development of the signal, the DAB+ chromogen system was used (K3468, DAKO). Counterstaining was carried out with haematoxylin.

### **Meso Scale Discovery Immunoassay**

A plate was designed to contain analytes of interest from the U-PLEX Biomarker Group 1 (ms) Assays (catalogue number K15069L-1). U-PLEX Mouse analytes: IL-1 $\beta$ , IL-6, IL-10, IL-17A, IL-21, TNF- $\alpha$ , and VEGF-A. The MSD plate was coated and loaded following the manufacturer's instructions. Blood samples from eleven female and one male 8-week-old Dp5Tyb mice and eight female and four male wild-type littermates were collected via retro-orbital bleed into brown z-gel tubes (no anti-coagulant). Serum was isolated by allowing the blood to clot at room temperature for 1 hour before centrifuging (16000 x g, 4°C, 5 min). The supernatant (serum) was loaded neat into the plate (25  $\mu$ l/well). To obtain middle ear fluids from eleven female and one male Dp5Tyb mice the tympanic membrane was removed with forceps. The fluid was collected from both ears of each mouse, added to 50  $\mu$ l ice cold PBS, vortexed for 30 seconds and centrifuged (500 x g, 4°C, 10 min) to pellet cells and debris. The supernatant was removed and added to the plate neat (25 $\mu$ l/well). The standard curve was created using 4-fold serial dilutions of the calibrators in Diluent 41, and diluent alone as the 8th standard.

### **Auditory brainstem response (ABR)**

8-week old mice, three from each genotype and gender, were anaesthetised and placed on a heated mat in a sound attenuating chamber. Acoustic stimuli were delivered to the right ear and ABR responses were collected, amplified and averaged using the BioSig software. Broadband click stimuli were presented at 90 dB SPL and gradually decreased in steps of 5 dB until a threshold was visually determined by the lack of replicable response peaks. The test was analysed, as previously described (Hardisty-Hughes et al., 2010).

### **Skull morphology**

Skulls from 8-week old mice were dissected, macerated in 1% potassium hydroxide and stained with alcian blue for cartilage and alizarin red for bone, following routine histological

## Appendix

procedures. The skulls were stored in glycerol until measurements were taken. ImageJ software was used to measure the skull length, nasal bone length, frontal bone length and skull width. Allometric comparisons were performed against skull length with at least three mice of each genotype and sex.

### **Scanning electron microscopy**

Inner ears, dissected from two female and one male 4-week-old Dp1Tyb mice and wild-type littermates, were fixed, washed and decalcified, as previously described (Mburu et al., 2010). The organ of Corti was exposed, the ears were dehydrated, critical-point dried, sputter coated with gold/platinum and then viewed on a JEOL 6010 LV scanning electron microscope.

Middle ears from: two female and one male 2-week-old Dp5Tyb mice and wild-type littermates, two female and one male 2-week-old Dp3Tyb mice and one female and two male wild-type littermates, three female and three male 2-month-old Dp5Tyb mice and two female and two male wild-type littermates, three female and three male 2-month-old Dp3Tyb mice and one female and two male wild-type littermates were prepared for imaging using the same methods as described for the cochleae, except no decalcification or fine dissection was required as the cilia are already exposed, and samples were additionally stained using osmium tetroxide. Images were taken at 2500x magnification.

### **Real-time quantitative PCR (RT-qPCR) analysis of blood and middle ear fluid**

Middle ear fluid and venous blood were collected from 8-week-old mice. For this study ear fluid from 10 female and 7 male mice; blood from 9 female and 7 male Dp1Tyb mice; blood from 13 female and 12 male wild-type mice was used. RNA from the blood samples was extracted using the Mouse RiboPure blood RNA isolation kit (1951, Ambion) and RNA from the ear fluid samples was extracted using RNeasy Plus micro kit (74034, Qiagen). For the Dp5Tyb mice, RNA was extracted from venous blood collected from nine female and ten male Dp5Tyb mice and eight female and five male wild type mice using the Maxwell RSC simplyRNA blood kit (AS1380), and from four female and five male Dp5Tyb ear fluids using the Maxwell RSC simplyRNA cells kit (AS1390). All mice were 8-weeks-old. After the RNA extraction cDNA was synthesised, RT-qPCR was performed and the data was analysed, as previously described (Crompton et al., 2017).

## Appendix

### **qPCR analysis of saliva samples**

Saliva samples were collected from six children with Down syndrome who underwent surgery for otitis media (4 male, 2 female; average age 5.7 years, range 0.5-14.8 years; 4 with COME, two with recurrent acute otitis media), and their unaffected mothers using Oragene saliva kits (DNA Genotek, Ottawa, Ontario, Canada). DNA samples were isolated from saliva according to the manufacturer's instructions. Primers were designed for the 12 genes within the mouse region of interest and control gene *ACTB* using the human reference sequence (hg19). Each of the 12 DNA samples were used for qPCR on a Bio-Rad machine (Hercules, CA, USA) in triplicate using the SYBR Green PCR Master Mix (Thermo Fisher Scientific). Fold change was determined based on  $\Delta$ CT values.

### **Data analysis**

We used the Chi-squared test to compare the difference between the observed and the expected number of the Dp1Tyb mice. Two-tailed t-test was used for comparing mean ABR thresholds, mucoperiosteal thickness, skull, and Eustachian tube measurements. We used two-tailed Fisher's exact test for comparing mutant and wild-type mice for prevalence of OME. A value of p less than 0.05 was considered significant. Tukey *post hoc* multiple comparisons analysis using ANOVA of the delta CT means against the genotype, gene expression probe and sample collection type were calculated to determine qPCR expression differences with a family-wise confidence level of 95%.

For MSD data pre-processing we replaced missing values with LOD / 2 for the specific assay (Lower LODs in pg/ml are IL-17A = 0.3, IL-21 = 6.5, IL-6 = 4.8, IL-10 = 3.8, IL-1B = 3.1, TNF-A = 1.3, VEGF-A = 0.77) and applied logarithmic (base 2) transformation. We regressed out plate effects (subtract plate means and add global mean) and calculated the mean of data for each sample (12 samples have four technical replicates averaged from across two plates, and 24 samples have two technical replicates averaged from a single plate).

For each pairwise comparison in a panel a two-sided Mann-Whitney-Wilcoxon (MWW) test was performed and raw p-values were denoted according to (\*\*\*\* < 0.0001, \*\*\* < 0.001, \*\* < 0.01, \* < 0.05). To control for multiple testing, we applied the Benjamin-Hochberg procedure to the complete set of 24 p-values arising from all the MWW tests across all assays and pairs of groups. Rejecting the null in all starred cases (\*, \*\*, \*\*\* and \*\*\*\*) controlled the FDR below 5%.

## Appendix

### **Acknowledgments**

The authors would like to thank the staff of the Mary Lyon Centre for animal husbandry, in particular Simona Oliveri, Elizabeth Joynson, Simon Gillard, Michelle Stewart and Heather Cater; Caroline Barker and Adele Austin for histology services; the genotyping core; Sara Johnson and Zsombor Szoke-Kovacs for the microCT scans; Lee Moir for the assistance using MSD plates and George Nicholson for the help with the statistical analysis of the data from the MSD plates. We also thank T Bootpetch for performing qPCR, and N Friedman, K Chan, M Scholes, S Haville and K Tholen for providing saliva DNA samples for study.

This work was supported by the Medical Research Council, UK (MC\_U142684175 to S.D.M.B.), Wellcome Trust (grant numbers 080174, 098327 and 098328, to E.M.C.F. and V.L.J.T.), National Institutes of Health – National Institute on Deafness and Communication Disorders (R01 DC015004 to R.L.P.S.C.) and the Ponzio Research Accelerator Award from the Center for Children’s Surgery, Children’s Hospital Colorado (to B.W.H.). V.L.J.T. was supported by the Francis Crick Institute which receives its core funding from Cancer Research UK (FC001194), the UK Medical Research Council (FC001194), and the Wellcome Trust (FC001194). This research was funded in whole, or in part, by the Wellcome Trust. For the purpose of Open Access, the authors have applied a CC-BY public copyright licence to any Author Accepted Manuscript version arising from this submission.

### **Author contributions**

H.T., S.D.M.B., A.S., E.L-E, V.L.J.T and E.M.C.F. conceived and designed the experiments and interpreted the results. E.L-E., S.W-S., B.W.H., R.S-C. and D. G. were involved in the provision of resources. H.T., A.S., P.V., D.W., T.P., P.M., and A.P. performed the experiments, A.S., P.V., H.V.L., R.S-C. and D.N. contributed to analysing the data, S.W. coordinated the management of the mouse colonies, H.T. and S.D.M.B. wrote the manuscript, A.S., E.L-E, V.L.J.T and E.M.C.F. were involved in correcting and editing of the manuscript.

## References

- ABDALA, C. & VISSER-DUMONT, L. 2001. Distortion Product Otoacoustic Emissions: A Tool for Hearing Assessment and Scientific Study. *Volta Rev*, 103, 281-302.
- ABDULLAH, S. N., ZAKARIA, M. N., SALIM, R., MD DAUD, M. K. & NIK OTHMAN, N. A. 2022. Comparing the diagnostic accuracy of audiometric Weber test and tuning fork Weber test in patients with conductive hearing loss. *Laryngoscope Investig Otolaryngol*, 7, 523-529.
- ABUHATZIRA, L., SHAMIR, A., SCHONES, D. E., SCHÄFFER, A. A. & BUSTIN, M. 2011. The chromatin-binding protein HMGN1 regulates the expression of methyl CpG-binding protein 2 (MECP2) and affects the behavior of mice. *J Biol Chem*, 286, 42051-42062.
- ALLEN, E. K., CHEN, W. M., WEEKS, D. E., CHEN, F., HOU, X., MATTOS, J. L., MYCHALECKYJ, J. C., SEGADÉ, F., CASSELBRANT, M. L., MANDEL, E. M., FERRELL, R. E., RICH, S. S., DALY, K. A. & SALE, M. M. 2013. A genome-wide association study of chronic otitis media with effusion and recurrent otitis media identifies a novel susceptibility locus on chromosome 2. *J Assoc Res Otolaryngol*, 14, 791-800.
- ALPAY, H. C., ETEM, E. O., KAYGUSUZ, I., YUCE, H., KARLIDAG, T., KELES, E., ORHAN, I. & YALCIN, S. 2010. Evaluation of the polymorphism in the Toll-like receptor 4 (TLR4) genes of tympanosclerosis patients. *Auris Nasus Larynx*, 37, 29-32.
- ANDERSEN, M. P., PARHAM, A. R., WALDREP, J. C., MCKENZIE, W. N. & DHAND, R. 2012. Alveolar fractal box dimension inversely correlates with mean linear intercept in mice with elastase-induced emphysema. *Int J Chron Obstruct Pulmon Dis*, 7, 235-43.
- ANGELO, L. S. & KURZROCK, R. 2007. Vascular endothelial growth factor and its relationship to inflammatory mediators. *Clin Cancer Res*, 13, 2825-30.
- ANNUNZIATO, F., COSMI, L., LIOTTA, F., MAGGI, E. & ROMAGNANI, S. 2012. Defining the human T helper 17 cell phenotype. *Trends Immunol*, 33, 505-12.
- ANTHWAL, N. & THOMPSON, H. 2016. The development of the mammalian outer and middle ear. *J Anat*, 228, 217-32.
- ANTONARAKIS, S. E. 2017. Down syndrome and the complexity of genome dosage imbalance. *Nature Reviews Genetics*, 18, 147-163.
- ANTONARAKIS, S. E., LYLE, R., DERMITZAKIS, E. T., REYMOND, A. & DEUTSCH, S. 2004. Chromosome 21 and down syndrome: from genomics to pathophysiology. *Nat Rev Genet*, 5, 725-38.
- ANTONARAKIS, S. E., SKOTKO, B. G., RAFII, M. S., STRYDOM, A., PAPE, S. E., BIANCHI, D. W., SHERMAN, S. L. & REEVES, R. H. 2020. Down syndrome. *Nat Rev Dis Primers*, 6, 9.
- ATAS-OZCAN, H., BRAULT, V., DUCHON, A. & HERAULT, Y. 2021. Dyrk1a from Gene Function in Development and Physiology to Dosage Correction across Life Span in Down Syndrome. *Genes (Basel)*, 12.
- BALKANY, T. J., DOWNS, M. P., JAFEK, B. W. & KRAJICEK, M. J. 1979. Hearing loss in Down's syndrome. A treatable handicap more common than generally recognized. *Clin Pediatr (Phila)*, 18, 116-8.

## Appendix

- BARR, E., DUNGWORTH, J., HUNTER, K., MCFARLANE, M. & KUBBA, H. 2011. The prevalence of ear, nose and throat disorders in preschool children with Down's syndrome in Glasgow. *Scott Med J*, 56, 98-103.
- BETTELLI, E., CARRIER, Y., GAO, W., KORN, T., STROM, T. B., OUKKA, M., WEINER, H. L. & KUCHROO, V. K. 2006. Reciprocal developmental pathways for the generation of pathogenic effector TH17 and regulatory T cells. *Nature*, 441, 235-8.
- BHUTTA, M. F. 2012. Mouse models of otitis media: strengths and limitations. *Otolaryngol Head Neck Surg*, 147, 611-4.
- BHUTTA, M. F., CHEESEMAN, M. T., HERAULT, Y., YU, Y. E. & BROWN, S. D. 2013. Surveying the Down syndrome mouse model resource identifies critical regions responsible for chronic otitis media. *Mamm Genome*, 24, 439-45.
- BHUTTA, M. F., LAMBIE, J., HOBSON, L., GOEL, A., HAFRÉN, L., EINARSDOTTIR, E., MATTILA, P. S., FARRALL, M., BROWN, S. & BURTON, M. J. 2017a. A mouse-to-man candidate gene study identifies association of chronic otitis media with the loci TGIF1 and FBXO11. *Sci Rep*, 7, 12496.
- BHUTTA, M. F., LAMBIE, J., HOBSON, L., WILLIAMS, D., TYRER, H. E., NICHOLSON, G., BROWN, S. D. M., BROWN, H., PICCINELLI, C., DEVAILLY, G., RAMSDEN, J. & CHEESEMAN, M. T. 2019. Transcript Analysis Reveals a Hypoxic Inflammatory Environment in Human Chronic Otitis Media With Effusion. *Front Genet*, 10, 1327.
- BHUTTA, M. F., THORNTON, R. B., KIRKHAM, L. S., KERSCHNER, J. E. & CHEESEMAN, M. T. 2017b. Understanding the aetiology and resolution of chronic otitis media from animal and human studies. *Dis Model Mech*, 10, 1289-1300.
- BLANC, F., AYACHE, D., CALMELS, M. N., DEGUINE, O., FRANCOIS, M., LÉBOULANGER, N., LESCANNE, E., MARIANOWSKI, R., NEVOUX, J., NICOLLAS, R., TRINGALI, S., TESSIER, N., FRANCO-VIDAL, V., BORDURE, P. & MONDAIN, M. 2018. Management of otitis media with effusion in children. Societe francaise d'ORL et de chirurgie cervico-faciale clinical practice guidelines. *Eur Ann Otorhinolaryngol Head Neck Dis*, 135, 269-273.
- BOSMAN, A., LETOURNEAU, A., SARTIANI, L., DEL LUNGO, M., RONZONI, F., KUZIAKIV, R., TOHONEN, V., ZUCHELLI, M., SANTONI, F., GUIPPONI, M., DUMEVSKA, B., HOVATTA, O., ANTONARAKIS, S. E. & JACONI, M. E. 2015. Perturbations of heart development and function in cardiomyocytes from human embryonic stem cells with trisomy 21. *Stem Cells*, 33, 1434-46.
- BOWL, M. R. & DAWSON, S. J. 2019. Age-Related Hearing Loss. *Cold Spring Harb Perspect Med*, 9.
- BROWN, S. D., HARDISTY-HUGHES, R. E. & MBURU, P. 2008. Quiet as a mouse: dissecting the molecular and genetic basis of hearing. *Nat Rev Genet*, 9, 277-90.
- BROWN, S. D. M. 2021. Advances in mouse genetics for the study of human disease. *Hum Mol Genet*, 30, R274-r284.
- BUSTAMANTE-MARIN, X. M. & OSTROWSKI, L. E. 2017. Cilia and Mucociliary Clearance. *Cold Spring Harb Perspect Biol*, 9.
- BUTTERFIELD, T. A., BEST, T. M. & MERRICK, M. A. 2006. The dual roles of neutrophils and macrophages in inflammation: a critical balance between tissue damage and repair. *J Athl Train*, 41, 457-65.

## Appendix

- CAMPBELL, H. & TOMKEIEFF, S. I. 1952. Calculation of the Internal Surface of a Lung. *Nature*, 170, 117-117.
- CARPINELLI, M. R., KRUSE, E. A., ARHATARI, B. D., DEBRINCAT, M. A., OGIER, J. M., BORIES, J. C., KILE, B. T. & BURT, R. A. 2015. Mice Haploinsufficient for *Ets1* and *Fli1* Display Middle Ear Abnormalities and Model Aspects of Jacobsen Syndrome. *Am J Pathol*, 185, 1867-76.
- CASSELBRANT, M. L., MANDEL, E. M., ROCKETTE, H. E., KURS-LASKY, M., FALL, P. A., BLUESTONE, C. D. & FERRELL, R. E. 2004. The genetic component of middle ear disease in the first 5 years of life. *Arch Otolaryngol Head Neck Surg*, 130, 273-8.
- CHEESEMAN, M. T., TYRER, H. E., WILLIAMS, D., HOUGH, T. A., PATHAK, P., ROMERO, M. R., HILTON, H., BALI, S., PARKER, A., VIZOR, L., PURNELL, T., VOWELL, K., WELLS, S., BHUTTA, M. F., POTTER, P. K. & BROWN, S. D. 2011. HIF-VEGF pathways are critical for chronic otitis media in Junbo and Jeff mouse mutants. *PLoS Genet*, 7, e1002336.
- CHEN, G. D., LI, L., MCCALL, A., DING, D., XING, Z., YU, Y. E. & SALVI, R. 2022. Hearing impairment in murine model of Down syndrome. *Front Genet*, 13, 936128.
- CHEN, J., ZHANG, X., LI, J., SONG, C., JIA, Y. & XIONG, W. 2016a. Identification of a Novel ENU-Induced Mutation in Mouse *Tbx1* Linked to Human DiGeorge Syndrome. *Neural Plast*, 2016, 5836143.
- CHEN, R., SCHWANDER, M., BARBE, M. F. & CHAN, M. M. 2016b. Ossicular Bone Damage and Hearing Loss in Rheumatoid Arthritis: A Correlated Functional and High Resolution Morphometric Study in Collagen-Induced Arthritic Mice. *PLoS One*, 11, e0164078.
- CHEN, Y., THAI, P., ZHAO, Y. H., HO, Y. S., DESOUZA, M. M. & WU, R. 2003. Stimulation of airway mucin gene expression by interleukin (IL)-17 through IL-6 paracrine/autocrine loop. *J Biol Chem*, 278, 17036-43.
- CHITTKA, L. & BROCKMANN, A. 2005. Perception space--the final frontier. *PLoS Biol*, 3, e137.
- CHOI, M., KIM, A. K., HAM, Y., LEE, J. Y., KIM, D., YANG, A., JO, M. J., YOON, E., HEO, J. N., HAN, S. B., KI, M. H., LEE, K. S. & CHO, S. 2021. Aristolactam BIII, a naturally derived DYRK1A inhibitor, rescues Down syndrome-related phenotypes. *Phytomedicine*, 92, 153695.
- COSMI, L., MAGGI, L., SANTARLASCI, V., LIOTTA, F. & ANNUNZIATO, F. 2014. T helper cells plasticity in inflammation. *Cytometry A*, 85, 36-42.
- COURCET, J.-B., FAIVRE, L., MALZAC, P., MASUREL-PAULET, A., LOPEZ, E., CALLIER, P., LAMBERT, L., LEMESLE, M., THEVENON, J., GIGOT, N., DUPLOMB, L., RAGON, C., MARLE, N., MOSCA-BOIDRON, A.-L., HUET, F., PHILIPPE, C., MONCLA, A. & THAUVIN-ROBINET, C. 2012. The DYRK1A gene is a cause of syndromic intellectual disability with severe microcephaly and epilepsy. *Journal of Medical Genetics*, 49, 731.
- CROMPTON, M., PURNELL, T., TYRER, H. E., PARKER, A., BALL, G., HARDISTY-HUGHES, R. E., GALE, R., WILLIAMS, D., DEAN, C. H., SIMON, M. M., MALLON, A. M., WELLS, S., BHUTTA, M. F., BURTON, M. J., TATEOSSIAN, H. & BROWN, S. D. M. 2017. A mutation in Nischarin causes otitis media via LIMK1 and NF-kappaB pathways. *PLoS Genet*, 13, e1006969.
- DANG, E. V., BARBI, J., YANG, H. Y., JINASENA, D., YU, H., ZHENG, Y., BORDMAN, Z., FU, J., KIM, Y., YEN, H. R., LUO, W., ZELLER, K., SHIMODA, L., TOPALIAN, S. L., SEMENZA, G. L., DANG, C. V., PARDOLL, D. M. &

## Appendix

- PAN, F. 2011. Control of T(H)17/T(reg) balance by hypoxia-inducible factor 1. *Cell*, 146, 772-84.
- DAUPHINOT, L., LYLE, R., RIVALS, I., DANG, M. T., MOLDRICH, R. X., GOLFIER, G., ETTWILLER, L., TOYAMA, K., ROSSIER, J., PERSONNAZ, L., ANTONARAKIS, S. E., EPSTEIN, C. J., SINET, P. M. & POTIER, M. C. 2005. The cerebellar transcriptome during postnatal development of the Ts1Cje mouse, a segmental trisomy model for Down syndrome. *Hum Mol Genet*, 14, 373-84.
- DAVISSON, M. T., SCHMIDT, C. & AKESON, E. C. 1990. Segmental trisomy of murine chromosome 16: a new model system for studying Down syndrome. *Prog Clin Biol Res*, 360, 263-80.
- DE SCHRIJVER, L., TOPSAKAL, V., WOJCIECHOWSKI, M., VAN DE HEYNING, P. & BOUDEWYNS, A. 2019. Prevalence and etiology of sensorineural hearing loss in children with down syndrome: A cross-sectional study. *Int J Pediatr Otorhinolaryngol*, 116, 168-172.
- DEL-POZO, J., MACINTYRE, N., AZAR, A., GLOVER, J., MILNE, E. & CHEESEMAN, M. 2019. Chronic otitis media is initiated by a bulla cavitation defect in the FBXO11 mouse model. *Dis Model Mech*, 12.
- DEMURO, S., DI MARTINO, R. M. C., ORTEGA, J. A. & CAVALLI, A. 2021. GSK-3 $\beta$ , FYN, and DYRK1A: Master Regulators in Neurodegenerative Pathways. *Int J Mol Sci*, 22.
- DESHMUKH, V., O'GREEN, A. L., BOSSARD, C., SEO, T., LAMANGAN, L., IBANEZ, M., GHAS, A., LAI, C., DO, L., CHO, S., CAHIWAT, J., CHIU, K., PEDRAZA, M., ANDERSON, S., HARRIS, R., DELLAMARY, L., KC, S., BARROGA, C., MELCHIOR, B., TAM, B., KENNEDY, S., TAMBIAH, J., HOOD, J. & YAZICI, Y. 2019. Modulation of the Wnt pathway through inhibition of CLK2 and DYRK1A by lorecivivint as a novel, potentially disease-modifying approach for knee osteoarthritis treatment. *Osteoarthritis Cartilage*, 27, 1347-1360.
- DESHMUKH, V., SEO, T., O'GREEN, A. L., IBANEZ, M., HOFILENA, B., KC, S., STEWART, J., DELLAMARY, L., CHIU, K., GHAS, A., BARROGA, C., KENNEDY, S., TAMBIAH, J., HOOD, J. & YAZICI, Y. 2021. SM04755, a small-molecule inhibitor of the Wnt pathway, as a potential topical treatment for tendinopathy. *J Orthop Res*, 39, 2048-2061.
- DESHPANDE, A., BORLEPAWAR, A., ROSSKOPF, A., FRANK, D., FREY, N. & RANGREZ, A. Y. 2021. SH3-Binding Glutamic Acid Rich-Deficiency Augments Apoptosis in Neonatal Rat Cardiomyocytes. *Int J Mol Sci*, 22.
- DOWJAT, W. K., ADAYEV, T., KUCHNA, I., NOWICKI, K., PALMINIELLO, S., HWANG, Y. W. & WEGIEL, J. 2007. Trisomy-driven overexpression of DYRK1A kinase in the brain of subjects with Down syndrome. *Neurosci Lett*, 413, 77-81.
- DUCHON, A. & HERAULT, Y. 2016. DYRK1A, a Dosage-Sensitive Gene Involved in Neurodevelopmental Disorders, Is a Target for Drug Development in Down Syndrome. *Front Behav Neurosci*, 10, 104.
- DUCHON, A., RAVEAU, M., CHEVALIER, C., NALESSO, V., SHARP, A. J. & HERAULT, Y. 2011. Identification of the translocation breakpoints in the Ts65Dn and Ts1Cje mouse lines: relevance for modeling Down syndrome. *Mamm Genome*, 22, 674-84.
- DUNLEVY, L., BENNETT, M., SLENDER, A., LANA-ELOLA, E., TYBULEWICZ, V. L., FISHER, E. M. & MOHUN, T. 2010. Down's syndrome-like cardiac

## Appendix

- developmental defects in embryos of the transchromosomal Tc1 mouse. *Cardiovasc Res*, 88, 287-95.
- DUTTA, A., VENKATAGANESH, H. & LOVE, P. E. 2021. New Insights into Epigenetic Regulation of T Cell Differentiation. *Cells*, 10, 3459.
- EINARSDOTTIR, E., HAFREN, L., LEINONEN, E., BHUTTA, M. F., KENTALA, E., KERE, J. & MATTILA, P. S. 2016. Genome-wide association analysis reveals variants on chromosome 19 that contribute to childhood risk of chronic otitis media with effusion. *Sci Rep*, 6, 33240.
- EMONTS, M., VEENHOVEN, R. H., WIERTSEMA, S. P., HOUWING-DUISTERMAAT, J. J., WALRAVEN, V., DE GROOT, R., HERMANS, P. W. & SANDERS, E. A. 2007. Genetic polymorphisms in immunoresponse genes TNFA, IL6, IL10, and TLR4 are associated with recurrent acute otitis media. *Pediatrics*, 120, 814-23.
- FAUSCH, C. & ROOSLI, C. 2015. The incudomalleolar articulation in Down syndrome (trisomy 21): a temporal bone study. *Otol Neurotol*, 36, 348-53.
- FORTNUM, H., LEIGHTON, P., SMITH, M. D., BROWN, L., JONES, M., BENTON, C., MARDER, E., MARSHALL, A. & SUTTON, K. 2014. Assessment of the feasibility and clinical value of further research to evaluate the management options for children with Down syndrome and otitis media with effusion: a feasibility study. *Health Technol Assess*, 18, 1-147, v-vi.
- FUCHS, J. C., LINDEN, J. F., BALDINI, A. & TUCKER, A. S. 2015. A defect in early myogenesis causes Otitis media in two mouse models of 22q11.2 Deletion Syndrome. *Hum Mol Genet*, 24, 1869-82.
- FUCHS, J. C. & TUCKER, A. S. 2015. Chapter Nine - Development and Integration of the Ear. In: CHAI, Y. (ed.) *Current Topics in Developmental Biology*. Academic Press.
- GALANTE, M., JANI, H., VANES, L., DANIEL, H., FISHER, E. M., TYBULEWICZ, V. L., BLISS, T. V. & MORICE, E. 2009. Impairments in motor coordination without major changes in cerebellar plasticity in the Tc1 mouse model of Down syndrome. *Hum Mol Genet*, 18, 1449-63.
- GALATI, D. F., SULLIVAN, K. D., PHAM, A. T., ESPINOSA, J. M. & PEARSON, C. G. 2018. Trisomy 21 Represses Cilia Formation and Function. *Dev Cell*, 46, 641-650 e6.
- GANUSOV, V. V. & DE BOER, R. J. 2007. Do most lymphocytes in humans really reside in the gut? *Trends in Immunology*, 28, 514-518.
- GARBIERI, T. F., BROZOSKI, D. T., DIONÍSIO, T. J., SANTOS, C. F. & NEVES, L. T. 2017. Human DNA extraction from whole saliva that was fresh or stored for 3, 6 or 12 months using five different protocols. *J Appl Oral Sci*, 25, 147-158.
- GARCÍA-CERRO, S., MARTÍNEZ, P., VIDAL, V., CORRALES, A., FLÓREZ, J., VIDAL, R., RUEDA, N., ARBONÉS, M. L. & MARTÍNEZ-CUÉ, C. 2014. Overexpression of Dyrk1A is implicated in several cognitive, electrophysiological and neuromorphological alterations found in a mouse model of Down syndrome. *PLoS One*, 9, e106572.
- GARCIA-CERRO, S., RUEDA, N., VIDAL, V., LANTIGUA, S. & MARTINEZ-CUE, C. 2017. Normalizing the gene dosage of Dyrk1A in a mouse model of Down syndrome rescues several Alzheimer's disease phenotypes. *Neurobiol Dis*, 106, 76-88.
- GESSNER, B. D., GILLINGHAM, M. B., WOOD, T. & KOELLER, D. M. 2013. Association of a genetic variant of carnitine palmitoyltransferase 1A with infections in Alaska Native children. *J Pediatr*, 163, 1716-21.

## Appendix

- GHADERSOHI, S., BHUSHAN, B. & BILLINGS, K. R. 2018. Challenges and outcomes of cholesteatoma management in children with Down syndrome. *Int J Pediatr Otorhinolaryngol*, 106, 80-84.
- GRIBBLE, S. M., WISEMAN, F. K., CLAYTON, S., PRIGMORE, E., LANGLEY, E., YANG, F., MAGUIRE, S., FU, B., RAJAN, D., SHEPPARD, O., SCOTT, C., HAUSER, H., STEPHENS, P. J., STEBBINGS, L. A., NG, B. L., FITZGERALD, T., QUAIL, M. A., BANERJEE, R., ROTHKAMM, K., TYBULEWICZ, V. L., FISHER, E. M. & CARTER, N. P. 2013. Massively parallel sequencing reveals the complex structure of an irradiated human chromosome on a mouse background in the Tc1 model of Down syndrome. *PLoS One*, 8, e60482.
- GUTIERREZ-HERVAS, A., GOMEZ-MARTINEZ, S., IZQUIERDO-GOMEZ, R., VEIGA, O. L., PEREZ-BEY, A., CASTRO-PINERO, J. & MARCOS, A. 2020. Inflammation and fatness in adolescents with and without Down syndrome: UP & DOWN study. *J Intellect Disabil Res*, 64, 170-179.
- HAFRÉN, L., EINARSDOTTIR, E., KENTALA, E., HAMMARÉN-MALMI, S., BHUTTA, M. F., MACARTHUR, C. J., WILMOT, B., CASSELBRANT, M., CONLEY, Y. P., WEEKS, D. E., MANDEL, E. M., VAARALA, O., KALLIO, A., MELIN, M., NIEMINEN, J. K., LEINONEN, E., KERE, J. & MATTILA, P. S. 2015. Predisposition to Childhood Otitis Media and Genetic Polymorphisms within the Toll-Like Receptor 4 (TLR4) Locus. *PLoS One*, 10, e0132551.
- HAN, F., YU, H., ZHANG, J., TIAN, C., SCHMIDT, C., NAVA, C., DAVISSON, M. T. & ZHENG, Q. Y. 2009. Otitis media in a mouse model for Down syndrome. *Int J Exp Pathol*, 90, 480-8.
- HARASHIMA, C., JACOBOWITZ, D. M., WITTA, J., BORKE, R. C., BEST, T. K., SIAREY, R. J. & GALDZICKI, Z. 2006. Abnormal expression of the G-protein-activated inwardly rectifying potassium channel 2 (GIRK2) in hippocampus, frontal cortex, and substantia nigra of Ts65Dn mouse: a model of Down syndrome. *J Comp Neurol*, 494, 815-33.
- HARDISTY-HUGHES, R. E., PARKER, A. & BROWN, S. D. 2010. A hearing and vestibular phenotyping pipeline to identify mouse mutants with hearing impairment. *Nat Protoc*, 5, 177-90.
- HARDISTY-HUGHES, R. E., TATEOSSIAN, H., MORSE, S. A., ROMERO, M. R., MIDDLETON, A., TYMOWSKA-LALANNE, Z., HUNTER, A. J., CHEESEMAN, M. & BROWN, S. D. 2006. A mutation in the F-box gene, Fbxo11, causes otitis media in the Jeff mouse. *Hum Mol Genet*, 15, 3273-9.
- HARDISTY, R. E., ERVEN, A., LOGAN, K., MORSE, S., GUIONAUD, S., SANCHO-OLIVER, S., HUNTER, A. J., BROWN, S. D. & STEEL, K. P. 2003. The deaf mouse mutant Jeff (Jf) is a single gene model of otitis media. *J Assoc Res Otolaryngol*, 4, 130-8.
- HILDEBRANDT, C., FULTON, A. & RODAN, L. H. 2021. Homozygous deletion of 21q22.2 in a patient with hypotonia, developmental delay, cortical visual impairment, and retinopathy. *Am J Med Genet A*, 185, 555-560.
- HILLE, S., DIERCK, F., KUHL, C., SOSNA, J., ADAM-KLAGES, S., ADAM, D., LULLMANN-RAUCH, R., FREY, N. & KUHN, C. 2016. Dyrk1a regulates the cardiomyocyte cell cycle via D-cyclin-dependent Rb/E2f-signalling. *Cardiovasc Res*, 110, 381-94.
- HIRSCH, S. D., ELLING, C. L., BOOTPETCH, T. C., SCHOLE, M. A., HAFRÉN, L., STREUBEL, S. O., PINE, H. S., WINE, T. M., SZEREMETA, W., PRAGER, J. D., EINARSDOTTIR, E., YOUSAF, A., BASCHAL, E. E., REHMAN, S.,

## Appendix

- BAMSHAD, M. J., NICKERSON, D. A., RIAZUDDIN, S., LEAL, S. M., AHMED, Z. M., YOON, P. J., KERE, J., CHAN, K. H., MATTILA, P. S., FRIEDMAN, N. R., CHONMAITREE, T., FRANK, D. N., RYAN, A. F. & SANTOS-CORTEZ, R. L. P. 2021. The role of CDHR3 in susceptibility to otitis media. *J Mol Med (Berl)*, 99, 1571-1583.
- HUANG, H., RAMBALDI, I., DANIELS, E. & FEATHERSTONE, M. 2003. Expression of the Wdr9 gene and protein products during mouse development. *Dev Dyn*, 227, 608-14.
- HUANG, Q., ZHANG, Z., ZHENG, Y., ZHENG, Q., CHEN, S., XU, Y., OU, Y. & QIU, Z. 2012. Hypoxia-inducible factor and vascular endothelial growth factor pathway for the study of hypoxia in a new model of otitis media with effusion. *Audiol Neurootol*, 17, 349-56.
- HUSSEMAN, J., PALACIOS, S. D., RIVKIN, A. Z., OEHL, H. & RYAN, A. F. 2012. The role of vascular endothelial growth factors and fibroblast growth factors in angiogenesis during otitis media. *Audiol Neurootol*, 17, 148-54.
- ISHIHARA, K., SHIMIZU, R., TAKATA, K., KAWASHITA, E., AMANO, K., SHIMOHATA, A., LOW, D., NABE, T., SAGO, H., ALEXANDER, W. S., GINHOUX, F., YAMAKAWA, K. & AKIBA, S. 2020. Perturbation of the immune cells and prenatal neurogenesis by the triplication of the Erg gene in mouse models of Down syndrome. *Brain Pathol*, 30, 75-91.
- JACKSON, S. J., ANDREWS, N., BALL, D., BELLANTUONO, I., GRAY, J., HACHOUMI, L., HOLMES, A., LATCHAM, J., PETRIE, A., POTTER, P., RICE, A., RITCHIE, A., STEWART, M., STREPKA, C., YEOMAN, M. & CHAPMAN, K. 2017. Does age matter? The impact of rodent age on study outcomes. *Lab Anim*, 51, 160-169.
- JENG, J. Y., CARLTON, A. J., JOHNSON, S. L., BROWN, S. D. M., HOLLEY, M. C., BOWL, M. R. & MARCOTTI, W. 2021. Biophysical and morphological changes in inner hair cells and their efferent innervation in the ageing mouse cochlea. *J Physiol*, 599, 269-287.
- JEON, S. H., CHAE, B. C., KIM, H. A., SEO, G. Y., SEO, D. W., CHUN, G. T., KIM, N. S., YIE, S. W., BYEON, W. H., EOM, S. H., HA, K. S., KIM, Y. M. & KIM, P. H. 2007. Mechanisms underlying TGF-beta1-induced expression of VEGF and Flk-1 in mouse macrophages and their implications for angiogenesis. *J Leukoc Biol*, 81, 557-66.
- JI, W., FERDMAN, D., COPEL, J., SCHEINOST, D., SHABANOVA, V., BRUECKNER, M., KHOKHA, M. K. & MENT, L. R. 2020. De novo damaging variants associated with congenital heart diseases contribute to the connectome. *Sci Rep*, 10, 7046.
- JIANG, L., KERCHBERGER, V. E., SHAFFER, C., DICKSON, A. L., ORMSETH, M. J., DANIEL, L. L., LEON, B. G. C., COX, N. J., CHUNG, C. P., WEI, W. Q., STEIN, C. M. & FENG, Q. 2022. Genome-wide association analyses of common infections in a large practice-based biobank. *BMC Genomics*, 23, 672.
- JOSHI, K., SHEN, L., CAO, F., DONG, S., JIA, Z., CORTEZ, M. A. & SNEAD, O. C. 2018. Kcnj6(GIRK2) trisomy is not sufficient for conferring the susceptibility to infantile spasms seen in the Ts65Dn mouse model of down syndrome. *Epilepsy Research*, 145, 82-88.
- JOSHI, K., SHEN, L., MICHAELI, A., SALTER, M., THIBAUT-MESSIER, G., HASHMI, S., EUBANKS, J. H., CORTEZ, M. A. & SNEAD, O. C. 2016.

## Appendix

- Infantile spasms in down syndrome: Rescue by knockdown of the GIRK2 channel. *Ann Neurol*, 80, 511-21.
- JUHN, S. K., JUNG, M.-K., HOFFMAN, M. D., DREW, B. R., PRECIADO, D. A., SAUSEN, N. J., JUNG, T. T. K., KIM, B. H., PARK, S.-Y., LIN, J., ONDREY, F. G., MAINS, D. R. & HUANG, T. 2008. The role of inflammatory mediators in the pathogenesis of otitis media and sequelae. *Clinical and experimental otorhinolaryngology*, 1, 117-138.
- JUNG, H. H., KIM, M. W., LEE, J. H., KIM, Y. T., KIM, N. H., CHANG, B. A., CHOI, J. O. & LIM, H. H. 1999. Expression of vascular endothelial growth factor in otitis media. *Acta Otolaryngol*, 119, 801-8.
- KAZUKI, Y., GAO, F. J., LI, Y., MOYER, A. J., DEVENNEY, B., HIRAMATSU, K., MIYAGAWA-TOMITA, S., ABE, S., KAZUKI, K., KAJITANI, N., UNO, N., TAKEHARA, S., TAKIGUCHI, M., YAMAKAWA, M., HASEGAWA, A., SHIMIZU, R., MATSUKURA, S., NODA, N., Ogonuki, N., INOUE, K., MATOBA, S., OGURA, A., FLOREA, L. D., SAVONENKO, A., XIAO, M., WU, D., BATISTA, D. A., YANG, J., QIU, Z., SINGH, N., RICHTSMEIER, J. T., TAKEUCHI, T., OSHIMURA, M. & REEVES, R. H. 2020. A non-mosaic transchromosomal mouse model of down syndrome carrying the long arm of human chromosome 21. *Elife*, 9.
- KERSCHNER, J. E., LI, J., TSUSHIYA, K. & KHAMPANG, P. 2010. Mucin gene expression and mouse middle ear epithelium. *Int J Pediatr Otorhinolaryngol*, 74, 864-8.
- KHOR, B., GAGNON, J. D., GOEL, G., ROCHE, M. I., CONWAY, K. L., TRAN, K., ALDRICH, L. N., SUNDBERG, T. B., PATERSON, A. M., MORDECAI, S., DOMBKOWSKI, D., SCHIRMER, M., TAN, P. H., BHAN, A. K., ROYCHOUDHURI, R., RESTIFO, N. P., O'SHEA, J. J., MEDOFF, B. D., SHAMJI, A. F., SCHREIBER, S. L., SHARPE, A. H., SHAW, S. Y. & XAVIER, R. J. 2015. The kinase DYRK1A reciprocally regulates the differentiation of Th17 and regulatory T cells. *Elife*, 4.
- KIM, S., KO, E., CHOI, H. G., KIM, D., LUCHI, M., KHOR, B. & KIM, S. 2023. FRTX-02, a selective and potent inhibitor of DYRK1A, modulates inflammatory pathways in mouse models of psoriasis and atopic dermatitis. *J Transl Autoimmun*, 6, 100185.
- KIM, T. H., CHAE, S. W., KIM, H. J. & JUNG, H. H. 2005. Effect of recombinant vascular endothelial growth factor on experimental otitis media with effusion. *Acta Otolaryngol*, 125, 256-9.
- KLESCHEVNIKOV, A. M., YU, J., KIM, J., LYSENKO, L. V., ZENG, Z., YU, Y. E. & MOBLEY, W. C. 2017. Evidence that increased *Kcnj6* gene dose is necessary for deficits in behavior and dentate gyrus synaptic plasticity in the Ts65Dn mouse model of Down syndrome. *Neurobiol Dis*, 103, 1-10.
- KNUDSEN, L., WEIBEL, E. R., GUNDERSEN, H. J., WEINSTEIN, F. V. & OCHS, M. 2010. Assessment of air space size characteristics by intercept (chord) measurement: an accurate and efficient stereological approach. *J Appl Physiol (1985)*, 108, 412-21.
- KOURTZELIS, I., MITROULIS, I., VON RENESSE, J., HAJISHENGALLIS, G. & CHAVAKIS, T. 2017. From leukocyte recruitment to resolution of inflammation: the cardinal role of integrins. *J Leukoc Biol*, 102, 677-683.
- KREICHER, K. L., WEIR, F. W., NGUYEN, S. A. & MEYER, T. A. 2018. Characteristics and Progression of Hearing Loss in Children with Down Syndrome. *J Pediatr*, 193, 27-33 e2.

## Appendix

- KUBINYECZ, O., VIKHE, P. P., PURNELL, T., BROWN, S. D. M. & TATEOSSIAN, H. 2020. The Jeff Mouse Mutant Model for Chronic Otitis Media Manifests Gain-of-Function as Well as Loss-of-Function Effects. *Front Genet*, 11, 498.
- KUHN, S., INGHAM, N., PEARSON, S., GRIBBLE, S. M., CLAYTON, S., STEEL, K. P. & MARCOTTI, W. 2012. Auditory function in the Tc1 mouse model of down syndrome suggests a limited region of human chromosome 21 involved in otitis media. *PLoS One*, 7, e31433.
- KUROKAWA, M., MITANI, K., IRIE, K., MATSUYAMA, T., TAKAHASHI, T., CHIBA, S., YAZAKI, Y., MATSUMOTO, K. & HIRAI, H. 1998. The oncoprotein Evi-1 represses TGF-beta signalling by inhibiting Smad3. *Nature*, 394, 92-6.
- KUSTERS, M. A., VERSTEGEN, R. H., GEMEN, E. F. & DE VRIES, E. 2009. Intrinsic defect of the immune system in children with Down syndrome: a review. *Clin Exp Immunol*, 156, 189-93.
- LACOMBE, J. M. & ROPER, R. J. 2020. Skeletal dynamics of Down syndrome: A developing perspective. *Bone*, 133, 115215.
- LANA-ELOLA, E., CATER, H., WATSON-SCALES, S., GREENAWAY, S., MULLER-WINKLER, J., GIBBINS, D., NEMES, M., SLENDER, A., HOUGH, T., KESKIVALI-BOND, P., SCUDAMORE, C. L., HERBERT, E., BANKS, G. T., MOBBS, H., CANONICA, T., TOSH, J., NOY, S., LLORIAN, M., NOLAN, P. M., GRIFFIN, J. L., GOOD, M., SIMON, M., MALLON, A. M., WELLS, S., FISHER, E. M. C. & TYBULEWICZ, V. L. J. 2021. Comprehensive phenotypic analysis of the Dp1Tyb mouse strain reveals a broad range of Down syndrome-related phenotypes. *Dis Model Mech*, 14.
- LANA-ELOLA, E., WATSON-SCALES, S., SLENDER, A., GIBBINS, D., MARTINEAU, A., DOUGLAS, C., MOHUN, T., FISHER, E. M. & TYBULEWICZ, V. 2016. Genetic dissection of Down syndrome-associated congenital heart defects using a new mouse mapping panel. *Elife*, 5.
- LARSEN, L. J. & MØLLER, L. B. 2020. Crosstalk of Hedgehog and mTORC1 Pathways. *Cells*, 9.
- LEE, Y. C., KIM, C., SHIM, J. S., BYUN, J. Y., PARK, M. S., CHA, C. I., KIM, Y. I., LEE, J. W. & YEO, S. G. 2008. Toll-like receptors 2 and 4 and their mutations in patients with otitis media and middle ear effusion. *Clin Exp Otorhinolaryngol*, 1, 189-95.
- LEICHTLE, A., HERNANDEZ, M., PAK, K., YAMASAKI, K., CHENG, C. F., WEBSTER, N. J., RYAN, A. F. & WASSERMAN, S. I. 2009. TLR4-mediated induction of TLR2 signaling is critical in the pathogenesis and resolution of otitis media. *Innate Immun*, 15, 205-15.
- LEONG, A. F., BUCKLEY, G. A., PAGANIN, D. M., HOOPER, S. B., WALLACE, M. J. & KITCHEN, M. J. 2014. Real-time measurement of alveolar size and population using phase contrast x-ray imaging. *Biomed Opt Express*, 5, 4024-38.
- LI, H., HELPARD, L., EKEROOT, J., ROHANI, S. A., ZHU, N., RASK-ANDERSEN, H., LADAK, H. M. & AGRAWAL, S. 2021. Three-dimensional tonotopic mapping of the human cochlea based on synchrotron radiation phase-contrast imaging. *Sci Rep*, 11, 4437.
- LI, Y. L., ZHANG, M. M., WU, L. W., LIU, Y. H., ZHANG, Z. Y., ZENG, L. H., LIN, N. M. & ZHANG, C. 2022. DYRK1A reinforces epithelial-mesenchymal transition and metastasis of hepatocellular carcinoma via cooperatively activating STAT3 and SMAD. *J Biomed Sci*, 29, 34.

## Appendix

- LIAO, Y. M., WANG, Y. H., HUNG, J. T., LIN, Y. J., HUANG, Y. L., LIAO, G. S., HSU, Y. L., WU, J. C. & YU, A. L. 2021. High B3GALT5 expression confers poor clinical outcome and contributes to tumor progression and metastasis in breast cancer. *Breast Cancer Res*, 23, 5.
- LIM, D. J., SHIMADA, T. & YODER, M. 1973. Distribution of mucus-secreting cells in normal middle ear mucosa. *Arch Otolaryngol*, 98, 2-9.
- LIN, J. J., GILLAM, L., SMITH, L., CAREW, P., KING, A., CHING, T. Y. C. & SUNG, V. 2022. Mild matters: parental insights into the conundrums of managing mild congenital hearing loss. *Int J Audiol*, 61, 500-506.
- LING, K. H., HEWITT, C. A., TAN, K. L., CHEAH, P. S., VIDYADARAN, S., LAI, M. I., LEE, H. C., SIMPSON, K., HYDE, L., PRITCHARD, M. A., SMYTH, G. K., THOMAS, T. & SCOTT, H. S. 2014. Functional transcriptome analysis of the postnatal brain of the Ts1Cje mouse model for Down syndrome reveals global disruption of interferon-related molecular networks. *BMC Genomics*, 15, 624.
- LIU, X., CONG, N., CHENG, X., MA, R., WANG, J., HUANG, Y. B., ZHAO, M., WANG, X. W., CHI, F. L. & REN, D. D. 2017. The Role of the Notch Signal Pathway in Mucosal Cell Metaplasia in Mouse Acute Otitis Media. *Sci Rep*, 7, 4588.
- LOHELA, M., BRY, M., TAMMELA, T. & ALITALO, K. 2009. VEGFs and receptors involved in angiogenesis versus lymphangiogenesis. *Curr Opin Cell Biol*, 21, 154-65.
- LUO, W., YI, H., TAYLOR, J., LI, J. D., CHI, F., TODD, N. W., LIN, X., REN, D. & CHEN, P. 2017. Cilia distribution and polarity in the epithelial lining of the mouse middle ear cavity. *Sci Rep*, 7, 45870.
- MACARTHUR, C. J., HEFENEIDER, S. H., KEMPTON, J. B. & TRUNE, D. R. 2006. C3H/HeJ mouse model for spontaneous chronic otitis media. *Laryngoscope*, 116, 1071-9.
- MACARTHUR, C. J., WILMOT, B., WANG, L., SCHULLER, M., LIGHTHALL, J. & TRUNE, D. 2014. Genetic susceptibility to chronic otitis media with effusion: candidate gene single nucleotide polymorphisms. *Laryngoscope*, 124, 1229-35.
- MALKOV, M. I., LEE, C. T. & TAYLOR, C. T. 2021. Regulation of the Hypoxia-Inducible Factor (HIF) by Pro-Inflammatory Cytokines. *Cells*, 10.
- MANCINO, A., SCHIOPPA, T., LARGHI, P., PASQUALINI, F., NEBULONI, M., CHEN, I. H., SOZZANI, S., AUSTYN, J. M., MANTOVANI, A. & SICA, A. 2008. Divergent effects of hypoxia on dendritic cell functions. *Blood*, 112, 3723-34.
- MANICKAM, V., SHOTT, G. S., HEITHAUS, D. & SHOTT, S. R. 2016. Hearing loss in Down Syndrome revisited - 15 years later. *Int J Pediatr Otorhinolaryngol*, 88, 203-7.
- MANN, Z. F., THIEDE, B. R., CHANG, W., SHIN, J. B., MAY-SIMERA, H. L., LOVETT, M., CORWIN, J. T. & KELLEY, M. W. 2014. A gradient of Bmp7 specifies the tonotopic axis in the developing inner ear. *Nat Commun*, 5, 3839.
- MARGOLIS, R. H., WILSON, R. H., POPELKA, G. R., EIKELBOOM, R. H., SWANEPOEL DE, W. & SALY, G. L. 2016. Distribution Characteristics of Air-Bone Gaps: Evidence of Bias in Manual Audiometry. *Ear Hear*, 37, 177-88.
- MARIS, M., WOJCIECHOWSKI, M., VAN DE HEYNING, P. & BOUDEWYNS, A. 2014. A cross-sectional analysis of otitis media with effusion in children with Down syndrome. *Eur J Pediatr*, 173, 1319-25.

## Appendix

- MAZZONI, D. S., ACKLEY, R. S. & NASH, D. J. 1994. Abnormal pinna type and hearing loss correlations in Down's syndrome. *J Intellect Disabil Res*, 38 ( Pt 6), 549-60.
- MBURU, P., ROMERO, M. R., HILTON, H., PARKER, A., TOWNSEND, S., KIKKAWA, Y. & BROWN, S. D. 2010. Gelsolin plays a role in the actin polymerization complex of hair cell stereocilia. *PLoS One*, 5, e11627.
- MCCARTHY, D. J. & SMYTH, G. K. 2009. Testing significance relative to a fold-change threshold is a TREAT. *Bioinformatics*, 25, 765-71.
- MCELYEA, S. D., STARBUCK, J. M., TUMBLESON-BRINK, D. M., HARRINGTON, E., BLAZEK, J. D., GHONEIMA, A., KULA, K. & ROPER, R. J. 2016. Influence of prenatal EGCG treatment and Dyrk1a dosage reduction on craniofacial features associated with Down syndrome. *Hum Mol Genet*, 25, 4856-4869.
- MCNAMEE, E. N., KORNS JOHNSON, D., HOMANN, D. & CLAMBEY, E. T. 2013. Hypoxia and hypoxia-inducible factors as regulators of T cell development, differentiation, and function. *Immunol Res*, 55, 58-70.
- MICHELS, T. C., DUFFY, M. T. & ROGERS, D. J. 2019. Hearing Loss in Adults: Differential Diagnosis and Treatment. *Am Fam Physician*, 100, 98-108.
- MITWALLI, M., WAHBA, Y., SHALTOUT, A. & GOUIDA, M. 2018. Lymphocyte subgroups and recurrent infections in children with Down syndrome - a prospective case control study. *Cent Eur J Immunol*, 43, 248-254.
- MORICE, E., ANDREAE, L. C., COOKE, S. F., VANES, L., FISHER, E. M., TYBULEWICZ, V. L. & BLISS, T. V. 2008. Preservation of long-term memory and synaptic plasticity despite short-term impairments in the Tc1 mouse model of Down syndrome. *Learn Mem*, 15, 492-500.
- MOWERY, C. T., REYES, J. M., CABAL-HIERRO, L., HIGBY, K. J., KARLIN, K. L., WANG, J. H., KIMMERLING, R. J., CEJAS, P., LIM, K., LI, H., FURUSAWA, T., LONG, H. W., PELLMAN, D., CHAPUY, B., BUSTIN, M., MANALIS, S. R., WESTBROOK, T. F., LIN, C. Y. & LANE, A. A. 2018. Trisomy of a Down Syndrome Critical Region Globally Amplifies Transcription via HMGN1 Overexpression. *Cell Rep*, 25, 1898-1911.e5.
- MOZZI, A., PONTREMOLI, C. & SIRONI, M. 2018. Genetic susceptibility to infectious diseases: Current status and future perspectives from genome-wide approaches. *Infect Genet Evol*, 66, 286-307.
- MULAY, A., AKRAM, K. M., WILLIAMS, D., ARMES, H., RUSSELL, C., HOOD, D., ARMSTRONG, S., STEWART, J. P., BROWN, S. D., BINGLE, L. & BINGLE, C. D. 2016. An in vitro model of murine middle ear epithelium. *Dis Model Mech*, 9, 1405-1417.
- NAGY, J. A., BENJAMIN, L., ZENG, H., DVORAK, A. M. & DVORAK, H. F. 2008. Vascular permeability, vascular hyperpermeability and angiogenesis. *Angiogenesis*, 11, 109-19.
- NEUMANN, F., GOURDAIN, S., ALBAC, C., DEKKER, A. D., BUI, L. C., DAIROU, J., SCHMITZ-AFONSO, I., HUE, N., RODRIGUES-LIMA, F., DELABAR, J. M., POTIER, M. C., LE CAËR, J. P., TOUBOUL, D., DELATOUR, B., CARIOU, K. & DODD, R. H. 2018. DYRK1A inhibition and cognitive rescue in a Down syndrome mouse model are induced by new fluoro-DANDY derivatives. *Sci Rep*, 8, 2859.
- NGUYEN, T. L., DUCHON, A., MANOUSOPOULOU, A., LOAEC, N., VILLIERS, B., PANI, G., KARATAS, M., MECHLING, A. E., HARSAN, L. A., LIMANTON, E., BAZUREAU, J. P., CARREAUX, F., GARBIS, S. D., MEIJER, L. & HERAULT,

## Appendix

- Y. 2018. Correction of cognitive deficits in mouse models of Down syndrome by a pharmacological inhibitor of DYRK1A. *Dis Model Mech*, 11.
- NICE 2008. Surgical management of otitis media with effusion in children. *Surgical Management of Otitis Media with Effusion in Children*. London.
- NIGHTENGAL, E., YOON, P., WOLTER-WARMERDAM, K., DANIELS, D. & HICKEY, F. 2017. Understanding Hearing and Hearing Loss in Children With Down Syndrome. *Am J Audiol*, 26, 301-308.
- NOLAN, P. M., PETERS, J., STRIVENS, M., ROGERS, D., HAGAN, J., SPURR, N., GRAY, I. C., VIZOR, L., BROOKER, D., WHITEHILL, E., WASHBOURNE, R., HOUGH, T., GREENAWAY, S., HEWITT, M., LIU, X., MCCORMACK, S., PICKFORD, K., SELLEY, R., WELLS, C., TYMOWSKA-LALANNE, Z., ROBY, P., GLENISTER, P., THORNTON, C., THAUNG, C., STEVENSON, J. A., ARKELL, R., MBURU, P., HARDISTY, R., KIERNAN, A., ERVEN, A., STEEL, K. P., VOEGELING, S., GUENET, J. L., NICKOLS, C., SADRI, R., NASSE, M., ISAACS, A., DAVIES, K., BROWNE, M., FISHER, E. M., MARTIN, J., RASTAN, S., BROWN, S. D. & HUNTER, J. 2000. A systematic, genome-wide, phenotype-driven mutagenesis programme for gene function studies in the mouse. *Nat Genet*, 25, 440-3.
- NOLZ, J. C. 2015. Molecular mechanisms of CD8(+) T cell trafficking and localization. *Cell Mol Life Sci*, 72, 2461-73.
- O'DOHERTY, A., RUF, S., MULLIGAN, C., HILDRETH, V., ERRINGTON, M. L., COOKE, S., SESAY, A., MODINO, S., VANES, L., HERNANDEZ, D., LINEHAN, J. M., SHARPE, P. T., BRANDNER, S., BLISS, T. V., HENDERSON, D. J., NIZETIC, D., TYBULEWICZ, V. L. & FISHER, E. M. 2005. An aneuploid mouse strain carrying human chromosome 21 with Down syndrome phenotypes. *Science*, 309, 2033-7.
- OLSON, L. E., RICHTSMIEIER, J. T., LESZL, J. & REEVES, R. H. 2004. A chromosome 21 critical region does not cause specific Down syndrome phenotypes. *Science*, 306, 687-90.
- OTTE, J., SCHUNKNECHT, H. F. & KERR, A. G. 1978. Ganglion cell populations in normal and pathological human cochleae. Implications for cochlear implantation. *Laryngoscope*, 88, 1231-46.
- OUKKA, M. 2008. Th17 cells in immunity and autoimmunity. *Annals of the rheumatic diseases*, 67, iii26-iii29.
- PAGE, E. C., HEATLEY, S. L., EADIE, L. N., MCCLURE, B. J., DE BOCK, C. E., OMARI, S., YEUNG, D. T., HUGHES, T. P., THOMAS, P. Q. & WHITE, D. L. 2022. HMG1 plays a significant role in CRLF2 driven Down Syndrome leukemia and provides a potential therapeutic target in this high-risk cohort. *Oncogene*, 41, 797-808.
- PALAZON, A., GOLDRATH, A. W., NIZET, V. & JOHNSON, R. S. 2014. HIF transcription factors, inflammation, and immunity. *Immunity*, 41, 518-28.
- PARK, A. H., WILSON, M. A., STEVENS, P. T., HARWARD, R. & HOHLER, N. 2012. Identification of hearing loss in pediatric patients with Down syndrome. *Otolaryngol Head Neck Surg*, 146, 135-40.
- PARK, H., LI, Z., YANG, X. O., CHANG, S. H., NURIEVA, R., WANG, Y. H., WANG, Y., HOOD, L., ZHU, Z., TIAN, Q. & DONG, C. 2005. A distinct lineage of CD4 T cells regulates tissue inflammation by producing interleukin 17. *Nat Immunol*, 6, 1133-41.
- PARKINSON, N., HARDISTY-HUGHES, R. E., TATEOSSIAN, H., TSAI, H. T., BROOKER, D., MORSE, S., LALANE, Z., MACKENZIE, F., FRAY, M.,

## Appendix

- GLENISTER, P., WOODWARD, A. M., POLLEY, S., BARBARIC, I., DEAR, N., HOUGH, T. A., HUNTER, A. J., CHEESEMAN, M. T. & BROWN, S. D. 2006. Mutation at the Evi1 locus in Junbo mice causes susceptibility to otitis media. *PLoS Genet*, 2, e149.
- PASH, J., POPESCU, N., MATOCHA, M., RAPOPORT, S. & BUSTIN, M. 1990. Chromosomal protein HMG-14 gene maps to the Down syndrome region of human chromosome 21 and is overexpressed in mouse trisomy 16. *Proc Natl Acad Sci U S A*, 87, 3836-40.
- PATTERSON, D. 2009. Molecular genetic analysis of Down syndrome. *Hum Genet*, 126, 195-214.
- PAULSON, L. M., WEAVER, T. S. & MACARTHUR, C. J. 2014. Outcomes of tympanostomy tube placement in children with Down syndrome--a retrospective review. *Int J Pediatr Otorhinolaryngol*, 78, 223-6.
- PELULLO, M., ZEMA, S., NARDOZZA, F., CHECQUOLO, S., SCREPANTI, I. & BELLAVIA, D. 2019. Wnt, Notch, and TGF-beta Pathways Impinge on Hedgehog Signaling Complexity: An Open Window on Cancer. *Front Genet*, 10, 711.
- PICKRELL, J. K., BERISA, T., LIU, J. Z., SEGUREL, L., TUNG, J. Y. & HINDS, D. A. 2016. Detection and interpretation of shared genetic influences on 42 human traits. *Nat Genet*, 48, 709-17.
- PLETCHER, M. T., WILTSHIRE, T., CABIN, D. E., VILLANUEVA, M. & REEVES, R. H. 2001. Use of comparative physical and sequence mapping to annotate mouse chromosome 16 and human chromosome 21. *Genomics*, 74, 45-54.
- POTIER, M. C., RIVALS, I., MERCIER, G., ETTWILLER, L., MOLDRICH, R. X., LAFFAIRE, J., PERSONNAZ, L., ROSSIER, J. & DAUPHINOT, L. 2006. Transcriptional disruptions in Down syndrome: a case study in the Ts1Cje mouse cerebellum during post-natal development. *J Neurochem*, 97 Suppl 1, 104-9.
- RAVEAU, M., NAKAHARI, T., ASADA, S., ISHIHARA, K., AMANO, K., SHIMOHATA, A., SAGO, H. & YAMAKAWA, K. 2017. Brain ventriculomegaly in Down syndrome mice is caused by Pcp4 dose-dependent cilia dysfunction. *Hum Mol Genet*, 26, 923-931.
- RAVEL, A., MIRCHER, C., REBILLAT, A. S., CIEUTA-WALTI, C. & MEGARBANE, A. 2020. Feeding problems and gastrointestinal diseases in Down syndrome. *Arch Pediatr*, 27, 53-60.
- REINHOLDT, L. G., DING, Y., GILBERT, G. J., CZECHANSKI, A., SOLZAK, J. P., ROPER, R. J., JOHNSON, M. T., DONAHUE, L. R., LUTZ, C. & DAVISSON, M. T. 2011. Molecular characterization of the translocation breakpoints in the Down syndrome mouse model Ts65Dn. *Mamm Genome*, 22, 685-91.
- REYNOLDS, L. E., WATSON, A. R., BAKER, M., JONES, T. A., D'AMICO, G., ROBINSON, S. D., JOFFRE, C., GARRIDO-URBANI, S., RODRIGUEZ-MANZANEQUE, J. C., MARTINO-ECHARRI, E., AURRAND-LIONS, M., SHEER, D., DAGNA-BRICARELLI, F., NIZETIC, D., MCCABE, C. J., TURNELL, A. S., KERMORGANT, S., IMHOF, B. A., ADAMS, R., FISHER, E. M., TYBULEWICZ, V. L., HART, I. R. & HODIVALA-DILKE, K. M. 2010. Tumour angiogenesis is reduced in the Tc1 mouse model of Down's syndrome. *Nature*, 465, 813-7.
- RICHTSMEIER, J. T., BAXTER, L. L. & REEVES, R. H. 2000. Parallels of craniofacial maldevelopment in Down syndrome and Ts65Dn mice. *Dev Dyn*, 217, 137-45.

## Appendix

- RODRIGUES, M., NUNES, J., FIGUEIREDO, S., MARTINS DE CAMPOS, A. & GERALDO, A. F. 2019. Neuroimaging assessment in Down syndrome: a pictorial review. *Insights Imaging*, 10, 52.
- ROSALES, C. 2018. Neutrophil: A Cell with Many Roles in Inflammation or Several Cell Types? *Front Physiol*, 9, 113.
- ROSENFELD, R. M., SHIN, J. J., SCHWARTZ, S. R., COGGINS, R., GAGNON, L., HACKELL, J. M., HOELTING, D., HUNTER, L. L., KUMMER, A. W., PAYNE, S. C., POE, D. S., VELING, M., VILA, P. M., WALSH, S. A. & CORRIGAN, M. D. 2016. Clinical Practice Guideline: Otitis Media with Effusion (Update). *Otolaryngol Head Neck Surg*, 154, S1-S41.
- ROZEN, E. J., ROEWENSTRUNK, J., BARALLOBRE, M. J., DI VONA, C., JUNG, C., FIGUEIREDO, A. F., LUNA, J., FILLAT, C., ARBONES, M. L., GRAUPERA, M., VALVERDE, M. A. & DE LA LUNA, S. 2018. DYRK1A Kinase Positively Regulates Angiogenic Responses in Endothelial Cells. *Cell Rep*, 23, 1867-1878.
- RUEDA, N., FLÓREZ, J. & MARTÍNEZ-CUÉ, C. 2013. Apoptosis in Down's syndrome: lessons from studies of human and mouse models. *Apoptosis*, 18, 121-34.
- RUMMAN, N., JACKSON, C., COLLINS, S., GOGGIN, P., COLES, J. & LUCAS, J. S. 2017. Diagnosis of primary ciliary dyskinesia: potential options for resource-limited countries. *Eur Respir Rev*, 26.
- RYE, M. S., BHUTTA, M. F., CHEESEMAN, M. T., BURGNER, D., BLACKWELL, J. M., BROWN, S. D. & JAMIESON, S. E. 2011a. Unraveling the genetics of otitis media: from mouse to human and back again. *Mamm Genome*, 22, 66-82.
- RYE, M. S., BLACKWELL, J. M. & JAMIESON, S. E. 2012. Genetic susceptibility to otitis media in childhood. *Laryngoscope*, 122, 665-75.
- RYE, M. S., WIERTSEMA, S. P., SCAMAN, E. S., OOMMEN, J., SUN, W., FRANCIS, R. W., ANG, W., PENNELL, C. E., BURGNER, D., RICHMOND, P., VIJAYASEKARAN, S., COATES, H. L., BROWN, S. D., BLACKWELL, J. M. & JAMIESON, S. E. 2011b. FBXO11, a regulator of the TGF $\beta$  pathway, is associated with severe otitis media in Western Australian children. *Genes Immun*, 12, 352-9.
- SACKS, B. & WOOD, A. Hearing disorders in children with Down syndrome. 2003.
- SAGO, H., CARLSON, E. J., SMITH, D. J., KILBRIDGE, J., RUBIN, E. M., MOBLEY, W. C., EPSTEIN, C. J. & HUANG, T. T. 1998. Ts1Cje, a partial trisomy 16 mouse model for Down syndrome, exhibits learning and behavioral abnormalities. *Proc Natl Acad Sci U S A*, 95, 6256-61.
- SAHM, A., BENS, M., SZAFRANSKI, K., HOLTZE, S., GROTH, M., GÖRLACH, M., CALKHOVEN, C., MÜLLER, C., SCHWAB, M., KRAUS, J., KESTLER, H. A., CELLERINO, A., BURDA, H., HILDEBRANDT, T., DAMMANN, P. & PLATZER, M. 2018. Long-lived rodents reveal signatures of positive selection in genes associated with lifespan. *PLoS Genet*, 14, e1007272.
- SALE, M. M., CHEN, W. M., WEEKS, D. E., MYCHALECKYJ, J. C., HOU, X., MARION, M., SEGADE, F., CASSELBRANT, M. L., MANDEL, E. M., FERRELL, R. E., RICH, S. S. & DALY, K. A. 2011. Evaluation of 15 functional candidate genes for association with chronic otitis media with effusion and/or recurrent otitis media (COME/ROM). *PLoS One*, 6, e22297.
- SÁNCHEZ-ELSNER, T., BOTELLA, L. M., VELASCO, B., CORBÍ, A., ATTISANO, L. & BERNABÉU, C. 2001. Synergistic cooperation between hypoxia and

## Appendix

- transforming growth factor-beta pathways on human vascular endothelial growth factor gene expression. *J Biol Chem*, 276, 38527-35.
- SANTOS-CORTEZ, R. L., CHIONG, C. M., REYES-QUINTOS, M. R., TANTOCO, M. L., WANG, X., ACHARYA, A., ABBE, I., GIESE, A. P., SMITH, J. D., ALLEN, E. K., LI, B., CUTIONGCO-DE LA PAZ, E. M., GARCIA, M. C., LLANES, E. G., LABRA, P. J., GLORIA-CRUZ, T. L., CHAN, A. L., WANG, G. T., DALY, K. A., SHENDURE, J., BAMSHAD, M. J., NICKERSON, D. A., PATEL, J. A., RIAZUDDIN, S., SALE, M. M., CHONMAITREE, T., AHMED, Z. M., ABES, G. T. & LEAL, S. M. 2015. Rare A2ML1 variants confer susceptibility to otitis media. *Nat Genet*, 47, 917-20.
- SANTOS-CORTEZ, R. L. P., BHUTTA, M. F., EARL, J. P., HAFREN, L., JENNINGS, M., MELL, J. C., PICHICHERO, M. E., RYAN, A. F., TATEOSSIAN, H. & EHRLICH, G. D. 2020. Panel 3: Genomics, precision medicine and targeted therapies. *Int J Pediatr Otorhinolaryngol*, 130 Suppl 1, 109835.
- SANTOS-CORTEZ, R. L. P., CHIONG, C. M., FRANK, D. N., RYAN, A. F., GIESE, A. P. J., BOOTPETCH ROBERTS, T., DALY, K. A., STERITZ, M. J., SZEREMETA, W., PEDRO, M., PINE, H., YARZA, T. K. L., SCHOLE, M. A., LLANES, E., YOUSAF, S., FRIEDMAN, N., TANTOCO, M. L. C., WINE, T. M., LABRA, P. J., BENOIT, J., RUIZ, A. G., DE LA CRUZ, R. A. R., GREENLEE, C., YOUSAF, A., CARDWELL, J., NONATO, R. M. A., RAY, D., ONG, K. M. C., SO, E., ROBERTSON, C. E., DINWIDDIE, J., LAGRANA-VILLAGRACIA, S. M., UNIVERSITY OF WASHINGTON CENTER FOR MENDELIAN, G., GUBBELS, S. P., SHAIKH, R. S., CASS, S. P., EINARSDOTTIR, E., LEE, N. R., SCHWARTZ, D. A., GLORIA-CRUZ, T. L. I., BAMSHAD, M. J., YANG, I. V., KERE, J., ABES, G. T., PRAGER, J. D., RIAZUDDIN, S., CHAN, A. L., YOON, P. J., NICKERSON, D. A., CUTIONGCO-DE LA PAZ, E. M., STREUBEL, S. O., REYES-QUINTOS, M. R. T., JENKINS, H. A., MATTILA, P., CHAN, K. H., MOHLKE, K. L., LEAL, S. M., HAFREN, L., CHONMAITREE, T., SALE, M. M. & AHMED, Z. M. 2018. FUT2 Variants Confer Susceptibility to Familial Otitis Media. *Am J Hum Genet*, 103, 679-690.
- SCHILDER, A. G., CHONMAITREE, T., CRIPPS, A. W., ROSENFELD, R. M., CASSELBRANT, M. L., HAGGARD, M. P. & VENEKAMP, R. P. 2016. Otitis media. *Nat Rev Dis Primers*, 2, 16063.
- SCHNABEL, F., SMOGAVEC, M., FUNKE, R., PAULI, S., BURFEIND, P. & BARTELS, I. 2018. Down syndrome phenotype in a boy with a mosaic microduplication of chromosome 21q22. *Mol Cytogenet*, 11, 62.
- SCHUON, R., SCHWARZENSTEINER, J., PAASCHE, G., LENARZ, T. & JOHN, S. 2021. Functional aspects of the Eustachian tube by means of 3D-modeling. *PLoS One*, 16, e0244909.
- SCHWARTZ, D. M. & SCHWARTZ, R. H. 1978. Acoustic impedance and otoscopic findings in young children with Down's syndrome. *Arch Otolaryngol*, 104, 652-6.
- SEGADE, F., DALY, K. A., ALLRED, D., HICKS, P. J., COX, M., BROWN, M., HARDISTY-HUGHES, R. E., BROWN, S. D., RICH, S. S. & BOWDEN, D. W. 2006. Association of the FBXO11 gene with chronic otitis media with effusion and recurrent otitis media: the Minnesota COME/ROM Family Study. *Arch Otolaryngol Head Neck Surg*, 132, 729-33.
- SEKIYAMA, K., OHORI, J., MATSUNE, S. & KURONO, Y. 2011. The role of vascular endothelial growth factor in pediatric otitis media with effusion. *Auris Nasus Larynx*, 38, 319-24.

## Appendix

- SELIKOWITZ, M. 1992. Health problems and health checks in school-aged children with Down syndrome. *J Paediatr Child Health*, 28, 383-6.
- SHI, L. Z., WANG, R., HUANG, G., VOGEL, P., NEALE, G., GREEN, D. R. & CHI, H. 2011. HIF1 $\alpha$ -dependent glycolytic pathway orchestrates a metabolic checkpoint for the differentiation of TH17 and Treg cells. *J Exp Med*, 208, 1367-76.
- SHIN, K. J. 2021. Navigational guidelines and positional relationships of the human auditory ossicles from three-dimensional topography for ensuring safe and effective malleostapedotomy : Stereotactic topography of the auditory ossicles and its clinical implication. *Surg Radiol Anat*, 43, 153-159.
- SHOTT, S. R., JOSEPH, A. & HEITHAUS, D. 2001. Hearing loss in children with Down syndrome. *Int J Pediatr Otorhinolaryngol*, 61, 199-205.
- SIMON, F., HAGGARD, M., ROSENFELD, R. M., JIA, H., PEER, S., CALMELS, M. N., COULOIGNER, V. & TEISSIER, N. 2018. International consensus (ICON) on management of otitis media with effusion in children. *European Annals of Otorhinolaryngology, Head and Neck Diseases*, 135, S33-S39.
- SINGH, N., DUTKA, T., REEVES, R. H. & RICHTSMEIER, J. T. 2016. Chronic up-regulation of sonic hedgehog has little effect on postnatal craniofacial morphology of euploid and trisomic mice. *Dev Dyn*, 245, 114-22.
- SINGH, R. & LAUTH, M. 2017. Emerging Roles of DYRK Kinases in Embryogenesis and Hedgehog Pathway Control. *J Dev Biol*, 5.
- SINGH, R. P., HASAN, S., SHARMA, S., NAGRA, S., YAMAGUCHI, D. T., WONG, D. T., HAHN, B. H. & HOSSAIN, A. 2014. Th17 cells in inflammation and autoimmunity. *Autoimmun Rev*, 13, 1174-81.
- SMIRNOVA, M. G., BIRCHALL, J. P. & PEARSON, J. P. 2002. In vitro study of IL-8 and goblet cells: possible role of IL-8 in the aetiology of otitis media with effusion. *Acta Otolaryngol*, 122, 146-52.
- SOJKA, S., AMIN, N. M., GIBBS, D., CHRISTINE, K. S., CHARPENTIER, M. S. & CONLON, F. L. 2014. Congenital heart disease protein 5 associates with CASZ1 to maintain myocardial tissue integrity. *Development*, 141, 3040-9.
- SOUCHET, B., DUCHON, A., GU, Y., DAIROU, J., CHEVALIER, C., DAUBIGNEY, F., NALESSO, V., CRÉAU, N., YU, Y., JANEL, N., HERAULT, Y. & DELABAR, J. M. 2019. Prenatal treatment with EGCG enriched green tea extract rescues GAD67 related developmental and cognitive defects in Down syndrome mouse models. *Sci Rep*, 9, 3914.
- STANKIEWICZ, M. J. & CRISPINO, J. D. 2013. AKT collaborates with ERG and Gata1s to dysregulate megakaryopoiesis and promote AMKL. *Leukemia*, 27, 1339-47.
- STARBUCK, J., REEVES, R. H. & RICHTSMEIER, J. 2011. Morphological integration of soft-tissue facial morphology in Down Syndrome and siblings. *Am J Phys Anthropol*, 146, 560-8.
- STERN, S., SEGAL, M. & MOSES, E. 2015. Involvement of Potassium and Cation Channels in Hippocampal Abnormalities of Embryonic Ts65Dn and Tc1 Trisomic Mice. *EBioMedicine*, 2, 1048-62.
- SUN, D., MATSUNE, S., OHORI, J., FUKUIWA, T., USHIKAI, M. & KURONO, Y. 2005. TNF- $\alpha$  and endotoxin increase hypoxia-induced VEGF production by cultured human nasal fibroblasts in synergistic fashion. *Auris Nasus Larynx*, 32, 243-9.
- TAKAHASHI, H. 2001. *The Middle Ear: The Role of Ventilation in Disease and Surgery*, Japan, Springer.

## Appendix

- TANG, S. H., SILVA, F. J., TSARK, W. M. & MANN, J. R. 2002. A Cre/loxP-deleter transgenic line in mouse strain 129S1/SvImJ. *Genesis*, 32, 199-202.
- TANG, Z., ZENG, X., LI, J., ZHANG, H., WU, H., ZHUANG, S. & ZHENG, Y. 2020. The immune imbalance of Treg/Th17 in secretory otitis media patients may be related to PI3K/Akt/mTOR signaling activation in the middle ear mucosa. *Authorea*.
- TATEOSSIAN, H., HARDISTY-HUGHES, R. E., MORSE, S., ROMERO, M. R., HILTON, H., DEAN, C. & BROWN, S. D. 2009. Regulation of TGF-beta signalling by Fbxo11, the gene mutated in the Jeff otitis media mouse mutant. *Pathogenetics*, 2, 5.
- TATEOSSIAN, H., MORSE, S., PARKER, A., MBURU, P., WARR, N., ACEVEDO-AROZENA, A., CHEESEMAN, M., WELLS, S. & BROWN, S. D. 2013. Otitis media in the Tgif knockout mouse implicates TGFbeta signalling in chronic middle ear inflammatory disease. *Hum Mol Genet*, 22, 2553-65.
- TATEOSSIAN, H., MORSE, S., SIMON, M. M., DEAN, C. H. & BROWN, S. D. 2015. Interactions between the otitis media gene, Fbxo11, and p53 in the mouse embryonic lung. *Dis Model Mech*, 8, 1531-42.
- TATEOSSIAN, H., SOUTHERN, A., VIKHE, P., LANA-ELOLA, E., WATSON-SCALES, S., GIBBINS, D., WILLIAMS, D., PURNELL, T., MBURU, P., PARKER, A., NORRIS, D. P., SANTOS-CORTEZ, R., WELLS, S., LAD, H. V., FISHER, E. M. C., TYBULEWICZ, V. L. J. & BROWN, S. D. M. 2022. DYRK1A kinase trisomy is the major cause of Otitis Media in Down Syndrome.
- TEJEDOR, F., ZHU, X. R., KALTENBACH, E., ACKERMANN, A., BAUMANN, A., CANAL, I., HEISENBERG, M., FISCHBACH, K. F. & PONGS, O. 1995. minibrain: a new protein kinase family involved in postembryonic neurogenesis in Drosophila. *Neuron*, 14, 287-301.
- TESMER, L. A., LUNDY, S. K., SARKAR, S. & FOX, D. A. 2008. Th17 cells in human disease. *Immunol Rev*, 223, 87-113.
- THOMPSON, H. & TUCKER, A. S. 2013. Dual origin of the epithelium of the mammalian middle ear. *Science*, 339, 1453-6.
- TIAN, C., HROMATKA, B. S., KIEFER, A. K., ERIKSSON, N., NOBLE, S. M., TUNG, J. Y. & HINDS, D. A. 2017. Genome-wide association and HLA region fine-mapping studies identify susceptibility loci for multiple common infections. *Nat Commun*, 8, 599.
- TOMKEIEFF, S. I. 1945. Linear Intercepts, Areas and Volumes. *Nature*, 155, 24-24.
- TORNALI, C., MIGLIORE, M., POLIZZI, A., BRAGAZZI, N. L., MARTINI, M., RUGGIERI, M., PRATICÒ, A. D. & VECCHIO, I. 2021. Reconstructive Surgery in Children with Down Syndrome: Bioethical Implications. *Journal of pediatric neurology*, 19, 001-006.
- TOUSSAINT, N., REDHEAD, Y., VIDAL-GARCÍA, M., LO VERCIO, L., LIU, W., FISHER, E. M. C., HALLGRÍMSSON, B., TYBULEWICZ, V. L. J., SCHNABEL, J. A. & GREEN, J. B. A. 2021. A landmark-free morphometrics pipeline for high-resolution phenotyping: application to a mouse model of Down syndrome. *Development*, 148.
- TSUCHIYA, K., KOMORI, M., ZHENG, Q. Y., FERRIERI, P. & LIN, J. 2008. Interleukin-10 is an essential modulator of mucoid metaplasia in a mouse otitis media model. *Ann Otol Rhinol Laryngol*, 117, 630-6.
- TYRER, H. E., CROMPTON, M. & BHUTTA, M. F. 2013. What Have We Learned from Murine Models of Otitis Media? *Current Allergy and Asthma Reports*, 13, 501-511.

## Appendix

- UBELL, M. L., KHAMPANG, P. & KERSCHNER, J. E. 2010. Mucin gene polymorphisms in otitis media patients. *Laryngoscope*, 120, 132-8.
- UGAZIO, A. G., MACCARIO, R., NOTARANGELO, L. D. & BURGIO, G. R. 1990. Immunology of Down syndrome: a review. *Am J Med Genet Suppl*, 7, 204-12.
- VAL, S., POLEY, M., ANNA, K., NINO, G., BROWN, K., PEREZ-LOSADA, M., GORDISH-DRESSMAN, H. & PRECIADO, D. 2018. Characterization of mucoid and serous middle ear effusions from patients with chronic otitis media: implication of different biological mechanisms? *Pediatr Res*, 84, 296-305.
- VAN INGEN, G., LI, J., GOEDEGEBURE, A., PANDEY, R., LI, Y. R., MARCH, M. E., JADDOE, V. W., BAKAY, M., MENTCH, F. D., THOMAS, K., WEI, Z., CHANG, X., HAIN, H. S., UITTERLINDEN, A. G., MOLL, H. A., VAN DUIJN, C. M., RIVADENEIRA, F., RAAT, H., BAATENBURG DE JONG, R. J., SLEIMAN, P. M., VAN DER SCHROEFF, M. P. & HAKONARSON, H. 2016. Genome-wide association study for acute otitis media in children identifies FNDC1 as disease contributing gene. *Nat Commun*, 7, 12792.
- VANNESTE, P. & PAGE, C. 2019. Otitis media with effusion in children: Pathophysiology, diagnosis, and treatment. A review. *J Otol*, 14, 33-39.
- VARJOSALO, M., KESKITALO, S., VAN DROGEN, A., NURKKALA, H., VICHALKOVSKI, A., AEBERSOLD, R. & GSTAIGER, M. 2013. The Protein Interaction Landscape of the Human CMGC Kinase Group. *Cell Reports*, 3, 1306-1320.
- VELDHOEN, M., HOCKING, R. J., ATKINS, C. J., LOCKSLEY, R. M. & STOCKINGER, B. 2006. TGFbeta in the context of an inflammatory cytokine milieu supports de novo differentiation of IL-17-producing T cells. *Immunity*, 24, 179-89.
- VIKHE, P. P., PURNELL, T., BROWN, S. D. M. & HOOD, D. W. 2019. Cellular content plays a crucial role in Non-typeable Haemophilus influenzae infection of preinflamed Junbo mouse middle ear. *Cell Microbiol*, 21, e12960.
- VIKHE, P. P., TATEOSSIAN, H., BHARJ, G., BROWN, S. D. M. & HOOD, D. W. 2020. Mutation in Fbxo11 Leads to Altered Immune Cell Content in Jeff Mouse Model of Otitis Media. *Front Genet*, 11, 50.
- WATSON-SCALES, S., KALMAR, B., LANA-ELOLA, E., GIBBINS, D., LA RUSSA, F., WISEMAN, F., WILLIAMSON, M., SACCON, R., SLENDER, A., OLERINYOVA, A., MAHMOOD, R., NYE, E., CATER, H., WELLS, S., YU, Y. E., BENNETT, D. L. H., GREENSMITH, L., FISHER, E. M. C. & TYBULEWICZ, V. L. J. 2018. Analysis of motor dysfunction in Down Syndrome reveals motor neuron degeneration. *PLoS Genet*, 14, e1007383.
- WATSON, D. R., MCCLELLAND, R. J. & ADAMS, D. A. 1996. Auditory brainstem response screening for hearing loss in high risk neonates. *Int J Pediatr Otorhinolaryngol*, 36, 147-83.
- WEI, G., GUO, J., DOSEFF, A. I., KUSEWITT, D. F., MAN, A. K., OSHIMA, R. G. & OSTROWSKI, M. C. 2004. Activated Ets2 is required for persistent inflammatory responses in the motheaten viable model. *J Immunol*, 173, 1374-9.
- WIESEN, B. M., HAFREN, L., EINARSDOTTIR, E., KERE, J., MATTILA, P. S. & SANTOS-CORTEZ, R. L. P. 2019. ABO Genotype and Blood Type Are Associated with Otitis Media. *Genet Test Mol Biomarkers*, 23, 823-827.
- WILLSEY, H. R., XU, Y., EVERITT, A., DEA, J., EXNER, C. R. T., WILLSEY, A. J., STATE, M. W. & HARLAND, R. M. 2020. The neurodevelopmental disorder

## Appendix

- risk gene DYRK1A is required for ciliogenesis and control of brain size in *Xenopus* embryos. *Development*, 147.
- WOLVETANG, E. J., WILSON, T. J., SANIJ, E., BUSCIGLIO, J., HATZISTAVROU, T., SETH, A., HERTZOG, P. J. & KOLA, I. 2003. ETS2 overexpression in transgenic models and in Down syndrome predisposes to apoptosis via the p53 pathway. *Hum Mol Genet*, 12, 247-55.
- XU, X., WOO, C.-H., STEERE, R. R., LEE, B. C., HUANG, Y., WU, J., PANG, J., LIM, J. H., XU, H., ZHANG, W., KONDURU, A. S., YAN, C., CHEESEMAN, M. T., BROWN, S. D. M. & LI, J.-D. 2012. EVI1 Acts as an Inducible Negative-Feedback Regulator of NF- $\kappa$ B by Inhibiting p65 Acetylation. *The Journal of Immunology*, 188, 6371-6380.
- YU, T., LI, Z., JIA, Z., CLAPCOTE, S. J., LIU, C., LI, S., ASRAR, S., PAO, A., CHEN, R., FAN, N., CARATTINI-RIVERA, S., BECHARD, A. R., SPRING, S., HENKELMAN, R. M., STOICA, G., MATSUI, S., NOWAK, N. J., RODER, J. C., CHEN, C., BRADLEY, A. & YU, Y. E. 2010. A mouse model of Down syndrome trisomic for all human chromosome 21 syntenic regions. *Hum Mol Genet*, 19, 2780-91.
- ZAITOUN, M., RAWASHDEH, M., ALQUDAH, S., H, A. L., NUSEIR, A. & AL-TAMIMI, F. 2021. Knowledge and Practice of Hearing Screening and Hearing Loss Management among Ear, Nose, and Throat Physicians in Jordan. *Int Arch Otorhinolaryngol*, 25, e98-e107.
- ZHU, B., PARSONS, T., STENSEN, W., MJØEN SVENDSEN, J. S., FUGELLI, A. & HODGE, J. J. L. 2022. DYRK1a Inhibitor Mediated Rescue of *Drosophila* Models of Alzheimer's Disease-Down Syndrome Phenotypes. *Front Pharmacol*, 13, 881385.

## Appendix

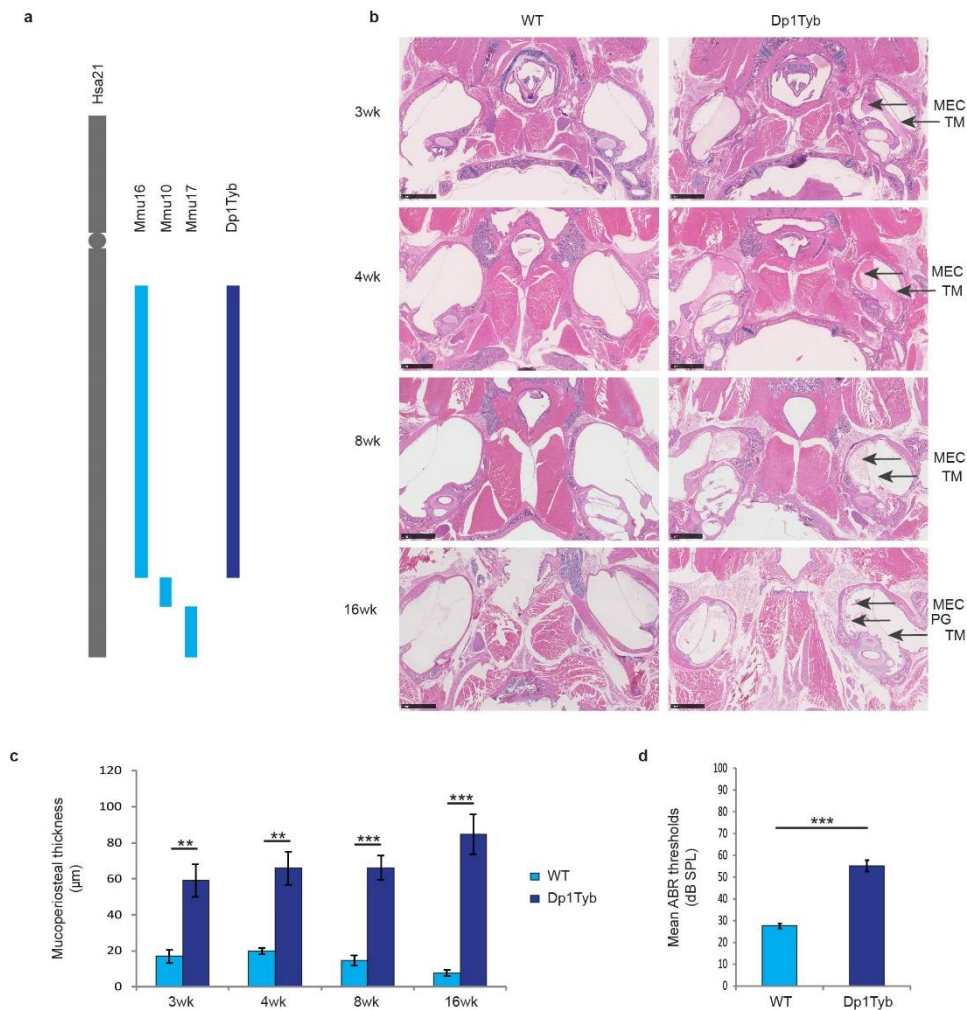


**Figure 1. Otitis media phenotype of Dp1Tyb mice.** **a**, Representation of Hsa21 (in grey), the orthologous regions on Mmu10, Mmu16 and Mmu17 (in light blue) and the region of the duplication in Dp1Tyb mice (in dark blue). **b**, Haematoxylin-eosin stained transverse sections through the middle ear of 3 week (3wk), 4 week (4wk), 8 week (8wk) and 16-week-old (16wk) wild-type (WT) and Dp1Tyb mice. MEC: middle ear cavity; TM: tympanic membrane; PG: polypoid growth. Scale bars: 1 mm. **c**, Comparison of the thickness of the epithelial lining of the middle ear for each genotype and age (3wk: WT n = 7 mice, Dp1Tyb n = 7 mice; 4wk: WT n = 5 mice, Dp1Tyb n = 4 mice; 8wk: WT n = 6 mice, Dp1Tyb n = 6 mice; 16wk: WT n = 4 mice, Dp1Tyb n = 7 mice). **d**, Broadband click stimuli ABR thresholds in the right ears of 2-month-old wild-type (WT) and Dp1Tyb mice. The graph shows elevated mean thresholds in Dp1Tyb mice (n = 6) compared to wild-type (WT) mice (n = 6). Bars: standard error of mean. P-values were determined using two-tailed t-test. \*\* p<0.01; \*\*\* p<0.001.

## Appendix

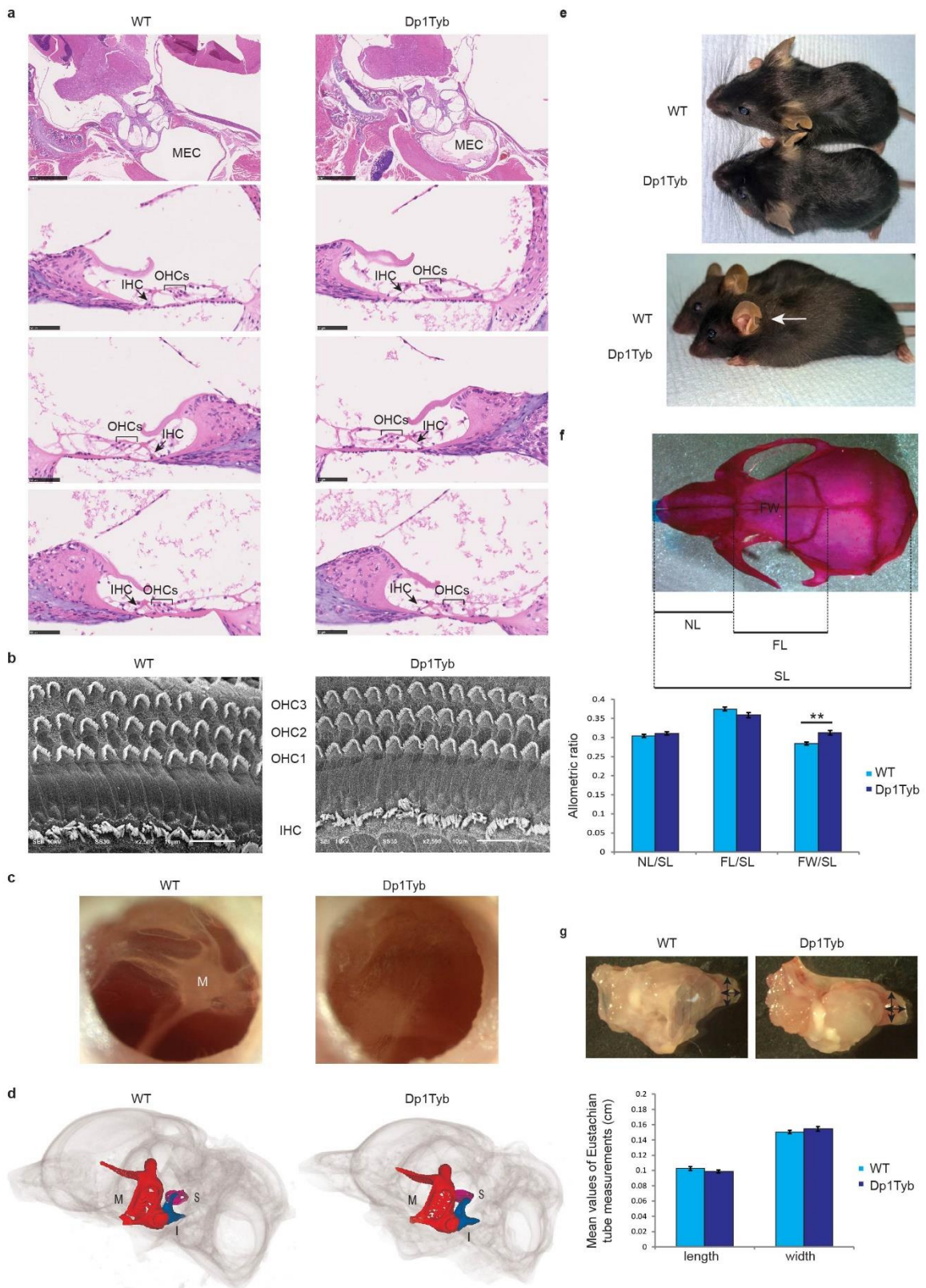


**Figure 2. Normal ear morphology and craniofacial dysmorphism in Dp1Tyb mice. a,** Histological analysis of the hair cells in 2-months old mice from both genotypes. No difference was observed between the genotypes. MEC: middle ear cavity. Scale bars: 1mm and 100 µm.

## Appendix

**b**, Scanning electron micrographs showing hair cell organisation and morphology in the mid turn of the cochlea of wild-type (WT) and Dp1Tyb mice. Three rows of OHCs and a row of IHCs were observed in both wild-type and mutant mice. Scale bars: 10  $\mu\text{m}$ . OHC, outer hair cell; IHC, inner hair cell. **c**, Microscopic views of tympanic membrane from wild-type (WT) and Dp1Tyb mice. No visible fluid behind the tympanic membrane and easily recognizable malleus was detected in the wild-type ears and cloudy appearance of the eardrum was detected in all inspected Dp1Tyb middle ears. Both wild-type and mutant ears had intact tympanic membranes. **d**,  $\mu\text{CT}$  images of the ear of a wild-type (WT) and a Dp1Tyb mouse showing no visible difference in the size of the malleus (in red), incus (in blue) and stapes (in magenta). M, malleus; I, incus; S, stapes. **e**, Images of a Dp1Tyb mouse and a wild-type littermate showing a different shape of the skull and different shape and position of the pinna in the mutant mouse. The arrow indicates the pinna in the Dp1Tyb mouse. **f**, Dorsoventral view of a 2-month-old wild-type mouse skull showing the measurements used to study the craniofacial defect of the Dp1Tyb mice and graphic comparison of the ratios of the nasal bone length (NL), frontal bone length (FL) and the frontal bone width (FW) to the full dorsal length of the skull (SL) for each genotype. The graph shows significant difference in the width of the Dp1Tyb mice ( $n = 6$ ) compared to wild-type mice (WT) ( $n = 8$ ). Bars: standard error of mean. P-values were determined using two-tailed t-test \*\*  $p < 0.01$ . **g**, Images of dissected ears from wild-type (WT) and Dp1Tyb mice. Arrows indicate the Eustachian tube measurements taken for this study. Comparison of the length and the width of the bony part of the Eustachian tubes in wild-type (WT) and Dp1Tyb mice. Bars: standard error of mean. P-values were determined using two-tailed t-test. No significant difference was detected.

## Appendix

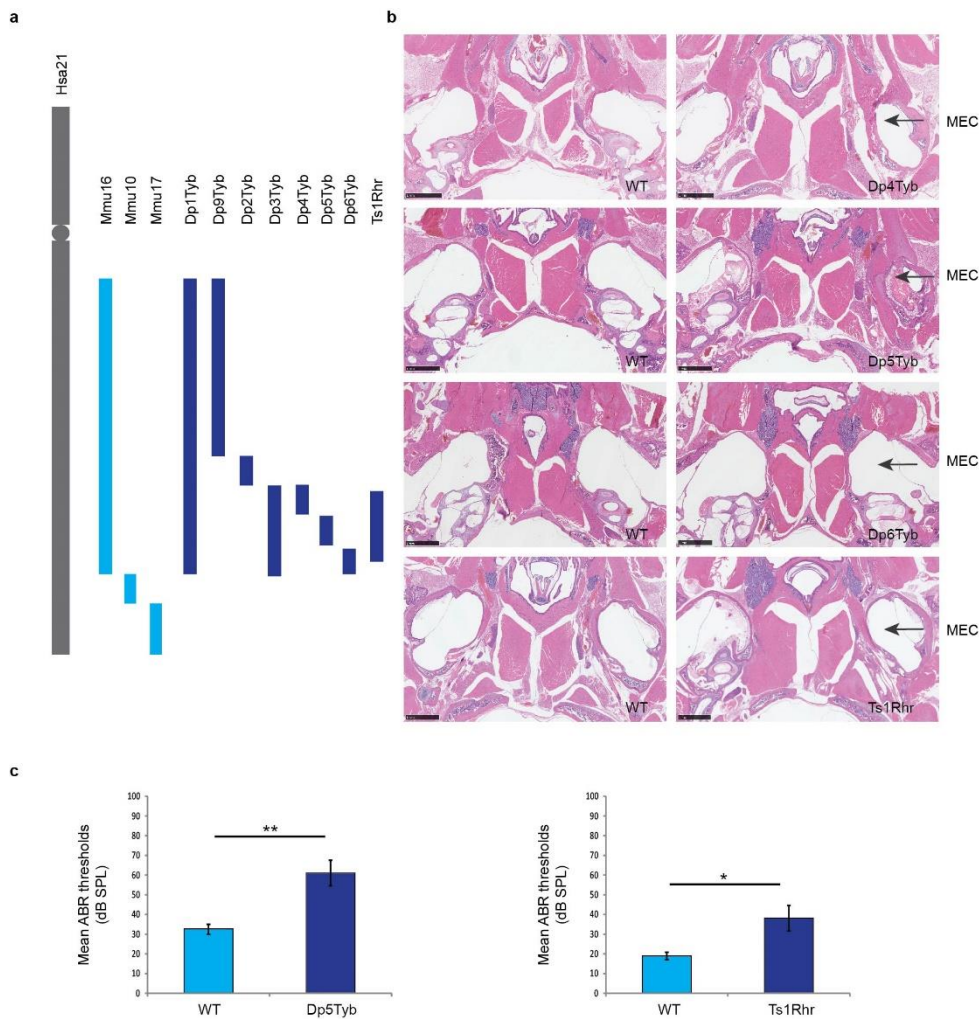


**Figure 3. OM phenotype of Dp4Tyb, Dp5Tyb, Dp6Tyb and Ts1Rhr mice.** **a**, Representation of Hsa21 (in grey), the orthologous regions on Mmu10, Mmu17 and Mmu16 (in light blue) and the region of the duplication in Dp1Tyb, Dp9Tyb, Dp2Tyb, Dp3Tyb, Dp4Tyb, Dp5Tyb, Dp6Tyb and Ts1Rhr mice (in dark blue). **b**, Haematoxylin-eosin stained transverse sections through the middle ear of 2-month-old wild type (WT) and mutant mice showing middle ear inflammation in Dp5Tyb and Ts1Rhr mice. MEC: middle ear cavity. Scale bars: 1 mm. **c**, Broadband click stimuli ABR thresholds in the right ears of 2-month-old wild-type (WT) and mutant (Dp5Tyb and Ts1Rhr) mice. The graph shows elevated mean thresholds in Dp5Tyb mice ( $n = 5$ ) compared to wild-type (WT) mice ( $n = 4$ ) and in Ts1Rhr mice ( $n = 5$ ) compared to wild-type (WT) mice ( $n = 5$ ). Bars: standard error of mean. P-values were determined using two-tailed t-test. \*  $p \leq 0.05$ ; \*\*  $p < 0.01$ .

## Appendix

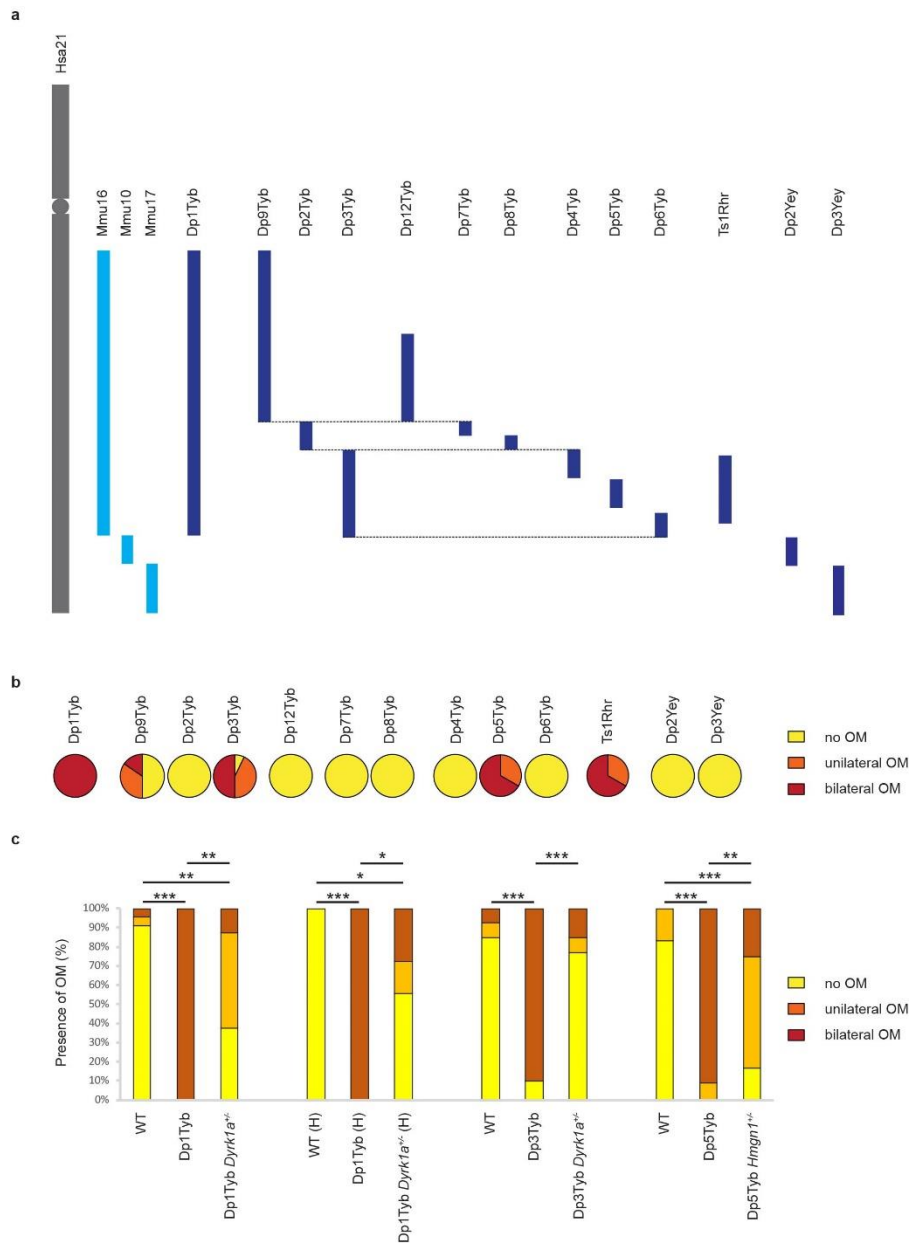


**Figure 4. Localisation and verification of the major gene, *Dyrk1a*, involved in OME in DS.**  
**a**, Representation of Hsa21 (in grey), the orthologous regions on Mmu10, Mmu17 and Mmu16 (in light blue) and the region of the duplication in all DpTyb mutants (in dark blue). **b**, The pie charts represent percentage of mutant mice with no effusion (in yellow) and with effusion in one (in orange) or in both ears (in red) for all the DpTyb lines tested along with Ts1Rhr, Dp2Yey and Dp3Yey. **c**, Normalisation of *Dyrk1a* dosage in Dp3Tyb mice leads to restoration of the wild-type phenotype. The graphs show the incidence of OM in wild-type (WT), DpTyb lines, and double mutant mice, carrying a DpTyb allele and heterozygous for a KO allele at either the *Dyrk1a* or *Hmggn1* gene. First panel, mice produced from Dp1Tyb mice crossed to *Dyrk1a*

## Appendix

knockout mice at the Francis Crick Institute - wild-type (WT), Dp1Tyb mice, and double mutant mice Dp1Tyb *Dyrk1a*<sup>+/-</sup>. Second panel, mice produced from Dp1Tyb mice crossed to *Dyrk1a* knockout mice at the MRC Harwell Institute (H) - wild-type (WT), Dp1Tyb mice, and double mutant mice Dp1Tyb *Dyrk1a*<sup>+/-</sup>. Third panel, mice produced from the Dp3Tyb mice crossed to *Dyrk1a* knockout mice in the Francis Crick Institute - wild-type (WT), Dp3Tyb mice, and double mutant mice Dp3Tyb *Dyrk1a*<sup>+/-</sup>. Fourth panel, mice produced from the Dp5Tyb mice crossed to *Hmgn1* knockout mice at the Francis Crick Institute - wild-type (WT), Dp5Tyb mice, and double mutant mice Dp5Tyb *Hmgn1*<sup>+/-</sup>. P-values were determined using two-tailed t-test. \* p≤0.05; \*\* p<0.01; \*\*\* p<0.001.

## Appendix

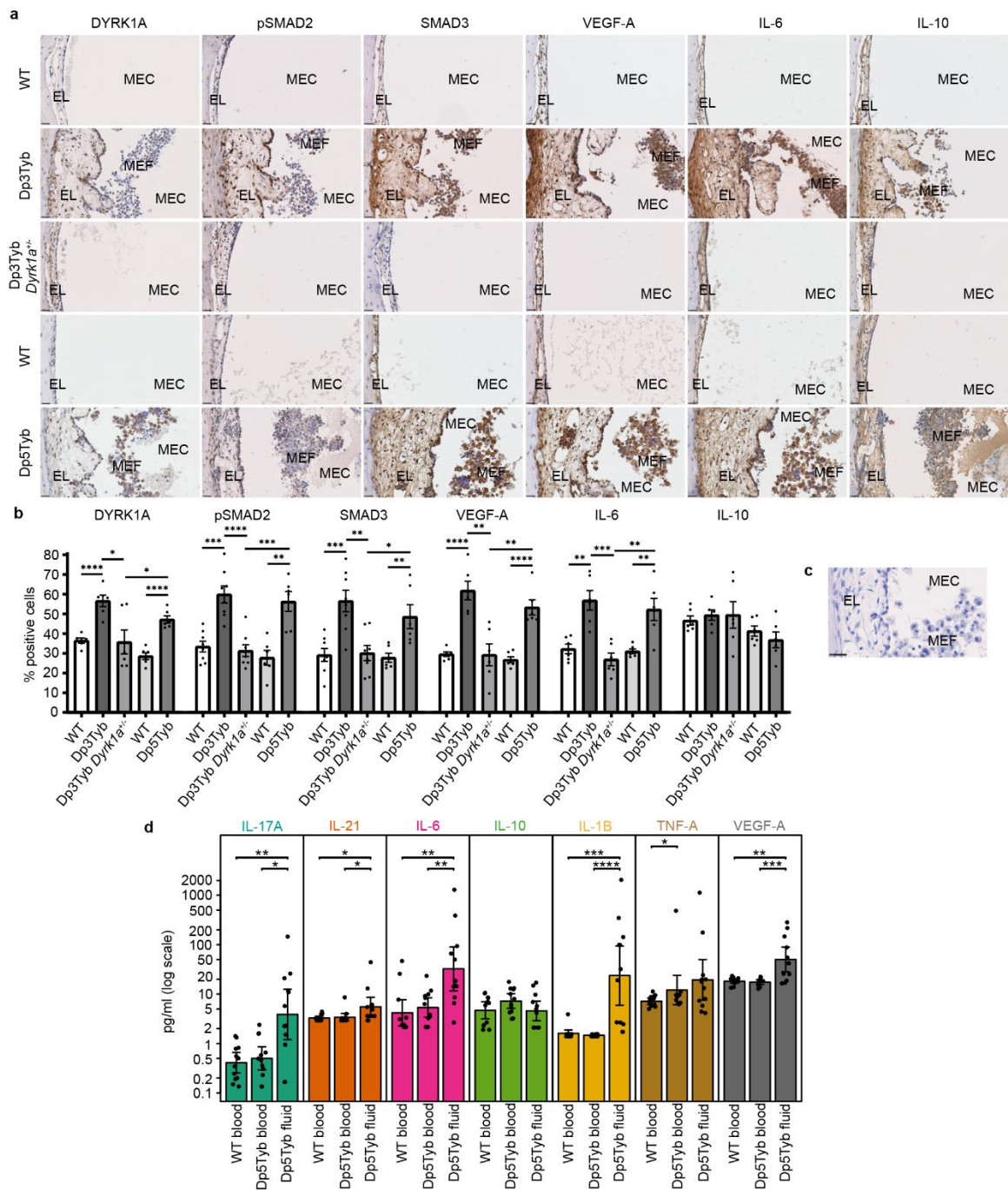


**Figure 5. Expression of DYRK1A and associated pathway members. a,** Immunohistochemical staining of transverse sections through the middle ear of mutant and wild-type (WT) mice with antibodies against DYRK1A, phospho SMAD2 (pSMAD2), SMAD3, VEGF-A, IL-6 and IL-10. Scale bar = 25  $\mu$ m. EL: epithelial lining; MEC: middle ear cavity; MEF: middle ear fluid. **b,** Bar graphs of the immunohistochemistry shown in a, represented as percentage of middle ear epithelial cells that express the protein. To quantify the results middle ear epithelial cells were counted in six ears from each genotype for each antibody

## Appendix

except for pSMAD2 and SMAD3 for the Dp3Tyb, Dp3Tyb *Dyrk1a*<sup>+/-</sup> mice and wild-type littermates (WT) where the cells were counted in eight ears. Error bars show standard error of the mean (SEM). Significance was established using two-tailed unpaired t-tests. P-values were denoted according to \*\*\*\*  $< 0.0001$ , \*\*\*  $< 0.001$ , \*\*  $< 0.01$ , \*  $< 0.05$ . **c**, Negative control (no primary antibody) for the immunohistochemistry shown in (a). **d**, Mesoscale Discovery (MSD) assay using blood from Dp5Tyb mice (n = 12), blood from wild-type (WT) littermates (n = 12) and middle ear fluid from Dp5Tyb mutants (n = 12). The results presented in the graphs are from two independent experiments for all antibodies. Each point corresponds to a single sample which has been measured repeatedly and averaged (see data pre-processing in methods). For each group in each panel the height of the coloured bar indicates the mean and whiskers extend to +/- 2 SEM. For each pairwise comparison in a panel a two-sided Mann–Whitney–Wilcoxon (MWW) test was performed and raw p-values were denoted according to: \*\*\*\*  $< 0.0001$ , \*\*\*  $< 0.001$ , \*\*  $< 0.01$ , \*  $< 0.05$ . To control for multiple testing, we applied the Benjamin-Hochberg procedure to the complete set of 24 p-values arising from all the MWW tests across all assays and pairs of groups. Rejecting the null in all starred cases (\*, \*\*, \*\*\* and \*\*\*\*) controlled the FDR below 5%.

## Appendix

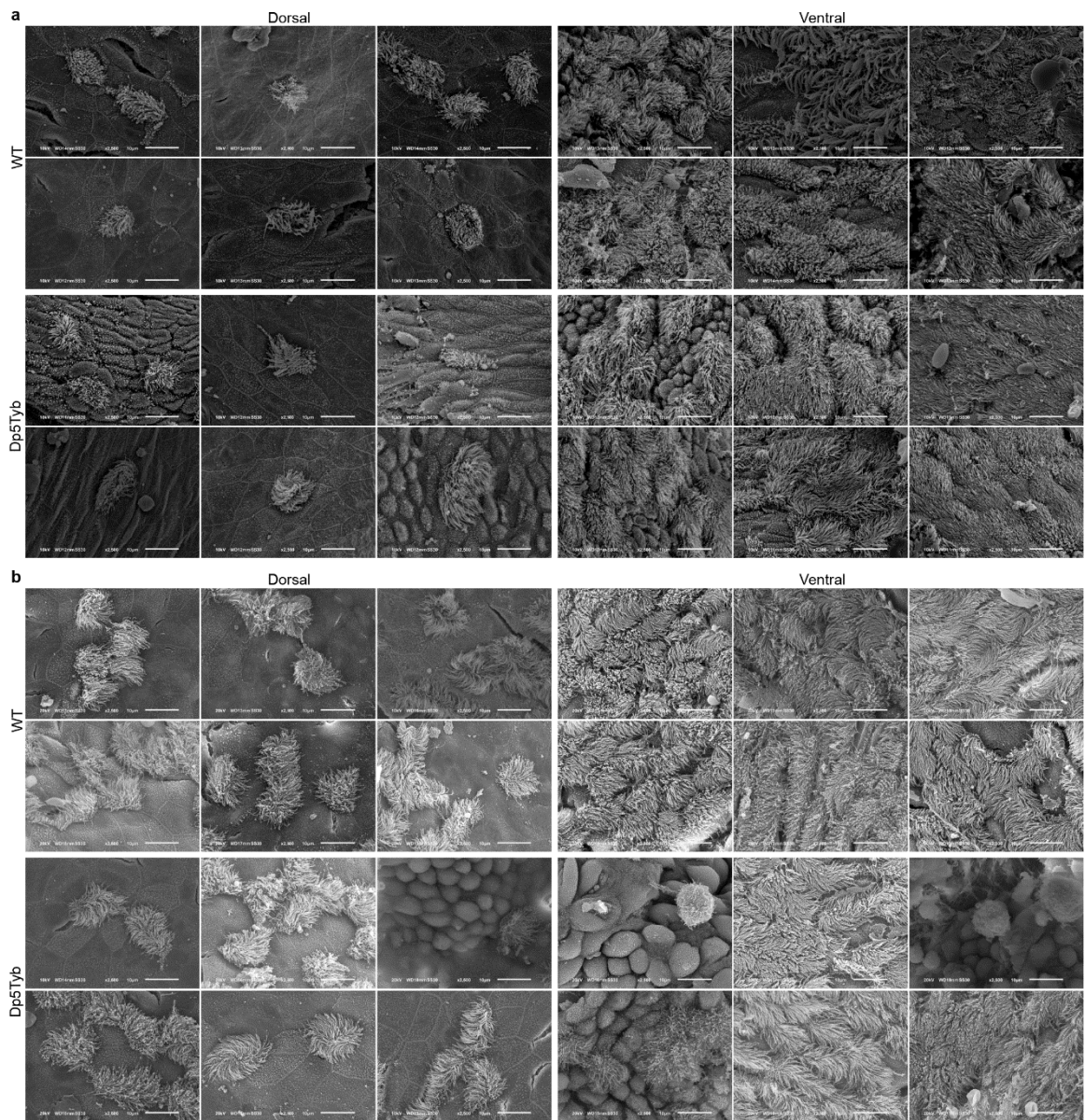
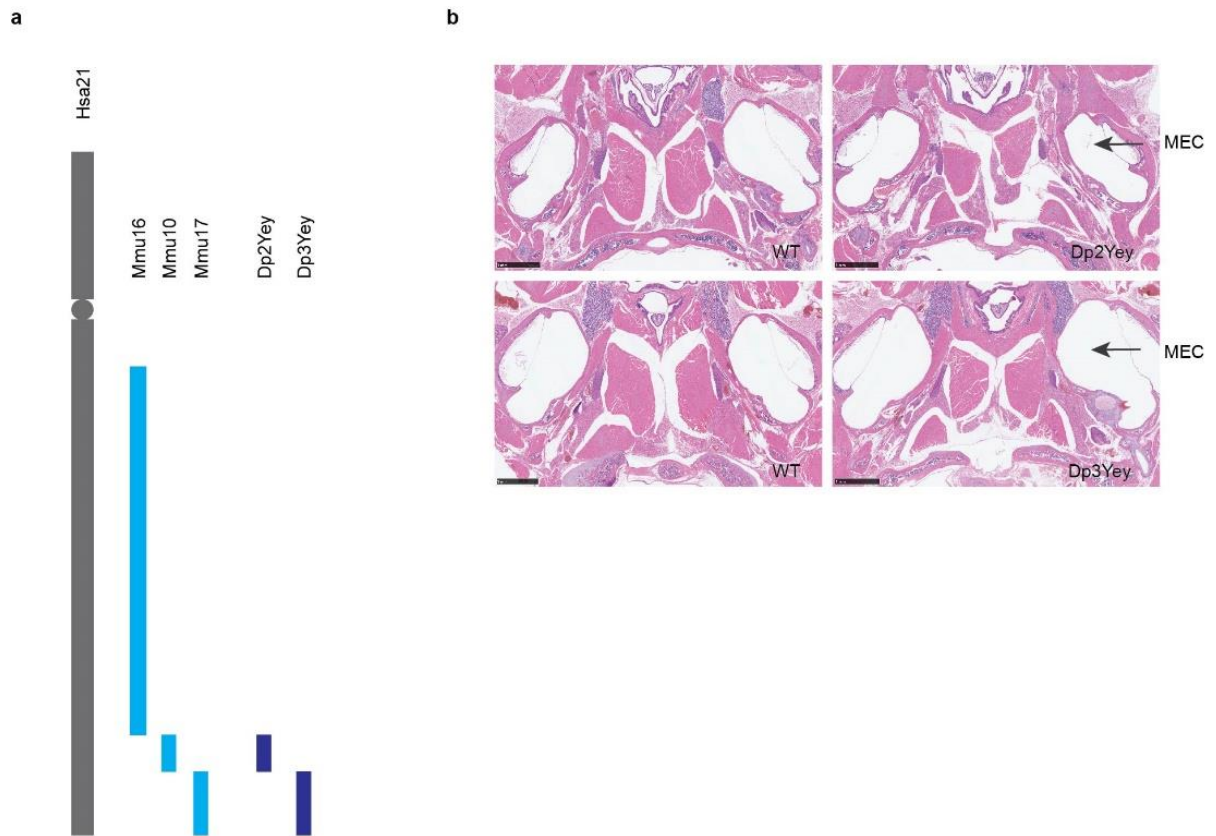


**Figure 6. Scanning electron micrographs of middle ear cavities of Dp5Tyb mice and littermate controls.** Scanning electron microscopy (SEM) images from the dorsal and ventral region of the middle ear of **a**, 2-week-old and **b**, 2-month-old Dp5Tyb mice and wild-type (WT) littermates. Images were taken of both ears of each mouse (2-week-old Dp5Tyb n = 3, WT n = 3; 2-month-old Dp5Tyb n = 6, WT n = 4). Representative SEM images of middle ears were chosen for the panels. For the 2-week-old time point the dorsal and ventral images of wild-type ears and the dorsal images of the Dp5Tyb ears are from three separate mice. The 2-week-old ventral images of the Dp5Tyb ears are from two separate mice. For the 2-month-old time point the dorsal images of wild-type ears are from six different ears of five mice, the ventral images of wild-type mice - six different ears from three mice. Both, dorsal and ventral images of middle

## Appendix

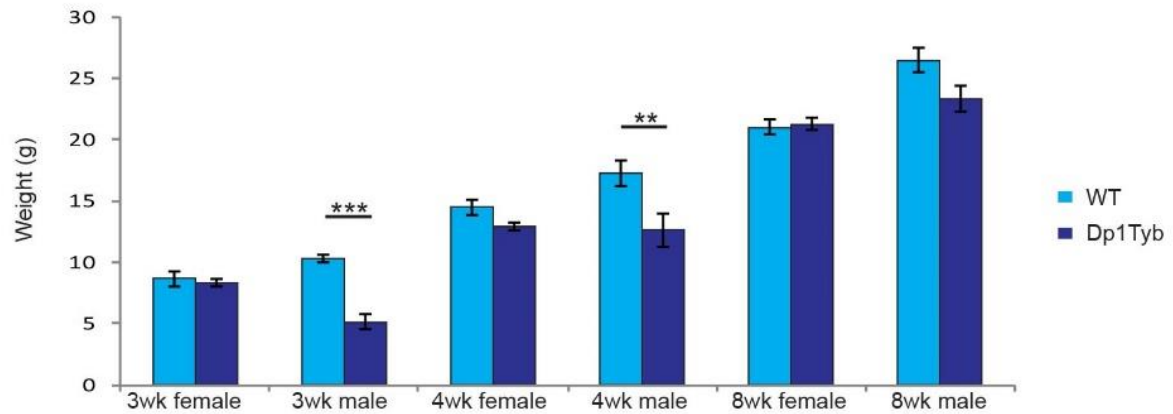
ear images of 2-month-old Dp5Tyb mice represented in the figure, at the time when the mice have fully developed OM, are from six different ears from five mice (for the dorsal) and from six different ears for four mice (for the ventral). Loss of cilia in the middle ear of epithelial cells was detected only in the ears of 2-month-old mutants but not in 2-week-old Dp5Tyb mice, indicating that the genes in three copies in the Dp5Tyb region, one of which is *Dyrk1a*, have no role in cilia development. Images taken at x2500 magnification. Scale bar = 10  $\mu\text{m}$ .

## Appendix



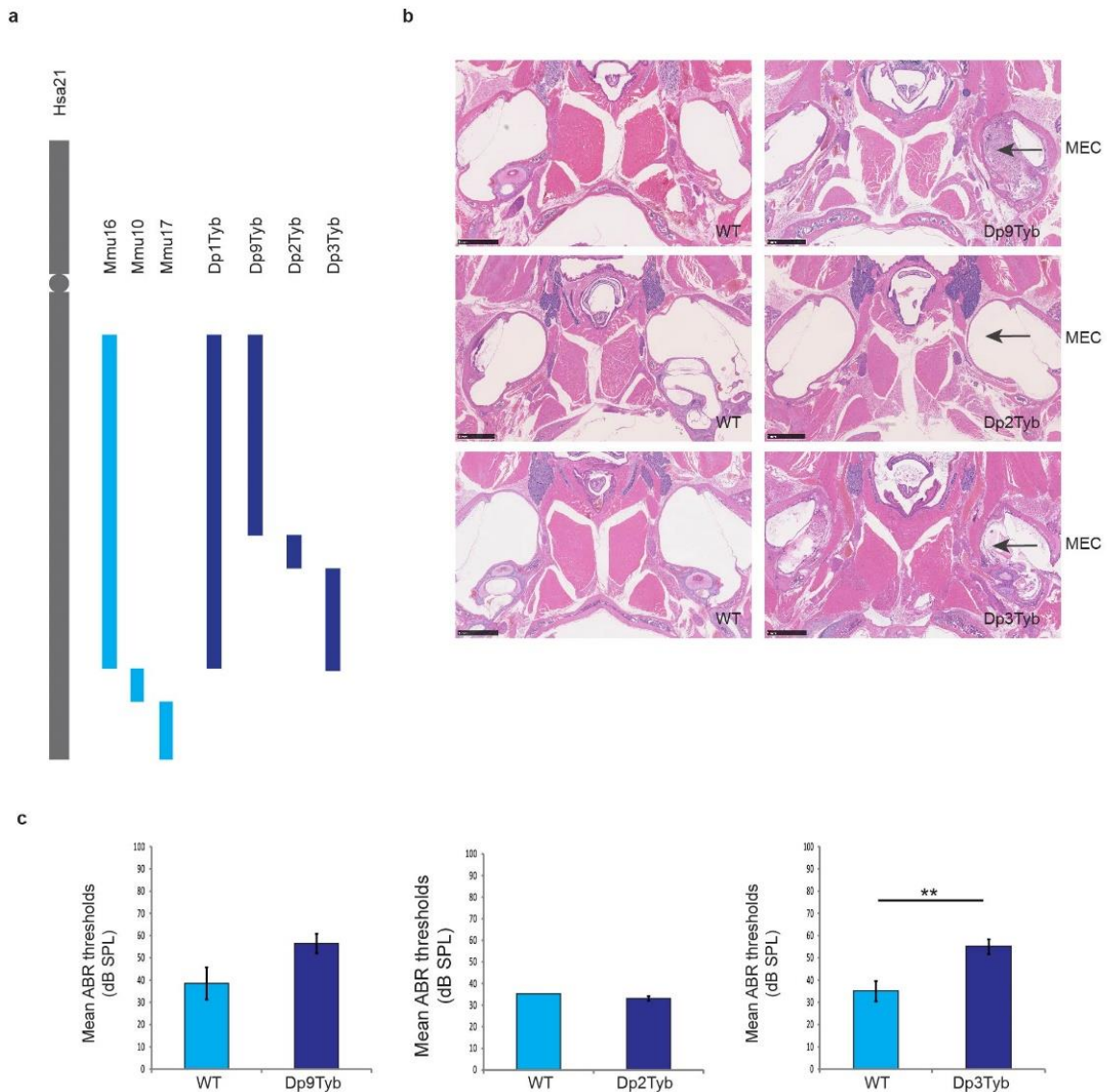
**Extended Data Fig. 1. Middle ear histology of Dp(10)2Yey and Dp(17)3Yey mice. a,** Representation of Hsa21 (in grey), the orthologous regions on Mmu10, Mmu17 and Mmu16 (in light blue) and the regions of the duplication in Dp(10)2Yey and Dp(17)3Yey (in dark blue). **b,** Haematoxylin-eosin stained transverse sections through the middle ear of 2-month-old wild type (WT) and mutant mice showing no middle ear inflammation in Dp(10)2Yey and Dp(17)3Yey mice. MEC: middle ear cavity. Scale bars: 1 mm.

## Appendix



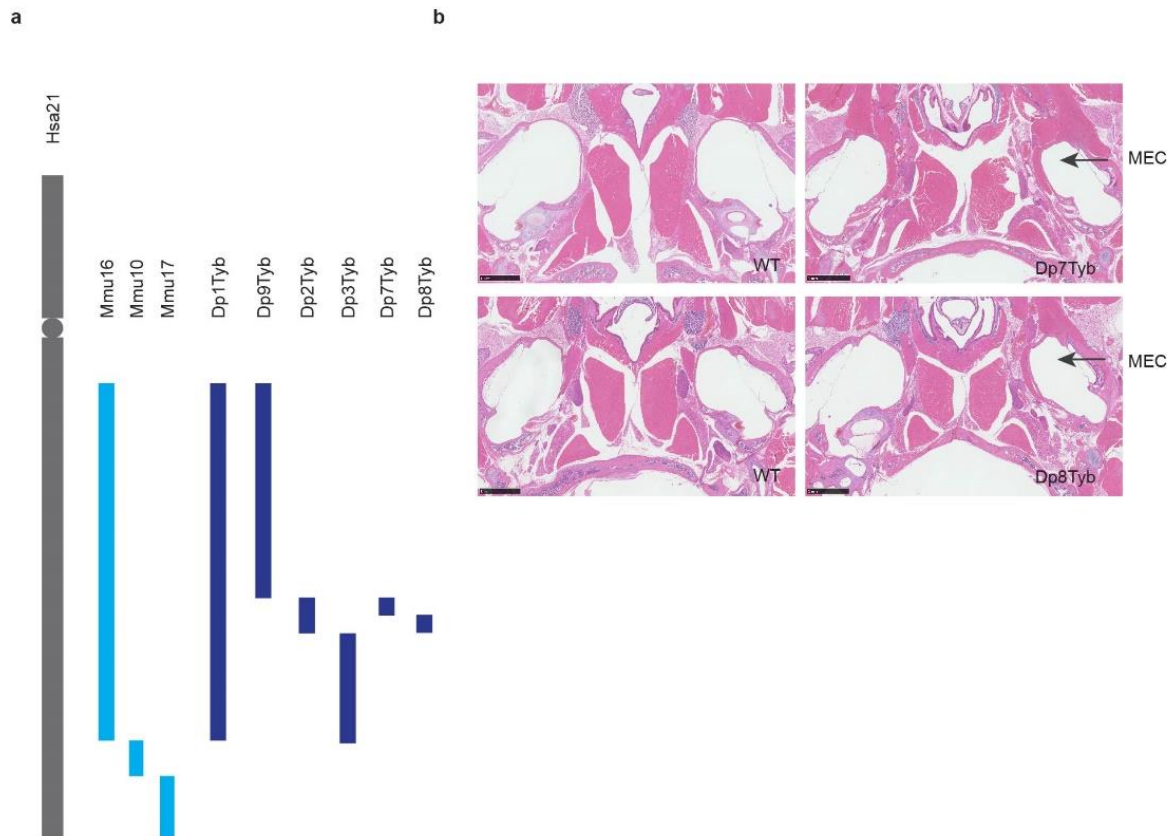
**Extended Data Fig. 2. Body weight of Dp1Tyb mice.** Comparison of the weights of Dp1Tyb mice to wild-type (WT) littermates at the age of 3 (3wk), 4 (4wk) and 8 (8wk) weeks for both male and female mice. The graph shows significant differences between males from the two genotypes at two of the time points (3wk and 4wk). 3wk: female Dp1Tyb n = 3 WT n = 5, male Dp1Tyb n = 3 WT n = 7; 4wk: female Dp1Tyb n = 5 WT n = 5, male Dp1Tyb n = 3 WT n = 6; 8wk: female Dp1Tyb n = 7 WT n = 9, male Dp1Tyb n = 3 WT n = 6. Bars: standard error of mean. P-values were determined using two-tailed t-test. \*\* p<0.01; \*\*\* p<0.001.

## Appendix



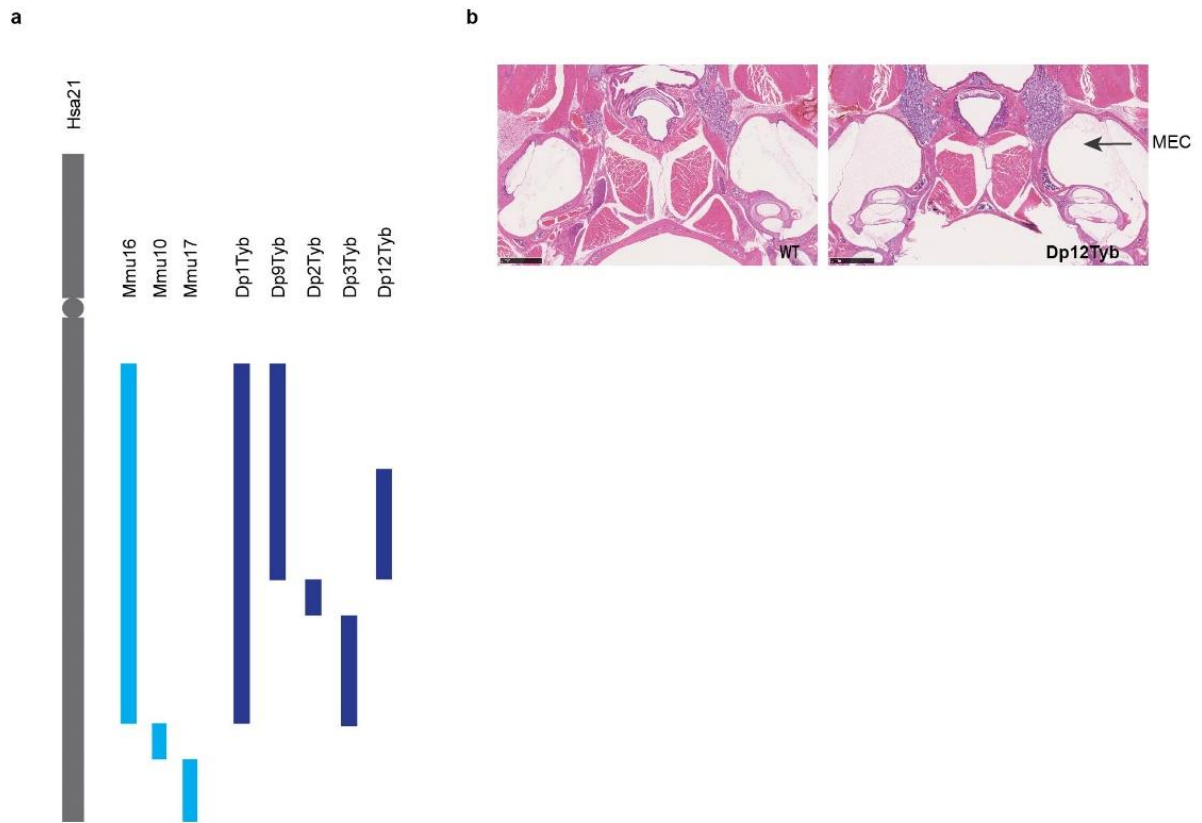
**Extended Data Fig. 3. OM phenotypes of Dp9Tyb, Dp2Tyb and Dp3Tyb mice. a**, Representation of Hsa21 (in grey), the orthologous regions on Mmu10, Mmu17 and Mmu16 (in light blue) and the region of the duplication in Dp1Tyb, Dp9Tyb, Dp2Tyb and Dp3Tyb mice (in dark blue). **b**, Haematoxylin-eosin stained transverse sections through the middle ear of 2-month-old wild type (WT) and mutant mice showing middle ear inflammation in Dp9Tyb and Dp3Tyb mice. MEC: middle ear cavity. Scale bars: 1 mm. **c**, Broadband click stimuli ABR thresholds in the right ears of 2-month-old wild-type (WT) and mutant (Dp9Tyb, Dp2Tyb and Dp3Tyb) mice. The graphs show elevated mean thresholds in Dp3Tyb mice ( $n = 6$ ) compared to wild-type mice ( $n = 4$ ) and no significant difference between Dp9Tyb ( $n = 4$ ) compared to wild-types ( $n = 3$ ) and Dp2Tyb mice ( $n = 5$ ) compared to wild-type ( $n = 1$ ). Bars: standard error of mean. P-values were determined using two-tailed t-test. \*\*  $p < 0.01$ .

## Appendix



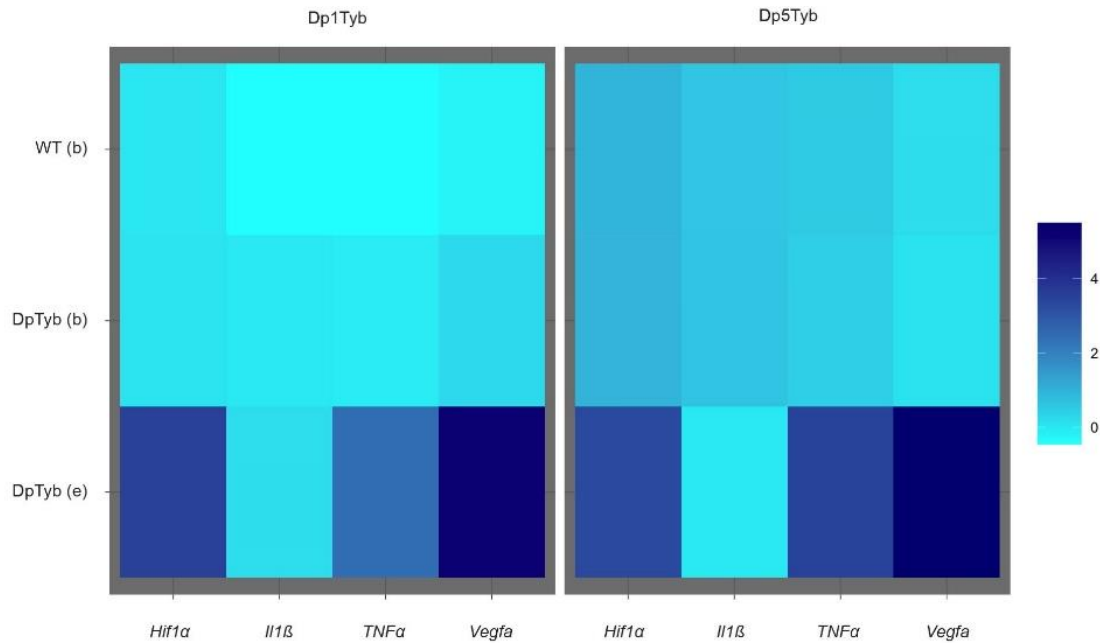
**Extended Data Fig. 4. Middle ear histology of Dp7Tyb and Dp8Tyb mice. a,** Representation of Hsa21 (in grey), the orthologous regions on Mmu10, Mmu17 and Mmu16 (in light blue) and the region of the duplication in Dp1Tyb, Dp9Tyb, Dp2Tyb, Dp3Tyb, Dp7Tyb and Dp8Tyb mice (in dark blue). **b,** Haematoxylin-eosin stained transverse sections through the middle ear of 2-month-old wild type (WT) and mutant mice showing no middle ear inflammation in Dp7Tyb and Dp8Tyb mice. MEC: middle ear cavity. Scale bars: 1 mm.

## Appendix



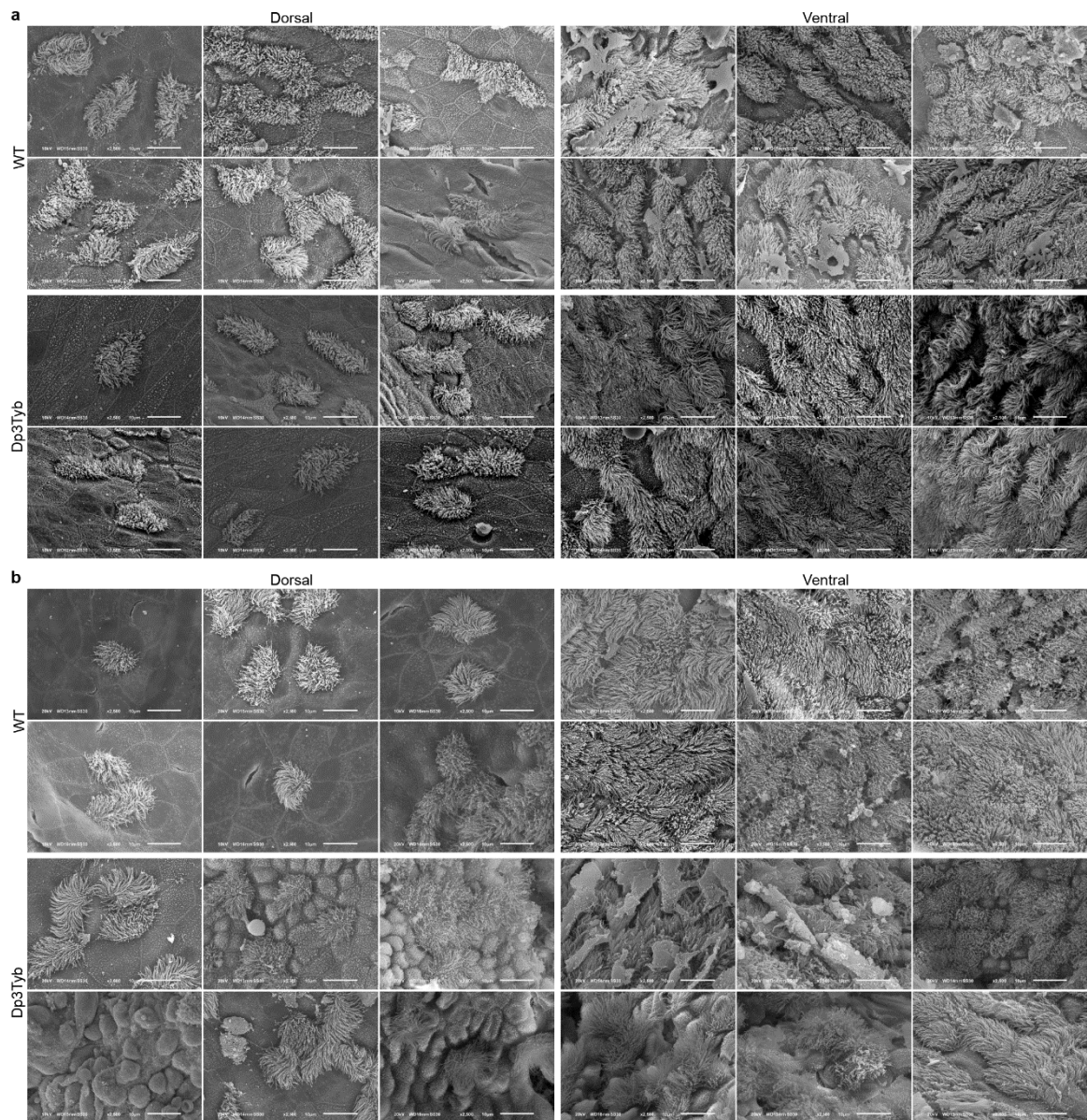
**Extended Data Fig. 5. Middle ear histology of Dp12Tyb mice.** **a**, Representation of Hsa21 (in grey), the orthologous regions on Mmu10, Mmu17 and Mmu16 (in light blue) and the region of the duplication in Dp1Tyb, Dp9Tyb, Dp2Tyb, Dp3Tyb and Dp12Tyb mice (in dark blue). **b**, Haematoxylin-eosin stained transverse sections through the middle ear of 2-month-old wild type (WT) and mutant mice showing no middle ear inflammation in Dp12Tyb mice. MEC: middle ear cavity. Scale bars: 1 mm.

## Appendix



**Extended Data Fig. 6. Expression levels of *Hif1α* and HIF responsive genes *Vegfa*, *Il-1β* and *Tnfa*.** Real-time quantitative PCR (RT-qPCR) analysis of cytokines in blood samples from Dp1Tyb (n = 16) mice, wild-type (WT) littermates (n = 25), middle ear fluid from Dp1Tyb mice (n = 17), Dp5Tyb (n = 19) mice, wild-type (WT) littermates (n = 13) and middle ear fluid from Dp5Tyb mice (n = 9). b: blood, e: ear fluid. RQ values were normalised using a log transformation.

## Appendix



**Extended Data Fig. 7. Scanning electron micrographs of middle ear cavities of Dp3Tyb mice and littermate controls.** Scanning electron microscopy (SEM) images from the dorsal and ventral region of the middle ear of **a**, 2-week-old and **b**, 2-month-old Dp3Tyb mice and wild-type (WT) littermates. Images were taken of both ears of each mouse (2-week-old Dp3Tyb  $n = 3$ , WT  $n = 3$ ; 2-month-old Dp3Tyb  $n = 6$ , WT  $n = 3$ ). Representative SEM images of middle ears were chosen for the panels. For the 2-week-old time point the dorsal images of wild-type ears are from three separate mice and the ventral images of wild-type ears as well as the dorsal and ventral images of the Dp3Tyb ears are from two separate mice for each group. For the 2-month-old time point the dorsal images of wild-type ears are from five different ears

## Appendix

of three mice, the ventral images of wild-type mice - six different ears from three mice. Both, dorsal and ventral images of middle ear images of 2-month-old Dp3Tyb mice represented in the figure, at the time when the mice have fully developed OM, are from six different ears from six mice (for the dorsal) and from six different ears for five mice (for the ventral). Loss of cilia in the middle ear of epithelial cells was detected only in the ears of 2-month-old mutants but not in 2-week-old Dp3Tyb mice, indicating that the genes in three copies in the Dp3Tyb region, one of which is *Dyrk1a*, have no role in cilia development. Images taken at x2500 magnification. Scale bar = 10  $\mu\text{m}$ .

## Appendix

### Extended Data Table 1. Prevalence of OM in Dp lines and wild-type (WT) mice.

The numbers of mice with unilateral and bilateral OM are given for each line along with wild-type controls. P-values were calculated using a two-tailed Fisher's exact test.

mouse line	Duplication segment	age (weeks)	OM in Dp mice			OM in WT mice			p value
			unilateral	bilateral	total	unilateral	bilateral	total	
Dp1Tyb	M mu16 <i>Lipi-Zbtb21</i>	3, 4, 8, 16, 28	0	31	31/31	8	0	8/34	<0.00001
Dp2Tyb	M mu16 <i>Mis 18a-Runx1</i>	8, 16, 28	0	0	0/8	0	0	0/6	1
Dp3Tyb	M mu16 <i>Mir802-Zbtb21</i>	8 and 28	6	7	13/14	2	0	2/11	0.0002
Dp4Tyb	M mu16 <i>Mir802-Dscr3</i>	8	1	0	1/8	0	0	0/8	1
Dp5Tyb	M mu16 <i>Dyrk 1a-B3galt5</i>	8	4	8	12/12	0	0	0/8	<0.00001
Dp6Tyb	M mu16 <i>Igsf5-Zbtb21</i>	8	1	10	11/11	0	0	0/6	1
Dp7Tyb	M mu16 <i>Mis 18a-Il10rb</i>	8	0	0	0/7	0	0	0/5	1
Dp8Tyb	M mu16 <i>fnar1-Runx1</i>	8	1	0	1/7	2	0	2/5	0.5227
Dp9Tyb	M mu16 <i>Lipi-Hunk</i>	8, 16, 28	9	4	13/26	3	1	4/22	0.0339
Dp12Tyb	M mu16 <i>Krtap24-1-Hunk</i>	8	0	0	0/7	1	0	1/5	0.3636
Dp2Yey	M mu10 <i>Prmt2-Mir6908</i>	8	1	0	1/7	1	0	1/6	1
Dp3Yey	M mu17 <i>Umodl1-Rrp1b</i>	8	1	0	1/9	0	0	0/6	1
Tsr1Rhr	M mu16 <i>Cbr3-Gm9242</i>	8	3	6	9/9	1	0	1/8	0.0004

## Appendix

**Extended Data Table 2. Comparison of the significant differences (p values) in the expression levels of *Hif1α* and HIF responsive genes *Vegfa*, *Il-1β* and *Tnfa* in middle ear fluids and blood of Dp1Tyb and Dp5Tyb mice and blood from wild-type littermates (WT). P-values were calculated using a tukey *post hoc* multiple comparisons analysis.**

WT blood/Dp1Tyb blood	1	1	1	1
WT blood/Dp1Tyb ear fluid	1.68E-09	6.37E-14	1	0.0000012
Dp1Tyb blood/Dp1Tyb ear fluid	1.01E-07	1.58E-13	1	5.49E-04
WT blood/Dp5Tyb blood	1	1	1	1
WT blood/Dp5Tyb ear fluid	8.74E-10	2.40E-13	1	4.00E-10
Dp5Tyb blood/Dp5Tyb ear fluid	1.34E-10	2.40E-13	1	2.45E-11

**Extended Data Table 3. qPCR analysis of duplicated genes from the Dp5Tyb region in saliva samples from paired Down syndrome children with OM and unaffected mothers (n = 6). P-values were calculated using paired t-test.**

Gene	ΔCt DS	ΔCt NonDS	ΔΔCt	Expression Fold Change	t.test_pval
<i>DYRK1A</i>	-0.38	0.25	-0.63	154	0.004
<i>KCNJ6</i>	2.67	-1.15	3.82	0.07	0.008
<i>KCNJ15</i>	0.38	-0.23	0.61	0.66	0.06
<i>ERG</i>	-0.46	-0.50	0.04	0.97	0.35
<i>ETS2</i>	1.90	1.47	0.43	0.74	0.08
<i>PSMG1</i>	0.69	0.65	0.04	0.97	0.21
<i>BRWD1</i>	0.62	1.08	-0.46	1.37	0.33
<i>HMG1</i>	-1.06	-0.87	-0.19	1.14	0.03
<i>WRB</i>	0.21	0.71	-0.50	1.41	0.25
<i>LCA5L</i>	0.69	0.76	-0.07	1.05	0.31
<i>SH3BGR</i>	1.93	1.08	0.85	0.55	0.14
<i>B3GALT5</i>	0.87	0.55	0.31	0.81	0.18